AD-A207 446 THE DEMONSTRATION OF THE FEASIBILITY OF THE TUNING AND STIMULATION OF NUCLEAR RADIATION(U) TEXAS UNIV AT DALLAS RICHARDSON C B COLLINS 31 OCT 88 1/3

UNCLASSIFIED N00014-81-K-0653 F/G 20/8 NL

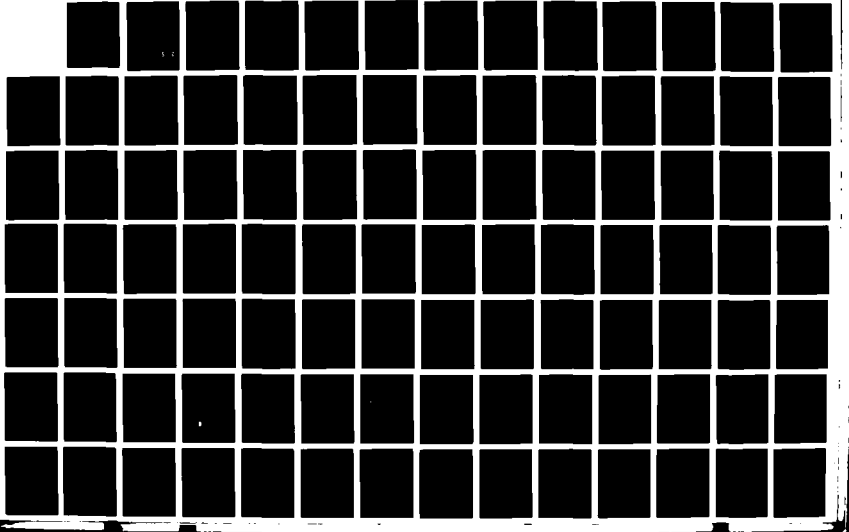

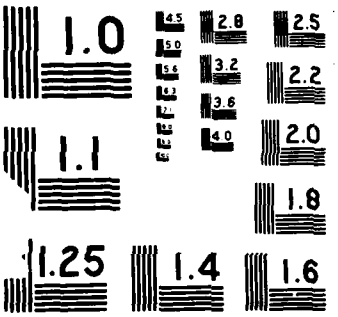
1.0
1.1
1.25
1.4
1.6
1.8
2.0
2.2
2.5
2.8
3.2
3.6
4.0
4.5
5.0
5.6

UTD Proposal #880259
Reference No: NR395-072

Final Report to the
U.S. Office of Naval Research

by

The University of Texas at Dallas
P.O. Box 830688
Richardson, TX 75083-0688
(214) 690-2864

describing effort applied to

THE DEMONSTRATION OF THE FEASIBILITY OF THE TUNING AND STIMULATION OF NUCLEAR RADIATION

Supported by
ONR Contract No. N00014-81-K-0653

July 1, 1981 to October 31, 1988

Principal Investigator: Carl B. Collins
Title: Professor
Soc. Sec. No.: 466-64-4951
Admin. Unit: School of Natural Sciences & Mathematics

ENDORSEMENT:

Carl B. Collins
Principal Investigator
Physics Program
Phone: (214) 690-2864

TABLE OF CONTENTS

INTRODUCTION

The problem of the tuning and stimulation of γ-radiation is one of a class of interesting concerns dealing with the properties of coherent nuclear states. It is generally recognized that studies of phenomena associated with the properties of coherently excited quantum states of matter at the atomic and molecular levels have revolutionized the traditional fields of optics and spectroscopy over the past decade. These efforts have benefited greatly from techniques that generally exchanged the readily available coherence of a radiation field for coherent states of material excitation. In contrast, it would seem at first that the low intensities of virtually all sources of quanta large enough to be used for the excitation of nuclear states, together with the shortened dephasing times that might characterize the coherent excitation of such levels, would deter comparable studies of excited nuclei.

Our early theoretical estimates[1-8] had suggested the opposite; namely that coherent superpositions of states of nuclear excitation might be produced or altered to a readily detectable extent by intense fields of longer wavelength electromagnetic radiation. Rather diverse processes involving such effects were discussed and modeled, including our efforts at quantitatively describing multiphoton absorption, emission, and mixed Raman-type scattering,[1-8] stimulated γ-radiation[3-8] and even some particle processes such as induced neutron capture and fission.[4,5,8] A very fertile interdisciplinary area of nuclear quantum electronics[7] appeared to be developing, encouraged by the further theoretical and experimental results of our subsequent work[9-22] under this contract.

Perhaps surprisingly, within the new field of research the conclusions of successively refined modeling studies are becoming progressively more positive. This is particularly so in our own case for the tuning and stimulation of nuclear radiations. As mentioned at the inception of this work, the feasibilities of both the coherent and incoherent pumping of nuclear transitions with "optical" radiation were dependent upon various nuclear properties that were (and still are) uncertain by several orders of magnitude. The amplitudes for upconversion were expected to depend critically upon the

energies and symmetries of potentially resonant intermediate states for the processes that lie in the "blind spots" of conventional nuclear spectroscopy and that cannot be resolved with existing technology. Reports in the literature continue to span a range of values which would cause threshold estimates for the stimulation of gamma radiation to vary from routine to impossible; and it still appears that much additional basic study of the structure and properties of nuclear excitation, particularly near isomeric levels, must precede any truly indicative estimate of the feasibility of any stimulated emission device. However, the results of the ongoing experiments continue to be extremely positive.

As a part of this contract work several new technologies were started, one of which has reached a high level of development, having emerged now as a dependable instrument.[23] It is the nuclear analog for gamma radiation of one of the methods for implementing laser spectroscopy at optical frequencies.

Most laboratory sources of gamma radiation emit at levels of intensity corresponding to single photon conditions and Mössbauer experiments are rarely conducted at such great intensities that the detection of two photons would be probable in the transit time spent between source and absorber. Under those conditions, the perception of gamma rays as streams of particles in instinctive. Nevertheless, as elements of electromagnetic radiation they must also be considered as carrier waves of high frequency. As the name would imply, our technique of Frequency Modulation Spectroscopy (FMS) developed under this contract derives its operation from the modulation of the gamma-ray carrier. It represents a translation into the nuclear domain of one of the powerful techniques of laser spectroscopy at the atomic level.[23]

TECHNICAL BACKGROUND AND SUMMARY OF ACHIEVEMENTS

All of the processes of interest in the new interdisciplinary field of nuclear quantum electronics that were mentioned in the introduction have a common requirement for the significant excitation of coherent superpositions of nuclear states with non-nuclear sources. This is actually the central issue. All conventional sources of nuclear radiations, including weapons level of power, are generally inadequate for the excitation of coherent

nuclear states. Principally because it can be focused, conventional laser radiation offers a unique possibility for the preparation of such states, provided certain conditions are met. If such states can be prepared, the essential control of nuclear processes will be at hand. Radioactive decay can be slowed, accelerated or stimulated for laser-like output at energies in the 10-100 keV range. All of the accelerated processes involving particles that were discussed in the introduction can be realistically pursued. Most of the processes of nonlinear optics can be conceived to have analogs at the nuclear level, if reasonable levels of coherent excitation of nuclear states can be accomplished with non-nuclear input energy.

Resolution of this critical issue depends upon the availability of intermediate states at the nuclear level and upon the magnitude of the interaction matrix elements coupling them to known stationary states. Since these questions lie outside the normal purview of nuclear physics, the answers are not available, and the techniques for obtaining them are arising mostly from our work. Our research under this contract has had the overall plan of first developing the methods while refining the modeling, and secondly, of approaching directly the question of accessibility of threshold for significant levels of stimulated emission.

One large-scale application of the basic concepts and technologies developed under this contract along the line of incoherent pumping was spun-off in 1986 for implementation under separate contract to SDIO/IST. More dependent upon continued basic research was this other line of coherent pumping, lying at the focus of efforts continued since 1986 under this ONR contract. As mentioned in the Introduction, in this direction technology has been advanced to yield a conceptual analog[23] of the narrow-line, tunable spectroscopic sources which supported the investigation of atomic and molecular properties with the level of resolution required for development of conventional types of lasers.

Surprisingly, the development of this promising field of nuclear quantum electronics has followed an excessively tortuous path dominated by a curious burden of history and counterproductive tradition. The most accessible sources of high power, coherent radiation lie in the radiofrequency and

microwave ranges and in 1980 a review was made of the comprehensive literature on hyperfine Mössbauer effects observed in the presence of intense radiofrequency fields. Remarkably enough, a major effect was found that had defied the construction of a completely satisfactory explanation in terms involving only conventional processes of incoherent excitation. It was the generation of radiofrequency sidebands on the hyperfine Mössbauer spectra of ^{57}Fe in ferromagnetic environments.[24-39] Through the application to a ferromagnetic iron foil of a magnetic field oscillating at radiofrequencies, several new spectral lines were produced in addition to the usual six hyperfine components of the 14.4 keV transition in ^{57}Fe. The rudiments of a multiphoton scheme had been advanced by Mitin[30] to explain the effect in 1971, but essential concerns were missed[33] and that attempt was apparently abandoned. Through a series of misleading but compelling experiments,[40] evidence was obtained that seemed to support an explanation attributing the sidebands to Doppler shifts caused by acoustic vibrations driven by magnetostriction of the foil. A persistent complication arose from the geometry in which the radiofrequency H field was generally applied in the plane of the absorber foil, so that magnetostriction occurred in the direction perpendicular to the axis of propagation of the γ-radiation. However, that was accommodated by the assumption[33] of mechanical resonances that drove the foil in a manner similar to the head of a drum. Quantitative agreement was never obtained with that model but it came to be believed with a fervor unusual in experimental physics.

In 1978, West and Matthias[41] reported the first clear case of the excitation of a coherent nuclear state with long wavelength radiation. They succeeded in producing at the level of the noise, two radiofrequency sidebands on the 6.1 keV transition of ^{181}Ta in nonmagnetic tungsten. Working with frequencies low enough to be comparable to the Mössbauer width of the transition, at kilowatt levels of input power sidebands finally became perceptible. In 1981, Olariu et al.[5] showed theoretically as a consequence of more general modeling of processes of coherent nuclear excitation[1-4] that a multiphoton model comparable to the Matthias estimate[41] could explain in both magnitude and detail that much stronger development of sidebands in the earlier ^{57}Fe experiments. However, the Olariu-Matthias representations had

been constructed under the assumption that static magnetization was absent in the Mössbauer absorber and as a result that model was rigorously appropriate only for nuclei embedded in paramagnetic samples. It was one of the first tasks of our group to test the Olariu-Matthias model as an approximation for ferromagnetic ^{57}Fe and, if possible, to resolve experimentally the conflict between magnetostrictive and multiphoton origins of the radiofrequency sidebands.

The completion of that task succeeded in confirming only the encouraging magnitudes of the sidebands while calling attention to the clear need for a theoretical description more appropriate than the Olariu-Matthias "paramagnetic" model. Subsequently, our group built a greatly extended database and still we found intense sidebands on hyperfine components of the 14.4 Mössbauer transition to be maximized under conditions that minimized chances for spurious magnetostrictive effects. Prominent sidebands were observed at only tenths of Watts in input power. Ambiguities in the identification of the order and parentage of particular sidebands were resolved by several changes of frequency. No sidebands were found on forbidden transitions in contrast to the predictions of the simple paramagnetic model.

Another of the early tasks under our ONR contract was to construct a multiphoton model for ferromagnetic environments. This description accommodated all phenomena previously reported and suggested that the sidebands developed in earlier experiments actually had been driven by the same excitation of coherent states, perhaps benefiting from some enhancement contributed by physical motions that could have developed if acoustic resonances were present as had been postulated. Our ferromagnetic model also showed that "forbidden sidebands" should not be expected for nuclei embedded in real magnetic materials.

Very significant was the result that unlike the paramagnetic case this new model predicted a dependence of sideband intensity upon power that was drastically different from the magnetostrictive theories. Gone were the nodes of power at which low order sidebands are quenched, a predicted phenomenon receiving no support from observations spanning the past 20 years. Even more significant was that the new multiphoton model of nuclear sidebands was

comprehensive enough to suggest new extrapolations and effects not previously apparent. The most exciting was the extensive range over which sidebands might be tuned. This together with indications that it should be possible to drive a large part of the modulated ferromagnetism (that is needed for a large effect) into a different material with other active nuclei seemed to imply the clear feasibility of the swept frequency source for nuclear spectroscopy which was subsequently realized.

Only a very brief summary of the theory was ever published,[11] but it suffices to show the unfortunate complexity of the problem. A detailed review of these theoretical accomplishments was presented in our Annual Report for 1986 and a copy is attached as Appendix I for convenience.

Despite the impressive agreement between results obtained with the new instrumentation developed under this contract and the multiphoton models, intense criticism continued to issue because of the belief that, somehow, all effects which appear as sidebands arise from spurious acoustic vibrations excited by magnetostriction of some of the various elements of the spectroscopic sample and its holder. In appearance our multiphoton spectra do resemble the transmission spectra which can be obtained by imposing periodic Doppler shifts of purely mechanical origin upon the Mössbauer source. This unfortunate similarity in appearance between phenomena arising from such different origins has provided the basis for years of critical controversy.

Quite independently and from completely difference directions,[42-45] concepts were converging upon the same means to excite multiphoton effects at significant levels. From a classical basis a Finnish group developed a model based upon the modulation of the phase of a nuclear state,[42-44] and from scattering theory a Soviet group[45] developed a quantum theory for an unrealistic type of magnetic material. Our own concepts are best characterized as a nuclear analog to the dressed state theory for atoms of Cohen-Tannoudji.[46]

Though completely obscured by different terminology and by the gulf between classical and quantum physics, ours and the Finnish representation are the same. Because of its clarity, the Finnish description is superior since we are able to justify it quantum mechanically.

For cases in which there is no static magnetic field[41] or in which the modulation is parallel to the static field[5] the effect of the time varying component, $H_o f(t)$ upon a nuclear eigenstate of the nucleus, $\Psi^o_{\alpha,m}$ can be written,

$$\Psi_{\alpha,m} = e^{-i\phi_\alpha(t)}\Psi^{(o)}_{\alpha,m} \quad , \tag{1}$$

where $\phi_\alpha(t)$ is the modulation angle of the phrase,

$$\phi_\alpha(t) = m\omega_\alpha \int_o^t f(t')dt' \quad , \tag{2}$$

and the Larmor frequency, ω_α is,

$$\omega_{\alpha m} = \mu_N g_\alpha H_o/\hbar \quad , \tag{3}$$

where μ_N is the nuclear magneton, g_α is the gyromagnetic ratio for the α-th excited or ground state of the nucleus, and m is the magnetic quantum number of the eigenstates.

In principle, the difference in phase modulation between the ground state, g, and an excited state, e, may be observed during an absorption transition because the Fourier components of $\phi_e(t)-\phi_g(t)$ will be manifest as sidebands. However, since the transition will have a width, Γ associated with the time-dependent decay of the states, unless,

$$\hbar\omega_\alpha \geq \Gamma \quad , \tag{4}$$

the sidebands will be buried in the natural wings of the probing transition.

The Finnish group had derived the factor exp. $[i(\phi_e-\phi_g)]$ and obtained the sidebands but only for this case of linear media. With this restriction coherent effects will inevitably be small. Our conceptual key to orders-of-magnitude of enhancement of phase modulation effects has been reported[11-13] to lie in the use of smaller powers to manipulate the greater magnetic fields arising from the natural correlations of individual spins in ferromagnetic materials. However, the modulation $\partial M/\partial t$ of the magnetization, M of a ferromagnetic material is rarely parallel to either the applied field H_o or even to M, itself.[47] For such cases of nuclei in ferromagnetic media the modulation angle of Eq. (2) takes a more complex form;[11] and one which causes a mixing of the eigenstates, $\Psi^{(o)}_{\alpha m}$. Nevertheless, the principal parameter is still a Larmor frequency, Ω_α which for magnetic environments becomes,

$$\Omega_\alpha = \mu_N g_\alpha M/\hbar \quad , \tag{5}$$

a value much larger than that found in Eq. (3) for nonmagnetic samples.

The approximate phase angle we developed[11] becomes,

$$\phi_\alpha(t) = \beta_\alpha(\omega_o\Omega_g/\omega^2) \sin \phi_\alpha \, (\sin \omega t - \omega t \cos \omega t) \quad , \qquad (6)$$

where ω is the frequency of reversal of the applied fields, ω_o is the magnon Larmor frequency, ϕ_α is the average angle between the perturbation and the easy axis of the material,

$$\beta_g \text{ is 1 and } \beta_e = -3|\omega_e/\omega_g| \quad .$$

In ferromagnetic foils our expression for the nuclear phase of Eq. (6) replaces the Finnish expression of Eq. (2) for linear materials. Sidebands are computed the same way from the Fourier coefficients of exp $[i(\phi_e - \phi_g)]$; while the dressed states come from the Fourier expansions of the individual exp $[i\ \phi_e]$ and exp $[i\ \phi_g]$.

Essentially, the results are the same with the ferromagnetic media scaling as $(\omega_o\Omega_g/\omega^2)$ while the nonmagnetic materials would be limited to the relative size of ω_g. Since $\Omega_g >> \omega_g$ by the ratio of magnetization to free space field strength, and $\omega_o >> \omega_g$ because of the ratios of nuclear mass to electron mass the effects will be much larger in magnetic media whenever applied frequencies ω are comparable to the static splittings of the nuclear transitions of the order of ω_e and ω_g.

Motivated by the convergence of theories arising in such disparate circumstances we focused considerable attention upon the disturbing impression in the Mössbauer community that an acoustic origin had been "proven" for all sidebands by the benchmark experiment of Chien and Walker[39] in 1976. In that experiment an absorbing foil composed of ferromagnetic and nonmagnetic layers was used to study transport of the causative agent from the ferromagnetic layer into the nonmagnetic region where the sidebands were produced upon Mössbauer transitions of embedded ^{57}Fe nuclei. Very clear evidence showed that the cause did arise in the ferromagnetic Ni layers, producing sidebands in the nonmagnetic stainless steel layers. The most ready explanation at that time was a transport of phonons from one layer to the next with a high acoustic Q. Those experiments were repeated[48] but with extensions which contradict the classic interpretation of Chien and Walker.[39] In fact, our

reexamination shows the original experiment to have been so flawed that any conclusions drawn from it must now be considered unproven.

As described in the Annual Summary Report for 1987 found in Appendix II, sideband effects scale with the square of the number of ferromagnetic sources. Interpreted as indicating the addition of fields from each source that are squared to communicate power into the sideband intensities, such scaling is completely inconsistent with an acoustic origin. In experiments such as these, acoustic phonons are the bosons associated with vector fields driven by tensor forces, not vector forces. Without invoking stimulated emission, we can conceive of no way in which tensor sources which are physically separated can produce coherent vector fields in a space between them, even if they are temporally synchronized. The stimulated emission of phonons to produce coherent additions of the displacements arising from the different sources would imply the existence of a threshold of power, above which two modulation indices of m would give an effect of $4m^2$ and below which only $2m^2$. No such threshold was suggested by the data which was obtained over an adequate range of powers. Sidebands scaled consistently with $4m^2$. Two years later, this work has finally been accepted for publication in Phys. Rev. B.

In the past year an even more critical experiment was conducted which further reduced the role possible for magnetostrictively generated phonons in sideband production. It represents a major milestone of achievement and is reviewed in the following section. However, before reviewing those results the completion of the instrumentation for Frequency Modulation Spectroscopy (FMS) should be mentioned. The successes of this device are detailed in the most recent Annual Report reproduced in Appendix II. There it is reported that our prototype Nuclear Raman Spectrometer was refined into more mature technology resulting in the Frequency Modulation Spectrometer (FMS) for gamma-ray energies.

The original prototype device had required a tedious level of manual interaction, and this was replaced with a fully automated and computerized control system during the most recent reporting period. In its present form the FMS device has an instrumental resolution of 100 Hz and a continuous tuning range 10^9 Hz with a stability of 0.1 Hz/sec with no mechanical move-

ments required anywhere. These characteristics are comparable to having a Mössbauer spectrometer with a means of shifting the gamma-ray source with a resolution of 10 nm/sec and a range of 100 mm/sec with a stability of 0.01 nm/sec/sec. Demonstration spectra were acquired with ^{57}Fe showing isomer shifts and thermal shifts. Because we were using a modulation type of spectroscopy, the static features could be suppressed and these different effects were obtained with great clarity.

Details of the mature FMS device are contained in the resulting article contained in the Annual Report in Appendix II. It shows data demonstrating the remarkable detail which can be readily obtained with this device. The crowning achievement is found in Fig. 6 of that reprint where 24 sidebands are seen in a tuning interval of 50 MHz, all having values of relative intensity confirmed in the companion plot of a computer synthesis of that region of the spectrum.

It appears that the FMS device developed in our laboratory has now proven its utility as a tool in Mössbauer spectroscopy. Besides standing ready to serve in our own search for nearly resonant intermediate states for a multiphoton process, it has the versatility to support many other kinds of experiments as well.

MAJOR MILESTONE ACCOMPLISHMENTS OF 1988

In 1988, we had completed a major milestone experiment in which we showed that effects attributed to multiphoton processes contained less than 1% contamination by any contributions from spurious acoustic phenomenon. From the beginning of this project we have maintained that the key to the excitation of significant levels of multiphoton phenomena lies in the use of small oscillating fields to manipulate the greater ferromagnetic and ferroelectric fields in which the nuclei are immersed. Unfortunately, such materials are almost always magnetostrictive or piezoelectric and the concern has lingered that all coherent phenomena would be overwhelmed and degraded by periodic Doppler shifts produced by vibrations excited by such mechanical efforts.

Reported in 1988 was the coherent excitation of magnetic sidebands on the unsplit 14.4 keV transition of ^{57}Fe in a stainless steel foil for which the

attenuation length for the transport of acoustic phonons was much smaller than the mean free path expected for the transport of spin waves. Stainless steel is a ferromagnetic substance having its Curie temperature well below room temperature. While the exchange energy between the constituent iron atoms is large enough to coordinate spins and produce spontaneous magnetization, at room temperatures thermal agitation destroys any long range ordering which may be imposed. When interfaced to a material in which the magnetization is oscillating, spin waves should be launched into the stainless at amplitudes comparable to saturation.

As a basis for comparison, sidebands were excited on the unsplit absorption transition of ^{57}Fe nuclei at 14.4 keV in a stainless steel foil by sinusoidal vibrations injected with a piezoelectric source as shown in Fig. 1a. In the usual longitudinal geometry for a transmission experiment a convenient level of input power produced a reference level of sideband development in which the 4th order contained 20% of the intensity remaining in the parent line. In the transverse geometry the effect of phonons transported in the foil about 1 cm around a bend of 90 degrees could not be detected, even with a tenfold increase in power above the reference level.

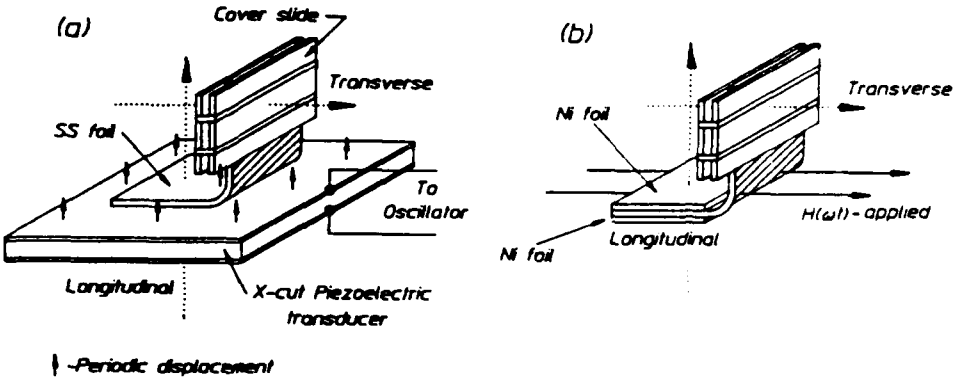

Figure 1: Schematic representation of the mounting of the enriched stainless steel foil 2.5 μm thick used in these transmission experiments. The vectors of the propagation of the gammas from sources to detectors are shown by the dotted arrows for the longitudinal and transverse arrangements shown.
a) (left) Sidebands driven by phonons from an X-cut quartz crystal.
b) (right) Sidebands driven by the oscillating magnetization of the two Ni foils immersed in the applied H field shown.

Replacing the piezoelectric source with a pair of 2.5 μm foils of ferromagnetic Ni sinusoidally magnetized as shown in Fig. 1b, gave the opportunity to launch what we believe are large amplitude spin waves into the paramagnetic stainless foil. Boundary effects known as flux refractions favor the transfer of ferromagnetic magnetization of the Ni across the interface where it can serve as a source term for local alignment of the magnons in the stainless foil. The longitudinal geometry was used to set the same reference level of sideband development at the source. In the transverse geometry at this same level of input power, the first order sidebands were found to have 20% of the intensity of the parent line, a level 10 times the threshold for detection and hence, 100 times any component contributed by acoustic phonons.

One of the pleasures of the conduct of research in an academic environment is that most of the work is incorporated in Ph.D. dissertations. Once in a while this produces a comprehensive review of outstanding merit. While three Ph.D.'s were earned by students pursuing this contract research, the most recent, detailing the milestone achievement was one of these rare products of exceptional merit. For this reason it is reproduced in Appendix III in order to report all aspects of the milestone work. Of course, all usual copyrights are retained by the author, Dr. T. W. Sinor. There is a twofold significance to the results described there.

1) In stainless steel spin waves can be transported more efficiently than phonons, thus providing a means for studying the direct modulation of nuclear states in an environment free from acoustic noise.

2) Even with transport the intensities of magnetic sidebands are greatly enhanced by ferromagnetic sources meaning that relatively large interaction energies can be developed at the nuclear level with modest applied powers.

The means have now been demonstrated to excite large scale modulations of the phases of nuclear state, even in nonmagnetic samples.

LONG RANGE IMPLICATIONS OF THE RESULTS

Of course, the most immediate implication of the successful conclusion of this contract work is that the techniques of nuclear spectroscopy could be considerably advanced through the subsequent development of a broadly tunable γ-ray source. The computational results referenced above suggest tuning ranges exceeding 10^{-6} or 10^{-5} of the transition energy without introducing any broadening of the natural linewidths of the transitions. This is at least 1,000 to 10,000 times in excess of the best that can be achieved with the conventional Doppler tuning of Mössbauer lines. Moreover, it can be done without any of the mechanical motion and vibration that currently set the instrumental width in the limited techniques currently available for γ-ray spectroscopy. It is interesting to reflect that if the result of these tasks in the direction of coherent pumping were to indicate that sum frequency generation would be practicable up to the addition of 76 μ FIR, the resulting shift of the γ-ray line would be equivalent to that obtained by conventional Doppler techniques at a relative velocity between source and absorber of Mach 1. To match by Doppler shifting the tuning achieved with the Raman conversion of laser photons at 2.3 μ wavelength would require the nuclei to attain relative velocities in excess of their escape velocity from earth. These values are to be compared to the normal tuning range of millimeters/sec encountered in conventional single photon Mössbauer spectroscopy.

The great extension in the tuning range over which stable, high resolution nuclear spectroscopy could be accomplished through implementation of these multiphoton methods would enhance basic research in many areas. For example, studies of photon spectra in solids and phonon scattering experiments would benefit from non-mechancial techniques of tuning. Of course, it is in the nuclear field that the greatest long-range implications lie. In principle, extremely high levels of energy storage exceeding one terajoule/liter can be achieved in concentrations of known isomeric states bred in a conventional reactor through neutron capture. Unfortunately, the controlled release of such energy through stimulated emission is unlikely to ever be achieved through single photon processes because of level broadening traceable to long

range interactions between nuclei. However, if a single system exists that has an intermediate state which would be resonant with any available high power laser, the Raman conversion of those laser photons at that resonant energy could lead to a stimulated cross section for the γ-ray step as large as the Breit-Wigner value. This in turn would be sufficient to induce the release of the stored energy at a power level comparable to that of a directed nuclear burst. There would be many incredible aspects to such a phenomenon whose enumeration is futile unless the necessary intermediate state can be found, at least for one exemplary transition.

Conventional Mössbauer spectroscopy has sufficient resolution but insufficient tuning range to support a search for nearly resonant intermediate states of a nucleus. X-ray spectroscopy with dispersion provided by grazing angle crystals presents the reverse dilemma, an adequate tuning range but inadequate resolution. Our technique of Frequency Modulation Spectroscopy that has developed from the preceding research would provide the optimum combination of resolution and tuning range to support the search for nearly degenerate nuclear levels which may prove essential in ultimately realizing a scalable γ-ray laser.

REFERENCES

1. C. B. Collins, S. Olariu, M. Petrascu, and I. Popescu, Phys. Rev. Lett. 42, 1397 (1979).

2. C. B. Collins, S. Olariu, M. Petrascu, and I. Popescu, Phys. Rev. C20, 1942 (1979).

3. C. B. Collins, in Proceedings of the International Conference on Lasers '80, edited by C. B. Collins (STS Press, McLean, VA, 1981) pp. 524-531.

4. S. Olariu, I. Popescu, and C. B. Collins, Phys. Rev. C23, 50 (1981).

5. S. Olariu, I. Popescu, and C. B. Collins, Phys. Rev. C23, 1007 (1981).

6. C. B. Collins, in Proceedings of the International Conference on Lasers '81, edited by C. B. Collins (STS Press, McLean, VA, 1982) pp. 291-295.

7. C. B. Collins, in Laser Techniques for Extreme Ultraviolet Spectroscopy, edited by T. J. McIlrath (AIP Conference Proceeding Series No. 90).

8. C. B. Collins, F. W. Lee, D. M. Shemwell, B. D. DePaola, S. Olariu, and I. I. Popescu, J. Appl. Phys. 53, 4645 (1982).

9. C. B. Collins, F. Davanloo, and T. S. Bowen, Rev. Sci. Instrum. 57, 863-865 (1986).

10. F. Davanloo, T. S. Bowen, and C. B. Collins, Rev. Sci. Instrum. 58, 2103 (1987).

11. C. B. Collins and B. D. Depaola, Optics Letters, 10, 25-27 (1985).

12. B. D. Depaola, S. S. Wagal, and C. B. Collins, J. Opt. Soc. Am. B. 1, 812-817 (1984).

13. B. D. Depaola, S. S. Wagal, and C. B. Collins, J. Opt. Soc. Am. B. 2, 541-543 (1985).

14. C. B. Collins, in Advances in Laser Science - I, edited by W. C. Swalley and M. Lapp (AIP Conference Proceedings No. 146, Dallas, 1985) p. 18.

15. F. Davanloo, T. S. Bowen, and C. B. Collins, in Advances in Laser Science - I, edited by W. C. Swalley and M. Lapp (AIP Conference Proceedings No. 146, Dallas, 1985) p. 60.

16. S. S. Wagal and C. B. Collins, in Advances in Laser Science - I, edited by W. C. Swalley and M. Lapp (AIP Conference Proceedings No. 146, Dallas, 1985) p. 62.

17. C. B. Collins, in Advances in Laser Science - I, edited by W. C. Swalley and M. Lapp (AIP Conference Proceedings No. 146, Dallas, 1985) p. 40.

18. C. B. Collins, in Advances in Laser Science - II, edited by M. Lapp, W. C. Swalley, and G. A. Kenney-Wallace (AIP Conference Proceedings, New York, 1987), pp. 45-54.

19. F. Davanaloo, T. S. Bowen, and C. B. Collins, in Advances in Laser Science - II, edited by M. Lapp, W. C. Swalley, and G. A. Kenney-Wallace (AIP Conference Proceedings, New York, 1987), pp. 63-65.

20. S. S. Wagal, P. Reittinger, E. Juengerman, C. D. Eberhard, and C. B. Collins, in Advances in Laser Science - II, edited by M. Lapp, W. C. Swalley, and G. A. Kenney-Wallace (AIP Conference Proceedings, New York, 1987), pp. 66-68.

21. T. S. Bowen, J. J. Coogan, F. Davanloo, and C. B. Collins, in Advances in Laser Science - II, edited by M. Lapp, W. C. Swalley, and G. A. Kenney-Wallace (AIP Conference Proceedings, New York, 1987), pp. 98-100.

22. P. Reittinger, S. S. Wagal, and C. B. Collins, in Advances in Laser Science - II, edited by M. Lapp, W. C. Swalley, and G. A. Kenney-Wallace (AIP Conference Proceedings, New York, 1987), pp. 101-103.

23. P. W. Reittinger, T. W. Sinor, S. S. Wagal, and C. B. Collins, Rev. Sci. Instrum. 59, 362 (1988).

24. N. D. Heiman, L. Pfeiffer, and J. C. Walker, Phys. Rev. Lett. 21, 93 (1968).

25. G. J. Perlow, Phys. Rev. 172, 319 (1968).

26. G. Asti. G. Albanese, and C. Bucci, Nuovo Cimento 57B, 531 (1968).

27. G. Asti. G. Albanese, and C. Bucci, Phys. Rev. 184, 260 (1969).

28. H. D. Heiman, J. C. Walker, and L. Pfeiffer, Phys. Rev. 184, 281 (1969).

29. L. Pfeiffer, J. Apply. Phys. 42, 1725 (1971).

30. V. Mitin, Dokl, Akad. Nauk SSSR 194, 59 (1970) [Sov. Phys. Dokl. 15, 827 (1971)].

31. N. D. Heiman, J. C. Walker, and L. Pfeiffer, in Mössbauer Effect Methodology, edited by I. Gruverman (Plenum, New York, 1971), Vol. VI.

32. L. Pfeiffer, in Mössbauer Effect Methodology, edited by I. Gruverman (Plenum, New York, 1971), Vol. VII.

33. L. Pfeiffer, N. D. Hieman, and J. C. Walker, Phys. Rev. B6, 74 (1972).

34. N. Heiman, R. K. Hester, and S. P. Weeks, Phys. Rev. B8, 3145 (1973).

35. C. L. Chien and J. C. Walker, Proceedings of the International Conference on Mössbauer Spectroscopy, Cracow, 1975 (unpublished), p. 47.

36. M. Kopcewicz, A. Kotlicki, and M. Szefer, see Ref. 24, p. 49.

37. M. Kopcewicz, see Ref. 24, p. 53.

38. Y. V. Baldokhin, V. A. Povitskii, V. A. Makarov, and E. F. Makarov, see Ref. 24, p. 55.

39. C. L. Chien and J. C. Walker, Phys. Rev. B13, 1876, (1976).

40. References 33 and 39 seem to have been particularly important in establishing the magnetostrictive model.

41. P. J. West and E. Matthias, Z. Physik A288, 369 (1978).

42. P. Helisto, E. Ikonen, T. Katila, and K. Riski, Phys. Rev. Lett. 49, 1209 (1982).

43. E. Ikonen, P. Helisto, T. Katila, and K. Riski, Phys. Rev. A 32, 2298 (1985).

44. E. Ikonen, P. Helisto, J. Hietaniemi, and T. Katila, Phys. Rev. Lett. 60, 643 (1988).

45. E. K. Sadykov and A. I. Skvortsov, Sov. Phys. Solid State 29, 1818 (1987).

46. C. Cohen-Tannoudji, Frontiers in Laser Spectroscopy, Session XXVII (North Holland, Amsterdam, 1975).

47. T. H. O'Dell, Ferromagnetodynamics (J. Wiley, N.Y., 1981) Ch. 2.

48. C. B. Collins, P. W. Reittinger, and T. W. Sinor, "Comments on 'Mössbauer Sidebands from a Single Parent Line'," Phys. Rev. B. 39, 1-5 (1989).

PUBLICATIONS OF THIS CONTRACT RESEARCH

"Tunability of Radiation Generated at Wavelengths below 1A by Anti-Stokes Scattering from Nuclear Levels," by B. D. DePaola and C. B. Collins, J. Opt. Soc. Am. B1, 812-817 (1984).

"Observation of Coherent Multiphoton Processes in Nuclear States," by C. B. Collins and B. D. DePaola, Opt. Lett. 10, 25-27 (1985).

"Nuclear Raman Spectroscopy," by B. D. DePaola, S. S. Wagal, and C. B. Collins, J. Opt. Soc. Am. B2, 541-543 (1985).

"Nuclear Raman Spectroscopy with No Mechanical Tuning," by B. D. DePaola, S. S. Wagal, and C. B. Collins, J. Opt. Soc. Am. B (pending).

"Flash X-Ray Source of Intense Nanosecond Pulses Produced at High Repetition Rates," by C. B. Collins, F. Davanloo, and T. S. Bowen, Rev. Sci. Instrum. 57, 863-865 (1986).

"Evidence for the Observation of Nuclear States Dressed by Radiofrequency Photons," by C. B. Collins and S. S. Wagal, Phys. Rev. Lett. (pending).

"Observation of Mössbauer Transitions between Dressed Nuclear States," by C. B. Collins, S. S. Wagal, C. D. Eberhard, E. M. Juengerman, G. Merk, W. R. Osborn, and P. W. Reittinger (pending).

"Comment on Mössbauer Sidebands from a Single Parent Line," by C. B. Collins, S. S. Wagal, P. W. Reittinger and E. M. Juengerman, Phys. Rev. B (pending).

"Nuclear Multiphoton Processes Excited by Modulated Field Gradients," by C. B. Collins, M. Barb, S. Olariu, and I. Popescu, J. Opt. Soc. Am. B (pending).

"Scaling to High Average Powers of a Flash X-Ray Source Producing Nanosecond Pulses," by F. Davanloo, T. S. Bowen, and C. B. Collins, Rev. Sci. Instrum. 58, 2103-2109 (1987).

"A Frequency Modulation Spectrometer for Mössbauer Studies," by P. W. Reittinger, T. W. Sinor, S. S. Wagal, and C. B. Collins, Rev. Sci. Instrum. 59, 362-367 (1987).

"Comment on 'Mössbauer Sidebands from a Single Parent Line'," by C. B. Collins, P. W. Reittinger, and T. W. Sinor, Phys. Rev. B 39, 1-5 1989).

"Large Scale Effects of the Magnetic Phase Modulation of Recoiless Gamma Transitions," T. W. Sinor, P. W. Reittinger, and C. B. Collins, Phys. Rev. Lett. (pending)

"Observation of Magnetic Phase Modulation Effects in Nonmagnetostrictive Permalloy," T. W. Sinor, P. W. Reittinger, and C. B. Collins, Phys. Rev. B (pending)

APPENDIX I

ANNUAL SUMMARY REPORT

1 JANUARY 1986 - 31 DECEMBER 1986

ANNUAL SUMMARY REPORT

for the period

1 January 1986 through 31 December 1986

for

Office of Naval Research
Contract N00014-81-K-0653
Task No. NR 395-072

THE DEMONSTRATION OF THE FEASIBILITY OF THE TUNING AND STIMULATION OF NUCLEAR RADIATION

Short Title: GAMMA-RAY LASER

Principal Investigator: Carl B. Collins

The University of Texas at Dallas
Center for Quantum Electronics
P.O. Box 830688, Richardson, TX 75083-0688

TABLE OF CONTENTS

PROJECT DESCRIPTION

This project concerns the demonstration of the feasibility of the tuning and stimulation of nuclear radiation. It represents a critical line of investigation in our overall program concerned with the feasibility of a gamma-ray laser.

Theory, supported by our experiments conducted under this contract, has indicated that anti-Stokes Raman upconversion of intense but conventional laser radiation produced by scattering from isomeric states of nuclear excitation could lead to significant sources of tunable gamma radiation characterized by the natural Mossbauer widths of the lines. Further computations have suggested that this type of coherent, as well as a type of incoherent, optical pumping could even lead to appreciable levels of inversion of the populations of nuclear levels, thus supporting the growth of stimulated gamma-ray intensities. Whether or not these processes can reach threshold depends upon the resolution of basic issues that have not been previously addressed in an interdisciplinary region between quantum electronics and nuclear physics. It is the purpose of this contract work to study these issues experimentally in order to guide the development of the technology and methods needed to exploit the enormous potential of this effect.

SCIENTIFIC PROBLEM

The viability of the concept for the tuning of gamma radiation by adding the variable energy of an optical photon produced by a tunable laser depends upon the existence in the

nucleus of a particular arrangement of excited states. A suitable energy difference would would make it possible to dress the nuclear states with the laser photons. Transitions between the dressed states would then occur at the sum and difference frequencies characteristic of the nuclear transition, plus or minus the energies of integral numbers of laser photons.

Whether the necessary arrangements of nuclear states do exist is the central issue being addressed in this contracted work. Surprisingly, such information is currently unknown because such potentially useful states would lie in the "blind spots" of the conventional techniques of nuclear spectroscopy. Normal Mossbauer spectroscopy provides enormous resolution, but a tuning range that is inadequate by orders of magnitude to support any possible study of transitions to the intermediate states of a multiphoton process. Conversely, crystal spectrometers provide broad tuning ranges, but levels of resolution that miss by two orders of magnitude the threshold that would be necessary to separate the transitions to the initial and intermediate states. As a consequence, the ideal arrangement of nuclear energy levels needed for the Raman upconversion process could be a common occurrence that has gone unnoticed because of the inadequacies of conventional nuclear spectroscopy.

The critical problem in this research has two facets: 1) the development of an appropriate spectroscopic technique, and 2) the search for a suitable medium for a large-scale effect. The dressing of the nuclear states not only affects their energies, but also changes their transition properties. Forbidden nuclear transitions should become allowed so that the metastability of

isomeric states would be "switched off" as the states were dressed. This would greatly enhance the prospects for stimulating the gamma-ray transition, in addition to rendering it tunable. It is the development of the investigative instrumentation and the verification of these predicted effects that comprise the scientific problem addressed by this contract research.

TECHNICAL APPROACH

For the resolution of the central issue of the existence of potentially useful intermediate states in a multiphoton upconversion of optical photons to gamma-ray energies, it was first intended to demonstrate sum frequency generation in one case in which nonresonant intermediate states were known to exist. This was the case in which both initial and intermediate states were magnetic sublevels of the same nucleonic state and in which the transitions were mediated by the M1, magnetic dipole operator. Experimental data reproduced in the literature suggested that such a process had already been unknowingly demonstrated for the generation of radiofrequency sidebands to Mossbauer transitions at the sum and difference frequencies. This suggested the development of a new instrument, a Frequency Modulation Spectrometer for gamma-ray energies, designed to support the needed studies of nuclear structure with the precision of Mossbauer spectroscopy applied over a tuning range of energies lying considerably beyond the state-of-the-art at the time our work began. Pursuant to this goal, we are conducting a conventional single-photon Mossbauer experiment in the presence of an intense radiofrequency

field with measurement and parameterization of the conversion efficiency into the sum frequency line to determine the practical limits on the ultimate linewidths and tuning ranges that can be achieved. This technique will then be used in a "bootstrap" approach to support a search for accidentally resonant intermediate states. By replacing the radiofrequency excitation with tunable higher frequencies, it is expected that the tuning range of Mossbauer spectroscopy can be extended by further orders-of-magnitude.

PROGRESS DURING THIS REPORTING PERIOD

Instrumentation of FMS

The sum and difference frequency sidebands produced on intrinsic Mossbauer transitions has made possible very effective new instrumentation for high resolution spectroscopy at gamma-ray energies. A prototype version of this Frequency Modulation Spectrometer (FMS) was first described[1] by our laboratory in 1985, and subsequent refinements were made during the current reporting period under this contract and under a related SDI contract directed by ONR. This device monitors changes in the intensity of transmitted single-frequency gamma photons as a function of frequency of the long wavelength photons of the alternating magnetic field in which the absorbing nuclei are immersed.

During the past year our prototype "Nuclear Raman Spectrometer" was refined into more mature technology resulting in the Frequency Modulation Spectrometer (FMS) for gamma-ray energies (Figure 1). The original prototype device had required

a tedious level of manual interaction, and this was replaced with a fully-automated and computerized control system during the current reporting period. At its heart is a multi-channel scalar (MCS) and IEEE-488 GPIB interface with an Apple II+ computer. The MCS was designed to have a 100% duty cycle. The GPIB enables the spectrometer to sweep continuously through the frequencies of an rf magnetic field produced with a Wavetek frequency synthesizer. The Mossbauer drive allows the frequency of the gamma photon to be biased by a constant Doppler shift, if desired. In its present form, the FMS device has an instrumental resolution of 100Hz and a continuous tuning range of 10^9Hz with a stability of 0.1Hz/sec with no mechanical movements required anywhere. These characteristics are comparable to a Mossbauer spectrometer with a means of shifting the gamma-ray source, having a resolution of 10nm/sec and a range of 100mm/sec with a stability of 0.01nm/sec/sec. Demonstration spectra were acquired with ^{57}Fe showing isomer shifts and thermal shifts. Because we were using a modulation type of spectroscopy, the static features could be suppressed, and these different effects were obtained with unprecedented clarity.

In operation, FMS of ^{57}Fe provides a direct measurement of rf sideband positions and intensities from which one can extrapolate information about the transitions between Zeeman split energy levels (parent transitions), labeled 1 through 6 in Figure 2. Radiofrequency sidebands have been labeled as a parent transition preceded by a number of +'s or -'s, the number of which corresponds to the number of rf field energy quanta

(order of the sideband) added to or subtracted from the parent transition. The symmetrically opposed parent transitions 1 and 6 are separated by 123.7 MHz in pure iron. Applying a 61.85 MHz alternating magnetic field to the Fe foil produces (+1) and (-6) sidebands which overlap in the symmetric center, or transition center, of the hyperfine structure of the ^{57}Fe. The energies of the gamma ray emitted by the source and the transition center of the absorber differ by the isomer shift, Δ (Figure 3a). In FMS the Stokes sideband from parent transition 6, (-6) would be detected at a frequency of (61.85-Δ) MHz while the anti-Stokes sideband from parent transition 1, (+1) would be detected at a frequency of (61.85+Δ) MHz (Figure 3b and c). Therefore, FMS should produce a spectrum with two peaks around 60 MHz, separated by 2Δ.

If we apply a small Doppler shift, ∂, to the source, we should obtain an FMS spectrum with two peaks around 60 MHz, separated by $2(\Delta + \partial)$ (Figure 4). Classically, the frequencies at which sidebands appear, fs, is simply

$$fs(MHz) = [\ v - (P_j + iso)] * (11.6/ord), \qquad (1)$$

where P_j is the position of the j'th parent transition (mm/sec), v is the velocity of the source (mm/sec), iso is the isomer shift (mm/sec), and ord is the order of the sideband of interest. The source used was in a Pd lattice (iso = -0.185).

Radiofrequency sideband positions are also apparently affected by the intensity of the rf magnetic field (Figure 5). It is yet to be determined whether sideband position is a function of intensity as well as frequency of the rf magnetic

field, or whether the temperature shift of the parent transitions is being detected, or both. Since we start with a negative isomer shift, raising the temperature of the absorber should reduce the energy difference between the source transition and the transition center of the absorber. Therefore, increasing the rf field intensity should raise the temperature of the absorber and in turn decrease the isomer shift.

It seems clear that, in addition to providing information about sideband intensity and position, FMS could also prove to be a means for direct and accurate measurement of isomer and temperature shifts, spectroscopic quantities that are difficult to measure with Mossbauer spectroscopy as usually practiced because of the difficulty in obtaining such small velocities with such precise control. For the purposes of the gamma-ray laser program, it is the combination of narrow instrumental width and large tuning range that offers the greatest attractions.

To dress an isomeric state requires a certain arrangement of nuclear levels that would make them undetectable to conventional techniques of nuclear spectroscopy. Our method of FMS is the only means found to date that can be used to search for this combination among the 29 best candidates for a gamma-ray laser. The successes of the new FMS apparatus for nuclear spectroscopy indicate that a much higher resolution, by perhaps several more orders of magnitude, can be achieved through a reasonable upgrade of the apparatus. If the range of tunability does extend to the ferromagnetic spin resonance (FSR) frequency, then it will be possible to construct a swept frequency device

capable of continuously tuning over a range of 10^{11} linewidths, an enormous improvement in the state-of-the-art of nuclear spectroscopy.

Theory of FMS

Most laboratory sources of gamma radiation emit at levels of intensity corresponding to single photon conditions. Mossbauer experiments are rarely conducted at such great intensities that the detection of two photons would be probable in the transit time spent between source and absorber. Under those conditions, the perception of gamma rays as streams of particles is instinctive. Nevertheless, as elements of electromagnetic radiation they must also be considered as carrier waves of high frequency. As the name implies, the Frequency Modulation Spectrometer derives its operation from the modulation of the gamma-ray carrier and represents a translation into the nuclear domain of one of the powerful techniques of laser spectroscopy at the atomic level. As described above, the device itself works better than the theory describing it, and during the current reporting period emphasis developed upon refining and validating the dressed state theory describing the origin of the carrier modulation. Reviewed in the following material will be five different approaches to a comprehensive theoretical description. Not published elsewhere, each is being reported here as each approach is useful in defining acceptable levels of approximation.

CONTEXT OF THEORETICAL EFFORTS

In our version of FMS, the spectrum of the gamma photons emitted by the source is modulated by its passage through a thin, ferromagnetic foil immersed in a radiofrequency magnetic field[2]. Most work has been done upon ^{57}Fe with the radiofrequency magnetic field being applied in the plane of the foil. Although the interaction energy of the nuclear magnetic moment directly with the applied magnetic field is insufficient to cause a significant perturbation of the system, the applied magnetic field is sufficient to cause the direction of the magnetization within the material, $\vec{M}(t)$, to precess in a complicated manner and this interaction of the nuclear moment with $\vec{M}$ is of significant magnitude.

Ferromagnetism is a cooperative magnetic behavior resulting from the exchange interaction between the electrons. In ferromagnetic materials, the principal effect of the exchange interaction is to cause parallel ordering or alignment of the atomic spins in a common direction, so that there is a large spontaneous magnetization even in the absence of an applied field. Maximum ordering is obtained at $0^{\circ}K$ where the randomizing effect of thermal agitation disappears. At the Curie temperature T_C the magnetic ordering is destroyed by thermal agitation, and the spontaneous magnetization disappears. Between these two extremes a sample of ferromagnetic material is usually divided into small volumes called domains, which may vary in size, shape and direction of magnetization. Within each domain, the magnetization is uniform and has the maximum or saturation value, M_s,

characteristic of the material and the temperature. *Within a ferromagnetic material, the magnetization vector $\vec{M}(t)$ may vary in direction but not in magnitude, even when traversing a domain wall.* Therefore, changes of the magnetization are precessions and must be described by equations which reflect this.

The magnetic field at the site of the ^{57}Fe nucleus is the sum of several large terms which may be positive or negative. In an ^{57}Fe foil the magnetic field at the nucleus has been determined to be about 330×10^3 Oersteds in the direction opposite to the local direction of the bulk magnetization, $\vec{M}(t)$. The electrons respond to the changes of $\vec{M}(t)$ quite rapidly since the magnetic moments of the electrons are strongly coupled to $\vec{M}(t)$ (the cooperative effect). Thus, in response to any applied fields, the magnetic field at the site of the nucleus also precesses in a manner which reflects the precession of the bulk magnetization. For this reason, the motion of the magnetization $\vec{M}(t)$ must be determined as a function of time as a part of any comprehensive description of the ultimate effects of applied H fields upon nuclear states.

The equation of motion of the magnetization vector $\vec{M}(t)$ is determined by the Landau-Lifshitz equation:

$$-(1/|\gamma|)\, d\vec{M}(t)/dt = (\vec{M} \times \vec{F}) - \lambda\, [\vec{F} - (\vec{M}\cdot\vec{F})\, \vec{M}/M_s^2] \quad . \quad (2)$$

The gyromagnetic ratio of the electron is given by $-|\gamma|$, and λ is an experimental parameter obtained from ferromagnetic resonance studies, $\lambda/M_s \sim 10^{-3}$. The magnetic field $\vec{F}$ in equation (2) is the vector sum of four contributions: 1) the magnetic field required to simulate the magnetic anisotropy effects inherent to

the crystal structure of the material, 2) the "magnetostatic" fields due to the finite size of the sample, 3) the exchange field, which represents a potential energy term leading to the ordering of neighboring magnetic dipole moments on a microscopic scale, and 4) the applied magnetic field. The solutions[3,4] to equation (2) depend strongly on the anisotropy of the material and on the geometry of the sample and are usually of an exceedingly complicated nature. Approximations were developed to varying degrees as part of each of the different approaches to the nuclear sideband problem.

During the past year our efforts to develop a model of the modulation of the gamma spectrum have focused upon the following five approaches, to be summarized in this report below:

1. The refinement of the theoretical approach initiated by C. B. Collins and B. D. DePaola[2] in Optics Letters 10, 25 (1985) culminating in the results presented at the 1986 IQEC meeting. We have referred to this as the multiphoton processes in nuclear states.

2. A literature search and study of the applicability of the "dressed atom" approach of C. Cohen-Tannoudji.

3. The development of a coherent switch model of the magnetization $\vec{M}(t)$ by integrating the Landau-Lifshitz equation. This model was specific for a thin ferromagnetic foil. The solution for $\vec{M}(t)$ is in agreement with results presented elsewhere.[4]

4. The development of a domain wall passage model. This research does not appear to have been fruitful, although it may

still be of use.

5. In collaboration with Professor P. Berman of New York University, the development of solutions to the time dependent Schroedinger equation utilizing information about the magnetization derived from approach 3. The resulting method appears to be the best approach. The computer code is in the process of development and is being verified first for the static case.

1) Multiphoton Processes in Nuclear States of ^{57}Fe in a Ferromagnetic Foil Immersed in a Radiofrequency Magnetic Field

The time-dependent Schroedinger equation of the ^{57}Fe nucleus embedded in a ferromagnetic foil immersed in an rf magnetic field is

$$i\hbar(d\Psi/dt) = H_A\Psi - \{\vec{H}_{app}(t)\cdot\vec{\mu} + \vec{M}(t)\cdot\vec{\mu} + \vec{H}_d(t)\cdot\vec{\mu} + \vec{H}_{dn}(t)\cdot\vec{\mu}\}\Psi \quad (3)$$

where

Ψ = the eigenstate of the system,

H_A = the atomic Hamiltonian associated with quantum number(s) α.

$\vec{\mu}$ = the magnetic moment of the nucleus,

$\vec{H}_{app}$ = the applied radiofrequency magnetic field (a few gauss) with frequency ω_1,

$\vec{M}$ = the magnetization of the material (kilogauss),

$\vec{H}_d$ = the demagnetizing field due to the surface poles developed when $\vec{M}$ rotates out of the plane of the foil (kilogauss),

$\vec{H}_{dn}$ = the demagnetizing field due to the poles developed when the nuclear magnetic moment $\vec{\mu}$ rotates out of the plane of the foil (very small).

The expression in the brackets represents the interaction of the nuclear magnetic moment, $\vec{\mu}$, with the vector sum of all of the magnetic fields to which the nucleus is subjected. The interaction of the magnetic field with the electrons is included in the behavior of $\vec{M}$ and therefore does not require another term. This notation and approach are essentially the same as outlined by Collins and DePaola[2].

Since the terms $\vec{H}_{app}(t)\cdot\vec{\mu}$ and $\vec{H}_{dn}(t)\cdot\vec{\mu}$ are small when compared to the other terms in the Hamiltonian, they are neglected.

The simplified time dependent Schroedinger equation becomes

$$i\hbar\,(\partial\Psi/dt) = H_A\,\Psi - \{\vec{M}(t)\cdot\vec{\mu} + \vec{H}_d(t)\cdot\vec{\mu}\}\,\Psi \qquad (4)$$

in the fixed laboratory coordinates.

A new coordinate system is defined in the laboratory, such that the magnetization $\vec{M}$ in the plane of the foil corresponds to the z axis, that is, as $\vec{M}$ responds to the applied magnetic field (by rotating in the plane of the foil), the foil is rotated about an axis perpendicular to the foil in such a way that $\vec{M}$ always lies along the z axis of the laboratory coordinates. Doppler shifts are introduced because the foil is moving, but since the absorption spectrum is observed along an axis perpendicular to the foil, only the second order transverse Doppler shift occurs, which should be negligible. This coordinate system is denoted as primed in the following material. In it $\vec{M}$ has constant magnitude and direction (z axis) as shown in Figure 6. Equation (4) may be rewritten

$$i\hbar\,(\partial\Psi'/\partial t) = H_A\,\Psi' - \{\vec{M}\cdot\vec{\mu} + \vec{H}_d(t)\cdot\vec{\mu}\}\,\Psi' \quad . \qquad (5)$$

The magnetic moment of the nucleus, $\vec{\mu}$, is related to its angular

momentum through the equality

$$\vec{\mu} = (g_x \mu_N / \hbar)\, \vec{J} \qquad (6)$$

where x denotes either the ground (g) or excited (e) state of the nucleus. The symbol μ_N stands for the nuclear magneton,

$$\mu_N = (e\hbar/2M) = 0.505 \times 10^{-26} \text{ amp-m}^2 \quad , \qquad (7)$$

in the MKS system of units.

The Hamiltonian of a particularly useful basis set of eigenstates and energies is obtained from,

$$H_B = H_A - \vec{M}\cdot\vec{\mu} = H_A - \hbar\omega_x J_z \quad , \qquad (8)$$

where $\hbar\omega_x$ corresponds to the total splitting of the x level by the magnetization $\vec{M}$,

$$\hbar\omega_x = g_x \mu_N M_s \quad . \qquad (9)$$

In the basis set, the time dependent Schroedinger equation of the x state,

$$i\hbar\,(\partial\Psi_o'/\partial t) = H_A\,\Psi_o' - \hbar\omega_x\, J_z\,\Psi_o' \quad , \qquad (10)$$

has solutions of the form,

$$\Psi_o'(\alpha_x, J', m') = |\alpha_x, J', m'\rangle \exp[-i(E_{\alpha_x}/\hbar - m'\omega_x)t]. \qquad (11)$$

The quantum number(s) α_x describe the nuclear state x with energy E_{α_x}, in the absence of any magnetization field in the material or any applied field. The angular momentum state of the nucleus in the primed coordinate system is described by J' and m'. These basis states of the system might be described as the "non-interacting basis" states.

The interacting state Ψ' can be derived from the basis state Ψ_o' by means of a rotation through an angle ϕ_x about an axis parallel to $\vec{H}_d(t)$. This rotation operator is Hermitian and unitary and of the form

$$R = \exp[i\phi_x \hat{n}\cdot\vec{J}] = \exp(i\phi_x J_d) \quad . \tag{12}$$

where $\hat{n}$ is a unit vector parallel to the axis of rotation. The interacting state is given by

$$\Psi'_x = e^{(i\phi_x J_d)}\, \Psi'_o(\alpha_x, J', m') \quad . \tag{13}$$

Combining equations (5) and (13), the time dependence of the angle ϕ_x is given by the equation

$$(\partial\phi_x/\partial t) = g_x \mu_N\, H_d(t)/\hbar \quad . \tag{14}$$

If $H_d(t)$ is known, the angle $\phi_x(t)$ can be computed numerically and therefore may be considered a known function.

The transition amplitude is determined by

$$i\hbar(da_{eg}/dt) = i\hbar\, \dot{a}_{eg} = \tag{15}$$

$$\int\left[e^{(+i\phi_e J_d)}\, \Psi'_o(\alpha_e, J', m')\right]^*\, V_\gamma e^{-i\omega_\gamma t}\left[e^{(+i\phi_g J_d)}\, \Psi'_o(\alpha_g, J', m')\right] d\tau \; .$$

Since R is Hermitian and unitary, this equation may be rewritten

$$i\hbar\, \dot{a}_{eg} = \tag{16}$$

$$e^{-i\omega_\gamma t}\int\left[e^{[+i(\phi_e - \phi_g)J_d]}\, \Psi'_o(\alpha_e, J', m')\right]^*\, W_\gamma\, \Psi'_o(\alpha_g, J', m')\, d\tau$$

where

$$W_\gamma = e^{(-i\phi_g J_d)}\; V_\gamma\; e^{(+i\phi_g J_d)} \approx V_\gamma \quad . \tag{17}$$

The operator J_d is not diagonal in the primed coordinate system since $\hat{n}$ is perpendicular to $\vec{M}$ (the z axis). It is necessary to use the finite rotation matrix[10] to transform into a system in which the z axis is parallel to $\hat{n}$. After operating with J_d, then the finite rotation matrix is again used to return to the primed laboratory system.

The time derivative of the total transition amplitude in terms of $\langle\Psi'_e(m_e)|W_\gamma|\Psi'_g(m_g)\rangle$ is given by

$$i\hbar\,\dot{a}_{eg} = (1/2)^2 \left[c_B \exp[i\Omega_1 t] \langle -3/2|W_\gamma|-1/2\rangle R_1(t) \right.$$
$$+ c_B \exp[i\Omega_2 t] \langle -1/2|W_\gamma|-1/2\rangle R_2(t)$$
$$+ c_B \exp[i\Omega_3 t] \langle +1/2|W_\gamma|-1/2\rangle R_2(t) \qquad (18)$$
$$+ c_A \exp[i\Omega_4 t] \langle -1/2|W_\gamma|+1/2\rangle R_2(t)$$
$$+ c_A \exp[i\Omega_5 t] \langle +1/2|W_\gamma|+1/2\rangle R_2(t)$$
$$\left. + c_A \exp[i\Omega_6 t] \langle +3/2|W_\gamma|+1/2\rangle R_1(t) \right]$$

where Ω_i is the detuning of the i^{th} transition as shown in Figure 7. That is,

$$\Omega_i = (\Delta E_i/\hbar) - \omega_\gamma \quad . \qquad (19)$$

where ΔE_i is the energy of the i^{th} transition. The concentrations of the ground state levels are c_A and c_B for $m = -1/2$ and $m = +1/2$ respectively. If the angle ϕ is defined by

$$\phi \equiv \phi_e - \phi_g \quad , \qquad (20)$$

the factors $R_1(t)$ and $R_2(t)$ which appear in the transition amplitudes are defined as follows:

$$R_1(t) = (1 + \sqrt{3})\, e^{-i(3\phi/2)} + (3 - \sqrt{3})\, e^{i\phi/2} \qquad (21a)$$

$$R_2(t) = (3 + \sqrt{3})\, e^{-i(3\phi/2)} + (1 - \sqrt{3})\, e^{i\phi/2} \quad . \qquad (21b)$$

The transitions probabilities are calculated from

$$\lim_{t\to\infty} \frac{1}{t}(-i\hbar\, a_{eg})(+i\hbar\, a^*_{eg}). \qquad (22)$$

When $R_1(t)$ and $R_2(t)$ are expanded in Fourier series,

$$R_j(t) = \sum_{-\infty}^{+\infty} n\, (R_j)_n\, e^{(-in\omega_1 t)} \quad . \qquad (23)$$

there are two components to the transition probability which survive the time averaging procedure. The first is the "normal" contribution given by

$$W_{eg} = \frac{2\pi}{\hbar^2}\left(\frac{1}{2}\right)^4 \sum_{-\infty}^{+\infty} n \left\{ (R_1)_n (R_1)_n^* \left[c_B^2 |\langle -3/2 | W_\gamma | -1/2 \rangle|^2 \, \delta(\Omega_1 - n\omega_1) \right.\right.$$
$$\left. + c_A^2 |\langle +3/2 | W_\gamma | +1/2 \rangle|^2 \, \delta(\Omega_6 - n\omega_1) \right]$$
$$+ (R_2)_n (R_2)_n^* \left[c_B^2 |\langle -1/2 | W_\gamma | -1/2 \rangle|^2 \, \delta(\Omega_2 - n\omega_1) \right.$$
$$+ c_B^2 |\langle +1/2 | W_\gamma | -1/2 \rangle|^2 \, \delta(\Omega_3 - n\omega_1)$$
$$+ c_A^2 |\langle -1/2 | W_\gamma | +1/2 \rangle|^2 \, \delta(\Omega_4 - n\omega_1)$$
$$\left. \left. + c_A^2 |\langle +1/2 | W_\gamma | +1/2 \rangle|^2 \, \delta(\Omega_5 - n\omega_1) \right] \right\} \quad . (24)$$

After $R_1(t)$ and $R_2(t)$ have been expanded in terms of their Fourier components, a typical term in the product of the two expansions shown in (22) is of the form

$$c_i(ME)_i \; c_j^*(ME)_j^* \sum_{m,n} (R_i)_n (R_j)_m^* \left[\frac{e^{i(\Omega_i - n\omega)t} - 1}{\Omega_i - n\omega} \right] \left[\frac{e^{-i(\Omega_j - m\omega)t} - 1}{\Omega_j - m\omega} \right], (25)$$

where $(ME)_i$ is the matrix element of the i^{th} transition. When the time average is taken as shown in expression (22), this term is zero for all $m \neq n$. The summation over m collapses to one term which does not vanish when the time average is taken. When $m = n$, the equality[10] in the limit $t \to \infty$,

$$\lim_{t \to \infty} \frac{\sin^2 \alpha t}{\pi t \alpha^2} = \delta(\alpha) \qquad (26)$$

may be used, which introduces the delta functions of frequency.

In reality, the delta functions of frequency must be replaced by Lorentzian distributions centered at the position of the delta function. The width of the Lorentzian corresponds to the lifetime of the excited state. The parent lines of the transition, that is, the spectrum in the absence of the rf magne-

tic field, correspond to the n = 0 amplitudes,

$$W_{eg}^{0} = \frac{2\pi}{\hbar^2}\left(\frac{1}{2}\right)^4 \Big\{ |(R_1)_0|^2 \Big[c_B^2 |\langle -3/2|W_\gamma|-1/2\rangle|^2 \, \delta(\Omega_1) + c_A^2 |\langle +3/2|W_\gamma|+1/2\rangle|^2 \, \delta(\Omega_6) \Big] + |(R_2)_0|^2 \Big[c_B^2 |\langle -1/2|W_\gamma|-1/2\rangle|^2 \, \delta(\Omega_2) + c_B^2 |\langle +1/2|W_\gamma|-1/2\rangle|^2 \, \delta(\Omega_3) + c_A^2 |\langle -1/2|W_\gamma|+1/2\rangle|^2 \, \delta(\Omega_4) + c_A^2 |\langle +1/2|W_\gamma|+1/2\rangle|^2 \, \delta(\Omega_5) \Big] \Big\} \quad (27)$$

The delta functions of frequency indicate that the parent lines will be observed at their normal frequencies,

$$\Omega_i = \text{detuning} = 0 \quad \text{or} \quad \Delta E_i/\hbar = \omega_\gamma . \quad (28)$$

The intensity of the first order sideband may be found in the same manner by taking either n = $\pm$1. For n = +1, the frequencies of the first order sidebands in the absorption spectrum is found by taking

$$\Omega_i - \omega_1 = (\Delta E_i/\hbar) - \omega_\gamma - \omega_1 = 0 \quad , \quad (29)$$

or

$$[(\Delta E_i/\hbar) - \omega_1] = \omega_\gamma \quad . \quad (30)$$

Thus, n = +1 corresponds to the first negative sideband and conversely n = -1 corresponds to the first positive sideband. The absolute magnitudes of $(R_i)_n$ govern the amplitudes of the sidebands. For this reason, it is vitally important to have an adequate model of the behavior the magnetization $\vec{M}$ as a function of time.

The second component is a quantum enhancement which adds on to the "normal" curve whenever the condition,

$$\Omega_i - \Omega_j = p\omega_1 \quad (31)$$

(p is any positive or negative integer) is satisfied, that is,

whenever two transition energies differ by an integral number of photons in the rf field. The intensity given by the "normal" curve is increased by the amount

$$\frac{2\pi}{\hbar^2}\left(\frac{1}{2}\right)^4 \sum_n \left[K(R_i)_n (R_j)^*_{n-p} + K^*(R_i)^*_n (R_j)_{n-p}\right] \delta(\Omega_i - n\omega_1), \quad (32)$$

where,

$$K = c_i\, c_j^*\, (ME)_i\, (ME)_j^* \quad . \quad (33)$$

As can be seen from expression (33), the enhancements to the absorption spectrum fall on the same frequencies as the usual sidebands, including the parent, and occur only when equation (31) is satisfied. If i = 1 or 6, then $R_i \rightarrow R_1$. For all other values of the index i, then $R_i \rightarrow R_2$. The index j follows the same rules. For this reason, the quantum enhancement must be determined on a case-by-case basis.

At this point the model is a direct extension of the one originally proposed by DePaola and Collins[2] which was limited in validity to the vicinity of a moving domain wall where the angle of rotation of the magnetization $\vec{M}(t)$ in the plane of the foil is large. The extension realized in this section as characterized in equations (24) and (32) is more generally valid. Unfortunately both models share the dependence on the rather simplified description of the magnetization which strictly confines $\vec{M}(t)$ to a plane. Not surprisingly, neither one adequately describes the enhancement of the sideband intensity observed in ^{57}Fe near the applied frequency of 45 MHz. This enhancement of the sideband amplitude was thought to be due to the mixing of the Zeeman levels of the ground state by the

applied magnetic field. For a better understanding of the mixing effects of an intense field, the 'dressed state theory' of C. Cohen-Tannoudji[5,6,7] and S. Haroche[8,9] was studied, because it had been refined and experimentally verified to a very high degree of accuracy for analogous cases in atomic physics.

Also, before proceeding further, it is necessary to develop a better model for the behavior of the magnetization $\vec{M}(t)$ in the presence of an applied rf field. To accomplish this, it is necessary to integrate the Landau-Lifshitz equation (equation 2) as discussed in sections 3 and 4.

2) "Dressed State" Theory

At first, the work of C. Cohen-Tannoudji[5,6,7] and S. Haroche[8,9] on atoms immersed in a strong electromagnetic field of a single frequency (optical or radio frequency) is very attractive conceptually. It departs considerably from the usual approach in which the interaction of the atom with the applied electromagnetic field is considered as a perturbation to be handled using standard perturbation theory. The need for an alternative arises from the fact that perturbation theory is not appropriate when the strength of the interaction is large due to the presence of very strong fields. In the dressed state theory, the quantized system consists of both the atom and the electromagnetic field. The electromagnetic field is handled as an integral part of the system, not a perturbation, and it is considered quantum mechanically, not classically.

Exact solutions of the Schroedinger equation are possible for some systems of atomic levels and polarizations. It is particularly interesting that the stationary states of the total Hamiltonian of the dressed atom no longer correspond to a fixed, well defined number of photons in the field. The number states $|n\rangle$ for the pure radiation field are no longer eigenstates of the total Hamiltonian. In addition, it can be shown that stationary solutions exist which are a superposition of one or more of the atomic states calculated in the absence of fields and one or more of the number states of the field. This theory was used to predict the sideband intensities of well-known atomic transitions which were modulated by the application of optical or rf fields states. The "dressed state" theory predicted sideband intensi-

ties as functions of the interaction energy (or field strength) very successfully. It is reasonable to inquire whether the same formalism could be adapted to the analogous case in nuclei.

Maxwell's equations, which govern the interaction and propagation of electromagnetic fields, are linear and may be solved in terms of a Fourier decomposition. Magnetization is a more complex phenomenon, and it is expected that the solutions to the Landau-Lifshitz equation for obtaining $\vec{M}(t)$ will contain a number of harmonics of the frequency of the applied magnetic field. Each of these harmonics may then be considered to be an independent "dressing field" in the sense that Cohen-Tannoudji uses the term. If done in this way, the results should be summed over the harmonics which appear.

With this approach in mind, an extensive study was made of the publications concerning the dressed atom. The most comprehensive treatise was written by S. Haroche and published in *Annales de Physique* in 1971 in French. The results of the literature search were condensed into an internal document titled "The Interaction of the Dressed Atom", copies of which are available upon request.

As before, a better understanding of the magnetization is required before this approach could be adapted. The next sections describe models of how the direction of the magnetization varies as a function of time.

3) <u>Development of the Coherent Switch Model of the Magnetization M(t) by Integrating the Landau-Lifshitz Equation</u>

As mentioned in the previous sections, both the extension of the early DePaola and Collins model and the dressed state theory

of Cohen-Tannoudji are critically dependent upon the use of a good approximation to the complex precession of the magnetization vector, $\vec{M}(t)$ under the influence of an applied rf field. This section describes an investigation of the solutions to the Landau- Lifshitz equation appropriate to a thin ferromagnetic foil immersed in an rf magnetic field.

There are many solutions in the literature to the Landau-Lifshitz equation that describe static domain walls for various configurations of the magnetization[3,11,12]. The domain walls in an ^{57}Fe foil of the type generally used in experiments are expected to be "180^{o}" walls, that is walls in which the magnetization rotates through 180^{o} as the wall is traversed from one side to the other. There are fewer models of moving domain walls[3,12] than static walls. The precursive model of the demagnetizing field developed by DePaola and Collins to describe the magnetic fields interacting with the nuclear moment was taken from Chen[12]. He had described the concept of the magnetization rotating under the influence of the demagnetizing field which in turn is due to the magnetic poles developed when the applied magnetic field causes the magnetization to precess out of its initial plane. Thus a moving domain wall is formed. This was the model presented by DePaola and Collins[2]. On the other hand, there is no reason to expect the foil to be a single domain with only one moving domain wall.

Experimentally, it has been found that the static spectrum of the ^{57}Fe foil with no applied rf field demonstrates the usual six hyperfine lines. The relative intensities of the parent

lines in this case suggest that the magnetic field causing the splitting (the magnetization) is confined to the plane perpendicular to the transmission axis, that is, the plane of the foil. When an rf magnetic field is applied, the spectrum becomes much more complex. There are the usual six hyperfine lines (parent lines) plus six systems of sidebands, that is, absorption lines displaced from the parent line by frequencies corresponding to an integer (positive or negative) number times the applied frequency. The relative intensities of the parent lines continue to suggest that the magnetic field remains confined to the plane perpendicular to the transmission axis.

Thus, the internal magnetic structure of the ^{57}Fe foil is considered to be a composite of many platelet-shaped microcrystals with the platelets aligned more or less parallel with the plane of the foil. Demagnetizing fields develop in the volume of the platelets due to the appearance of magnetic poles on the surfaces. Each microcrystal or platelet is considered to be a single domain. In the coherent switching model, the magnetization at all points within the domain rotates in phase, that is, together as a unit without the usual domain wall (where the rotation is concentrated within the wall). Since the platelets are not identical, there are discontinuities in the magnetization between the platelets, but inside the platelet, the magnetization is uniform. A second mode which includes the effects of the traversal of a domain wall through a nuclear site will be considered in section 4.

Equation (2) describes the motion of $\vec{M}(t)$ under the influence of the four magnetic fields (real and fictitious) mentioned

previously. The problem was solved using a combination of spherical polar coordinates and the Cartesian components of $\vec{M}(t)$ as shown in Figure 8. The Cartesian components of $\vec{M}(t)$ are

$$M_x = M_s \sin\theta \cos\phi \tag{34a}$$

$$M_y = M_s \sin\theta \sin\phi \tag{34b}$$

$$M_z = M_s \cos\theta \quad . \tag{34c}$$

These four fields, the applied field, the magnetostatic field, the anisotropy field, and the exchange field, will each be considered as part of this model.

A) The Applied Field. Consistent with the initial conditions, the applied magnetic field is written as

$$\vec{H}_{app}(t) = - H_1 \sin \omega_1 t \quad . \tag{35}$$

B) The Magnetostatic Field. The Magnetostatic field is given by

$$\vec{B} = \mu_o(\vec{H} + \vec{M}) \tag{36}$$

where $\vec{H}$ is given by the solution to the Poisson equation

$$\vec{H} = (1/4\pi) \text{ grad } \int_V \frac{\text{div } \vec{M}}{r_{ij}} dV + \int_S \frac{\vec{M}\cdot\hat{n}}{r_{ij}} dS \tag{37}$$

The distance between the point of integration, i surrounded by the volume of integration dV, and the point j, at which $\vec{H}$ is to be evaluated, is denoted by r_{ij}. The first integral is taken throughout the entire volume of the magnetized body. The second integral is taken over the entire surface of the magnetized body, $\hat{n}$ being the inwardly directed unit vector normal to the surface.

The magnetostatic field is best considered on a case-by-case basis. The divergence of a vector field is a measure of the "sources" or "sinks" of that vector within a volume. Since the

magnitude of $\vec{M}$ remains the same throughout the body, div $\vec{M}$ = 0. The first integral resembles the volume integration of a charge density equal to div $\vec{M}$ which vanishes throughout the volume.

The second integral resembles an integration of a surface charge density over a surface. The non-zero magnetic pole density arises from the discontinuity of $\vec{M}$ at the surface and the continuity boundary requirement on $\vec{B}$ and $\vec{H}$. If $\vec{M}$ has a component normal to the surface, the magnetic pole density is $(\vec{M}\cdot\hat{n})$ on the surface. As the applied magnetic field increases parallel to the x axis, the magnetization begins to precess about the applied field, and $\vec{M}(t)$ moves out of the xy plane. A magnetic pole density develops on the faces of the foil parallel to the xy plane (boundary conditions on $\vec{B}$ and $\vec{H}$). These magnetic poles, whose density is given by $- M_z(t)$, are the source of the magnetostatic field, which then simplifies to the single term,

$$\vec{H}_d(t) = - \vec{M}_\perp = - M_s \cos\theta\, \hat{e}_z . \qquad (38)$$

C) The Anisotropy Field. The ferromagnetic foil is assumed to consist of many small microcrystals shaped like platelets or "microfoils". This is consistent with the amplitude distribution of the observed six-line spectrum in the absence of any applied field which is a rather sensitive function of the average orientation of the magnetization of each domain in the sample.

A magnetic material is said to have an easy or preferred direction of magnetization if a minimum energy state is obtained by having the magnetization lying along this easy direction. In a uniaxial material (the approximation used for each platelet of the ferromagnetic foil), any deviation of $\vec{M}(t)$ away from the easy

direction by an angle $(\phi-\phi_o)$ results in an increase in the energy density which may be accurately represented[3] by the expression $K_u \sin^2(\phi-\phi_o)$. The anisotropy constant K_u has units of energy/volume.

The effect of anisotropy is often represented[3] by an equivalent (but fictitious) magnetic field which lies along the easy direction of the crystal. The exchange field and the anisotropy field are derived in the same way: the expression for the interaction energy is derived from basic principles and then a fictitious magnetic field is deduced which yields the same functional expression for the energy, based on the relation,

$$E_{int} = -(1/2)\ \mu_o \vec{M}\cdot\vec{H}. \qquad (39)$$

A unit vector in the direction of the easy axis, as shown in Figure 8, is designated $\hat{e}_{x'}$. Thus the anisotropy field is given by

$$\vec{H}_a = Q\ (\vec{M}\cdot\hat{e}_{x'})\ \hat{e}_{x'} = Q\ M_s \sin\theta \cos(\phi-\phi_o)\ \hat{e}_{x'}, \qquad (40)$$

where

$$\hat{e}_{x'} = \cos\phi_o\ \hat{e}_x + \sin\phi_o\ \hat{e}_y \qquad (41)$$

and where $Q = (2K_u/\mu_o M_s^2)$ is a parameter of the crystal. The angle ϕ_o is the acute angle between the easy axis and the x axis of the foil coordinates.

D) The Exchange Field. Since the magnetization at every point within the domain precesses in the same manner, that is, in the domain where

$$\vec{M}(\vec{r},t) = \vec{M}(\vec{r}+d\vec{r},t)\ , \qquad (42)$$

the exchange field is zero. However, in materials where $\vec{M}$ depends on the position of the point of observation, such as in a

Landau-Lifshitz wall, the "exchange field" (fictitious) is given by

$$\vec{H}(\vec{r},t) = (2A/\mu_o M_s^2)\ \nabla^2\ \vec{M}(\vec{r},t) \qquad (43)$$

where A is a constant of the material.

The total magnetic field $\vec{F}$ in equation (2) is the sum of the fields given in equations (35), (38) and (40):

$$\vec{F} = \mu_o\ (\vec{H}_{app} + \vec{H}_d + \vec{H}_a) \quad . \qquad (44)$$

The equations of motion of the components of $\vec{M}(t)$ can be reduced and combined to yield equations for $d\phi/dt$ and $d\theta/dt$ in terms of the components of $\vec{F}$.

$$\begin{aligned} \sin\theta\ (d\phi/dt) = &- |\gamma| F_x\ [\ (\lambda/M_s)\sin\phi + \cos\phi\ \cos\theta\ ] \\ &+ |\gamma| F_y\ [\ (\lambda/M_s)\cos\phi - \sin\phi\ \cos\theta\ ] \\ &+ |\gamma| F_z\ \sin\theta \end{aligned} \qquad (45)$$

$$\begin{aligned} (d\theta/dt) = &- |\gamma| F_x\ [\ \sin\phi - (\lambda/M_s)\cos\phi\ \cos\theta\ ] \\ &+ |\gamma| F_y\ [\ \cos\phi + (\lambda/M_s)\sin\phi\ \cos\theta\ ] \\ &- |\gamma| F_z\ (\lambda/M_s)\ \sin\theta \end{aligned} \qquad (46)$$

The components of the total magnetic field $\vec{F}$ are given below.

$$F_x = -\mu_o H_1\ \sin\omega_1 t + \mu_o M_s Q\ \sin\theta\ \cos(\phi-\phi_o)\ \cos\phi_o \qquad (47a)$$

$$F_y = +\mu_o M_s Q\ \sin\theta\ \cos(\phi-\phi_o)\ \sin\phi_o \qquad (47b)$$

$$F_z = -\mu_o M_s\ \cos\theta \qquad (47c)$$

These are first order differentials in time but very complicated functions of the angles θ and ϕ. A program was written in FORTRAN for the Hewlett-Packard Series 9000/560 Computer in which the angles θ and ϕ were built up in small steps from the initial conditions to obtain the magnetization $\vec{M}(t)$. An example solution is shown in Figure 9A.

The motion of $\vec{M}(t)$ seen in Figure 9A is quite consistent with the expectations reached by purely qualitative arguments. At t=0, the magnetization lies in the plane of the foil at $\theta_o = \pi/2$ radians along the easy axis at an initial angle ϕ_o, assumed to be 0.35 radian in this example. The initial angles θ_o and ϕ_o are solution parameters. As the magnetostatic field increases through the precession of $\vec{M}(t)$ out of the xy plane, the effect of the magnetostatic field (in the z direction) completely dominates the motion of $\vec{M}(t)$, causing it to rotate in the xy plane rapidly until it nears the easy axis. After $\sin \omega_1 t$ reaches its maximum and begins to decrease, the M_z begins to decrease as $\vec{M}(t)$ returns to the xy plane. The magnetization now lies along the easy axis but antiparallel to its initial direction. The motion of $\vec{M}(t)$ proceeds in a similar manner through the second half cycle of the applied field (although the motion is rotated about the z axis through 180^o from its initial position).

The angle $\phi(t)$ as a function of time is also shown in Figure 9A. The oscillations of $\vec{M}(t)$ about the equilibrium position between the easy direction and the direction of the applied field are clearly shown. When $\vec{M}(t)$ switches, it is carried past its equilibrium position. The second term of equation (2) behaves as a restoring force which brings $\vec{M}(t)$ more nearly parallel to the equilibrium direction. The equilibrium direction is determined by the local minimum of the sum of the interaction energies of the magnetization with the anisotropy field and with the applied field. If the applied field were very strong, in time the restoring force would bring the magnetization parallel to the applied field. Figure 9B, which is from Chikazumi's book[4], tends

to confirm this initially surprising result.

Figures 10A and 10B show the dependence of the motion of $\vec{M}(t)$ on the initial value of the angle θ for the values of θ_o equal to 91^o and 89^o, respectively. From these figures it is evident that the starting value of θ_o determines the direction of the initial rotation only. After the initial cycle, the behavior of $\vec{M}(t)$ is the same in all three cases. Since the magnetization is expected to lie in the plane of the foil (which minimizes the magnetostatic energy) only values near 90^o can be realistic. The maximum expected deviation from 90^o would be on the order of

$$\delta\theta_o \sim \text{(thickness of the foil/linear dimension of the foil)}$$
$$\sim 5 \times 10^{-6} \text{ m} / 1 \times 10^{-2} \text{ m} \sim 0.03 \text{ degree} .$$

For this reason, an initial value of $\theta_o \sim 90^o$ is considered reasonable.

Finally, parameter studies have shown that for small values of H_1 and/or certain values of ϕ_o, the direction of magnetization in the foil does not switch. This is consistent with the picture above in that the applied field never develops enough interaction energy to overcome the effective anisotropy energy barrier, K_u.

The most important output of this model is the decomposition of $\sin \phi(t)$ and $\cos \phi(t)$ in terms of harmonics of the applied field frequency. The amplitudes of the harmonics then become the input to the program for solutions to the time dependent Schroedinger equation from which sideband intensities are computed according to one or another of the approaches being discussed. The amplitudes of the harmonic decompositions of $\cos \phi(t)$ and $\sin \phi(t)$ versus the order of the harmonic are shown in

Figure 11 for a typical set of input parameters.

Since this type of numerical integration of the Landau-Lifshitz equation must be condsidered "exact" to within the limits of numerical methods, its principal shortcoming is that coherence is limited to a single domain. The possible importance of domain walls is considered next. That is, this picture requires the magnetization of the entire domain to switch without the presence of a moving domain wall.

4) The Domain Wall Passage Model[3]

In the coherent switching model, magnetization within the domain is required to rotate uniformly (equation 42). It is also possible for the direction of the magnetization to change by means of passage of a domain wall through the material.

There are several different kinds of domain walls, for example the 90° wall where the direction changes by 90°, and the 180° wall between two domains whose magnetizations are antiparallel. An example containing a 180° wall is shown in Figure 12.

The position and shape of a domain wall is determined by the minimization of all the interaction energies. In the absence of an applied magnetic field, the domain walls remain static. When a magnetic field is applied, the domain wall moves in such a way that the volume of the domain whose magnetization is parallel to the applied field increases. The static and moving domain walls will be discussed next.

A) The Static Domain Wall.

Within the domain wall, the direction of $\vec{M}$ rotates while its magnitude remains fixed at the saturation value M_s.

The fundamental equation of micromagnetics states that the torque, given by the vector product of the magnetization and the total magnetic field, must vanish at every point in a medium which is in magnetostatic equilibrium. That is,

$$(\vec{M} \times \vec{F}) = 0. \tag{48}$$

For an infinitely long sample, the $\vec{H}$ field calcaulated from equation (37) is neglible. Since the magnitude of $\vec{M}$ remains constant, the divergence vanishes. There is no normal component of $\vec{M}$ at the surface of the sample, except either on faces which are far removed in the z direction from the point of observation or at the very small area where the domain wall meets the surface. Therefore, the contribution to $\vec{F}$ from the magnetostatic field is simply $\mu_o \vec{M}$ by equation (37).

However, since $\vec{M}$ is not uniform within the wall, there is a contribution from the exchange field. The easy direction of magnetization is taken to be parallel to the z axis. The components of $\vec{F}$ are

$$F_x = -(2K_u/M_s^2)\, M_x + (2A/M_s^2)\, \nabla^2 M_x + \mu_o M_x \tag{49a}$$

$$F_z = (2A/M_s^2)\, \nabla^2 M_z + \mu_o M_z \quad . \tag{49b}$$

In this case there is assumed to be no applied magnetic field, so that $H_{app} = 0$. The equation determining the spatial dependence of $\vec{M}$ is obtained by substituting equations (49a) and (49b) into equation (48).

$$\frac{A}{M_s^2}\left(M_z \frac{d^2 M_x}{dy^2} - M_x \frac{d^2 M_z}{dy^2}\right) - \frac{K_u}{M_s^2} M_z M_x = 0 \tag{50}$$

which is an ordinary differential equation since $\vec{M}$ is a function of y only. The components of $\vec{M}$ may be written

$$M_x = M_s \sin \theta \qquad (51a)$$

$$M_z = M_s \cos \theta \quad . \qquad (51b)$$

and the solution is found to be

$$\pm \tan(\theta/2) = \exp (y/\Delta) \qquad (52)$$

where Δ is the well known wall-width parameter,

$$\Delta = (A/K_u)^{1/2} \quad . \qquad (53)$$

One should note that the angle θ is that angle θ defined in Figure 12.

The choice of sign in equation (52) indicates that the domain wall may have either a clockwise or an anticlockwise screw-sense associated with the rotation of $\vec{M}$ in the xz plane. The components of $\vec{M}$ are

$$M_x = - M_s \tanh (y/\Delta) \qquad (54a)$$

$$M_z = \pm M_s \operatorname{sech} (y/\Delta) \quad . \qquad (54b)$$

B) The Moving Domain Wall.

In 1935 Landau and Lifshitz applied their equation [equation (2)] to the case of the motion of the static domain wall structure described above. They assumed that, although the wall was moving due to the influence of the applied magnetic field, the wall structure remained almost identical to its previous static structure [equations (54a) and (54b)]. That is, they assumed a "rigid wall structure".

If the wall moves as a rigid structure, then the spatial derivatives of $\vec{M}$ are defined. If the wall moves at a constant velocity, the time derivatives are defined as well. The problem

becomes algebraic and may be solved at any convenient point, such as the center of the domain wall. At the center of the domain wall, $M_x = M_s$ and $M_z = 0$. The other assumption which follows, once a rigid wall model is adopted, is that the anisotropy field and the exchange field remain antiparallel to $\vec{M}$ in the moving wall as in the stationary wall. Then only the applied field must be considered.

The domain on the left in Figure 13A is magnetized in the same direction as the applied field and consequently grows through the motion of the wall to the right with velocity v_y. This figure only shows $\vec{M}$ in the two domains and at the center of the wall, assuming a positive screw-sense of the rotation. Here only B_z enters into equation (37):

$$(dM_y/dt) = |\gamma| M_s B_z \qquad (55a)$$

$$(dM_z/dt) = |\gamma| \lambda B_z \quad . \qquad (55b)$$

The damping constant, λ, can only be determined experimentally by ferromagnetic resonance (FMR) on single crystal, spherically-shaped samples. In general[3], the dimensionless ratio (λ/Ms) has been found to be on the order of 10^{-3} or less. Since $(\lambda/M_s) \sim 10^{-3}$, equation (55a) is the more important of the two. This equation indicates that the proposal that the wall can move forward under the influence of the applied field must involve the vector $\vec{M}$ developing a component in the direction of motion. It is not possible to assume that the wall is really rigid and maintains exactly the same form which it has when stationary. As shown in Figure 13B, $\vec{M}$ must tilt by the angle ϕ to satisfy equation (55a).

At the center of the wall, the components of $\vec{M}$ are

$$M_x = M_s \cos \phi \qquad (56a)$$

$$M_y = M_s \sin \phi \qquad (56b)$$

$$M_z = 0 \quad . \qquad (56c)$$

In the original development of the model, Landau and Lifshitz continued to assume that the contributions to $\vec{F}$ due to the exchange and anisotropy fields remain antiparallel to $\vec{M}$, as when $\phi=0$. The component M_z is assumed to have the same form as given in equation (54b). Then equation (37) is solved using only the magnetostatic field and the applied field.

$$-(dM_x/dt) = |\gamma| \sin \phi \, [B_z M_s - \lambda \mu_o M_s \cos \phi \sin \phi] \qquad (57a)$$

$$+(dM_y/dt) = |\gamma| \cos \phi \, [B_z M_s - \lambda \mu_o M_s \cos \phi \sin \phi] \qquad (57b)$$

$$+(dM_z/dt) = |\gamma| \, [\mu_o M_s^2 \cos \phi \sin \phi + \lambda B_z] \qquad (57c)$$

From this, one sees that domain wall motion may be visualized as follows: as the wall moves forward, the vector $\vec{M}$ rotates about y. Since $\vec{M}$ has constant magnitude and ϕ is constant for a constant velocity, equations (57a) and (57b) are zero. The angle ϕ is related to the applied field B_z through

$$\sin 2\phi = (2B_z/\mu_o\lambda) \quad . \qquad (58)$$

Since a rigid wall has been assumed, at the center of the wall

$$dM_z/dt = (\partial M_z/\partial y)(dy/dt) = (M_s/\Delta)\, v_y \quad , \qquad (59)$$

which when combined with (57c) leads to an expression for v_y,

$$v_y = (|\gamma|\Delta/M_s)[\lambda B_z + \mu_o M_s^2 \sin \phi \cos \phi] \quad . \qquad (60)$$

This gives the picture of a domain wall moving forward at a constant velocity v_y under the influence of a constant applied field B_z. Combining equations (58) and (60), the velocity is

given by

$$v_y = (|\gamma|\Delta M_s/\lambda)[1 + \lambda^2/M_s^2]\, B_z \quad . \tag{61}$$

In conducting materials where eddy currents complicate the calculations, it is possible to derive an expression for the domain wall velocity in terms of the product of a domain wall mobility and the applied field, that is,

$$v_y = \mu_w B_z \quad . \tag{62}$$

The domain wall mobility is given by

$$\mu_w = (\mu_o^2 \sigma M_s h)^{-1} \tag{63}$$

where σ is the conductivity and h is the thickness of the material.

From this domain wall velocity, a tilt angle ϕ could be deduced. If ϕ developed to approximately 45°, its maximum possible value, a significant amount of the magnetization field might be transmitted to an adjacent material. However, it was found that the passage of a wall at the surface transferred only on the order of 0.1 to 10.0 H_{app}, which was calculated to be at the most 20 gauss. Excitation of single non-magnetic stainless steel foils enriched with ^{57}Fe at this level failed to show sidebands. Thus it was concluded that the wall passage alone could not add significantly to the transfer of an effect from a magnetic to a non-magnetic foil at the level of magnitude seen in experiments.

In general, computer analyses of the static domain wall equations in conductors yield only solutions in which the magnetization remains parallel to the surface. A. Aharoni has made extensive analyses of domain walls in conducting materials, and his solution for a uniaxial material is shown in Figure 14.

These analyses reinforce the conclusion that the effects of moving domain walls in conductors are insufficient to transfer excitation to the non-magnetic foil. The problem of the transfer of sidebands from magnetic to non-magnetic layers lies at the focus of evolving concepts for the next year, but it must be recognized that such transfer leads to a relatively small effect, anyway. The largest effect, by an order-of-magnitude, is the development of sidebands in a single magnetic foil and this seems to be able to be described by the model synthesized from the previous approaches as described in the following section.

5) Solutions to the Time-dependent Schroedinger Equation at a Higher Level of Approximation

A more tractable approach to the solution of the time dependent Schroedinger equation discussed earlier was suggested by Professor Paul Berman of New York University. It is similar to some developed earlier but proves useful in more general cases for single foils.

In continued collaboration with Professor Berman, this approach has been programmed for the Hewlett-Packard Series 9000/560 Computer and is in the process of checkout. This approach combines the exact solution of the time dependent Schroedinger equation for the system of the ^{57}Fe nucleus in a ferromagnetic foil with perturbation theory solution of the absorption of the gamma-ray photon.

Figure 7 shows the energy levels and angular momentum assignments of the Mossbauer hyperfine transitions in ^{57}Fe. Before detailing the calculations, the matrix indices of the va-

rious states of the nucleus must be defined. To avoid the unnecessary complication of carrying both J and M_J as subscripts denoting a specific level, each magnetic sublevel of the ground state and excited state has been assigned a single index as follows:

1 is J = 1/2, M_J = +1/2 (ground state)

2 is J = 1/2, M_J = -1/2 (ground state)

3 is J = 3/2, M_J = +3/2 (excited state)

4 is J = 3/2, M_J = +1/2 (excited state)

5 is J = 3/2, M_J = -1/2 (excited state)

6 is J = 3/2, M_J = -3/2 (excited state) .

The total Hamiltonian of the ^{57}Fe nucleus in a foil immersed in an rf magnetic field is given by

$$H = H_o + V_1(t) + V_2(t) \qquad (64)$$

where H_o is the nuclear Hamiltonian with $\vec{M}(t) = 0$ and no gamma ray interaction. The matrix H_o is

$$H_o = \left[\begin{array}{cc|cccc} 0 & 0 & 0 & 0 & 0 & 0 \\ 0 & 0 & 0 & 0 & 0 & 0 \\ \hline 0 & 0 & \hbar\omega_o & 0 & 0 & 0 \\ 0 & 0 & 0 & \hbar\omega_o & 0 & 0 \\ 0 & 0 & 0 & 0 & \hbar\omega_o & 0 \\ 0 & 0 & 0 & 0 & 0 & \hbar\omega_o \end{array}\right] \qquad (65)$$

In Eq. (64), $V_1(t)$ is the potential of the interaction of the magnetization $\vec{M}(t)$ with the nucleus having magnetic moment $\vec{\mu}_n$.

$$V_1(t) = -\vec{\mu}_n \vec{M}(t) = (-g_x\mu_N/\hbar)(\vec{M}\cdot\vec{J}) \quad . \qquad (66)$$

where g_x is the gyromagnetic ratio of the nuclear state x, μ_N is the nuclear magneton, and $\vec{J}$ is the vector total angular momentum operator.

The matrix $V_1(t)$ is given by

$$V_1(t) = \frac{\hbar\mu_N}{2}\left[\begin{array}{cc|cccc} g_g M_z & g_g M_- & 0 & 0 & 0 & 0 \\ g_g M_+ & g_g M_z & 0 & 0 & 0 & 0 \\ \hline 0 & 0 & 3g_e M_z & 3g_e M_- & 0 & 0 \\ 0 & 0 & 3g_e M_+ & g_e M_z & 2g_e M_- & 0 \\ 0 & 0 & 0 & 2g_e M_+ & -g_e M_z & 3g_e M_- \\ 0 & 0 & 0 & 0 & 3g_e M_+ & -3g_e M_z \end{array}\right] \quad (67)$$

The geometry is the same as shown in Figure 8. If $\vec{M}(t)$ has no z component, the diagonal elements of $V_1(t)$ vanish. The components of $\vec{M}(t)$ in the plane of the foil are

$$M_{\pm} = M_x(t) \pm i\, M_y(t) = M_s\, e^{\pm i\phi(t)} \quad . \quad (68)$$

The time dependence of the angle $\phi(t)$ is determined from the techniques described in Sections 3 and 4.

The coupling of the gamma ray field to the nucleus is given by $V_2(t)$. The selection rules for nuclear magnetic dipole transitions (M1 transitions) are $\Delta J = 0,\ 1$ and $\Delta M_J = \pm 1, 0$. The matrix $V_2(t)$ has the form

$$V_2(t) = \left[\begin{array}{cc|cccc} 0 & 0 & K_{13} & K_{14} & K_{15} & 0 \\ 0 & 0 & 0 & K_{24} & K_{25} & K_{26} \\ \hline K_{13}^* & 0 & 0 & 0 & 0 & 0 \\ K_{14}^* & K_{24}^* & 0 & 0 & 0 & 0 \\ K_{15}^* & K_{25}^* & 0 & 0 & 0 & 0 \\ 0 & K_{26}^* & 0 & 0 & 0 & 0 \end{array}\right] \quad (69)$$

where K_{jk} is the matrix element of the gamma ray absorption operator,

$$K_{jk} = \langle j | V_\gamma \cos \omega_\gamma t | k \rangle \quad . \quad (70)$$

The time dependent Schroedinger equation,

$$i\hbar\, (d\vec{a}/dt) = H\, \vec{a} \quad , \quad (71)$$

is written for this system as

$$i\hbar\,(d\vec{a}/dt) = (H_o + V_1(t) + V_2(t))\,\vec{a} \quad . \tag{72}$$

The problem can be divided into two parts. First, the time dependent Schroedinger equation is solved exactly for the Hamiltonian, $H = H_o + V_1(t)$. Then the solutions are used to treat $V_2(t)$ as a perturbation of the system.

First, the state of the system is transformed into the interaction representation,

$$\vec{a} = e^{-(iH_o t/\hbar)}\,\vec{b} \quad . \tag{73}$$

Explicitly,

$$a_k = b_k \qquad \text{for } k = 1,2 \text{ (ground state)} \quad ,$$

$$a_k = (e^{-i\omega_o t})\,b_k \qquad \text{for } k = 3,4,5,6 \text{ (excited state)}.$$

When equation (73) is substituted into equation (72), the equation for $(d\vec{b}/dt)$ becomes

$$i\hbar\,(d\vec{b}/dt) = (V_1' + V_2')\,\vec{b} \tag{74}$$

where the V' matrix is defined by

$$V' = e^{(iH_o t/\hbar)}\,V\,e^{-(iH_o t/\hbar)} \quad . \tag{75}$$

or

$$V'_{ij} = V_{ij}\,e^{(i\omega_{ij}t)} \tag{76a}$$

$$\omega_{ij} = (E_i - E_j)/\hbar \quad . \tag{76b}$$

Since $V_1(t)$ does not have matrix elements between the ground state and the excited state, $V'_1(t) = V_1(t)$.

However, $V_2(t)$ does have matrix elements linking the ground state to the excited state. The non-zero matrix elements of V_2' are

$$(V_2')_{13} = K_{13}\,e^{-i\omega_o t} = (V_2')^*_{31} \tag{77a}$$

$$(V_2')_{14} = K_{14}\,e^{-i\omega_o t} = (V_2')^*_{41} \tag{77b}$$

$$(V_2')_{15} = K_{15}\, e^{-i\omega_o t} = (V_2')^*_{51} \qquad (77c)$$

$$(V_2')_{24} = K_{24}\, e^{-i\omega_o t} = (V_2')^*_{42} \qquad (77d)$$

$$(V_2')_{25} = K_{25}\, e^{-i\omega_o t} = (V_2')^*_{52} \qquad (77e)$$

$$(V_2')_{26} = K_{26}\, e^{-i\omega_o t} = (V_2')^*_{62} \quad . \qquad (77f)$$

The gamma ray interaction may be written as

$$V_2 = V_\gamma \cos \omega_\gamma t = (1/2)\, V_\gamma\, (e^{i\omega_\gamma t} + e^{-i\omega_\gamma t}) \quad . \qquad (78)$$

The rotating wave approximation consists of neglecting all of the terms which contain the sum of the frequencies, $\pm(\omega_\gamma + \omega_o)$, in the exponential time dependence. In this approximation, the non-zero matrix elements of V_2' become

$$(V_2')_{13} = (V_\gamma)_{13}\, e^{i\Delta t} = (V_2')^*_{31} \qquad (79a)$$

$$(V_2')_{14} = (V_\gamma)_{14}\, e^{i\Delta t} = (V_2')^*_{41} \qquad (79b)$$

$$(V_2')_{15} = (V_\gamma)_{15}\, e^{i\Delta t} = (V_2')^*_{51} \qquad (79c)$$

$$(V_2')_{24} = (V_\gamma)_{24}\, e^{i\Delta t} = (V_2')^*_{42} \qquad (79d)$$

$$(V_2')_{25} = (V_\gamma)_{25}\, e^{i\Delta t} = (V_2')^*_{52} \qquad (79e)$$

$$(V_2')_{26} = (V_\gamma)_{26}\, e^{i\Delta t} = (V_2')^*_{62} \qquad (79f)$$

where the angular frequency Δ is defined by

$$\Delta = \omega_\gamma - \omega_o \quad . \qquad (80)$$

The matrix U(t) is defined as the V'_2 matrix in the rotating wave approximation as shown in equations (79a) through (79f) above. In the rotating wave approximation, equation (73) is rewritten,

$$i\hbar\,(d\vec{b}/dt) = (V_1 + U)\,\vec{b} \quad . \tag{81}$$

Furthermore, the vector $\vec{b}$ may be written as the matrix product

$$\vec{b} = \exp[(i/\hbar)\int_0^t V_1(t')dt']\,\vec{c} \equiv T(t)\,\vec{c} \quad . \tag{82}$$

The equation of motion for the matrix $T(t)$ is

$$i\hbar\,(dT(t)/dt) = V_1\,T(t) \tag{83}$$

with the initial condition, $T(t=0) = 1$, the unit matrix.

The equation of motion of the vector $\vec{c}$ is now given by

$$i\hbar\,(d\vec{c}/dt) = U'(t)\,\vec{c} \tag{84}$$

where $U'(t)$ is defined by

$$U'(t) = T^{+}\,U(t)\,T \quad . \tag{85}$$

The matrix $U'(t)$ has the same general form as V_2' shown above in equations (79a) through (79f). The ground states and the excited states are now mixed as a result of both V_1 and V_2. The relaxation effects of the natural decay of the excited state are now added into equation (84),

$$(d\vec{c}/dt) = (-i/\hbar)\,U'(t)\,\vec{c} - (1/2)\gamma\,\vec{c} \tag{86}$$

where the matrix γ is defined

$$\gamma = \left[\begin{array}{cc:cccc} 0 & 0 & 0 & 0 & 0 & 0 \\ 0 & 0 & 0 & 0 & 0 & 0 \\ \hdashline 0 & 0 & \gamma & 0 & 0 & 0 \\ 0 & 0 & 0 & \gamma & 0 & 0 \\ 0 & 0 & 0 & 0 & \gamma & 0 \\ 0 & 0 & 0 & 0 & 0 & \gamma \end{array}\right] \quad . \tag{87}$$

The quantity γ has the dimensions $(\sec^{-1})$ and is defined as the inverse of the natural lifetime of the excited state, $\gamma = (1/\tau)$.

The net absorption of the gamma rays is proportional to $\sum_{m=3}^{6} |a_m(t)|^2$ for times $t \gg (2/\gamma)$. However,

$$\sum_{m=3}^{6} |a_m(t)|^2 = \sum_{m=3}^{6} |b_m(t)|^2 = \sum_{m=3}^{6} |c_m(t)|^2 \qquad (88)$$

since H_o and V_1 are Hermitian. The components of $\vec{c}(t)$ are given by

$$c_j(t) = (-i/\hbar) \sum_{k=1}^{2} \int_0^t U'_{jk}(t')\, e^{(-\gamma/2)(t-t')}\, c_k(t')\, dt'. \qquad (89)$$

For $t \gg (2/\gamma)$, the absorption is proportional to

$$\langle \sum_{k=3}^{6} |c_k(t)|^2 \rangle \quad ,$$

where the time average is taken over the time response of the detector. This completes the formal solution.

If the decay of the excited state into the ground state is neglected, then to the zeroth order in $V_2(t)$,

$$c_k \simeq c_k(0) \qquad k = 1,2 \qquad (90)$$

since $V_2(t)$ does not couple the ground states, 1 and 2, in the first order. Furthermore, since H_o and V_1 are Hermitian, the amplitude $c_k(t)$ for the ground states may be written

$$c_k(t) = c_k(0) = a_k(0) \quad \text{for } k = 1,2 \quad . \qquad (91)$$

The ground state splitting is small compared to the thermal energy at room temperature, so that the ground states are equally populated. Thus,

$$a_k(0) = (1/\sqrt{2}) \qquad \text{for } k = 1,2 \quad . \qquad (92)$$

The absorption spectrum then becomes the result of six computational steps.

Step 1: To determine the $V_1(t)$ matrix given by equations (67), equation (68) may be expanded to

$$M_{\pm} = M_s \, (\cos \phi(t) \pm i \sin \phi(t)) \quad . \qquad (93)$$

The output of the program written for the coherent switching

model described above includes the Fourier decomposition amplitudes A_n, B_n, A_n', and B_n', where

$$\cos \phi(t) = \sum_{n=0}^{\infty} [A_n \cos n\omega_1 t + B_n \sin n\omega_1 t] \qquad (94)$$

$$\sin \phi(t) = \sum_{n=0}^{\infty} [A_n' \cos n\omega_1 t + B_n' \sin n\omega_1 t] \quad . \qquad (95)$$

These amplitudes may be used as inputs which specify $V_1(t)$.

Step 2: Step 2 is the numerical solution of equation (83) for the matrix T(t) subject to the initial condition, T(t=0) = 1. Equation (83) is a first order differential equation for the matrix T(t). Since the elements of the matrix (dT(t)/dt) are known, the elements of T(t) are integrated numerically from the initial values specified at t=0.

Step 3: With the elements of T(t) tabulated as a function of time, the elements of U'(t) are calculated as a function of time. The matrix $U'(t) = T^+ U T$ (equation 85) is formed for a given gamma-ray frequency ω_γ.

Step 4: The integral of equation (89) is numerically computed as a function of time, the magnitude squared, and then the summation over the indices of the excited states is taken. The calculation of $\langle \sum_{k=3}^{6} |c_k(t)|^2 \rangle$ as a function of time is taken for this value of ω_γ.

Step 5: This summation is averaged over a time comparable to several natural lifetimes.

Step 6: Steps 1 through 5 are repeated for another value of ω_γ until the spectrum has been covered.

A program which performs steps 1 through 3 has been written and is in the process of checkout. Since these equations are quite complicated, a simple case was chosen which could also be verified without resorting to numerical analysis. This is the static case where $\vec{M}(t) = M_s \hat{e}_x$ or $\phi = 0^\circ$. The magnetization lies in the xy plane, so the diagonal elements of V_1 vanish.

With V_1 given, and the splittings of the ground and excited levels given by

$$g_g \mu_N M_s = - \hbar\omega_g \tag{96a}$$

$$g_e \mu_N M_s = + \hbar\omega_e \quad . \tag{96b}$$

the differential equations for the elements of T(t) are

$$i \dot{T}_{1j} = -(\omega_g/2)\, T_{2j} \tag{97a}$$

$$i \dot{T}_{2j} = -(\omega_g/2)\, T_{1j} \tag{97b}$$

$$i \dot{T}_{3j} = (\sqrt{3}/2)\omega_e\, T_{4j} \tag{97c}$$

$$i \dot{T}_{4j} = (\sqrt{3}/2)\omega_e\, T_{3j} + \omega_e\, T_{5j} \tag{97d}$$

$$i \dot{T}_{5j} = \omega_e\, T_{4j} + (\sqrt{3}/2)\omega_e\, T_{6j} \tag{97e}$$

$$i \dot{T}_{6j} = (\sqrt{3}/2)\omega_e\, T_{5j} \quad . \tag{97f}$$

The elements of the T matrix in this special case are found to be

$$T_{11} = \cos K_g x = T_{22} \tag{98a}$$

$$T_{12} = i \sin K_g x = T_{21} \tag{98b}$$

$$T_{33} = (1/4)\,[3 \cos K_e x + \cos 3K_e x] = T_{66} \tag{98c}$$

$$T_{34} = (-i/4)(\sqrt{3})\,[\sin K_e x + \sin 3K_e x] = T_{43} \tag{98d}$$

$$T_{35} = (1/4)(\sqrt{3})\,[-\cos K_e x + \cos 3K_e x] = T_{53} \tag{98e}$$

$$T_{36} = (+i/4)\,[3 \sin K_e x - \sin 3K_e x] = T_{63} \tag{98f}$$

$$T_{44} = (1/4)\,[\cos K_e x + 3 \cos 3K_e x] = T_{55} \tag{98g}$$

$$T_{45} = (i/4)\,[\sin K_e x - 3 \sin 3K_e x] = T_{54} \tag{98h}$$

$$T_{46} = (1/4)(\sqrt{3})\,[-\cos K_e x + \cos 3K_e x] = T_{64} \tag{98i}$$

$$T_{56} = (-i/4)(\sqrt{3})\,[\sin K_e x + \sin 3_e x] = T_{65} \qquad (98j)$$

where, in terms of the parameters of the computer program,

$$x = \omega_1 t \qquad (99a)$$

$$K_g x = (\omega_g/2\omega_1)(\omega_1 t) = (\omega_g/2) \qquad (99b)$$

$$K_e x = (\omega_e/2\omega_1)(\omega_1 t) = (\omega_e/2) \quad . \qquad (99c)$$

All other $T_{ij} = 0$. That T is symmetric in this case is due to the choice $M_+ = M_- = M_s$. This is not the usual property of T.

The matrices T(t) and U'(t) have been calculated and compared with the functions above. There is very good agreement. Discrepancies are oscillatory in nature and do not seem to build up in time. The worst case deviations of U'(t) are about 0.3%.

Work continues on this approach with the next step being the checkout of each computational step.

SIGNIFICANCE

To dress an isomeric state requires a certain arrangement of nuclear levels that would make them undetectable to conventional techniques of nuclear spectroscopy. Our method of FMS is the only means found to date that can be used to search for this combination among the 29 best candidates.

In order to advance the theory of FMS during the current reporting period we have generated a computer program to integrate the Landau-Lifshitz equation for the foil geometry. Also we are in the process of completing the checkout of the program described in section 5 which theoretically predicts the sideband amplitudes when the time dependence of $\vec{M}(t)$, given by the solution of the Landau-Lifshitz equation, is known. Since this program is rather general, it can also be utilized to predict the Mossbauer absorption spectrum of other nuclear species embedded in the ferromagnetic foil, for example a Sn nucleus embedded in Fe. Further modifications of the program are planned to extend its capacity so that more general motions of $\vec{M}(t)$ may be incorporated.

The successes to date of the new FMS apparatus for nuclear spectroscopy indicate that a much higher resolution, by perhaps six orders of magnitude, can be achieved through a reasonable upgrade of the apparatus. If the range of tunability does extend to the ferromagnetic spin resonance (FSR) frequency, then it will be possible to construct a swept frequency device capable of continuously tuning over a range of 10^{11} linewidths, an enormous improvement in the state-of-the-art of nuclear spectroscopy.

REFERENCES

1. B. D. DePaola, S. S. Wagal and C. B. Collins, J. Opt. Soc. Am. B 2, 541 (1985).

2. C. B. Collins and B. D. DePaola, Optics. Lett. 10, 25 (1985).

3. T. H. O'Dell, Ferromagnetodynamics, Wiley, New York (1981).

4. S. Chikazumi, Physics of Magnetism, Wiley, New York (1964).

5. C. Cohen-Tannoudji, Cargese Lectures in Physics, Vol. 2, ed. by M. Levy, Gordon and Breach (1968).

6. C. Cohen-Tannoudji and S. Haroche, J. Physique, 30, 125 (1969).

7. C. Cohen-Tannoudji, Frontiers in Laser Spectroscopy, Session XXVII, North Holland Publishing Co. (1975).

8. S. Haroche, Annales de Physique, 6, 189, (1971).

9. S. Haroche, Annales de Physique, 6, 327 (1971).

10. L. D. Landau and E. M. Lifshitz, Quantum Mechanics, Pergamon Press, New York (1976).

11. A. Aharoni, J. Appl. Phys., 46, 1783 (1975).

12. C. Chen, Magnetism and Metallurgy of Soft Magnetic Materials, North Holland Publishing Co. (1977).

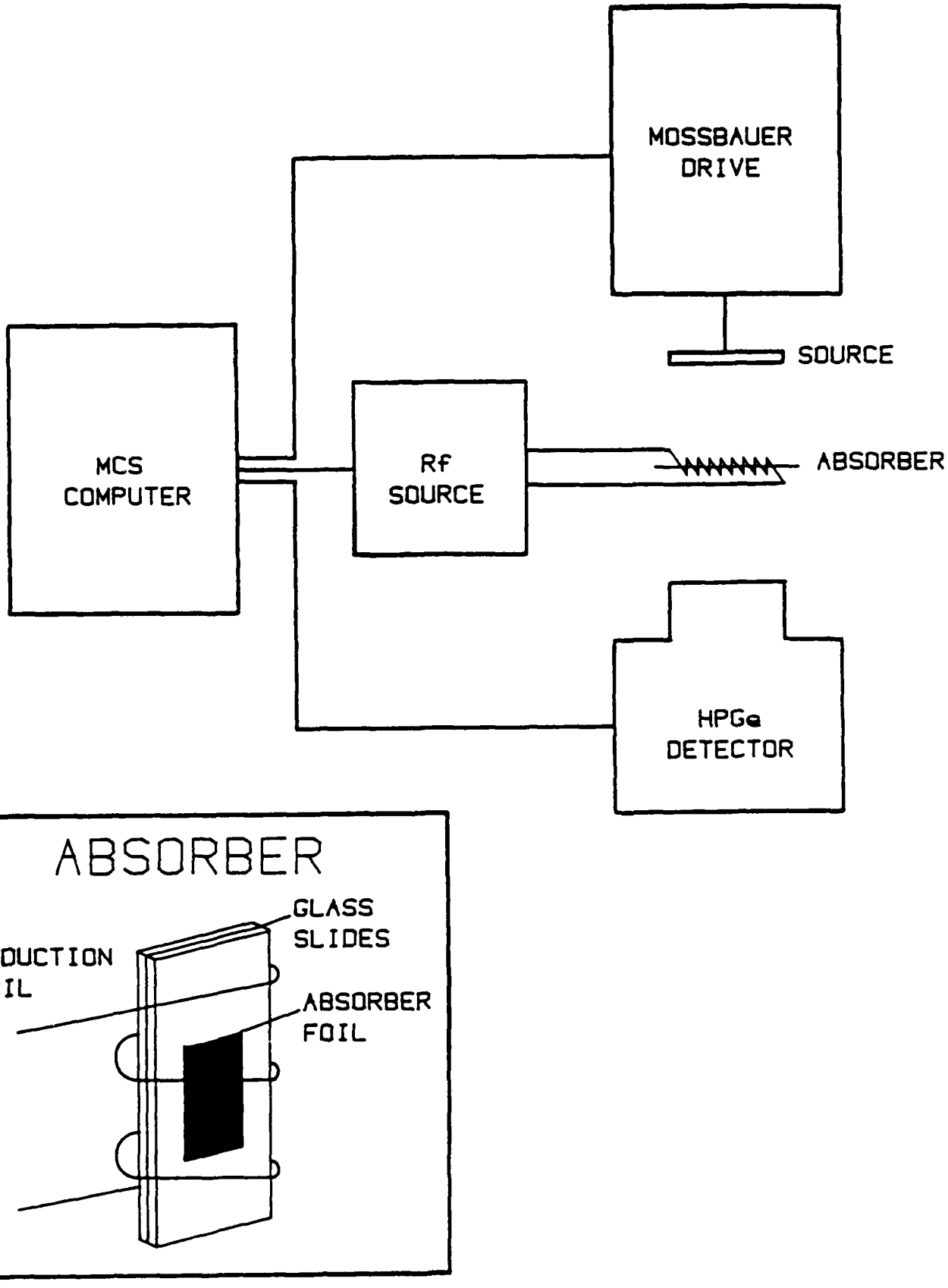

Figure 1. The heart of the Frequency Modulated Spectrometer (FMS) is a real time computer interface with a linear motor, an Rf signal generator, and a γ-ray detector. The γ-ray absorber, mounted in thin cover glass slides for rigidity, is subjected to an Rf alternating magnetic field. The computer scans through frequencies of the Rf field to obtain a spectrum.

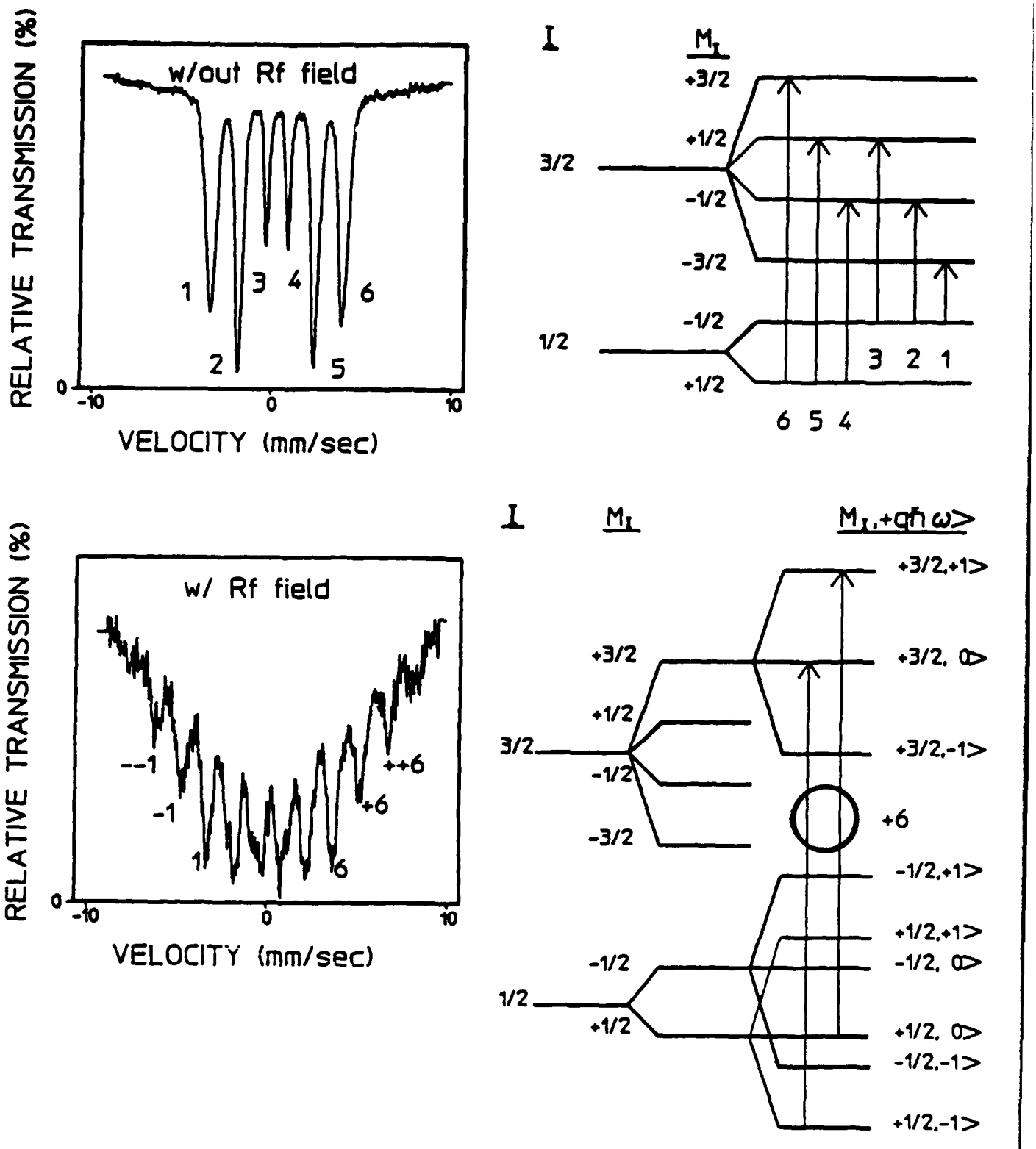

Figure 2. The effects of an alternating magnetic field on the hyperfine structure of ^{57}Fe are readily observable in conventional Mossbauer spectra. Without the Rf field there are 6 allowed transitions (parent transitions). The additional structure in the spectrum taken in the presence of the Rf field has the appearance of additional allowed transitions (sidebands).

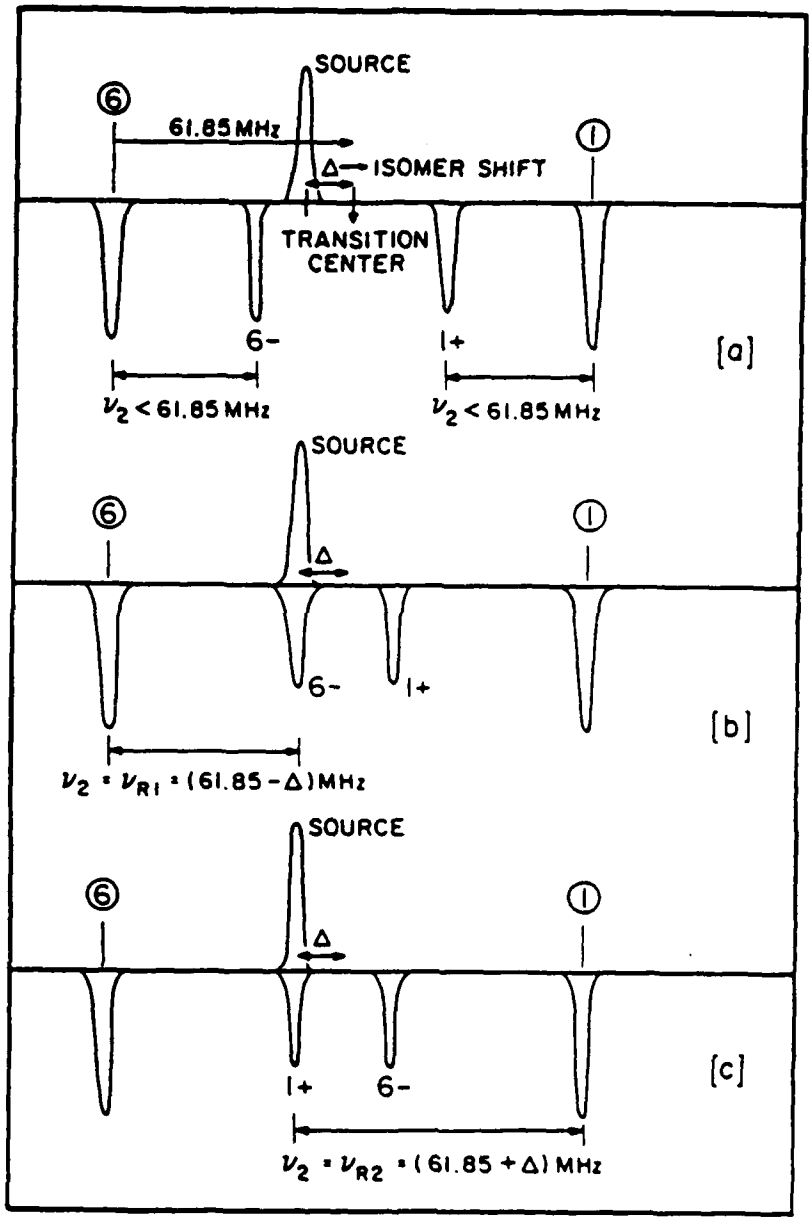

Figure 3. As the frequency of the RF field is increased, sidebands from symmetrically opposed transitions approach the transition center. For a stationary source, the probing radiation's energy is separated from the transition center by the isomer shift (Δ) between the source and absorber. Therefore, these two sidebands will move through the point of observation separated by twice the isomer shift.

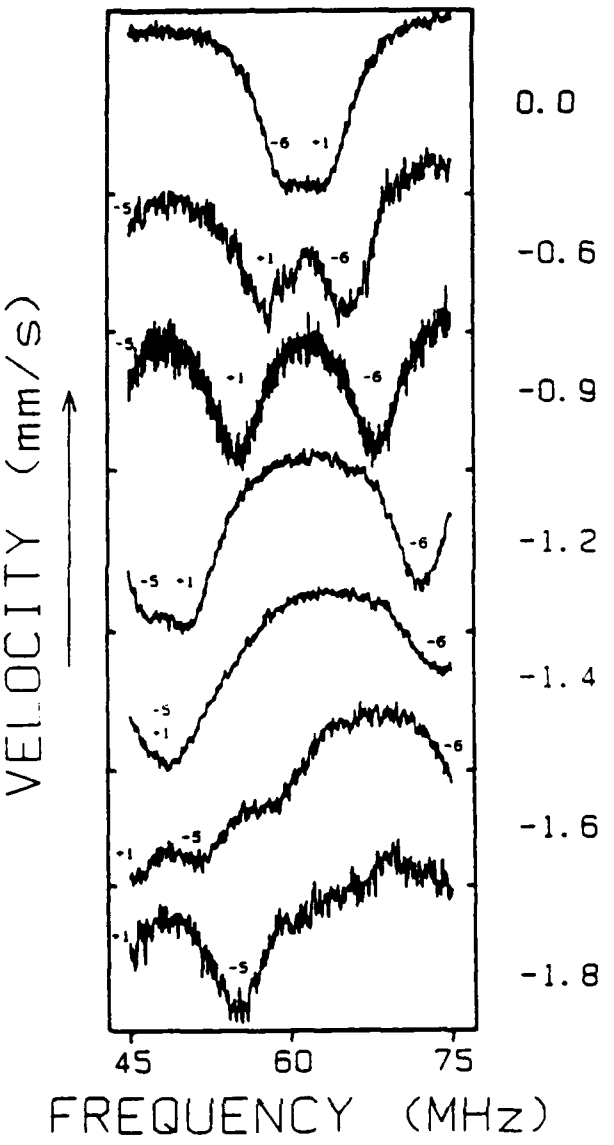

Figure 4. For a stationary source, the sidebands from the parent transitions 1 and 6 in ^{57}Fe overlap at 60 MHz separated by twice the isomer shift. If the source is given a small constant velocity, then the sidebands are separated by twice the isomer shift plus twice the velocity offset. At sufficiently high velocities a sideband from parent transition 5 comes within the frequency range scanned.

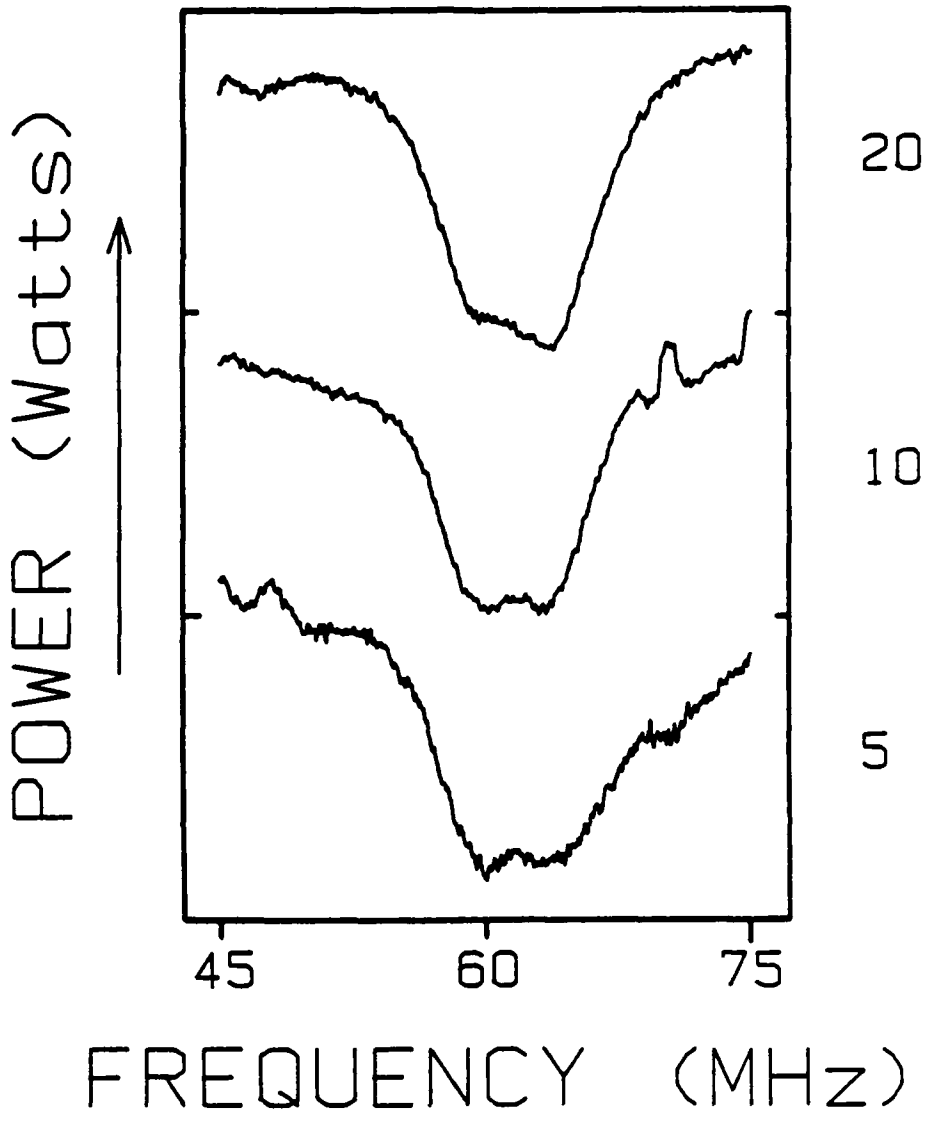

Figure 5. The amplitude of the sideband absorptions is dependent on the power of the applied Rf field. These are FMS spectra taken at three different powers.

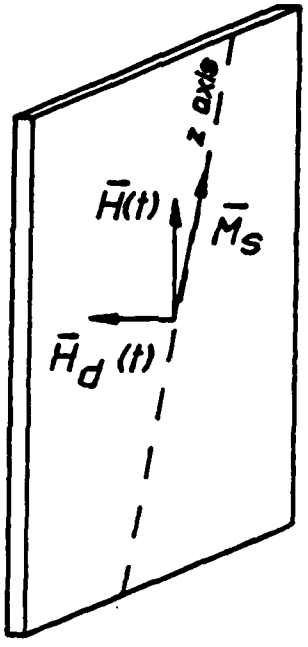

Figure 6. Primed coordinate system defined in the plane of the foil such that $\vec{M}$ always cooresponds to the z axis. The vector $\vec{H}_d$ is perpendicular to the plane of the foil.

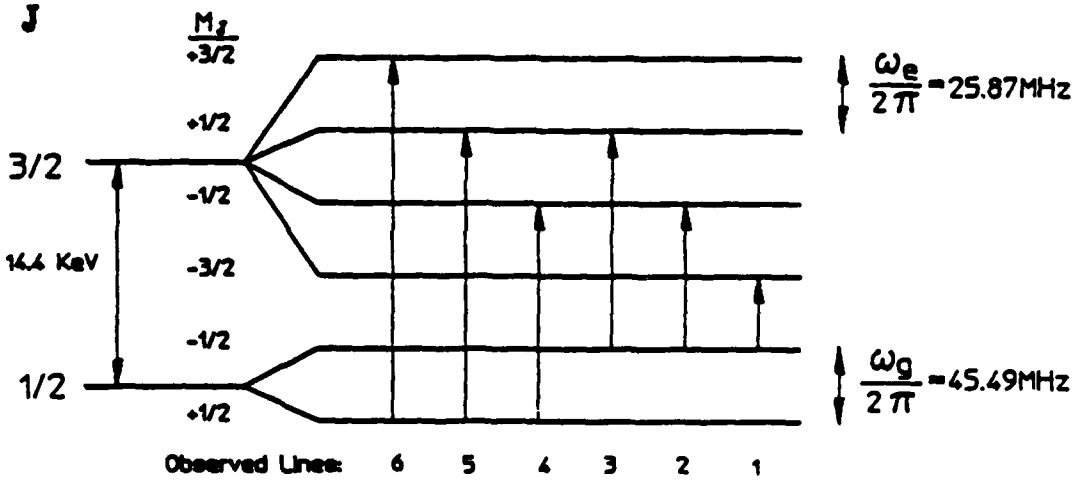

Figure 7. Energy levels of the Mossbauer transition of the ^{57}Fe nucleus in a ferromagnetic Fe foil indicating the total angular momentum, the magnetic sublevels, and the observed transitions.

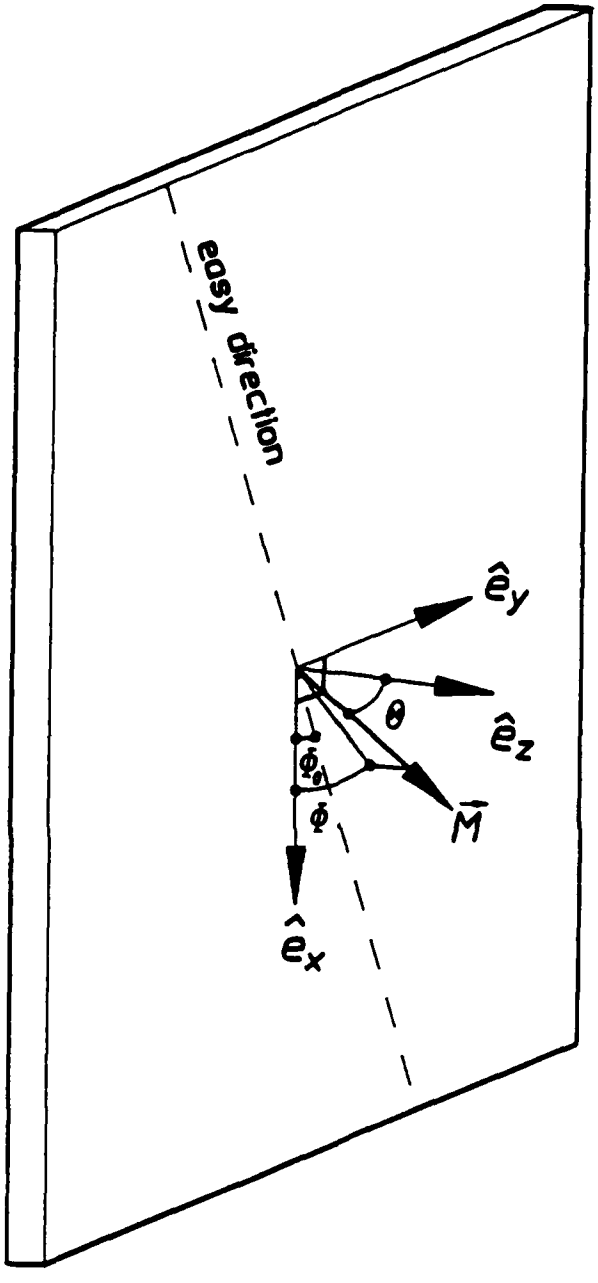

Figure 8. In the coherent switching model, coordinate system of the ^{57}Fe foil showing $\vec{M}(t)$ in relation to coordinates ϕ and θ. The foil lies in the xy plane.

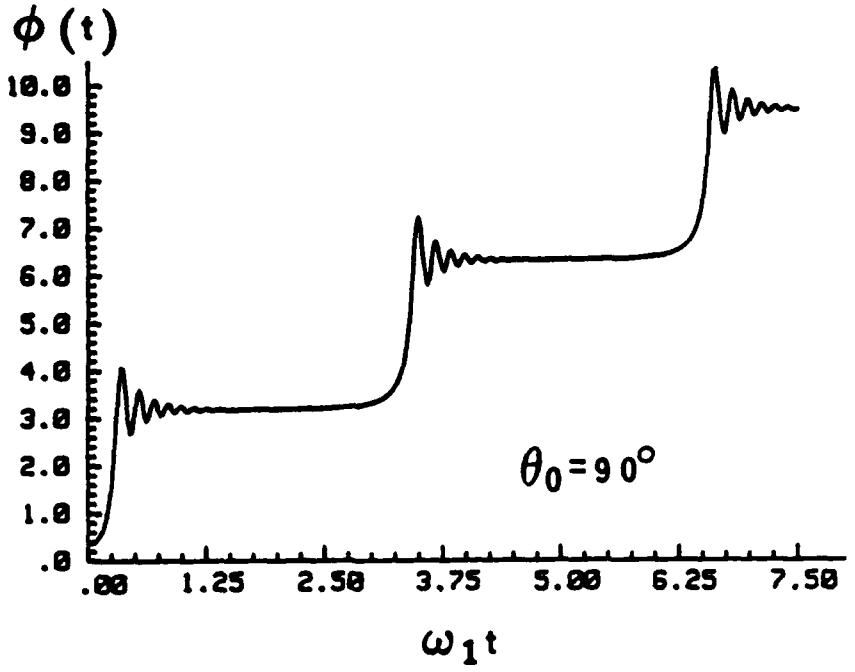

Figure 9A. Results of integrating the Landau-Lifshitz equation, $\phi(t)$ as a function of $(\omega_1 t)$, for the following initial conditions and input parameters:

Initial conditions: $\phi_o = 0.35$ rad $= 20^o$

$\theta_o = \pi/2$ rad $= 90^o$

Input parameters: $|\gamma| H_{app} = 33.61 \times 10^6$ rad/sec

$\omega_1 = 6\pi \times 10^7$ rad/sec (ν = 30 MHz)

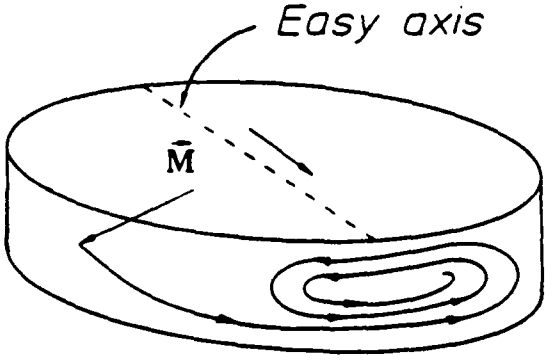

Figure 9B. The motion of the magnetization $\vec{M}(t)$ for a thin film switching. Adapted from Figure 16.13 of Physics of Magnetism by S. Chikazumi[4].

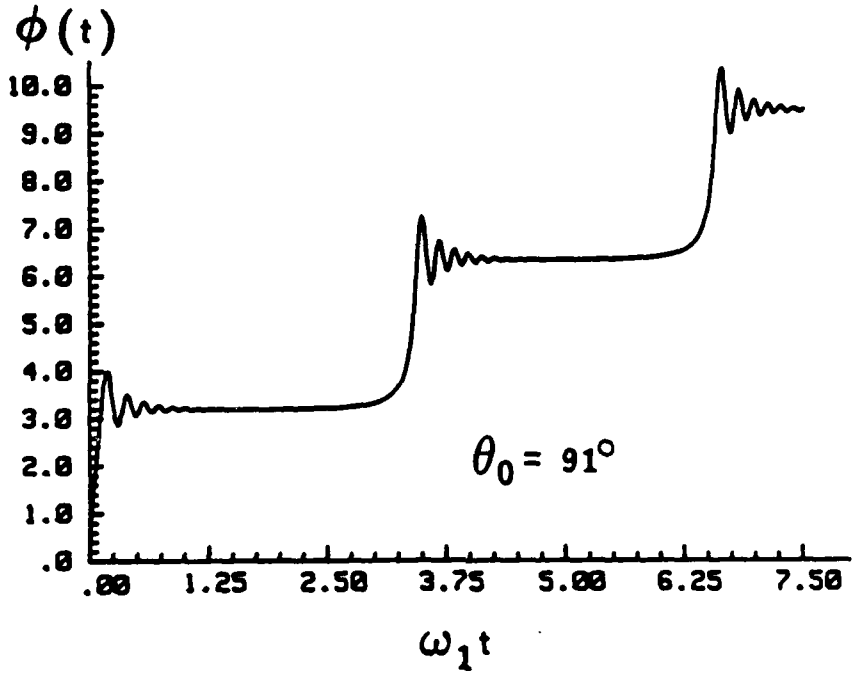

Figure 10A. Results of integrating the Landau-Lifshitz equation for $\theta_0 = 91^\circ$. All other parameters are the same as in Figure 9A.

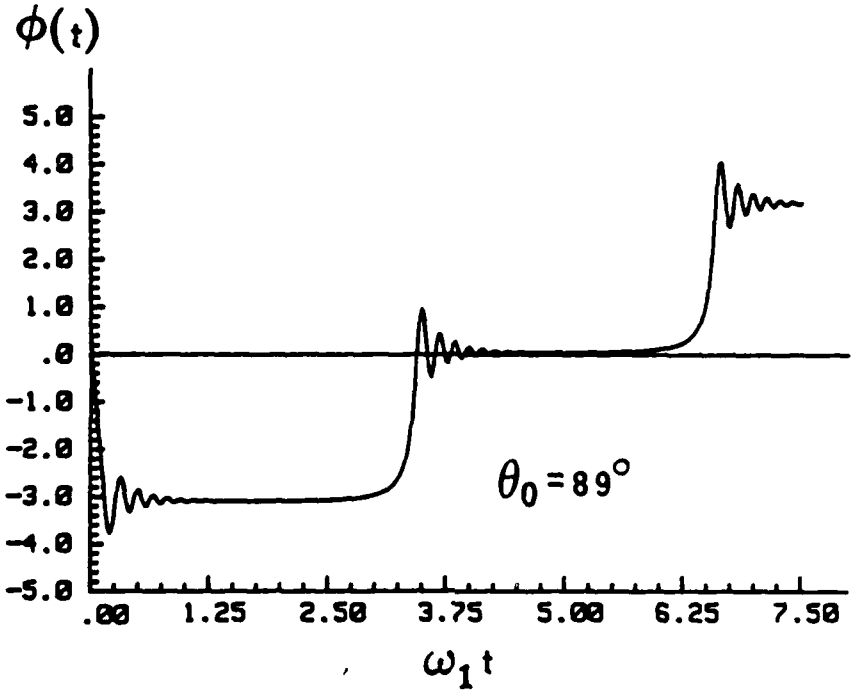

Figure 10B. Results of integrating the Landau-Lifshitz equation for $\theta_0 = 89^\circ$. All other parameters are the same as in Figure 9A.

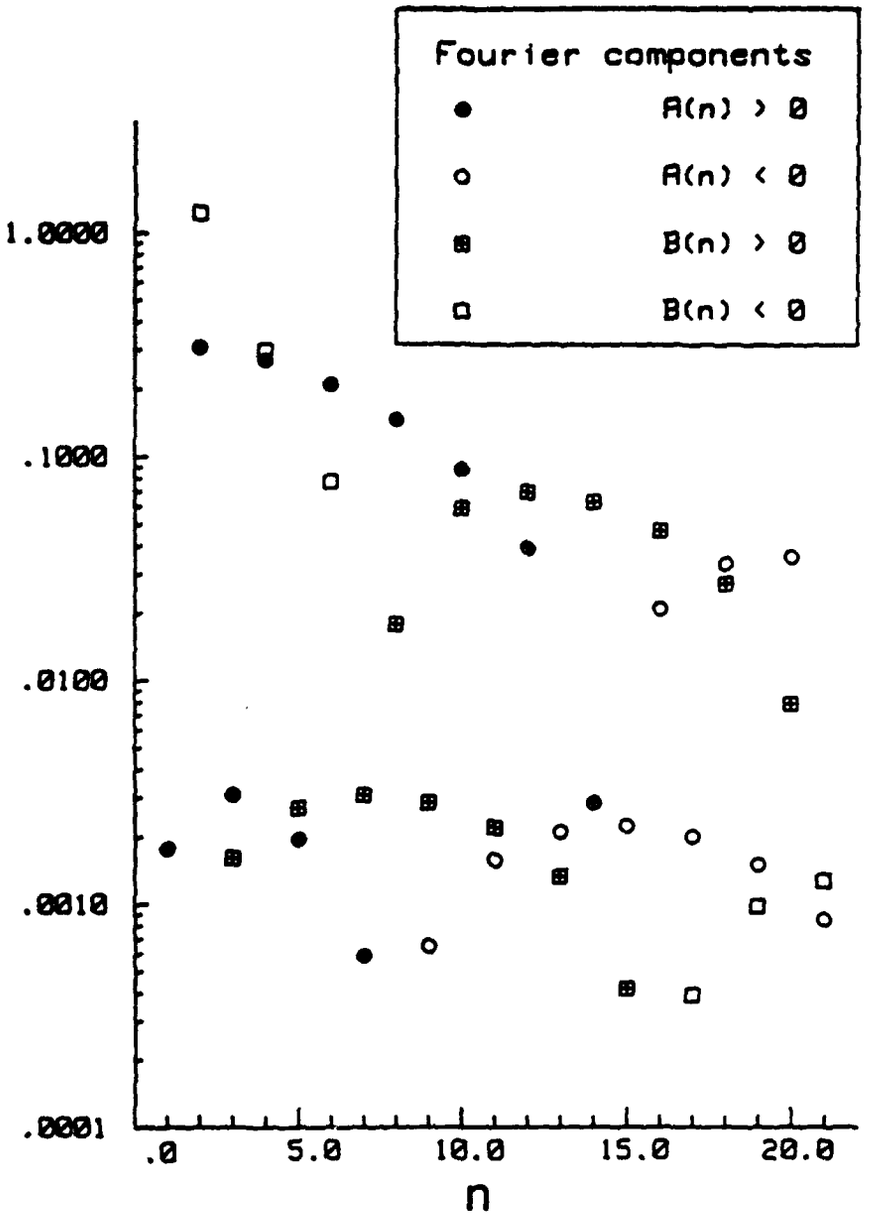

Figure 11. The Fourier decomposition of cos $\phi(t)$ derived from $\phi(t)$ as shown in Figure 9A according to the expansion

$$\cos \phi(t) = \sum_{n=0}^{\infty} [A(n) \cos n\omega_1 t + B(n) \sin n\omega_1 t].$$

The absolute values of the components A(n) and B(n) are plotted as functions of the order n. The sign of the component may be inferred from the legend.

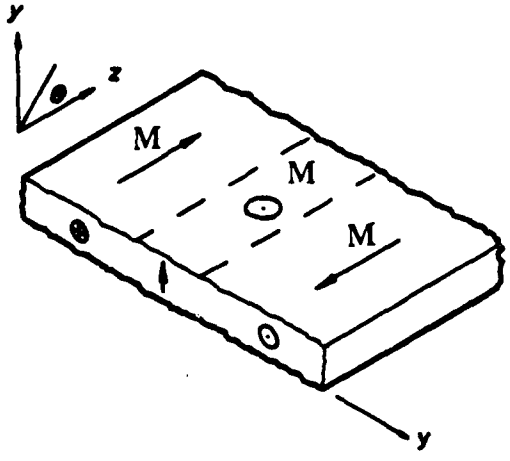

Figure 12. The magnetization $\vec{M}$ in a static Landau-Lifshitz 180^{o} domain wall. When the magnetization lies in the plane, there is no surface divergence $(\vec{M}\cdot\hat{n})$ except over the small region where the domain wall cuts the surface. Adapted from Figure 2.2 of Ferromagnetodynamics by T. H. O'Dell[3].

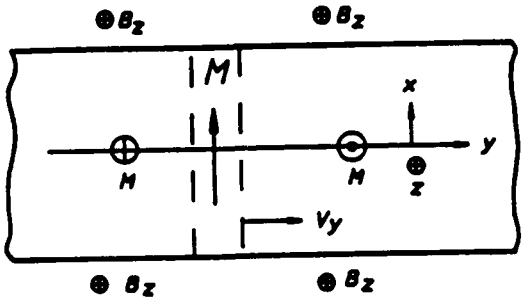

Figure 13A. Coordinate system for a "rigid" domain wall motion under the influence of an externally applied field B_z. Adapted from Figure 2.4 of Ferromagnetodynamics by T. H. O'Dell[3].

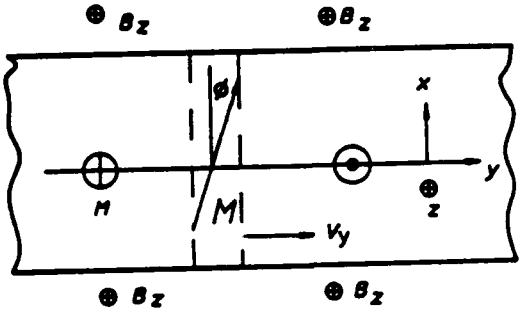

Figure 13B. Coordinate system for domain wall motion in which the magnetization is tilted slightly out of the xz plane. Analysis shows that the moving wall must develop a component of $\vec{M}$ which lies along the direction of motion. Adapted from Figure 2.5 of Ferromagnetodynamics by T. H. O'Dell[3].

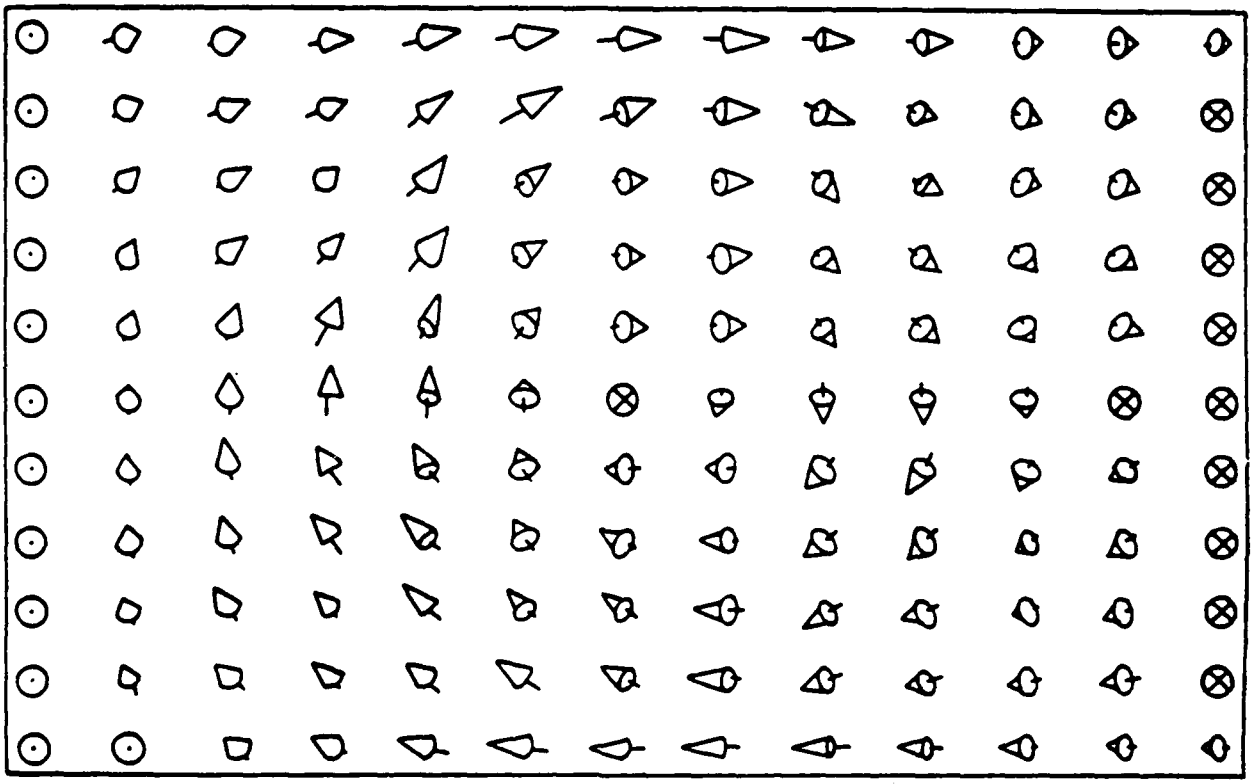

Figure 14. The magnetization in a wall region of a permalloy film 0.1 μm thick. The computation of the exact behavior of domain walls in conductors is based on the minimization of the interaction energies, including the magnetostatic energy. Of note is the fact that the magnetization always lies parallel to the surface of the conductor, thus minimizing the magnetostatic energy. Adapted from A. Aharoni[11].

APPENDIX II

ANNUAL SUMMARY REPORT

1 JANUARY 1987 - 31 DECEMBER 1987

ANNUAL SUMMARY REPORT

for the period

1 January 1987 through 31 December 1987

for

Office of Naval Research
Contract N00014-81-K-0653
Task No. NR 395-072

THE DEMONSTRATION OF THE FEASIBILITY OF THE TUNING AND STIMULATION OF NUCLEAR RADIATION

Short Title: GAMMA-RAY LASER

Principal Investigator: Carl B. Collins

The University of Texas at Dallas
Center for Quantum Electronics
P.O. Box 830688, Richardson, TX 75083-0688

TABLE OF CONTENTS

PROJECT DESCRIPTION

This project concerns the demonstration of the feasibility of the tuning and stimulation of nuclear radiation. It represents a critical line of investigation in our overall program concerned with the feasibility of a gamma-ray laser.

Theory, supported by our experiments conducted under this contract, has indicated that anti-Stokes Raman upconversion of intense but conventional laser radiation produced by scattering from isomeric states of nuclear excitation could lead to significant sources of tunable gamma radiation characterized by the natural Mössbauer widths of the lines. Further computations have suggested that this type of coherent, as well as a type of incoherent, optical pumping could even lead to appreciable levels of inversion of the populations of nuclear levels, thus supporting the growth of stimulated gamma-ray intensities. Whether or not these processes can reach threshold depends upon the resolution of basic issues in an interdisciplinary region between quantum electronics and nuclear physics that have not been addressed elsewhere. It is the purpose of this contract work to study these issues experimentally in order to guide the development of the technology and methods needed to exploit the enormous potential of this effect.

SCIENTIFIC PROBLEM

The viability of the concept for the tuning of gamma radiation by adding the variable energy of an optical photon produced by a tunable laser depends upon the existence in the nucleus of a particular arrangement of excited states. A suitable energy difference would make it possible to dress the nuclear states with the laser photons. Transitions between the dressed states would then occur at the sum and difference

frequencies characteristic of the nuclear transition, plus or minus the energies of integral numbers of laser photons.

Whether the necessary arrangements of nuclear states do exist is the central issue being addressed in this contracted work. Surprisingly, such information is currently unknown because such potentially useful states would lie in the "blind spots" of conventional techniques of nuclear spectroscopy. Normal Mössbauer spectroscopy provides enormous resolution, but a tuning range that is inadequate by orders of magnitude to support any possible study of transitions to the intermediate states of a multiphoton process. Conversely, crystal spectrometers provide broad tuning ranges, but levels of resolution that miss by two orders of magnitude the threshold that would be necessary to separate the transitions to the initial and intermediate states. As a consequence, the ideal arrangement of nuclear energy levels needed for the Raman upconversion process could be a common occurrence that has gone unnoticed because of the inadequacies of conventional nuclear spectroscopy.

The critical problem in this research has two facets: 1) the development of an appropriate spectroscopic technique, and 2) the search for a suitable medium for a large-scale effect. The dressing of the nuclear states not only affects their energies, but also changes their transition properties. Forbidden nuclear transitions should become allowed so that the metastability of isomeric states would be "switched off" as the states were dressed. This would greatly enhance the prospects for stimulating the gamma-ray transition, in addition to rendering it tunable. It is the development of the investigative instrumentation and the verification of these predicted effects that comprise the scientific problem addressed by this contract research.

TECHNICAL APPROACH

For the resolution of the central issue of the existence of potentially useful intermediate states in a multiphoton upconversion of optical photons to gamma-ray energies, it was first intended to demonstrate sum frequency generation in one case in which nonresonant intermediate states were known to exist. This was the case in which both initial and intermediate states were magnetic sublevels of the same nucleonic state and in which the transitions were mediated by the M1, magnetic dipole operator. Experimental data reproduced in the literature suggested that such a process had already been unknowingly demonstrated for the generation of radiofrequency sidebands to Mössbauer transitions at the sum and difference frequencies. This suggested the development of a new instrument, a Frequency Modulation Spectrometer for gamma-ray energies, designed to support the needed studies of nuclear structure with the precision of Mössbauer spectroscopy applied over a tuning range of energies lying considerably beyond the state-of-the-art at the time our work began. With this instrument, we are conducting Mössbauer experiments in the presence of intense radiofrequency fields with measurement and parameterization of the conversion efficiency into the sum frequency lines to determine the practical limits on the ultimate linewidths and tuning ranges that can be achieved. This technique will then be used in a "bootstrap" approach to support a search for accidentally resonant intermediate states. By replacing the radiofrequency excitation with tunable higher frequencies, it is expected that the tuning range of Mössbauer spectroscopy can be extended by further orders-of-magnitude.

PROGRESS DURING THIS REPORTING PERIOD

Instrumentation of FMS

The sum and difference frequency sidebands produced on intrinsic Mössbauer transitions have made possible very effective new instrumentation for high resolution spectroscopy at gamma-ray energies. A prototype version of this Frequency Modulation Spectrometer (FMS) was first described[1] by our laboratory in 1985, and subsequent refinements were made during the successive reporting periods under this contract. This device monitors changes in the intensity of transmitted single-frequency gamma photons as a function of frequency of the long wavelength photons of the alternating magnetic field in which the absorbing nuclei are immersed.

With this contract support our prototype "Nuclear Raman Spectrometer" was refined into mature technology resulting in the Frequency Modulation Spectrometer, (FMS) for gamma-ray energies[2]. The original prototype device had required a tedious level of manual interaction, and this was replaced with a fully-automated and computerized control system. At its heart is a multi-channel scalar (MCS) and IEEE-488 GPIB interface with an Apple II+ computer. The MCS was designed to have a 100% duty cycle. The GPIB enables the spectrometer to sweep continuously through the frequencies of an rf magnetic field with a Wavetek frequency synthesizer. The Mössbauer drive allows the frequency of the gamma photons to be biased by a constant Doppler shift, if desired. In its present form, the FMS device has an instrumental resolution of 100Hz and a continuous tuning range of 10^9Hz with a stability of 0.1Hz/sec with no mechanical movements required anywhere. These characteristics are comparable to a Mössbauer spectrometer with a means of shifting the gamma-ray source, having a resolution of 10nm/sec and a range of 100mm/sec with a stability of 0.01nm/sec/sec. Demonstration spectra were acquired with ^{57}Fe showing isomer shifts and thermal shifts. Because we were using a modulation

type of spectroscopy, the static features could be suppressed, and these different effects were obtained with unprecedented clarity.

Details of the mature FMS device are contained in the article "Frequency-modulation spectrometer for Mössbauer studies", by P. W. Reittinger, T. W. Sinor, S. S. Wagal and C. B. Collins, Rev. Sci. Instrum. 59, 362 (1988). A copy is reproduced in Appendix I and shows data demonstrating the remarkable detail which can be readily obtained with this device. The crowning achievement is found in Fig. 6 of that reprint where 24 sidebands are seen in a tuning interval of 50 MHz, all having values of relative intensity confirmed in the companion plot of a computer synthesis of that region of the spectrum.

It appears that the FMS device developed under this contract has now proven its utility as a tool in Mössbauer spectroscopy. Besides standing ready to serve in our own search for nearly resonant intermediate states for a multiphoton process, it has the versatility to support many other kinds of experiments as well.

Spurious Acoustic Effects

Despite the impressive agreement between results obtained with the new instrumentation developed under this contract and rudimentary multiphoton models[2,3] intense criticism has continued to issue because of the belief that, somehow, all effects which appear as sidebands arise from spurious acoustic vibrations excited by magnetostriction of some of the various elements of the spectroscopic sample and its holder. In appearance our multiphoton spectra resemble the transmission spectra which Ruby and Bolef[4] obtained by imposing periodic Doppler shifts of purely mechanical origin upon the Mössbauer source. This unfortunate similarity in appearance between phenomena arising from such different origins has provided the basis for years of critical controversy.

There is the disturbing impression in the Mössbauer community that an acoustic origin had been "proven" for all sidebands by the benchmark

experiment of Chien and Walker[5] in 1976. In that experiment an absorbing foil composed of ferromagnetic and nonmagnetic layers was used to study transport of the causative agent from the ferromagnetic layer into the nonmagnetic region where the sidebands were produced upon Mössbauer transitions of embedded ^{57}Fe nuclei. Very clear evidence showed that the cause did arise in the ferromagnetic Ni layers, producing sidebands in the nonmagnetic stainless steel layers. The most ready explanation at that time was a transport of phonons from one layer to the next with a high acoustic Q. Those experiments were repeated in the current reporting period[6] but with extensions which contradict the classic interpretation of Chein and Walker.[1] In fact, our reexamination shows the original experiment to have been so flawed that any conclusions drawn from it now must be considered unproven.

As detailed in the manuscript[6] "Comment on Mössbauer sidebands from a single parent line," by C. B. Collins, P. W. Reittinger, and T. W. Sinor, submitted to Phys. Rev. B, sideband effects scale with the square of the number of ferromagnetic sources. Interpreted as indicating the addition of fields from each source that are squared to communicate power into the sideband intensities, such scaling is completely inconsistent with an acoustic origin. In experiments such as these, acoustic phonons are the bosons associated with vector fields driven by tensor forces, not vector forces. Without invoking stimulated emission, we can conceive of no way in which tensor sources which are physically separated can produce coherent vector fields in a space between them, even if they are temporally sychronized. The stimulated emission of phonons to produce coherent additions of the displacements arising from the different sources would imply the existence of a threshold of power, above which two modulation indices of m would give an effect of $4m^2$ and below which only $2m^2$. No such threshold was suggested by the data which was obtained

over an adequate range of powers. Sidebands scaled consistently with $4m^2$.

At the time of reporting a critical experiment was initiated which will go much further in eliminating the possibilities of an acoustic origin to the large scale Mössbauer sidebands we observe by studying the transport of the causative effect over greater distances than the thickness of a layer. However, at this juncture it can already be said that the experiment of Chein and Walker which is considered to be the bulwark of the acoustic model for Mössbauer sidebands actually showed nothing but a fortuitious arrangement of errors.

SIGNIFICANCE

The significance of the work completed during this past year is twofold. The first arises from completion of the FMS instrument which now stands as a powerful tool for use in the search for accidentally resonant intermediate states needed to dress nuclear states with photons to an extent necessary for large scale effects. The second significance accrues from the increased confidence in the identification of Mössbauer sidebands in magnetic media as manifestation of the successful excitation of dressed states. Destruction of the "proof" that all such large effects were caused by spurious phonons leaves the field open for other explanations. Indeed, the dressed state model is adequate to explain the phenomena but had never been proven necessary. When another explanation was available it had been the extraneous alternative.

Now there is no longer any proof or even evidence of the general pervasiveness of acoustic sidebands in magnetic materials. The next experiments emphasizing transport of sidebands should make a definitive statement about the origins of radiofrequency sidebands in Mössbauer spectroscopy.

REFERENCES

1. B. D. DePaola, S. S. Wagal, and C. B. Collins, J. Opt. Soc. Am. B 2, 541 (1985).

2. P. W. Reittinger, T. W. Sinor, S. S. Wagal, and C. B. Collins, Rev. Sci. Instrum. 59, 362 (1988).

3. C. B. Collins and B. D. DePaola, Optics Lett. 10, 25 (1985).

4. S. L. Ruby and D. I. Bolef, Phys. Rev. B 5, 5 (1960).

5. C. L. Chien and J. C. Walker, Phys. Rev. B 13, 1876 (1976).

6. C. B. Collins, P. W. Reittinger, and T. W. Sinor, Phys. Rev. B (pending).

Appendix I

"Frequency modulation spectrometer for Mössbauer studies," by P. W. Reittinger, T. W. Sinor, S. S. Wagal, and C. B. Collins, Rev. Sci. Instrum. 59, 362 (1988).

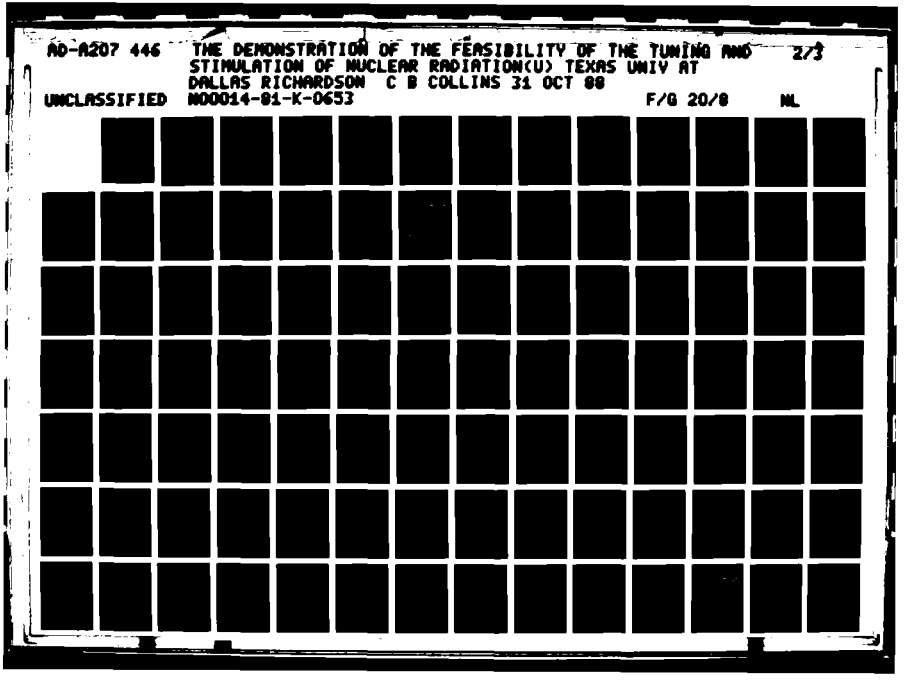
AD-A207 446
THE DEMONSTRATION OF THE FEASIBILITY OF THE TUNING AND STIMULATION OF NUCLEAR RADIATION(U) TEXAS UNIV AT DALLAS RICHARDSON C B COLLINS 31 OCT 88
2/3
UNCLASSIFIED
N00014-81-K-0653
F/G 20/8
NL

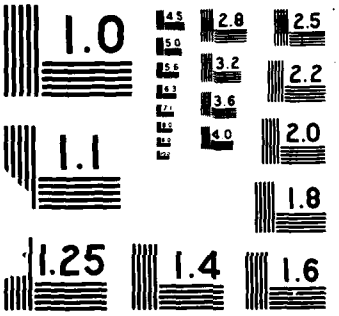
1.0
1.1
1.25
1.4
1.6
1.8
2.0
2.2
2.5
2.8
3.2
3.6
4.0
4.5
5.0
5.6

Frequency-modulation spectrometer for Mössbauer studies

P. W. Reittinger, T. W. Sinor, S. S. Wagal, and C. B. Collins

Center for Quantum Electronics, University of Texas at Dallas, Richardson, Texas 75080

(Received 30 July 1987; accepted for publication 13 October 1987)

A nuclear frequency-modulation spectrometer (NFMS) for high-resolution gamma-ray spectroscopy is described in this article. As the name implies, this device operates by modulating the cross section for gamma-ray absorption. The automation of this spectrometer required the development of an interface to an Apple computer which provides a real-time data display. This interface also enables the Apple computer to control up to two Mössbauer spectrometers at once, with a real-time data display for each. A nuclear frequency-modulation spectrometer makes it possible to observe directly the phenomenon known as "rf sidebands" in Mössbauer spectroscopy, without interference from the "parent transitions." The high resolution of NFMS makes it possible to examine the "rf sidebands" for any fine structure.

INTRODUCTION

As early as 1960 it had been noted that radio-frequency (rf) sidebands to the hyperfine structure of ^{57}Fe could be observed with a Mössbauer spectrometer.[1] The six lines (parent transitions) in a normal absorption spectrum of ^{57}Fe in iron [Fig. 1(a)] are accompanied by additional absorption peaks (rf sidebands) when the absorber is subjected to a rf field [Fig. 1(b)]. In 1960, Ruby and Bolef reported the observation of rf sidebands in iron produced by mounting a ^{57}Co Mössbauer gamma-ray source on an ultrasonic transducer driven at MHz frequencies.[1] It should be noted that the rf transducer was used in addition to a long-period oscillator which provided the energy range for the Mössbauer spectrum by introducing controlled Doppler shifts. In 1968, Perlow reported the generation of rf sidebands in iron directly, by subjecting the gamma ray source to a rf field without the involvement of any external ultrasonic source.[2] In that same year, Heiman, Pfeiffer, and Walker reported observing rf sidebands in iron as a result of subjecting the iron foil absorber to a rf field.[3] Finally, in 1976, Chien and Walker presented a method for producing rf sidebands in a nonferromagnetic stainless-steel absorber with a rf field, by using nickel as a ferromagnetic nonabsorbing driver.[4] In all cases, the rf sidebands appeared at integral multiples of the frequency of the applied rf (Fig. 2). Figure 2 shows rf sidebands produced in a stainless-steel foil driven by a nickel foil immersed in rf fields of different frequencies. The frequency dependence of these rf sidebands can be utilized to make a high-resolution adaptation of Mössbauer spectroscopy which is freed from many of the mechanical constraints tending to limit conventional devices.

In 1967, Bolef and Mishory reported the development of a spectrometer which was based upon rf sidebands induced in a Mössbauer source with a rf electromechanical transducer (an X-cut quartz crystal).[5] As the frequency of the applied rf was changed, the energies of the sideband gamma-ray emissions changed. This phenomenon enabled Bolef and Mishory to obtain an absorption spectrum as a function of the frequency of the applied rf. In 1985, DePaolo, Wagal, and Collins reported success in developing a spectroscopic technique using rf sidebands induced in a ferromagnetic absorber by a rf field.[6] Modulating the absorber has numerous advantages over modulating the source. It is easier and safer to work with a stable isotope, and it is also easier to interpret a spectrum from a single line source, as opposed to a Zeeman split source or a source with rf sidebands. Therefore, we have improved the technique for a modulated gamma-ray absorption cross-section spectroscopy which we call nuclear frequency-modulation spectroscopy (NFMS).

The technique reported by DePaolo, Wagal, and Collins was slow and laborious, with data collection times on the order of months for tens of data points. We would like to report the automation of this technique, with resulting data collection times of two days for 1024 data points and a sig-

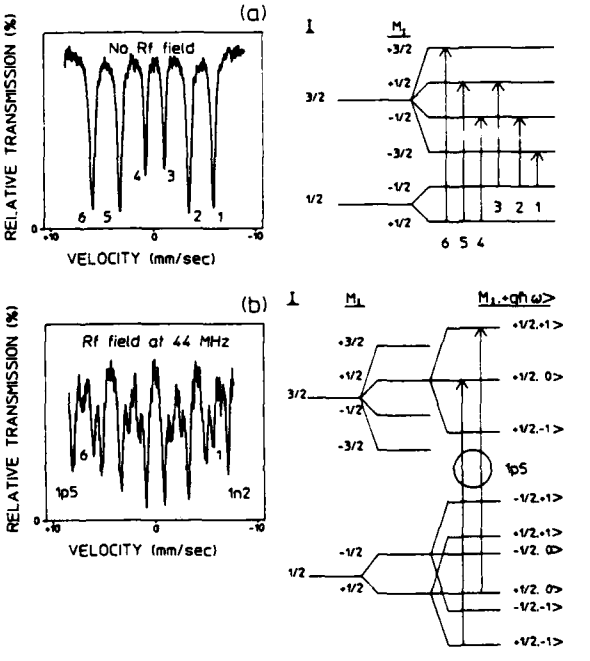

FIG. 1. Mössbauer absorption spectra and energy level diagrams for ^{57}Fe in iron; (a) with no rf field at the absorber, and (b) with a 4-Oe rf field applied to the absorber at a frequency of 44 MHz, showing the effect of the rf field.

 0034-6748/88/020362-06$01.30

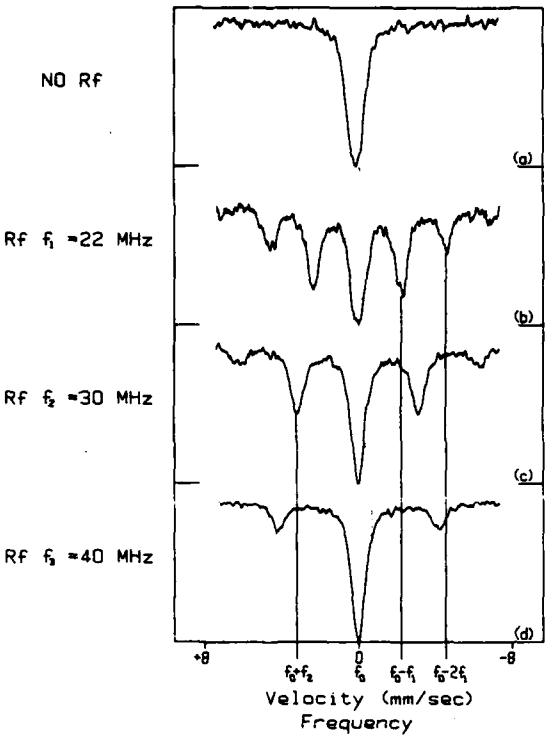

FIG. 2. Mössbauer absorption spectra of ^{57}Fe in 310-stainless-steel driven by a nickel foil, showing the effect of a rf field applied to the absorber–nonabsorber sandwich at frequencies of (b) 22 MHz, (c) 30 MHz, and (d) 40 MHz in comparison to (a) a no rf spectra. It can be seen from the figure that sidebands appear at integral multiples of the frequency of the rf field.

nal-to-noise ratio of 8:1 for a signal that represents a relative absorption of 3%. This article describes the NFMS apparatus, describes the interface to an Apple computer which automates NFMS data collection, and presents some typical NFMS data.

I. SPECTROMETER DESIGN

The NFMS is a modification of a conventional Mössbauer spectrometer comprised of the equipment in the dotted box in the schematic of Fig. 3. A Kr gas-filled proportional counter (ASA PC-KR-1) biased with 1.8 kV from a Bertran Associates model 303 dc voltage supply was used as our gamma-ray detector. The signal from the detector was amplified by an ASA CSP-400A preamp and ASA LA-200 amplifier. The amplified signal was then fed into an ASA LG-200 linear gate which produced 1-μs TTL pulses for counting.

A 10-mCi ^{57}Co Mössbauer source in a Pd matrix was mounted on an ASA K-4 linear motor capable of operating at a constant velocity or with constant acceleration. A stable means of Doppler shifting the energy of the emitted gamma ray is needed, therefore, an ASA S-700 motor controller is used to produce the voltage waveforms which drive the linear motor. The constant acceleration voltage waveform is derived from a 5-Hz square wave which must be provided by the multichannel scalar (MCS). If the motor is driven at a constant velocity, then the motor controller gates off data to the MCS while the motor is rewinding.

The key to NFMS is the presence of the rf field at the absorber, for which a very stable rf signal generator and amplifier are needed. A Wavetek 3510 signal generator, with a frequency range of 1 MHz to 1 GHz, and a 100-Hz resolution with a 500-Hz/(10-min) stability, was used. The rf amplifier was an ENI 550L 50-W linear amplifier with a range of 1.5–400 MHz. There were two basic circuits used to generate the rf field at the absorber. One was a series LC circuit in parallel with an impedance matching capacitor (Fig. 3). This series-resonant tank circuit was designed to have either a low Q when used in a narrow-band NFMS, or a high Q when used to obtain a Mössbauer spectrum in the presence of a single-frequency rf field. It should be noted that narrow band in these instances refers to a 12 MHz or less bandwidth.

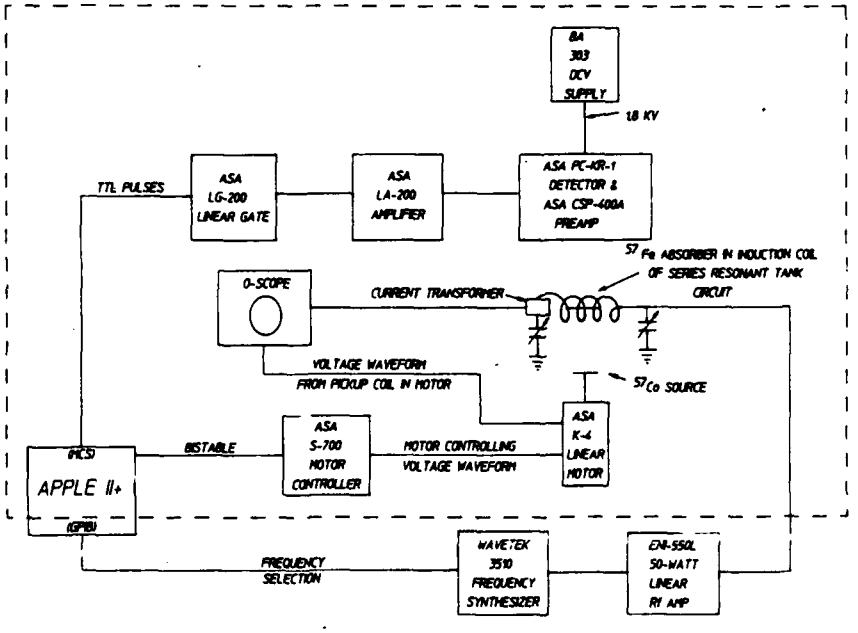

FIG. 3. This schematic shows the NFMS, while the portion of the apparatus which is in the dotted box can be used as a conventional Mössbauer spectrometer.

The other circuit, used in the wideband NFMS, simply incorporated an inductor in series with an impedance matching noninductive load. The absorber was then mounted in the induction coil of the appropriate circuit and subjected to field intensities on the order of 1–5 Oe.

In order to monitor the field intensity in the coil, a Pearson 2877 current transformer was used to measure the current flowing into the induction coil. This transformer outputs 1 V/A with a usable range of 300 Hz to 200 MHz and an insertion impedance of 0.02 Ω. In order to monitor the velocity of the motor, there is a pickup coil mounted in the linear motor. The output from this pickup is used to stabilize the driving voltage waveform, but it can also be monitored on an oscilloscope. The velocity of the motor was established by correlating the pickup coil voltages to the positions of the peaks in the six-line spectrum of ^{57}Fe. Currently, work is underway building an interface to an Apple II + from an ASA LC-9A laser interferometer. This interface will enable the computer to display real-time velocity information as well as track any drifting.

The heart of the NFMS, however, is the MCS/GPIB interface (Fig. 4). It enables an Apple II + computer to be used for data acquisition and real-time data display with either the conventional Mössbauer spectrometer (constant acceleration mode) or with the NFMS (constant velocity mode with GPIB interface to signal generator). The MCS is a card designed around two VIAs, or versatile interface adapters (6522's). The GPIB, or IEEE-488 General Purpose Interface Bus (9914), is a commercially available interface card available for the Apple computer. The GPIB is necessary only for scanning frequencies of the signal generator. Therefore, the GPIB is not needed if one intends to use only the Mössbauer spectrometer.

The central components of the MCS are the two 6522's, the multiplexing logic, and a 12-bit counter. Each 6522 is a 40-pin chip which has a 16-bit counter with a 16-bit latch, a 16-bit counter with an 8-bit latch, two 8-bit parallel ports, and a serial port. The counter with the full latch can be set to count down in a free running mode and generate interrupts. In other words, the 6522 can be set to generate evenly spaced interrupts so that the Apple's CPU need not be wasted keeping track of time. The counter with the half-latch can be set to count negative logic pulses at one of the pins of the 6522. The multiplexing logic is an assortment of gates which channel the pulses to be counted to one of the 6522's while channeling the Apple's data bus to the other 6522. When an interrupt is generated, the pulses to be counted are gated to the other 6522 while the Apple's data bus is then channeled to the first 6522. As a result, the time it takes the Apple's CPU to add a count to the proper channel is not dead time for the MCS. The 12-bit counter, actually three 4-bit counters, is needed to count 512 interrupts. This counting produces the 5-Hz square wave which is used by the motor controller to generate a constant acceleration voltage waveform for the linear motor. Therefore, the time between interrupts, hence the dwell time per channel, must be 195 μs for a 1024 data point Mössbauer spectrum. The NFMS, on the other hand, does not require an accelerating source. Therefore, when using the MCS in a NFMS, the dwell time can be user selected. The optimum dwell time minimizes the total dead time, which arises from the time needed to allow the rf signal to stabilize each time the frequency is changed, without compromising the stability of the signal.

Use of this hardware as a NFMS or a Mössbauer spectrometer is determined by the software. Written in 6502 assembly language, the software for the two spectrometers is similar in principle but different in particulars. In both spectrometers the MCS transfers data to the Apple on an interrupt basis. Both programs consist of four basic routines: an initialization routine, a display routine, a keyboard-inter-

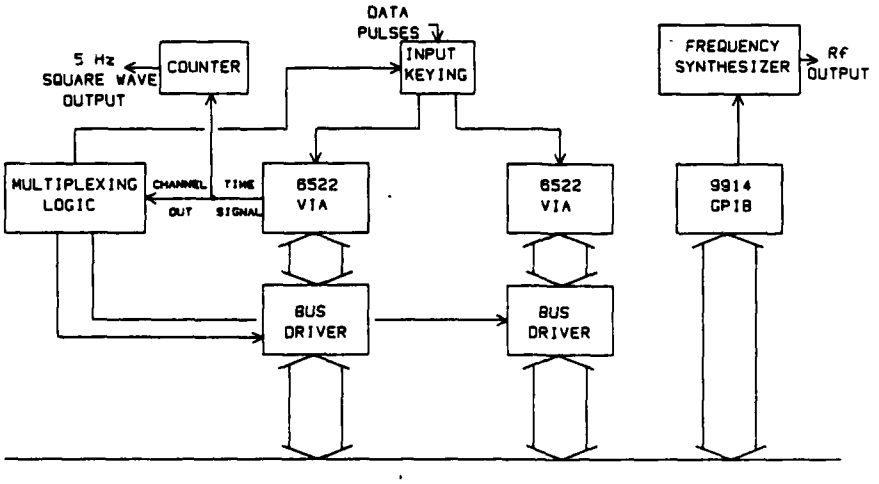

FIG. 4. This block diagram shows the basic components of the interface to the Apple II + computer. This interface enables the computer to be used for automatic NFMS data acquisition, or it can enable one computer, with two cards, to control and collect data from up to two Mössbauer spectrometers.

MCS/GPIB INTERFACE

preting routine, and an interrupt routine. The initialization routine uses the multiplexing logic on the MCS card to address each of the 6522's and set the appropriate registers. The display routine has two options. The data can be displayed graphically at different resolutions, or counts can be displayed as counts per channel and total counts per sweep. The graphics data display uses table lookup and two graphics screens to provide a real-time data display. The initialization routine generates a table in memory which stores the address for a given vertical coordinate on the screen in a memory location which is correlated to the value of the vertical coordinate. The value of the horizontal coordinate is correlated to the memory address of the channel to be displayed. As the display routine scans through memory at the data, the datum value and the channel value are used to address indirectly the appropriate graphics screen coordinate through this table. Therefore, by using table lookup, all of the mathematical operations necessary to obtain the appropriate screen addresses (including a division by seven) are performed only once. While one graphics screen is displayed, the other is cleared and plotted with the current data. The updated screen is then activated and the first screen is cleared and replotted, and so on. The keyboard-interpreting routine allows one to change the display, change the resolution of the graphics display, or stop the spectrometer and store the data on a disk, all with single key codes. A table of these key codes is displayed at the bottom of the counts display screen, the default display. Finally, the interrupt routine collects the count from the currently accessible 6522 and stores it in the appropriate 3-byte location. The display and keyboard routines for the two spectrometers are identical, but the initialization and interrupt routines for the two spectrometers are necessarily very different.

In the Mössbauer spectrometer, the initialization routine must enable the MCS card to generate interrupts at 195-μs intervals. Next, the interrupt routine must be capable of pushing all values in the CPU's registers to the stack, accessing the count from the appropriate 6522 and adding it to the appropriate memory locations, and then reloading the CPU's registers with their initial values, all in less than 195 μs, with enough time left over to update the display between interrupts. This feat was best accomplished by using four separate interrupt routines. Since the spectrometer has 1024 channels, the data is stored in twelve 256-byte pages for 3 bytes per channel. Each interrupt routine addresses a channel comprising 3 bytes through the sum of base addresses plus a counter value. Upon completion, each routine stores the address of the next interrupt routine in the interrupt vector. The fourth routine stores the address for the first routine in the interrupt vector and increments the addressing counter. The result is an interrupt routine that lasts 50–60 μs from interrupt to return, depending on the number of bytes which must be incremented. As a result, one Apple II + computer can easily handle two Mössbauer spectrometers with a real-time data display for each.

In the NFMS, the initialization routine enables the MCS card to generate interrupts at $\frac{1}{20}$ of a second intervals. This routine also initializes the signal generator through the GPIB. The interrupt routine must then translate the number of interrupts generated into an elapsed time and compare this time to the selected dwell time. In addition, this interrupt routine must perform all of the functions of the Mössbauer spectrometer interrupt routine. After the elapsed dwell time, the interrupt routine must step the frequency of the signal generator and change the address (channel) for data storage. When the frequency of the signal generator is changed, and for a time thereafter, the data to the MCS must be gated off and the timing stopped until the signal is stabilized. In the NFMS, the speed of the interrupt routine is no longer a major concern due to the significant increase in the time between interrupts and the fact that the data is gated off while the interrupt routine is delaying for the signal generator. Unfortunately, however, the time required to change the frequency is unavoidable dead time. Yet the total dead time in a run can be minimized by selecting a sufficiently long dwell time which does not allow the signal to drift significantly.

II. DATA AND DISCUSSION

Figures 1 and 2 show data collected with our Mössbauer spectrometer and processed with a five-point running average. These figures show rf sidebands in an iron foil absorber, and the frequency dependence of the rf sideband energies in a stainless-steel foil absorber. All NFMS spectra to be shown were obtained from a 1.5-cm$\times$0.85-cm$\times$2.5-μm iron foil absorber enriched with 95% ^{57}Fe . This foil is the same absorber which gave us the spectra in Fig. 1. All spectra shown were obtained from an absorption geometry, using a ^{57}Co source in a Pd matrix. All NFMS spectra have been processed with a five-point running average.

The first set of NFMS data concentrates on the first-order sidebands from the 1 and 6 parent transitions (Fig. 5). The nomenclature for identifying the rf sidebands is as follows. The first digit corresponds to the order of the sideband. Radio-frequency sidebands of the jth order from a given parent transition are found at the sum and difference frequencies of the static field, or Zeeman splitting, and j times the frequency of the applied rf field. The letter after the first digit, either an "n" or a "p," indicates whether the sideband is a negative or positive sideband, respectively. A negative sideband appears at an energy lower than the energy of the parent transition, while a positive sideband is at a higher energy. The last digit identifies the parent transition of the sideband. There are six allowed transitions for ^{57}Fe in a metallic iron foil, of which the lowest-energy transition is identified as parent transition 1 and the highest-energy transition is identified as 6. The energy difference between parent transitions 1 and 6 is 123 MHz, therefore, at 61.5 MHz the 1n6 and 1p1 sidebands should overlap at the transition center of the spectrum. If the gamma-ray source is stationary, then the energy of the gamma rays emitted differ from the energy of the transition center of the absorber by the isomer shift. Therefore, a stationary source should provide a NFM spectrum of the 1n6 and 1p1 sidebands displaced from 61.5 MHz by plus and minus the isomer shift, respectively [Fig. 5(a)]. The source used was in a Pd lattice, which has an isomer shift of -0.185 mm/s relative to metallic iron. If the source is

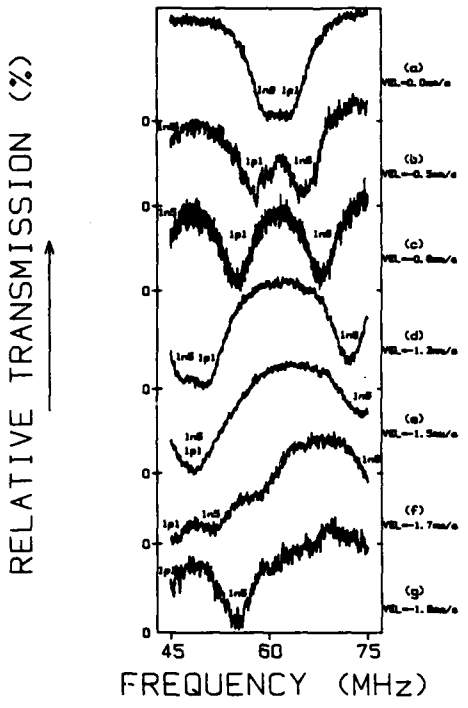

FIG. 5. Typical NFMS data showing first-order sidebands from the highest- and lowest-energy transitions of ^{57}Fe in iron, 1n6 and 1p1, respectively; (a) in the vicinity of the transition center of this Zeeman split absorber. An "n" in the sideband label indicates that the sideband is at a lower energy than its parent transition, whereas a "p" indicates that the sideband is at a higher energy. As the velocity of the source is decreased (b)–(g), the energy of the probing radiation is decreased, and as a result, the sideband from the lower-energy transition, 1p1, appears at lower frequencies. The sidebands from the higher energy transitions, 1n5 and 1n6, appear separated by the excited state splitting frequency of ^{57}Fe in iron, 26 MHz.

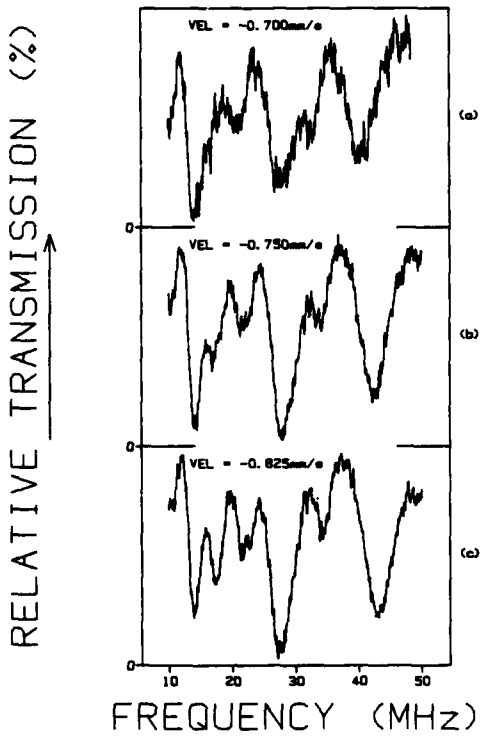

FIG. 6. Nuclear frequency-modulation spectrometer data obtained at lower frequencies has an appearance which belies the underlying complexity of the spectra. Sidebands add together to produce composite sidebands which have amplitudes, widths, and line shapes with a high degree of dependence upon the energy of the probing radition. As a result, a small change in the source velocity can lead to a significant change in the appearance of a spectrum.

then given a constant velocity, the 1n6 and 1p1 sidebands should be displaced from 61.5 MHz by plus and minus (isomer shift − velocity), respectively [Figs. 5(b)–5(g)]. The sign convention is to define a velocity as negative when the source and absorber are moving away from each other. Note that the rf sideband 1n5, which appears in Fig. 5, should be separated from 1n6 by 25.9 MHz, the excited state splitting frequency in metallic iron.

The second set of NFM spectra [Figs. 6(a)–6(c)] were obtained at a lower-frequency range. Higher-order sidebands add together at these lower frequencies and present significant cross sections. These particular spectra are comprised of 24 different sidebands, if one takes into account sidebands out to the fifth order. Following the spectra are computer-generated simulations [Figs. 7(a)–7(c)]. The model, a simple algorithm, shows remarkable agreement with the data. The frequency at which a sideband will appear is

$$F_{j,\mathrm{ord}}(\mathrm{MHz}) = [\mathrm{vel} - (P_j + \mathrm{iso})](K/\mathrm{ord}), \qquad (1)$$

where P_j is the position of the jth parent transition in mm/s, vel is the velocity of the source in mm/s, iso is the isomeric shift between the source and absorber, ord is the order of the sideband, and K is a conversion factor = 11.6 MHz/(mm/s) for the 14.4-keV gamma ray being detected.

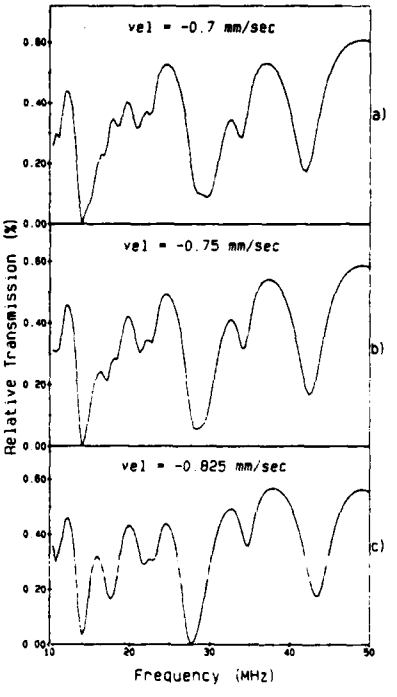

FIG. 7. Computer-generated simulations of the NFM spectra in Fig. 6 obtained from Eqs. (1)–(3). Each simulation is composed of 24 different sidebands.

The linewidth of the sideband as it will appear in the NFM spectrum is

$$\Gamma_{j,\mathrm{ord}} = (\Gamma_{P_j} + \Gamma_g)/\mathrm{ord}, \quad (2)$$

where Γ_{P_j} is the linewidth of the sideband's parent transition and Γ_g is the linewidth of the 14.4-keV gamma ray emitted by the source. The apparent linewidth's dependence on sideband order can be understood by realizing that an nth-order sideband will be displaced by n frequency units, while a first-order sideband is displaced by one frequency unit. Since we were concerned only with the relative amplitudes of a sideband within a given NFM spectrum, the amplitude of a sideband in a spectrum was assumed to be

$$A_{j,\mathrm{ord}} = A_{P_j}/\mathrm{ord}, \quad (3)$$

where A_{P_j} is the amplitude of the sideband's parent transition. By using this equation we have assumed that our spectra were not exhibiting the saturation effects discussed in Ref. 6. This assumption was a convenient mechanism for introducing a sideband amplitude dependence on the relative amplitudes of the parents. For the iron foil used, the relative amplitudes of the parents were taken as 2:2:1:1:2:2 [Fig. 1(a)]. The NFMS is a tool for directly measuring rf sideband position, width, and amplitude. This model shows that the NFMS is a powerful means of indirectly measuring isomeric shifts and the positions and relative amplitudes of the parent transitions.

The NFMS apparatus is versatile. This apparatus is a conventional Mössbauer spectrometer with or without a rf field, as well as a rf sideband spectrometer. A conventional Mössbauer spectrometer is not capable of measuring rf sidebands when they overlap a parent transition, and resonances have been predicted for certain such overlappings. The NFMS enables one to observe the behavior of rf sidebands in the vicinity of a parent transition, with high enough resolution to discern any fine structure in the sideband which might result from such resonances, because in NFMS, the parent transition appears only as a base line due to its lack of any frequency dependence. With the NFMS, it is also possible to observe directly the effect of the rf field intensity on sideband position, amplitude, and width. It should also be noted that the MCS described in this paper may also be used in a spectrometer similar to the type described by Bolef and Mishory in Ref. 5.

ACKNOWLEDGMENTS

Support for this project was provided in part by the Office of Naval Research and in part by IST/SDIO, directed by the Naval Research Laboratory.

[1]S. L. Ruby and D. I. Bolef, Phys. Rev. Lett. **5**, 5 (1960).
[2]G. J. Perlow, Phys. Rev. **172**, 319 (1968).
[3]N. D. Heiman, L. Pfeiffer, and J. C. Walker, Phys. Rev. Lett. **21**, 93 (1968).
[4]C. L. Chien and J. C. Walker, Phys. Rev. B **13**, 1876 (1976).
[5]D. I. Bolef and J. Mishory, Appl. Phys. Lett. **11**, 321 (1967).
[6]B. D. DePaolo, S. S. Wagal, and C. B. Collins, J. Opt. Soc. Am. B **2**, 541 (1985).

Appendix II

"Comment on Mössbauer sidebands from a single parent line," by C. B. Collins, P. W. Reittinger, and T. W. Sinor, Phys. Rev. B (submitted).

Comment on "Mössbauer sidebands from a single parent line"

by

C. B. Collins, P. W. Reittinger, and T. W. Sinor
Center for Quantum Electronics
University of Texas at Dallas
P.O. Box 830688
Richardson, Texas 75083-0688

Foils composed of alternating layers of ferromagnetic and nonmagnetic materials immersed in magnetic fields oscillating at radiofrequencies display sidebands on Mössbauer transitions from the nuclei contained in the nonmagnetic regions. Attributed by Chien and Walker [Phys. Rev. B13, 1876 (1976)] to the transfer into the nonmagnetic layer of acoustic phonons excited by magnetostriction in the ferromagnetic layers, this accepted cause of such effects is challenged by new data resulting from a reexamination and extension of that classic experiment.

The paper of Chien and Walker[1] was of such critical importance that it warrants comment over a decade later. Generally perceived as reporting an unarguable proof of a certain basic proposition, it has now been found to have rested upon a demonstrably false assumption. A reexamination of the original experiment shows it to have been so flawed that any conclusions drawn from it must now be considered unproven.

The point of inception had been the original proposal of Mitin[2,3] that Mössbauer transitions could be excited as part of a multiphoton process in nuclei immersed in intense radiofrequency (rf) fields. In those cases the Mössbauer spectrum was expected to show additional sum and difference frequency lines displaced from the normal lines by integral multiples of the perturbing frequency. In appearance such multiphoton spectra are expected to resemble the transmission spectra which Ruby and Bolef[4] obtained by imposing periodic Doppler shifts of purely mechanical origin upon the Mössbauer source. This unfortunate similarity in appearance between phenomena arising from such different origins provided the basis for years of critical controversy seemingly resolved by the work of Chien and Walker.[1] The purpose of this comment is to report new data from a repetition and extension of the Chien and Walker experiment that shows their conclusions to be unjustified. Without the force of conviction conveyed by their work, the controversy must be reopened to further investigation.

The earliest experiment in radiofrequency sideband production, reported by Perlow[5] in 1968, focused upon the components of the 14.4 keV transition in ^{57}Fe. Several ^{57}Co sources diffused into ferromagnetic hosts were immersed into intense magnetic fields oscillating at radiofrequencies. Those results were explained[5] as the magnetodynamic modulation of the hyperfine fields and generally conformed to the Mitin hypothesis for multiphoton transitions. Two

of the three groups who initially documented this phenomena favored the magnetodynamic explanation which required no mechanical action[5,6,7] while the other group began to develop an alternative based entirely upon magnetostriction.[8,9] Most of the actual experiments had used ferromagnetic hosts to enhance the applied magnetic fields, and such materials are almost invariably magnetostrictive. In the model finally synthesized, periodic Doppler shifts were assumed to be driven by acoustic phonons which were excited by magnetostriction along the greatest dimensions of the material and scattered onto the axis connecting source and absorber. To be effective, this mechanism required the sample to have a large acoustic Q so that displacements of the active nuclei could build to significant values.

Despite the accretion over the years of a large body of phenomenology presumed to describe rf sidebands on Mössbauer transitions, the magnetostrictive-acoustic theory never quantitatively predicted the amplitudes of the sidebands as functions of either applied power or frequency. However, the magnetodynamic models of that time fared no better, and attention turned to "proving" a magnetostrictive origin by distressing the alternative explanations.[10] The obvious difficulty with proving a theory by distressing the alternatives is that those other explanations may not have reached comparable levels of maturation. The magnetodynamic models of the late 60's were relatively easy to destroy.[10] However, the recent successes of ferromagnetodynamics[11,12] show the early models[5] of sideband formation to have been inspired, but inadequate approximations. These models simply did not embody the level of sophistication necessary to describe the complex switching behavior of magnetization in ferromagnetic foils subjected to various combinations of static and oscillating fields in those geometries employed.

More recent experiments[13,14] have shown that the applications of such oscillating magnetic fields to Mössbauer nuclei embedded in nonmagnetic hosts

do produce radiofrequency sidebands by directly modulating the phases of the nuclear states involved in the transitions. However, amplitudes were rather small in those experiments because the driving forces depended only upon the value of applied field, $\mu_o H$. In 1984, we extended such approaches further by deriving the phase modulation of a nuclear state in a magnetic material.[15] In this case driving forces were proportional to the magnetization $\mu_o M$ and effects were found to be large.[15,16,17] It appears that many prior results attributed exclusively to acoustic effects driven by magnetostriction could have also benefited from an unrecognized contribution from direct phase modulations of the nuclear states involved.

From a current perspective it is the experiment reported by Chien and Walker[1] that forms the bulwark of the magnetostrictive-acoustic explanation of Mössbauer sidebands. In that experiment an absorbing foil composed of ferromagnetic and nonmagnetic layers was used to study transport of the causitive agent from the ferromagnetic layer into the nonmagnetic region where the sidebands were produced upon Mössbauer transitions of embedded ^{57}Fe nuclei. Very clear evidence showed that the cause did arise in the ferromagnetic Ni layers, producing sidebands in the nonmagnetic stainless steel layers. The most ready explanation at that time was a transport of phonons from one layer to the next with a high acoustic Q. Those experiments were repeated in the work reported here, but with extensions which contradict the classic interpretation of Chien and Walker.[1]

Although not unique for all sidebands in a spectrum,[1] the idea of a modulation index m as a measure of the strength of the development of the sidebands offers practical convenience for descriptions. For a magnetostrictive origin,[1]

$$m = x_0/\pi \quad , \tag{1}$$

where x_0 is the amplitude of the periodic displacement of the nuclei and λ = 0.137 A for the 14.4 keV line of ^{57}Fe. In the corresponding magnetodynamic model,[15]

$$m = bH \quad , \tag{2}$$

where H is the applied magnetic field and b provides proportionality between M_s, the saturation magnization of the medium, and H. For relatively small m, the ratio of the magnitude of the first order sidebands to the intensity in the original parent line is proportional to m^2, which in turn is proportional to P, the applied radiofrequency power.

One of the most compelling results presented by Chien and Walker[1] was a demonstration supposed to show the enhancement of m^2 afforded by tighter acoustic coupling of the layers. They found that electroplating Ni upon a stainless steel foil produced much higher values of m^2 in absorption experiments than could be obtained by gluing a Ni foil to the stainless foil. They attributed the difference to the obviously poorer acoustic properties of the glue. However, as part of this report we observe that their stainless steel foil was electroplated on <u>both</u> sides with Ni while the epoxied bond was used to join a <u>single</u> Ni foil to one side of the stainless absorber. While the m defined by Eq. (1) for a single foil could not be additive if produced in different magnetostrictive layers, in principle the M_s upon which m depends in Eq. (2) could add coherently. Two sources of m arising from distinctly separate sources could give a resulting modulation of $4m^2$ in a magnetodynamic model. Chien and Walker failed to recognize[1] that even in the magnostrictive model two sources of m generated in the two electroplated layers should give a modulation index of $2m^2$ in the absorber foil. Instead, they attributed the increased sideband intensity developed by the two plated sources in comparison to the one glued source only to the advantage they assumed for a plated contact over a glued interface. They reported no comparison of the effects of

gluing or plating the *same number of ferromagnetic layers to the absorber foil*. Reported here is a repetition of the Chien and Walker experiment which showed that the effect of two foils varied from two to four times that produced by a single foil joined in the same fashion, depending upon the static magnetic bias applied.

In our experiment the absorber was a 2.5 μm paramagnetic stainless steel (SS) foil with 90.6% enrichment of ^{57}Fe. For the nonabsorbing ferromagnetic drivers, 2.5 μm Ni foils were used, all of which were cut from a single sheet of polycrystalline Ni. The stainless-steel absorber was sandwiched between two Ni foils and held in rigid contact by mounting the foils between glass cover slides of 100 μm thickness. A conventional Mössbauer spectrometer, modified for rf experiments, Fig. 1, utilized a 25 mCi source in a Rh matrix to obtain the ^{57}Fe absorption spectra. The 14.4 keV gamma rays were detected with a Kr gas filled proportional counter biased with 1.8 kV.

A 25 MHz rf magnetic field was applied by mounting the foils in the cylindrical induction coil of an L-C tank circuit. In obtaining data for a direct comparison between the effect of one Ni driver versus two, the product of the applied rf power P and the electrical Q of the circuit containing the rf induction coil was maintained at constant values. Elementary analysis shows that if PQ is constant the rf current in the coil of such a circuit is also constant and hence the two absorber arrangements are subjected to applied fields of the same intensity H. The results of the first experiment verified the linearity of the first order sideband amplitudes at 25 MHz for SS with two Ni drivers with PQ products of 75, 150, and 300 W Fig. 2. The spectra are scaled so that the intensity of the central Mössbauer absorption peak of ^{57}Fe in SS is held constant in order to make direct comparisons of the sideband amplitudes.

Having established the linearity of the first order sidebands in the Ni-SS-Ni sandwich, one of the Ni drivers was removed and the experiment was repeated with the same PQ products as before. Figure 3 shows a comparison of the sideband amplitude for two Ni drivers versus one; in this configuration two Ni drivers give twice the effect of one driver foil.

In the next experiment a comparison between the effect of one source of excitation with that from two sources when both were biased with a static magnetic field. Rare earth magnets were placed about the induction coil such that the static magnetic field was mutually orthogonal to the rf magnetic field and the direction of gamma-ray propagation.

The linearity of the sideband amplitudes at 25 MHz as a function of PQ was again established (Fig. 4) to insure that the introduction of the static magnetic field did not introduce any nonlinearities to the system. The scale thus established was used to measure the decrease in the sideband amplitude when one of the sources of excitation was removed from this biased sandwich. As is clearly shown in Fig. 5, the sideband amplitudes obtained with two driver foils are four times the amplitudes obtained with one driver foil. Therefore, with the application of a static B-field, two sources of excitation give four times the effect.

The results of this reexamination of the Chien and Walker experiment support only the first conclusion reached in that original work, namely that the causitive agent of rf sidebands can be produced in a ferromagnetic layer and then transported into a nonmagnetic layer. Their other conclusion is completely refuted by this demonstration because the effects they attributed to the type of coupling between layers most probably resulted from the relative numbers of magnetic and nonmagnetic layers.

These new results go beyond the propositions tested by Chien and Walker[1] and display behaviors completely inconsistent with the traditional magne-

tostrictive-acoustic origin of Mössbauer sidebands. In experiments such as these, acoustic phonons are the bosons associated with vector fields driven by tensor forces, *not vector forces.* Without invoking stimulated emission, we can conceive of no way in which tensor sources which are physically separated can produce coherent vector fields in a space between them, even if they are temporally synchronized. The stimulated emission of phonons to produce coherent additions of the displacements arising from the different sources would imply the existence of a threshold of power, above which two modulation indices of m would give an effect of $4m^2$ and below which only $2m^2$. No such threshold was suggested by data similar to that of Fig. 5 which was obtained over an adequate range of powers.

In view of the growing number of successes of the model for the direct modulation of the phases of the nuclear states and these new results which question the validity of the conclusions of the Chien and Walker[1] experiment, it would appear that the controversy over the origin of Mössbauer sidebands must be reopened.

The authors gratefully acknowledge the support of this work by the Office of Naval Research, by the Naval Research Laboratory, and by the Innovative Science and Technology Directorate of the Strategic Defense Initiative Office.

REFERENCES

1. C. L Chien and J. C. Walker, Phys. Rev. B 13, 1876 (1976).
2. A. V. Mitin, Sov. Phys. JETP 25, 1062 (1967).
3. A. V. Mitin, Sov. Phys. Dok. 15, B27 (1971).
4. S. L. Ruby and D. I. Bolef, Phys. Rev. Lett. 5, 5 (1960).
5. G. L. Perlow, Phys. Rev. 172, 319 (1968).
6. G. Asti, G. Albanese, and C. Bucci, II Nuovo Cimento 57B, 531 (1968).
7. G. Asti, AB. Albanese, and C. Bucci, Phys. Rev. 184, 260 (1969).
8. N. D. Heiman, L. Pfeiffer, and J. C. Walker, Phys. Rev. Lett. 21, 93 (1968).
9. N. D. Heiman and J. C. Walker, Phys. Rev. 184, 281 (1969).
10. L. Pfeiffer, N. D. Heiman, and J. C. Walker, Phys. Rev. B 6, 74 (1972).
11. T. H. O'Dell, Ferromagnetodynamics (Wiley, New York, 1981), Chap. I.
12. C. W. Chen, Magnetism and Metallurgy of Soft Magnetic Materials (North-Holland, Amsterdam, 1977).
13. P. J. West and E. Matthias, Z. Phys. A 288, 369 (1978).
14. E. Ikonen, P. Helistö, J. Hietanieni, and T. Katila, Phys. Rev. Lett. 60, 643 (1988).
15. C. B. Collins and B. D. DePaola, Optics Lett. 10, 25 (1985).
16. B. D. DePaola and C. B. Collins, J. Opt. Soc. Am. B 1, 812 (1984).
17. B. D. DePaola, S. S. Wagal, and C. B. Collins, J. Opt. Soc. Am. B 2, 541 (1985).

CAPTIONS

Fig. 1: Schematic drawing of the experimental arrangement used.

Fig. 2: Experimental verification of the linearity of the first order sidebands at 25 MHz as a function of the applied rf power. The product of the applied rf power, P, and the quality factor, Q, of the circuit are used to insure reproducibility of the rf field strengths.

Fig. 3: Comparison of first order sideband amplitudes for one Ni driver foil versus two at 25 MHz with a PQ product of 300 W.

Fig. 4: Establishment of linearity of the first order sidebands at 25 MHz with PQ = 75, 150 and 300 W when the foils are biased with a static B-field.

Fig. 5: Comparison of sideband amplitudes for one driver foil versus two when both are biased by a static B-field with PQ = 300 W. Here two foils give four times the effect of one thus giving a modulation index of $4m^2$.

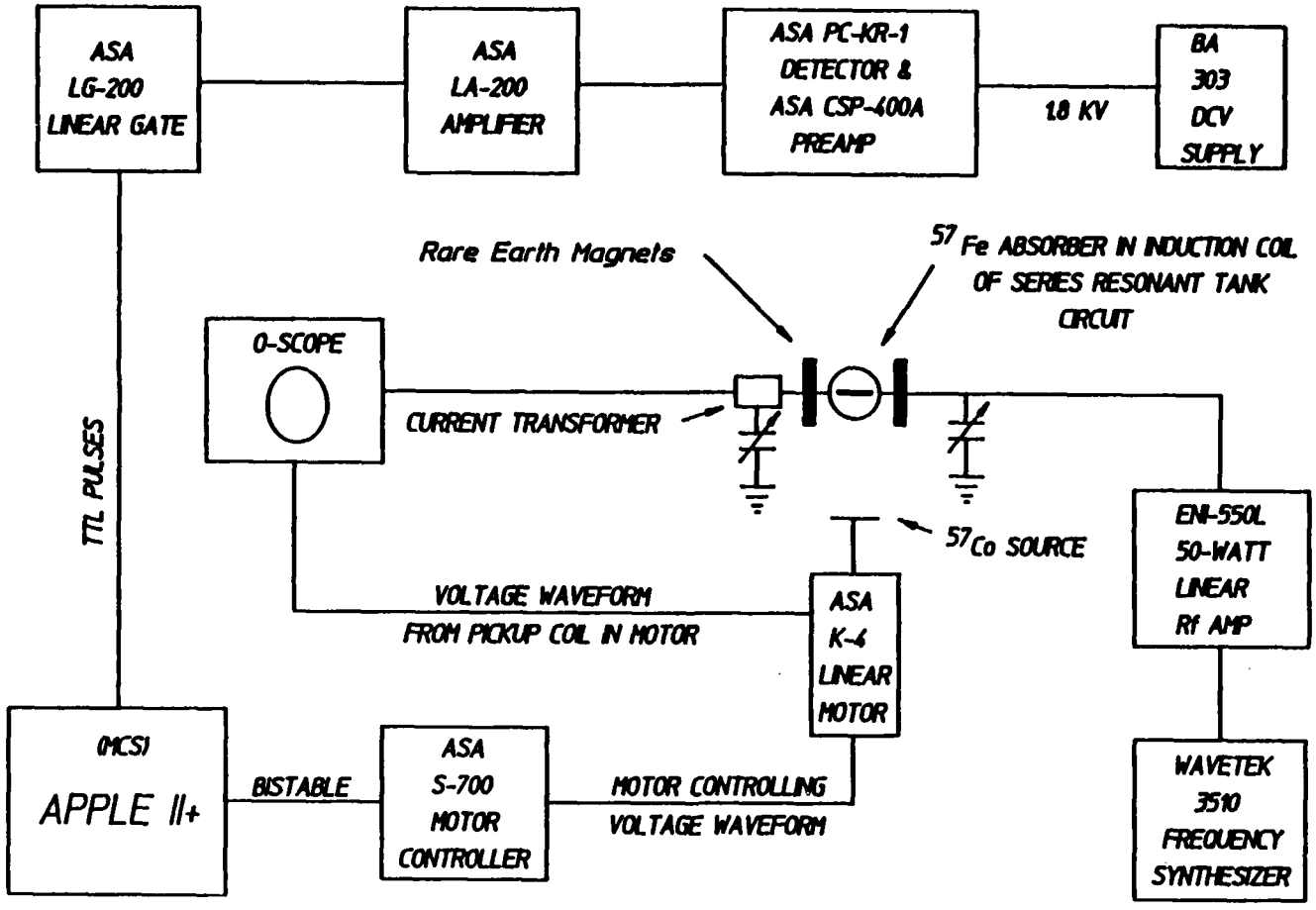
ASA
LG-200
LINEAR GATE
ASA
LA-200
AMPLIFIER
ASA PC-KR-1
DETECTOR &
ASA CSP-400A
PREAMP
1.8 KV
BA
303
DCV
SUPPLY
Rare Earth Magnets
57 Fe ABSORBER IN INDUCTION COIL
OF SERIES RESONANT TANK
CIRCUIT
O-SCOPE
CURRENT TRANSFORMER
TTL PULSES
57Co SOURCE
VOLTAGE WAVEFORM
FROM PICKUP COIL IN MOTOR
ASA
K-4
LINEAR
MOTOR
ENI-550L
50-WATT
LINEAR
Rf AMP
OMCSI
APPLE II+
BISTABLE
ASA
S-700
MOTOR
CONTROLLER
MOTOR CONTROLLING
VOLTAGE WAVEFORM
WAVETEK
3510
FREQUENCY
SYNTHESIZER

Linearity of First Order Sidebands

as a Function of Rf Power

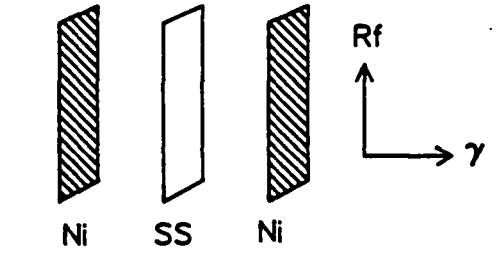

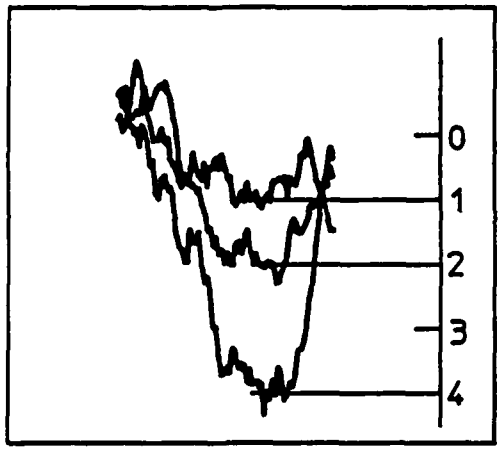

Details of First Order Sidebands

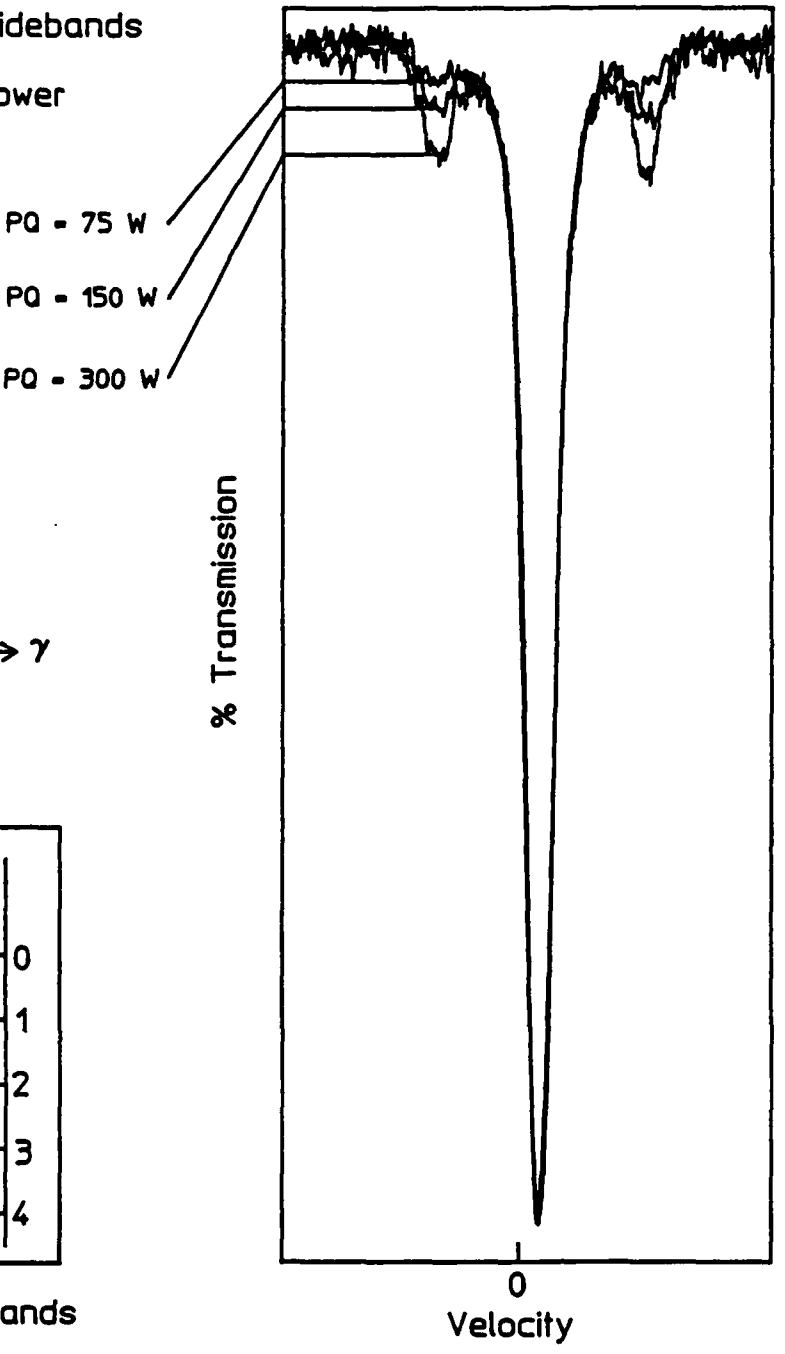

Comparison of Sideband Amplitudes
for One Driver Foil vs Two
PQ = 300 W

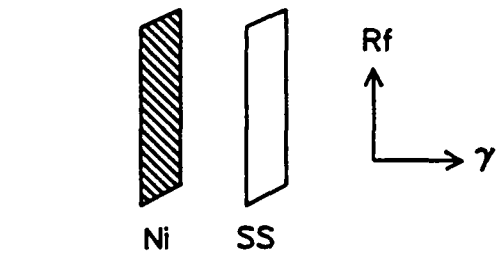

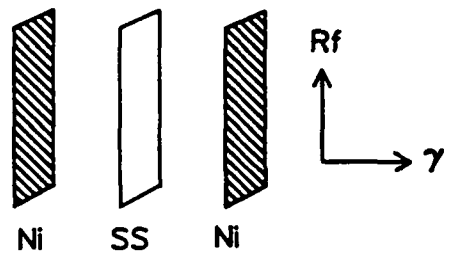

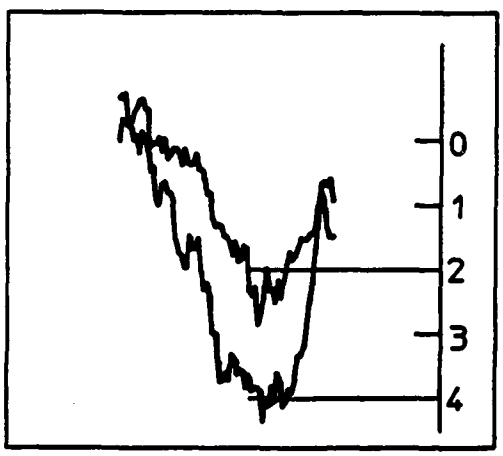

Details of First Order Sidebands

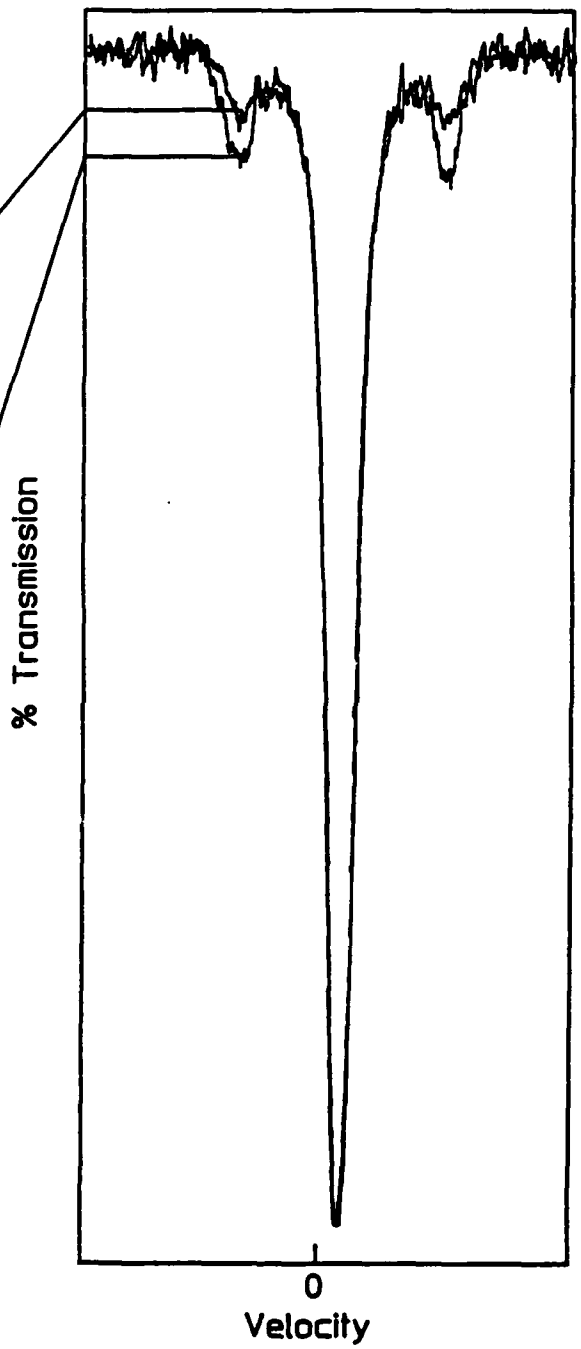

Linearity of First Order Sidebands
Under the Influence of a Static B-Field

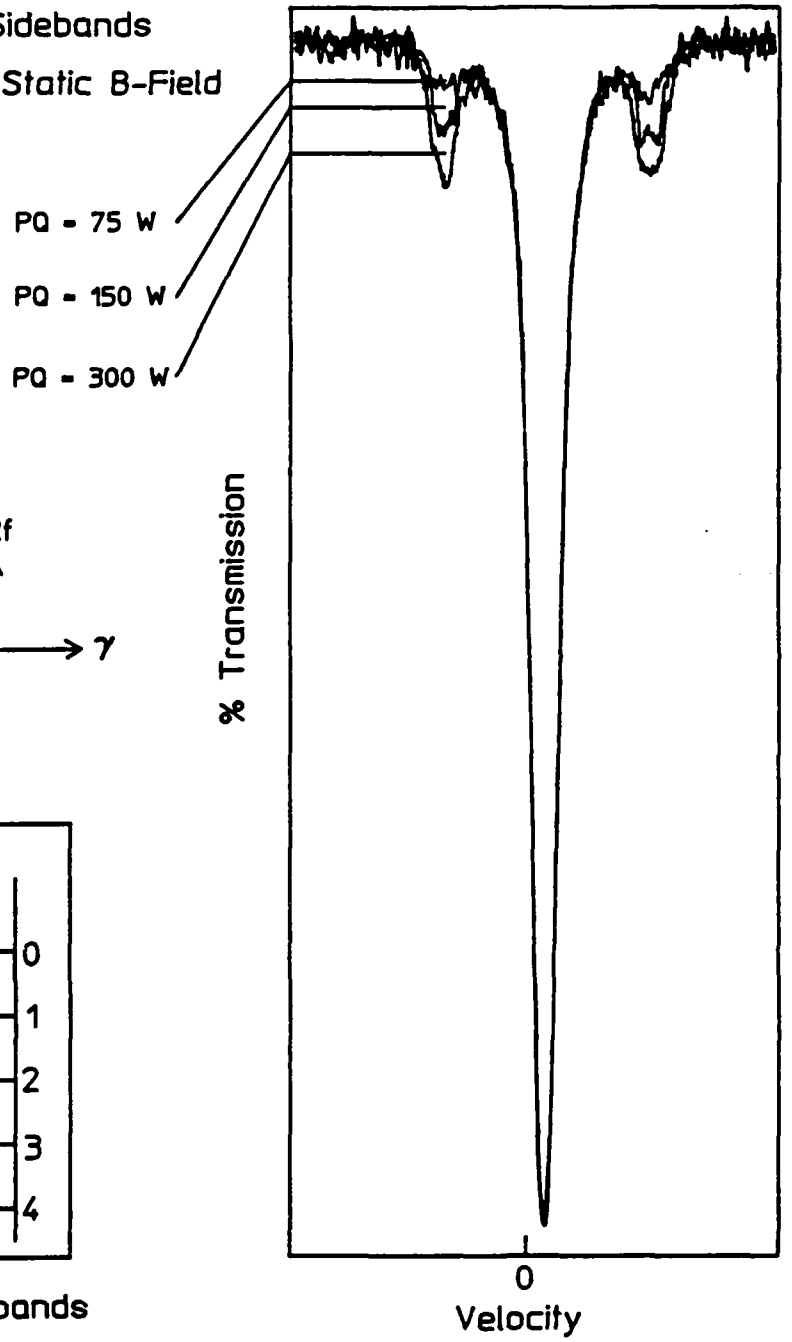

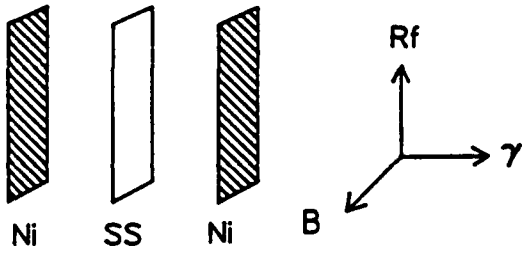

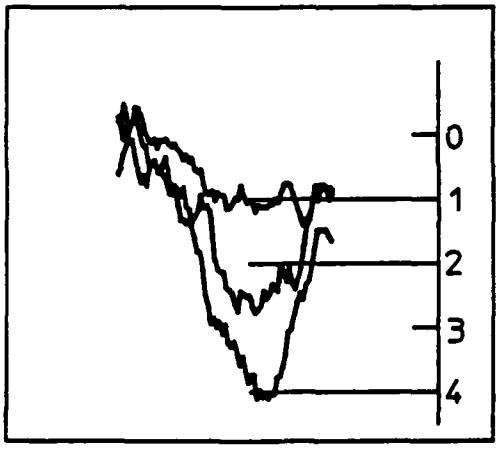

Details of First Order Sidebands

APPENDIX III

PH.D. DISSERTATION DESCRIBING DETAILS OF THE MAJOR MILESTONE ACHIEVEMENT OF 1988

T. W. Sinor, Observation of Large Scale Nuclear Phase Modulation Effects, (unpublished Ph.D. Thesis, University of Texas at Dallas, 1989).

OBSERVATION OF LARGE SCALE NUCLEAR PHASE MODULATION EFFECTS

by

TIMOTHY WAYNE SINOR, B. S., M. S.

DISSERTATION

Presented to the Faculty of

The University of Texas at Dallas

in Partial Fulfillment

of the Requirements

for the Degree of

DOCTOR OF PHILOSOPHY IN PHYSICS

THE UNIVERSITY OF TEXAS AT DALLAS

DECEMBER, 1988

OBSERVATION OF LARGE SCALE NUCLEAR PHASE MODULATION EFFECTS

Publication No._____

Timothy Wayne Sinor, Ph.D.

The University of Texas at Dallas, 1988

Supervising Professor: Carl B. Collins

The excitation of coherent transients in Mössbauer spectra has been previously limited to a low range of frequencies by the high powers required to modulate the nuclear phases. Reported here is an eleven-orders-of magnitude increase in the efficiency through which such phenomena can be produced. Magnetic modulation of the quantum phases of ^{57}Fe nuclei in paramagnetic media has been produced by spin waves of large amplitude transported from ferromagnetic sources. Excited on one end by the oscillating magnetization of a strip of ferromagnetic Ni, the absorber foil showed the strong development of sidebands at the other end where mechanical vibrations were shown to contribute less than 1% of the signal. In these experiments the driving amplitude, H_0 in the Ni was only 0.07 mT while the frequency was 23.74 MHz.

It was further demonstrated that spin waves can transport nuclear phase modulation effects through a paramagnetic bridge which connects physically separated Ni source foils and the ^{57}Fe enriched stainless which was used to detect the effect. It was found that sidebands resulting from nuclear phase modulation are not observed in the Mössbauer absorption spectra of ^{119}Sn when thin foils of diamagnetic tin are used as the absorber. However, the effect can be observed by embedding the tin nuclei into

ferromagnetic or antiferromagnetic materials. This was demonstrated in the magnetic compounds $FeSn_2$ and NiSn.

It was also demonstrated that large scale nuclear phase modulation was a dominant effect in nonmagnetostrictive permalloy and that the effect correlated with the high permeability of these magnetically soft materials.

TABLE OF CONTENTS

LIST OF ILLUSTRATIONS

LIST OF TABLES

CHAPTER 1

INTRODUCTION

The discovery by Mössbauer[1] that gamma-rays can be resonantly emitted and absorbed by nuclei bound in a crystal made possible the direct observation of many phenomena formerly thought to be unmeasurable. The terrestrial measurement of the gravitational red shift,[2,3] the testing of the equivalence principle for rotating systems,[4] and the observation of nuclear hyperfine interactions[5,6] are but a few of the experiments made feasible by the Mössbauer effect.

Mössbauer's observation is attributed to the fact that in the case of a nucleus bound in a crystal a gamma-ray can be emitted or absorbed without any measurable transfer of energy to or from the lattice. This means that neither thermal motion nor recoil can broaden or displace such transitions in energy. The high Q of such resonances, approximately 10^{12} for ^{57}Fe, provides photons of well defined energy which are useful for probing phenomena involving very small energies. In this way Mössbauer spectroscopy can provide a highly detailed account of the way in which the nucleus interacts with its environment. It is only through the existence of the Mössbauer effect that a practical source of very narrow line radiation can be produced, and with such a source very small changes in frequency can be measured.

With Mössbauer techniques there is sufficient frequency resolution that spectral changes produced by ultrasonic and magnetic perturbations to the nucleus can be observed in the short wavelength limit where quantum effects are dominant. For example, consider a classical emitter of radiation which has a negligible recoil energy. If the source is made to oscillate harmonically about some point with an amplitude x_0 and a frequency Ω, the emitted electromagnetic wave can be Fourier analyzed into a

component with frequency ω_0 and "sidebands" at frequencies $\omega_0 \pm n\Omega$ where n = 1, 2,...,. From a quantum viewpoint, this mechanical vibration of the nuclei generates a sharp peak in the phonon spectra of the solid at the oscillation frequency. The emission of the Mössbauer gamma-ray is then accompanied by the emission or absorption of n phonons, with the resulting gamma-ray spectrum consisting of a central absorption line accompanied by equally spaced sidebands.

In 1960, during their efforts to utilize Mössbauer spectroscopy as a tool to study the phonon spectra of solids, Ruby and Bolef[7] demonstrated the feasibility of producing ultrasonic sidebands to the single absorption line of ^{57}Fe in stainless-steel. These ultrasonic sidebands were produced by mounting the Mössbauer source onto a quartz transducer which was excited at megahertz frequencies. In addition, the source-transducer assembly was simultaneously driven at low frequencies (15 Hz) to tune the absorption in and out of resonance with the Doppler shifts produced by the lower frequency motion. With the use of a stainless-steel absorber, they were able to obtain spectra which consisted of a central unshifted absorption line accompanied by symmetrically located sidebands occurring at integral multiples of the ultrasonic driving frequency. Subsequent experiments similiar to those of Ruby and Bolef's have been performed by Burov et al.,[8] using ^{119}Sn and by Cranshaw and Reivari[9] with ^{57}Fe. Classical frequency modulation theory successfully predicts both the intensity and position of these ultrasonically induced sidebands as will be presented in Chapter 2.

Eight years after the initial observation of ultrasonic sidebands it was found that when either a ferromagnetic source or absorber was subjected to a magnetic field oscillating at radiofrequencies additional lines appeared in the gamma ray spectra. The resulting pattern of lines strongly resembled the sidebands that had been produced earlier by the ultrasonic effects. Since these rf sidebands were initially observed in ferromagnetic materials, they were incorrectly explained as ultrasonic sidebands driven

by the magnetostrictive oscillations of the source or absorber foils when exposed to an oscillating rf magnetic field.

More recently, some variations in the recoilless gamma-ray spectra have been reported[10] to result from direct modulation of the interaction energies arising from the couplings of the nuclear magnetic moments to the hyperfine fields. Described in terms of the phase modulation of the nuclear states involved in the transition,[10] those results demonstrate that even the earlier rf effects reported in ferromagnetic materials could have been the result of this type of phase modulation. It was not necessary to associate them with the time dependent magnetostrictive oscillations of the source or absorber foils.

This dissertation reports a reexamination of the question of radiofrequency sidebands and demonstrates that the effect arises from a direct interaction of the rf magnetic field with the energy levels of the nucleus and that magnetostriction effects produce a negligible contribution to the sideband intensities.

Literature Survey

Radiofrequency (rf) sidebands in Mössbauer spectroscopy, a well documented yet poorly understood phenomena, was first proposed in 1967 by Mitin,[11,12] who predicted that Mössbauer transitions could be excited as the result of a multiphoton interaction for nuclei immersed in intense radiofrequency fields. In cases where there was the simultaneous absorption of a gamma ray quantum under Mössbauer conditions and a quantum of the external radiofrequency field, the Mössbauer spectrum was predicted to show each recoilless gamma transition to be accompanied by sum and difference frequency lines displaced from it by integral multiples of the frequency of the applied rf field. In appearance these multiphoton spectra were expected to strongly resemble the transmission spectra obtained by Ruby and

Bolef[7] by imposing periodic Doppler shifts of mechanical origin on the source. This unfortunate similiarity between two phenomena arising from completely different origins subsequently provided years of critical controversy.

When radiofrequency sidebands were initially observed, they were seen only in ferromagnetic materials where there exists a coupling between the magnetic and elastic energy of the lattice. In such materials there are time dependent magnetostrictive oscillations when they are subjected to rf magnetic fields. Therefore, sidebands observed in ferromagnetic materials could possibly contain a certain contribution due to mechanical frequency modulation, as well as to multiphoton gamma-transitions. It is precisely this combination of effects which has led to considerable controversy as to the dominant mechanism producing the rf sidebands which have been observed in ferromagnetic media.

The earliest experiment investigating the influence of radiofrequency magnetic fields on Mössbauer transitions was reported by Perlow[13] in 1968. In this experiment, Perlow subjected several ^{57}Co sources which radiated the 14.4-keV transition of ^{57}Fe to intense magnetic fields oscillating at radiofrequencies. He was able to demonstrate the destruction of the Mössbauer hyperfine pattern by the action of the rf field. Even though rf sidebands were unresolved, Perlow attributed the observed change in the recoilless absorption to the random flipping of the hyperfine field due to domain wall motion.

It was later in 1968 that Heiman, Pfeiffer, and Walker[14] reported the first clear evidence of radiofrequency sidebands in ^{57}Fe as a result of subjecting an iron foil absorber rather than a source to an rf field. In addition to the usual six-line Zeeman pattern of ^{57}Fe, a set of sidebands were observed at energies $\hbar\omega_\gamma \pm n\hbar\omega_{rf}$, where $\hbar\omega_\gamma$ is the energy of the resonant gamma-radiation. Heiman et al.,[14] interpreted the additional lines as acoustically modulated sidebands arising from time-dependent

magnetostrictive oscillation within the foil and dismissed the possibility that the sidebands resulted from multiphoton processes. A later paper by the same authors[15] provided considerable experimental evidence supporting the magnetostrictive hypotheses. However, these results were challenged by other researchers in the field because the magnetostrictive-acoustic theory did not quantitatively predict the observed sidebands intensities in terms of a single modulation index which would be a measure of the sideband development.[16] In order to get reasonable predictions of the sideband intensities, it was necessary to postulate a large acoustic Q for these samples that provided a remarkable amplification of the vibrational amplitude of the acoustic vibrations inside the foil.[17]

It was the experiment reported by Chien and Walker[18] which gave the most compelling evidence in favor of the magnetostrictive-acoustic theory as an explanation of rf sidebands in ferromagnetic materials. In that experiment a composite absorber composed of ferromagnetic and nonmagnetic layers was used to study the transport of the causitive agent from the ferromagnetic layer into the nonmagnetic region where the sidebands were observed upon Mössbauer transitions of the ^{57}Fe nuclei. Very clear evidence showed that the cause did arise in the ferromagnetic nickel layers producing sidebands in the nonmagnetic stainless steel layers. The most ready explanation at that time was a transport of phonons from one layer to the next with a high acoustic Q, but as will be shown in this dissertation, this explanation is inadaquate and does not explain the new experimental evidence to be presented.

The possibility that rf sidebands might be produced by modulating the interaction energies of the nucleus with an rf field were all but dismissed until 1978 when West and Mattias[19] observed first-order sidebands from a single parent line by subjecting a non-magnetic ^{181}W Mössbauer source of the 6.2-keV line of ^{181}Ta to a strongly oscillating field of up to 230 Oe amplitude at a frequency of about one megahertz. The appearance of the

sidebands was due to the modulation of the interaction energy between the applied radiofrequency magnetic field and the nuclear magnetic moments of the two states of ^{181}Ta, linked by the 6.2-keV transition. The sideband positions, and intensities agreed well with theoretical analysis, assuming a pure magnetic interaction, and successfully yielded the g-factor ratio of the nuclear states involved in the transition that was in good agreement with values obtained by other techniques.[19] The results of that experiment, however, have not been widely accepted because the sidebands were obscured by the dispersive shape of the unperturbed Mössbauer resonance.

More recently, time-resolved Mössbauer spectroscopy[10] (TMS) has been used to analyze the influence of a periodically varying magnetic field on the high resolution Mössbauer resonance of ^{67}Zn in order to unambiguously demonstrate the pure magnetic phase modulation of the nuclear Zeeman levels in diamagnetic ZnO. This benchmark experiment required magnetic field amplitudes as large as 13.4 mT for sinusoidal modulation at applied frequencies, ω, of 10 kHz. In a complimentary frequency domain experiment where the time average of the recoilless gamma-radiation was measured, the Mössbauer spectrum resulting from magnetic phase modulation effects showed each absorption line to be split into an infinite set of sidebands displaced apart from it by integral multiples of the applied driving frequency. In essence, a Mössbauer spectrum resulting from magnetic phase modulation effects is identical in appearence to the ultrasonic and radiofrequency sidebands previously reported in the gamma-resonance spectrum of ^{57}Fe.

Since magnetic phase modulation effects were reported to scale as $(H_0/\omega)^2$, it would appear that such studies cannot be extended to nuclear systems with transition widths much greater than that of ^{67}Zn through a simple extension of efforts. The conceptual key to orders-of-magnitude enhancement of the phase modulation effects was developed in a series of three papers by Depaola and Collins[20-22] in 1984. In a critical reexamina-

tion of the phenomenology of rf sidebands in a ferromagnetic material, they suggested that the effect could be enhanced by the use of smaller powers used to manipulate the hyperfine magnetic fields arising from the natural correlations of the individual spins in ferromagnetic materials. The magnetization of the sample was then controlled by the internal magnetic field B_0 and by a perpendicular radiofrequency field B_{rf}. In this way the applied radiofrequency field could be enhanced at the nuclear sites by the ratio of the hyperfine magnetic field to the static field B_0.

Summary

Even though a tremendous amount of literature has been published on radiofrequency sidebands in ferromagnetic materials, a comprehensive understanding of their origins remains elusive. It has been the goal of this work to investigate and characterize certain phenomenological aspects of radiofrequency sidebands in two Mössbauer isotopes, ^{57}Fe and ^{119}Sn, in an effort to provide new insights into the origins of these controversial sidebands. To this end three specific series of experiments were performed.

In the first set of experiments, use was made of the well known fact that foils composed of alternating layers of ferromagnetic and nonmagnetic materials immersed in a radiofrequency field will display sidebands on the Mössbauer nuclei contained in the nonmagnetic layer (following the technique of Chien and Walker[18]). Using the concept of a modulation index, which is a measure of the strength of sideband development, this first experiment demonstrated that the sideband intensity measured as a function of the applied rf power scaled as the square of the number of sources, an observation not consistent with the magnetostrictive hypothesis.

Continuing this series, the next experiment was another direct attack of the magnetostrictive hypothesis. In this experiment we presented clear

evidence of radiofrequency modulation of the hyperfine fields of ^{57}Fe in a nonmagnetostrictive iron-nickel alloy. Such alloys, or permalloys as they are called, are of great scientific and technical interest because of their unusual magnetic properties. In particular, the magnetostriction of a polycrystaline permalloy passes through zero when the composition of the permalloy approaches 81 percent nickel.[23,24] At this critical composition in well annealed alloys, hystersis losses are at a minimum and the permeability is nearly maximum. Making use of two professionally prepared permalloy foils with compositions near the magnetostrictive null, this experiment demonstrated that the appearence of sidebands in these ferromagnetic iron-nickel alloys correlated with their permeability and not with their magnetostrictive properties.

The second series of experiments was performed using ^{119}Sn as the Mössbauer isotope. Pure tin, which is diamagnetic, can be readily alloyed with nickel and iron to form ferromagnetic and antiferromagnetic compounds. These alloys allowed a direct comparision of sideband behavior in materials with different magnetic properties.

The third and final series of experiments dealt with the transport properties of ultrasonic and radiofrequency sidebands. Here it was demonstrated conclusively that rf sidebands induced in paramagnetic materials via an interaction with a ferromagnetic driver are the result of spin waves propagating in the absorber foil. These spin waves interact with the nucleus and the net effect is to induce sidebands upon the Mössbauer transitions of the nucleus by modulating the phases of the nuclear states.

REFERENCES

1. R. L. Mössbauer, Z. Physik 151, 124 (1958).
2. R. V. Pound and G. A. Rebka, Jr. Phys. Rev. Letters 4, 337 (1960).
3. T. Katila and K. J. Riski, Phys. Lett. 83A, 51 (1981).
4. H. J. Hay, J. P. Schiffer, T. E. Cranshaw and P. A. Egelstaff, Phys. Rev. Letters 4, 165 (1960).
5. R. V. Pound and G. A. Rebka, Jr. Phys. Rev. Letters 3, 554 (1959).
6. S. S. Hanna, J. Heberle, C. Littlejohn, G. J. Perlow, R. S. Preston and D. H. Vincent, Phys. Rev. Letters 4, 177 (1960).
7. S. L. Ruby and D. I. Bolef, Phys. Rev. Lett. 5, 5 (1960).
8. V. A. Burov, V. A. Krasil'nikov, and O. Yu. Sukharevskaya, Sov. Phys. JETP 43, 837 (1962).
9. T. E. Cranshaw and P. Reivari, Proc. Phys. Soc., 90, 1059 (1967).
10. E. Ikonen, P. Helistö, J. Hietanieni, and T. Katila, Phys. Rev. Lett. 60, 643 (1988).
11. A. V. Mitin, Sov. Phys. JETP 25, 1062 (1967).
12. A. V. Mitin, Sov. Phys. Dok. 15, B27 (1971).
13. G. L. Perlow, Phys. Rev. 172, 319 (1968).
14. N. D. Heiman, L. Pfeiffer, and J. C. Walker, Phys. Rev. Lett. 21, 93 (1968).
15. L. Pfeiffer, N. D. Heiman, and J. C. Walker, Phys. Rev. B 6, 74 (1972).
16. G. Asti, AB. Albanese, and C. Bucci, Phys. Rev. 184, 260 (1969).
17. N. Heiman, R. K. Hester, and S. P. Weeks, Phys. Rev. B 8, 8 (1973).
18. C. L Chien and J. C. Walker, Phys. Rev. B 13, 1876 (1976).
19. P. J. West and E. Matthias, Z. Phys. A 288, 369 (1978).
20. C. B. Collins and B. D. DePaola, Optics Lett. 10, 25 (1985).
21. B. D. DePaola and C. B. Collins, J. Opt. Soc. Am. B 1, 812 (1984).

22. B. D. DePaola, S. S. Wagal, and C. B. Collins, J. Opt. Soc. Am. B 2, 541 (1985).

23. L. W. McKeehan and P. P. Cioffi, Phys. Rev. 28, 146 (1926).

24. M. Kersten, Z. tech Physik, 12, 665 (1931).

CHAPTER 2

THEORY

THE MÖSSBAUER EFFECT: AN OVERVIEW

The Mössbauer effect can be readily described by considering a nucleus which decays from some excited state to its ground state by the emission of a gamma-ray. The recoil energy of the nucleus, E_r, reduces the energy of the gamma-ray and also serves to increase the Doppler broadening of the line due to the thermal motions of the nuclei. The recoil energy of the nucleus is given by

$$E_r = E_\gamma^2/2Mc^2 \quad , \tag{2.1}$$

where E_γ is the transition energy, M is the mass of the nucleus, and c is the speed of light.

According to the Debye theory of specific heat,[1] a solid may be considered to consist of a large number of linear oscillators with a distribution of frequencies ranging from zero to some maximum frequency ω_D; the total number of oscillators being equal to 3N, where N is the number of atoms in the solid. If the recoil energy of the nucleus is less than the quantum of energy necessary to excite the oscillator to the next higher energy level, the gamma-ray may be emitted without recoil. The probability of such recoilless emission is, in most cases, governed by the Debye-Waller factor, a familiar quantity in the theory of x-ray and neutron scattering. The Debye-Waller fraction[2,3] is given by the Debye model as

$$f = \exp\ (-3E_r/2k_B\Theta_D);\ T \ll \Theta_D \quad , \tag{2.2}$$

$$f = \exp\ (-6E_rT/k_B\Theta_D^2);\ T > \Theta_D \quad , \tag{2.3}$$

where T is the absolute temperature, k_B is the Boltzman constant and θ_D is the Debye temperature. The Debye temperature, which is a measure of the stiffness of the lattice, is defined by the expression $\hbar\omega_D = k_B\theta_D$.

Practical considerations dictate that to observe the Mössbauer effect it is necessary to have $E_r < k\theta_D$, where $k = 2\pi/\lambda$. This condition requires the emitted gamma-rays to be of relatively low energy and the material in which the Mössbauer nuclei are embedded to have a high Debye temperature. Typical Debye temperatures are on the order of a few hundred degrees Kelvin (θ_D = 470 K for Fe and 200 K for Sn) while typical gamma-ray energies used in Mössbauer spectroscopy lie between 10-100-keV (E_γ = 14.4-keV for ^{57}Fe and 23.875-keV for ^{119}Sn). To date the Mössbauer effect has been observed in over 100 nuclei.[3] The best known are ^{57}Fe and ^{119}Sn, both of which have large recoilless fractions at room temperature.

Although experiments involving the Mössbauer effect can be performed with either a transmission or a scattering geometry, only the former is of interest for the current research. A typical transmission experiment consists of measuring the intensity of the resonance radiation passing through the absorber as a function of the relative velocity between the source and absorber. Because of the Doppler shift in energy produced by such a velocity, a resonance line shape is traced out.

In the work being presented here, two Mössbauer isotopes were used: ^{57}Fe and ^{119}Sn. The energy level diagram of the nuclear emission for ^{57}Fe is shown in Figure 2.1a. The gamma-ray source is ^{57}Co, in either a Pd or Rh lattice. It decays by electron capture into an excited state of ^{57}Fe, with its 3/2 - 1/2 transition emitting a 14.4-keV gamma-ray as seen in Figure 2.1a. This transition is very long-lived by nuclear standards with a mean lifetime, τ of 1.4×10^{-7} sec. From Heisenberg's uncertainty principle; $\Delta E = \Gamma = \hbar/\tau$, the natural line width of the transition is $\Gamma = 5 \times 10^{-9}$ eV. Since the ratio of the natural line width and the photon energy, E_γ/Γ is a measure of the accuracy of the determination of the relative frequency or

Figure 2.1

Energy level diagram for a ^{57}Co source and ^{57}Fe absorber showing (a) the emission process for the 14.4-keV gamma-ray and (b-d) static perturbations of the nuclear energy levels. Note: In (b-d) the energy scale is about 10^{13} smaller than in (a).

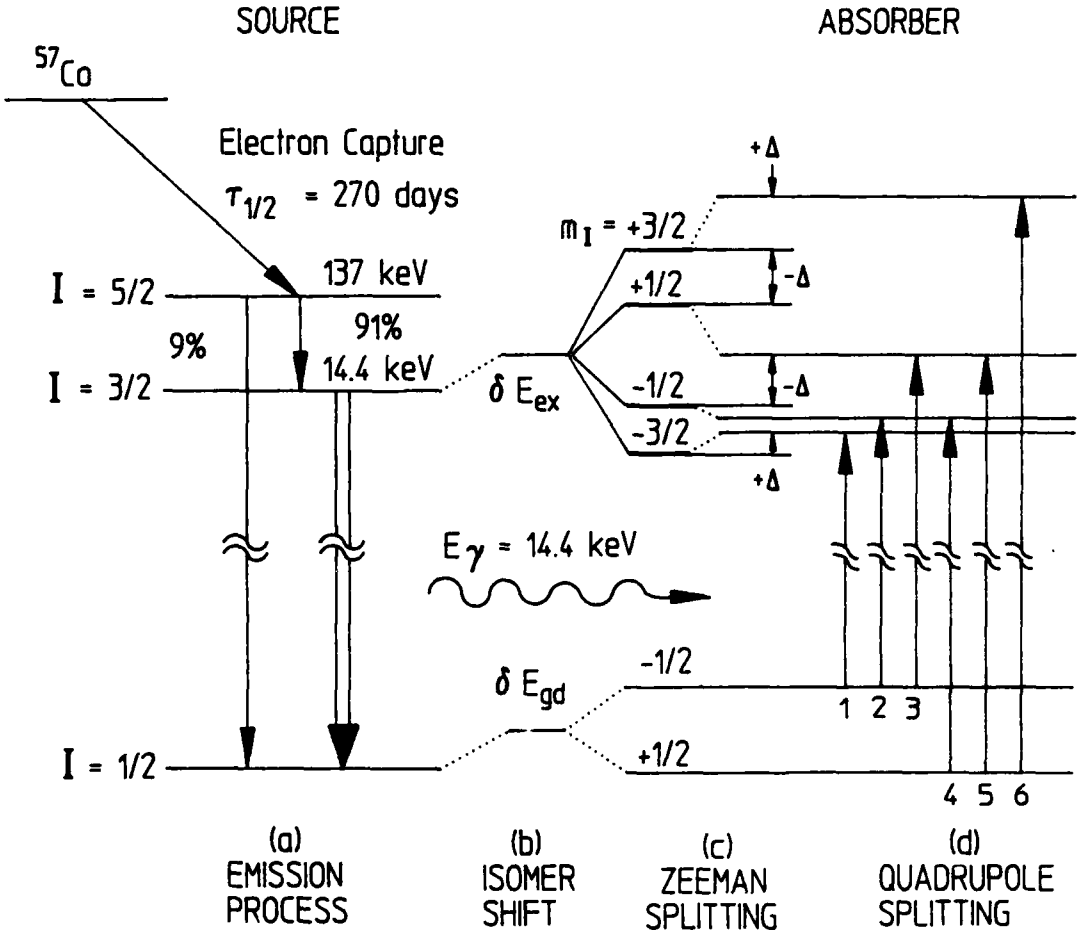
SOURCE
ABSORBER
^{57}Co
Electron Capture
$\tau_{1/2}$ = 270 days
137 keV
I = 5/2
9%
91%
14.4 keV
I = 3/2
δE_{ex}
m_I = +3/2
+1/2
-1/2
-3/2
+Δ
-Δ
-Δ
+Δ
E_γ = 14.4 keV
δE_{gd}
-1/2
+1/2
I = 1/2
1 2 3
4 5 6
(a) EMISSION PROCESS
(b) ISOMER SHIFT
(c) ZEEMAN SPLITTING
(d) QUADRUPOLE SPLITTING

energy changes of the system, the 14.4-keV transition is sharply defined with $E_\gamma/\Gamma = 2.9 \times 10^{12}$.

In Pd or Rh lattices the 14.4-keV transition can emit its gamma-ray without recoil in about 80% of the cases; therefore, resonant absorption can occur when the nuclear energy levels of the source and absorber match. With the frequency of the photon so well-defined, the Doppler effect (i.e., moving the source relative to the absorber) can be used to tune the absorption in and out of resonance with respect to the source. The relative velocity of the source to the absorber in order to scan a full width, 2Γ, of the gamma-ray line is given by the Doppler shift

$$E_D = (v/c)E_\gamma \cos\alpha \quad , \tag{2.4}$$

where E_γ is the gamma-ray energy, v is the relative velocity of the source and absorber, and α is the angle between the velocity direction and the direction of the gamma-ray propagation.

Since a Mössbauer spectrum is obtained by determining the intensity of the gamma radiation that reaches the detector as a function of the Doppler modulating velocity, the spectrum can be represented by a plot of intensity verses velocity. Under ideal conditions the velocity-dependent intensity is given by

$$I(v) = I(0) \frac{\Gamma^2/4}{(v-v_0)^2 + \Gamma^2/4} \quad , \tag{2.5}$$

where I(0) is the intensity of the resonance peak when the energies of the emitted and absorbed gamma-ray are equal, v is the Doppler velocity, v_0 is the velocity at the resonance maximum and Γ is the full width of the absorption peak at one-half the maximum intensity (FWHM).

In terms of the resonant cross-section the energy distribution of the emission or absorption line has a Breit-Wigner or Lorenzian line shape given by

$$\sigma(E) = \sigma_0 \frac{(\Gamma^2/4)}{(E-E_\gamma)^2 + (\Gamma^2/4)} \quad . \tag{2.6}$$

The total cross section, σ_0, for the absorption of nuclear radiation is given by

$$\sigma_0 = \frac{\lambda}{2\pi} \frac{2I_e+1}{2I_g+1} \frac{1}{\alpha_t+1} \quad , \tag{2.7}$$

where $k = 2\pi/\lambda$, and α is the total internal conversion coefficient for the gamma transition. The quantity $(2I_e+1)/(2I_g+1)$ is a statistical factor which is simply the ratio of the degeneracy of the excited to the ground state where I_e and I_g are the spins of the excited and ground states of the gamma transition. The quantity $1/(1+\alpha)$ gives the fraction of transitions which occur by the emission of a gamma photon. Since the emission and absorption resonances have the same line shape, the experimentally observed spectrum is a convolution of the source and absorber lines with a full width at half maximum (FWHM) of 2Γ.

In order to extract as much information as possible from a Mössbauer spectrum, there are two important features that must be understood. The first is why the resonance may be shifted between source and absorber by some finite, non-zero value of the velocity. The second is why the spectra from two level transitions are often composed of a number of resonance lines instead of just a single line.

In a Mössbauer spectrum the change in the position of a resonance line, or the center of a resonance pattern, is called the isomer shift. It is due to the electrostatic interaction of the nucleus with the electron charge density at the nucleus and can be considered an electric monopole interaction as shown in Figure 2.1b. More specifically, the excited and ground state nuclei differ in radius by a small yet significant amount (about 0.02% in ^{57}Fe). It is this change in the radius of the nucleus which causes the electrostatic interaction between the nucleus and the surrounding electrons to change upon excitation of the nucleus. If the Mössbauer nuclei in the source and absorber are in different chemical environments so that different electron distributions are experienced, the isomer shift is given by

$$I.S. = \frac{2\pi}{5} Ze^2[|\Psi_a(0)|^2 - |\Psi_s(0)|^2](R_e^2 - R_g^2) \quad , \quad (2.8)$$

where $|\Psi(0)|^2$ is the electron charge density at the nucleus, and R_e and R_g are the effective radii of the excited and ground state nuclei, respectively.

The fine structure of the Mössbauer spectrum arises from two principle static interactions; the magnetic dipole and electric quadrupole interactions, as shown in Fig. 2.1c and 2.1d, respectively. Since both the excited and ground states of ^{57}Fe and ^{119}Sn have non-zero nuclear spin, the magnetic dipole moment of the nucleus can interact with a magnetic field H, to produce a nuclear Zeeman effect, splitting the nuclear levels with spin I (I > 0) into (2I + 1) sublevels, with eigenvalues

$$E_m = -\mu_N H m_I / I = -g_N \beta_N H m_I \quad , \quad (2.9)$$

where m_I is the magnetic quantum number with values $m_I = I, I-1, \ldots, -I$, H is the magnetic field intensity at the site of the nucleus and μ_N is the

nuclear magnetic dipole moment. The nuclear magnetic moment is related to the nuclear Bohr magneton, β_N by the Lande' factor, g_N defined by the relation $\mu_N = g_N\beta_N I$. In the case of ^{57}Fe, which has a 330 kOe internal magnetic field, the absorption spectrum is split into six lines as shown in Figure 2.2. One of the most important applications of the Mössbauer effect has been the observation of this nuclear Zeeman interaction which can, in principle, be studied in practically all cases simply by placing either the source or the absorber in a field of convenient size while observing the splitting of the resonant line.

The electric quadrupole interaction is the interaction of the nuclear quadrupole moment, Q, with the gradient of the electrostatic field at the nucleus as shown in Figure 2.1d. The nuclear quadrupole moment arises from the deviation of the nucleus from a spherical symmetry;[2] hence, Q = 0 for nuclear spin states I = 0 or 1/2, but Q is non-zero for the 14.4-keV state of ^{57}Fe. However, the quadrupole interaction is much smaller than the magnetic splitting of interest in this work and, therefore, can be neglected.

MECHANICAL FREQUENCY MODULATION

Ruby and Bolef[4] were the first to produce frequency modulated sidebands in Mössbauer spectra. They did so by mechanically vibrating the source with a piezoelectric quartz transducer which was made to oscillate at megahertz frequencies. Several other investigations of frequency modulated sidebands have since been reported.[5-8]

The formalism of frequency modulated sidebands produced by periodic Doppler shifts is as follows. Consider a source of electromagnetic radiation which is made to execute a simple harmonic motion with frequency, Ω, and amplitude x_0. The time dependent displacement of the nucleus from its equilibrium position is given by

Figure 2.2

Mössbauer absorption spectrum of an iron foil enriched with ^{57}Fe. The six lines observed are the result of a magnetic dipole interaction. The separation of the outermost lines is ± 5.3 mm/sec while the innermost lines are separated by ± 0.84 mm/sec.

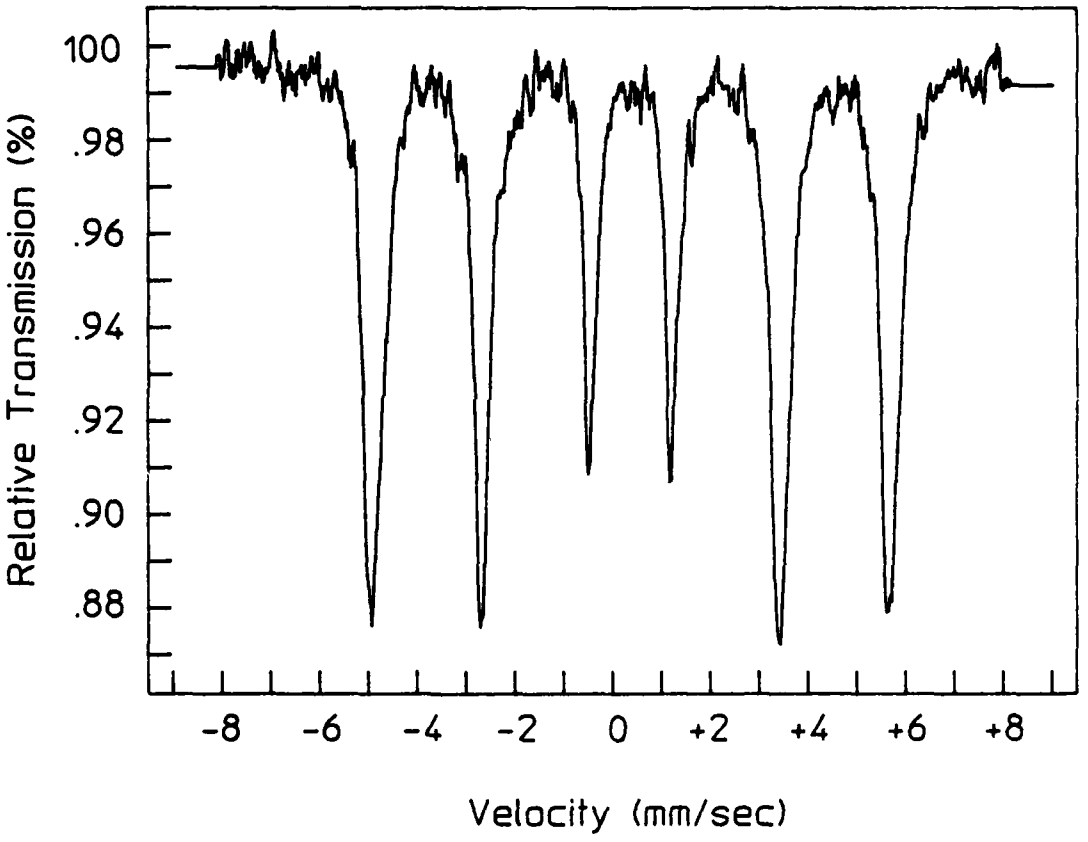
Relative Transmission (%)
100
.98
.96
.94
.92
.90
.88
-8
-6
-4
-2
0
+2
+4
+6
+8
Velocity (mm/sec)

$$x(t) = x_0 \sin\Omega t \quad . \tag{2.10}$$

The resulting time dependence of the recoilless gamma radiation as observed in the transmission through a resonant absorber has been given to be[9]

$$E(t,t_0) = \lambda^{1/2}\exp[i(\omega_0 t + a\sin\Omega t) - (\lambda/2)(t-t_0) \quad , \quad \begin{matrix} t \geq t_0 \\ t < t_0 \end{matrix} \tag{2.11}$$

where the constant $\lambda (= \tau^{-1} = \Gamma/\hbar)$ is the reciprocal of the mean lifetime of the decaying state, ω_0 is the frequency of the unperturbed radiation and $a = \omega_0 x_0/c$ is called the modulation index. Choosing the formation of the excited state to occur at time $t_0 = 0$ the observed intensity of the emitted radiation is proportional to the absolute square of the its amplitude: Eq. (2.11) shows that I(t) is given by

$$I(t) \propto |E(t)|^2 = \lambda e^{-\lambda t} = \lambda e^{-\Gamma t/2\hbar} \quad , \tag{2.12}$$

However, since the wave is not monotonic, the frequency distribution of the wave is obtained by expanding E(t) as

$$E(t) = (2\pi)^{-1/2} \int_{-\infty}^{\infty} d\omega \Phi(\omega) e^{i\omega t} \quad . \tag{2.13}$$

The term $\Phi(\omega)$ gives the weight with which the frequency ω appears in E(t).

Fourier inversion gives

$$\Phi(\omega) = (2\pi)^{-1/2} \int_{-\infty}^{\infty} dt E(t) e^{i\omega t} \quad , \tag{2.14}$$

or with Eq. (2.11), along with the Jacobi-Anger Bessel function identity;

$$e^{ia\sin\Omega t} = \sum_{n=0} J_n(a)e^{in\Omega t} \quad , \tag{2.15}$$

after integeration yields

$$\Phi(\omega) = -\lambda^{1/2} i \exp[-i(\omega t + a\sin\Omega t)] \sum_{n=0} \frac{J_n(a)\exp[in\Omega t]}{\omega - \omega_0 - n\Omega - i(\lambda/2)} \quad , \tag{2.16}$$

The intensity distribution of the wave is then

$$I(\omega) = \lambda \sum_{n=0} \frac{J_n^2(a)}{[(\omega - (\omega_0 - n\Omega)^2 + \lambda^2/4]} \quad , \tag{2.17}$$

where $J_n(a)$ is a Bessel function of the first kind.

The spectrum of Eq. (2.17) reveals that the electromagnetic wave is a superposition of partial waves with frequencies $\omega_0 \pm n\Omega$ where n = 0, 1, 2,...,. Since the intensity of the Mössbauer absorption line goes as the square of the electric field vector, the intensity of the n^{th} sideband is related to the square of the n^{th} Bessel coefficient

$$J_n^2(x_0/\chi) \quad . \tag{2.18}$$

The argument of the Bessel function, x_0/χ where χ is the normalized wavelength of the gamma-ray, is usually referred to as the modulation index and is denoted by a. The intensity of the unperturbed absorption line is given by

$$f = |E_{n=0}(\omega,t)|^2 = J_0^2(x_0/\chi) \quad . \tag{2.19}$$

Since E_0 is normalized, f is the fraction of the radiated energy with frequency ω_0.

MAGNETIC PHASE MODULATION

Magnetic phase modulation theory[10] was derived to analyze the influence of a periodically varying magnetic field on the Mössbauer resonance of ^{67}Zn in diamagnetic ZnO. Pure magnetic modulation of the nuclear Zeeman levels by an alternating magnetic field was observed to produce phase changes of the nuclear states which were manifested as time-dependent oscillations of the transmission intensity measured as a function of the oscillating magnetic field.

For cases in which there is no static magnetic field[11] or in which the modulation is parallel to the static field,[12] the effect of the time varying component, $H_0 f(t)$ upon an eigenstate of the nucleus, $\Psi^{(o)}_{\alpha,m}$ can be written,

$$\Psi_{\alpha,m} = e^{-i\varphi_\alpha(t)}\, \Psi^{(o)}_{\alpha,m} \quad , \tag{2.20}$$

where $\varphi_\alpha(t)$ is the modulation angle of the phase,

$$\varphi_\alpha(t) = m_I \omega_\alpha \int_o^t f(t')dt' \quad , \tag{2.21}$$

and the Larmor frequency, ω_α is,

$$\omega_\alpha = \mu_N g_\alpha H_o/\hbar \quad , \tag{2.22}$$

where μ_N is the nuclear magneton, g_α is the gyromagnetic ratio for the α-th excited or ground state of the nucleus, and m_I is the magnetic quantum number of the eigenstates.

In principle, the difference in phase modulation between the ground state, g, and an excited state, e, may be observed during an absorption transition because the Fourier components of $\Delta\varphi(t) = \varphi_e(t) - \varphi_g(t)$ will be manifested as sidebands. However, since the transition will have a width, Γ associated with the time-dependent decay of the states, unless,

$$\hbar\omega_\alpha \geq \Gamma \quad , \tag{2.23}$$

the sidebands will be buried in the natural wings of the probing transition.

The modulation angle of the phase is easily calculated for a nucleus with spin I under the influence of a sinusoidally oscillating magnetic field, $B(t) = B_0\cos\Omega t$. The nuclear magnetic dipole moment interacts with the magnetic field according to

$$\mu_N \cdot B = g_N \frac{e}{2m_p} \beta_N I \cdot B \quad . \tag{2.24}$$

The modulation angle of the phase $\varphi_\alpha(t)$ is calculated as the integral of the time-dependent Zeeman energy, hence by Eq. (2.18) we have

$$\Delta\varphi(t) = \frac{1}{\hbar}\int_0^t g_e\mu_N I_e \cdot B(t)dt - \frac{1}{\hbar}\int_0^t g_g\mu_N I_g \cdot B(t)dt \quad , \tag{2.25}$$

$$= \pm\, a_i \sin\Omega t$$

where $a_i = g_e\mu_N B_0/2\hbar\Omega$ is the amplitude of the phase modulation.

This last expression may be expanded as a Fourier series by using Eq. (2.15). The Fourier coefficient $C_n(a_i)$ is calculated from $\varphi_\alpha(t)$ over the period of the oscillating magnetic field ($T = 2\pi/\Omega$):

$$C_n(a_i) = \frac{1}{T}\int_0^T dt \exp[i(\varphi(t) - n\Omega t)] \quad , \tag{2.26}$$

for sinusodial modulation $C_n(a) = J_n(a)$.

Equation (2.27) indicates that the radiation consists of sidebands which are separated by the modulation frequency with relative amplitudes given by $|C_n(a_i)|^2$:

$$|C_n(a_i)|^2 = \frac{16a_i^2}{[n^2\pi^2 - 4a_i^2]^2}\sin^2 a_i \quad , \tag{2.27}$$

for even n. For odd indices the sine function is replaced by cosine.[10]

Large Scale Magnetic Phase Modulation Effects

The phase modulation theory presented in the last section was specifically developed to explain the response of a diamagnetic material to a rapidly oscillating rf magnetic field. Next, it is interesting to address the question of what happens when these same fields are applied to paramagnetic and ferromagnetic materials.

It is well known that when an external magnetic field is imposed on a diamagnetic material, there is an induced atomic EMF which opposes the externally applied field in accordance with Lenz's law. The induced magnetization of the material is directed opposite to the imposed field; therefore, the magnetic field seen by the nucleus within a diamagnetic material is smaller than the applied field would be in a vacuum.

When an atomic system has a permanent magnetic moment due to the presence of unpaired electrons, the material is either paramagnetic or ferromagnetic. In paramagnetic materials these moments are weakly coupled together and undergo random fluctuations due to thermal agitations. In ferromagnetic materials the unpaired electron spins are coupled together throughout the lattice producing strong magnetic fields at the nuclear sites. For example, in ^{57}Fe the unpaired electrons are in the 3d orbital and produce the 330 kOe internal magnetic field.

If an external field is applied to a paramagnetic material it becomes energetically favorable for the moments to align with the field, but this energy gain has to compete with the loss of entropy that would be associated with the loss of the random movement of the atomic moments.

With the application of an alternating magnetic field it is possible to excite spin waves in materials possessing a permanant magnetic moment. Spin waves which are oscillations in the relative orientations of the spins in a material provide a mechanism through which phase modulation effects can be propagated from ferromagnetic materials; where spin wave excitations are strong, into paramagnetic materials where the individual spins are weakly coupled.

The conceptual key to orders-of-magnitude of enhancement of phase modulation effects has been reported[11-13] to lie in the use of smaller powers to manipulate the greater magnetic fields arising from the natural correlations of individual spins in ferromagnetic materials. However, the modulation, $\partial M/\partial t$ of the magnetization, M of a ferromagnetic material is rarely parallel to either the applied field, H_o or even to M, itself.[14] For such cases of nuclei in ferromagnetic media, the modulation angle of Eq. (2.20) takes a more complex form;[11] and one which causes a mixing of the eigenstates, $\Psi^{(o)}_{\alpha,m}$. Nevertheless, the principal parameter is still a Larmor frequency, Ω_α which for magnetic environments becomes,

$$\Omega_\alpha = \mu_N g_\alpha M/\hbar \quad , \tag{2.28}$$

a value much larger than that found in Eq. (2.19) for nonmagnetic samples. Unfortunately, magnetic materials are almost invariably magnetostrictive and the concern has lingered that even the enhanced effects of phase modulation might always be overwhelmed by the periodic Doppler shifts produced by vibration in the lattices excited by magnetostriction.

The propagation of magnetoelastic waves is a complex problem which has been intensively studied since 1958.[15] For many magnetic media the dispersion equation for such waves displays several branches[16-17] which can be individually identified with spin waves, magnetostatic waves or elastic waves. Mixed waves coupling magnons and phonons occur principally when branches intersect, so that the frequencies and wavelengths for both are nearly equal.[15] Away from those values of parameters magnetic and acoustic waves can be separated. In principle this offers a means to propagate only the former to a sample in which it is desired to magnetically modulate the phases of the states of the nuclei to be observed there without the concomitant introduction of acoustic noise. This possibility was realized in the third set of experiments reported in this dissertation and seems to provide the key for separating phase modulation effects from those of acoustic origin.

REFERENCES

1. G. Burns, Solid State Physics, (Academic Press, New York, 1985).
2. H. Frauenfelder, The Mössbauer Effect, (Benjamin, New York, 1962).
3. U. Gonser, Topics in Applied Physics Vol. 5: Mössbauer Spectroscopy, (Springer-Verlag, New York, 1975).
4. S. L. Ruby and D. I. Bolef, Phys. Rev. Letters 5, 5 (1960).
5. V. Burov, V. Krasilnikov, and O. Sukharevskaya, Sov. Phys. JETP 16, 837 (1963).
6. T. E. Cranshaw and P. Reivari, Proc. Phys. Soc. (London) 90, 1059 (1967).
7. L. Mishory and D. Bolef, in Mossbauer Effect Methodology, edited by I. Gruverman (Plenum, New York, 1968), Vol. 4, p. 13.
8. R. P. Vardapetyan and A. H. Mkrtchyan, Solid State Commun. 60, 357, (1986).
9. J. E. Monahan and G. J. Perlow, Phys. Rev. A, 20, 1499 (1979).
10. E. Ikonen, P. Helisto, J. Hietaniemi and T. Katila, Phys. Rev. Lett. 60, 643 (1988).
11. C. B. Collins, S. Olarui, M. Petrascu, and I. Popescu, Phys. Rev. Lett, 42, 1397 (1979).
12. S. Olariu, I. Popescu, and C. B. Collins, Phys. Rev. C 23, 1007 (1981).
13. B. D. DePaola, S. S. Wagal, and C. B. Collins, J. Opt. Soc. Am. B2, 541 (1985).
14. T. H. O'Dell, Ferromagnetodynamics (J. Wiley, New York, 1981) Ch. 2.
15. C. Kittel, Phys. Rev. 110, 836 (1958).
16. P. C. Fletcher and C. Kittel, Phys. Rev. 120, 2004 (1960).
17. E. Schlömann, J. Appl. Phys. 31, 1647 (1960).
18. R. W. Damon and J. R. Eshback, J. Appl. Phys. Supp. 31, 1045 (1960).

19. H. A. Mook, J. W. Lynn, and R. M. Nicklow, Phys. Rev. Lett. 30, 556 (1973).

20. P. Grünberg, J. Appl. Phys. 51, 4338 (1980).

CHAPTER 3

INSTRUMENTATION AND PROCEDURES

The Mössbauer Spectrometer

In this chapter the fundamental aspects of the experimental design are presented which describe how the Mössbauer effect is used to study the influence of an rf magnetic field on the energy levels of the nucleus. Since a variety of experimental results are presented in this dissertation, a general overview of the experimental appartus and techniques will be presented in this chapter. The specific details pertaining to individual experiments which deviate from what is discussed here will be presented in the appropriate chapters covering the experimental results. The basic spectrometer used in all experiments consisted of an electromechanical transducer and its driving system, a gamma-ray detector with its associated electronics and a computer used as a multichannel scalar to collect and analyze the data. In addition to the above components, to apply the rf magnetic field to the absorber required a MHz signal generator, power amplifier, in-line power meter and a tuneable LC circuit.

The basic experimental arrangement is schematically shown in Fig. 3.1. The spectrometer consisted of an Austin Science Associates (ASA) model S-600 controller, an ASA linear motor and a multichannel scalar. The Mössbauer source was mounted on the motor which serves as an electromechanical velocity transducer to Doppler shift the frequency of the recoilless γ-radiation. The motion of the transducer is enslaved to a velocity reference signal (VRS) generated by the S-600. It could be operated in either a constant acceleration or a constant velocity mode. The Mössbauer resonance spectrum was generated by storing counts registered by a nuclear

Figure 3.1

Block diagram of the standard Mössbauer spectrometer used in all experiments.

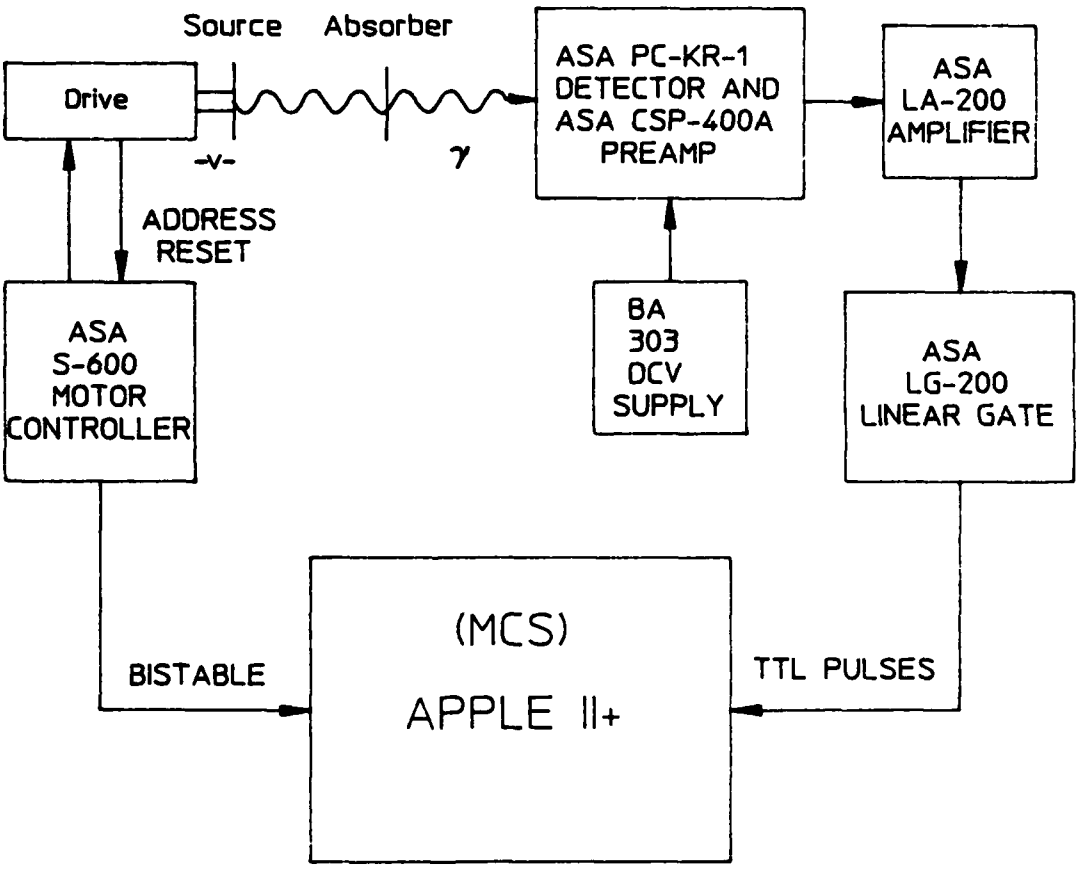
Source
Absorber
Drive
-v-
γ
ASA PC-KR-1
DETECTOR AND
ASA CSP-400A
PREAMP
ASA
LA-200
AMPLIFIER
ADDRESS
RESET
ASA
S-600
MOTOR
CONTROLLER
BA
303
DCV
SUPPLY
ASA
LG-200
LINEAR GATE
(MCS)
APPLE II+
BISTABLE
TTL PULSES

detector as a function of the velocity in an Apple II+ computer which served as a 1024 channel analyzer.

The S-600 requires a bistable signal from the MCA to properly time the drive waveform with the channel sweep. The memory channels were sequentially addressed with the velocity sweep using two triangular reference signals, 6 Hz and 24 Hz, to control both the channel advance and the velocity reference signal controlling the transducer.

For constant acceleration spectra the velocity of the motor was varied linearly with time in synchronism with the MCS. This was achieved by using a symmetric or asymmetric triangular waveform so that the VRS had a constant slope. In contrast, when the VRS had a constant voltage, the velocity of the motor was constant within a limited range. At the endpoints of its motion, the motor required a flyback signal to bring the drive back to its starting position. Different review articles concerning this type of instrumentation used to study the Mössbauer effect have been published; two excellent examples are those by Cohen and Wertheim[1] and Herber and Hazony[2].

The velocity calibration of the spectrometer was usually done by measuring the peak positions of the six absorption lines of ^{57}Fe. The outer absorption peaks span ± 5.3 mm/sec while the inner lines are separated by ± 0.84 mm/sec. For velocity ranges greater than this it was convenient to use the rf sidebands produced in stainless steel driven by a nickel foil immersed in rf fields or by using an ultrasonic piezoelectric transducer to generate the sidebands. Since these sidebands appear at integral multiples of the driving frequency, their spacing from the parent transitions provides an ideal velocity calibration scale.[3,4] For absolute velocity calibration the velocity transducer was also equipped with an ASA LC-9A laser interferometer.

Mössbauer Sources

In this work two Mössbauer isotopes were used: ^{57}Fe and ^{119}Sn. Both of these isotopes have large recoil-free fractions at room temperature. The precursor nuclide for the 14.4-keV gamma radiation of ^{57}Fe is ^{57}Co. The decay scheme and energy levels for this isotope was presented in Chapter II and will not be repeated here. The energy level diagram for ^{119}Sn is shown in Figure 3.2. This nuclide is produced by the (n,γ) reaction of ^{118}Sn (24.01% natural abundance), using the thermal neutron flux of a nuclear reactor. The Mössbauer transition at 23.875-keV from the first excited state (3/2 - 1/2), is populated by the decay of the more energetic metastable $^{119}Sn^{m}$ which has a half-life of 245 days. The ^{119}Sn was embedded in a $CaSnO_3$ matrix which gave it a recoilless fraction of 0.6 at room temperature. The initial activity of the source was 2.1 mCi.

A variety of ^{57}Co sources in Pd and Rh lattices were availble for use, with activities ranging from 2-25 mCi. Furthur details will be presented along with the experimental results.

Nuclear Detection System

To detect the 14.4-keV γ-rays in ^{57}Fe a Kr gas-filled proportional counter, ASA PC-KR-1, was used. A biasing voltage of 1.8 kV was supplied from a Bertran Associates model 303 dc voltage power supply. Krypton gas has a K-edge at 14.32-keV, so it is preferred for ^{57}Fe work despite an efficiency of only 50%. The resolution of a proportional counter is determined by the statistics of the conversion of the energy of the γ-rays into an electrical signal which scale as $2N^{-1/2}$, where N is the number of primary electrons. A charge sensitive preamplifier, ASA CSP-400A, amplified the signals from the proportional counter and delivered them to an ASA LA-200A linear amplifier. The amplifier output was then routed to an

Figure 3.2

Decay scheme and energy levels for the production of the 23.875-keV Mössbauer line of ^{119}Sn. Note the parasitic 24.8-keV x-ray line which can be electronically filtered out by using a high resolution high purity Ge solid state gamma-ray detector.

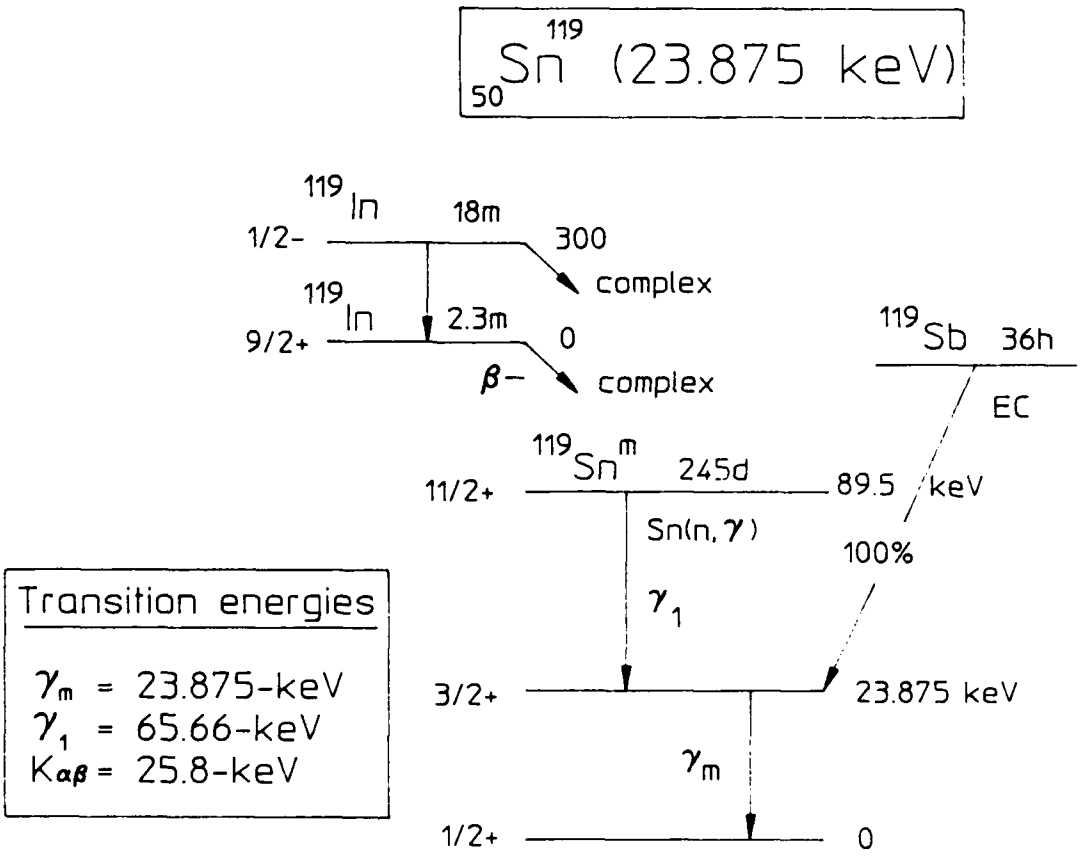
$^{119}_{50}Sn$ (23.875 keV)
^{119}In 18m
1/2-
300
complex
^{119}In 2.3m
9/2+
0
β−
complex
^{119}Sb 36h
EC
$^{119}Sn^{m}$ 245d
11/2+
89.5 keV
Sn(n, γ)
100%
γ1
3/2+
23.875 keV
γm
1/2+
0
Transition energies
γm = 23.875-keV
γ1 = 65.66-keV
Kαβ = 25.8-keV

LG-200A linear gate which included upper and lower descrimination to allow the selection of pulses produced by the desired γ-rays. It also produced a TTL pulse used by the MCS for counting.

Because of the presence of a parasitic 25.8-keV x-ray line in the energy spectrum of the decay of $^{119}Sn^{m}$ it was necessary to use a different type of nuclear detector to detect the 23.875-keV Mössbauer line. The problem of resolving low energy lines in the presence of a background radiation caused by higher energy x-ray or γ-ray is best solved by using a high resolution semiconductor detector.[2] Therefore, to resolve the 23.875-keV Mössbauer transition from the 25.8-keV x-ray line an EG&G high purity Ge detector was used to collect the ^{119}Sn absorption spectra. In a semiconductor detector the incident γ-rays produce electron-hole pairs in the depletion layer of a pn junction of the semiconductor. The electrons and holes are collected at opposite terminals due to the influence of a negative bias across the pn junction.

Solid state detectors are highly sensitive, requiring only a few eV of energy to create electron-hole pairs. The statistical factor that contributed predominately to the resolution in a proportional counter is of much less importance for solid-state detectors. The lower limits on the resolution of the semiconductor detector are due to thermal noise and defects in manufacturing. These detectors must be operated at liquid nitrogen temperatures because of the large thermal noise present at room temperature which causes spurious pulses due to thermal excitations in the crystal.

The Rf Apparatus

The rf apparatus consisted of a signal generator for operation in the MHz range, amplifier, in-line power meter, and a parallel-series resonant circuit as shown in Figure 3.3. A Wavetek model 3510 frequency synthesiz-

Figure 3.3

Modification to the Mössbauer spectrometer to allow the application of an rf magnetic field to the absorber foils. Proper rf shielding of the Doppler motor was required to prevent rf interference from entering into the velocity drive wave form.

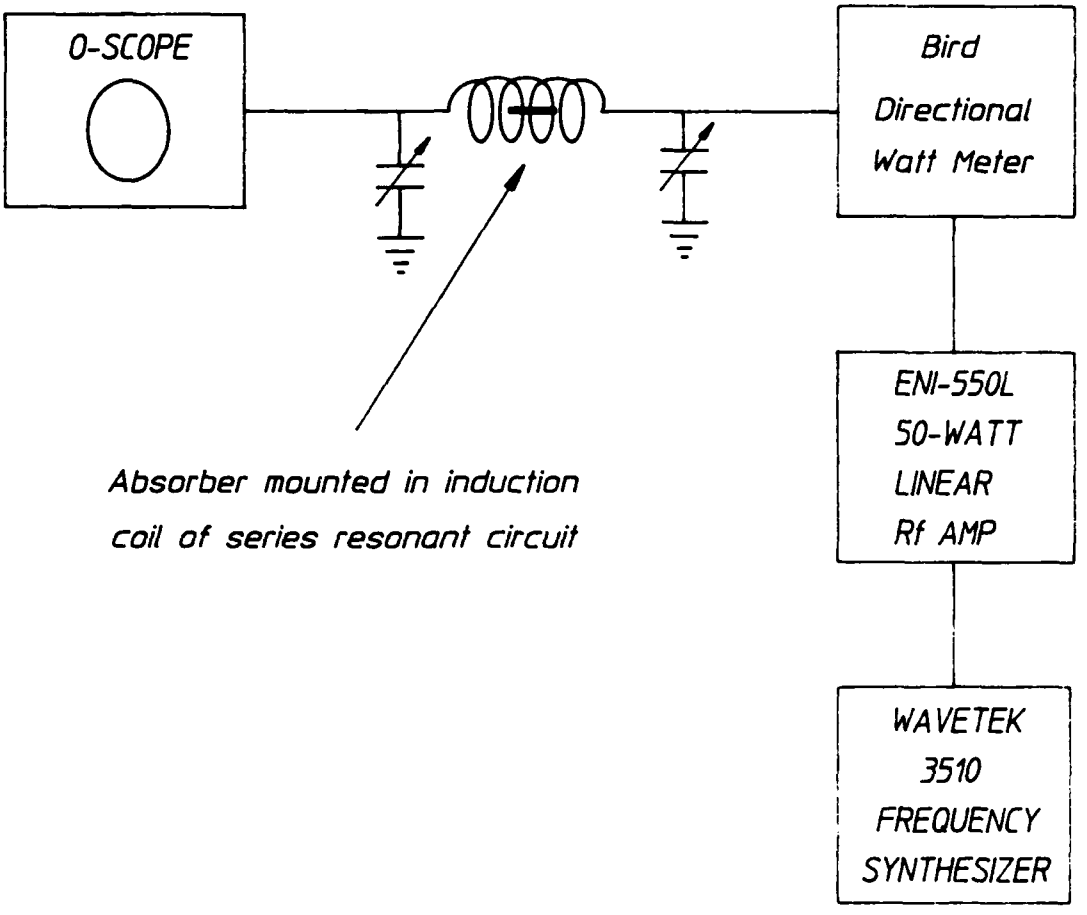
O-SCOPE
Bird
Directional
Watt Meter
ENI-550L
50-WATT
LINEAR
Rf AMP
WAVETEK
3510
FREQUENCY
SYNTHESIZER
Absorber mounted in induction
coil of series resonant circuit

er with a very low intrinsic frequency modulation of only ± 100 Hz with an 500 Hz/(10-min) stability supplied the rf signal and was tunable over a frequency range of 1-1000 MHz. The output of the signal generator was then amplified by an ENI model 550L linear amplifier which had a flat frequency response over the range of operation. The amplified signal was monitored by a Bird directional power meter. With the use of different elements both the forward and reflected rf power could be accurately measured. A more detailed discussion of the rf apparatus may be found in reference 8.

The magnetic field strength inside the induction coil in the absence of any magnetic material is approximated by[9]

$$H_{rf} = 6(PQ/V\nu)^{1/2} \quad , \qquad (3.1)$$

where P is the rf power in watts, Q is the Quality factor of the circuit ($Q = \omega/\Delta\omega$), V is the volume of the coil in cm^3 and ν is the resonance frequency in MHz. It is clear from Eq. (3.1) that if the product PQ is held constant, the rf current in the coil of such a circuit is also constant and, hence, different absorber arrangements could be subjected to applied fields of the same intensity, H.

Oxide Reduction of Absorbers

In experiments where the applied rf power exceeded more than about 5 watts cw, great care had to be taken to avoid oxidizing the absorber foils. This was particularly troublesome for experiments with tin absorbers. Stannic oxide, SnO_2, forms when metallic tin is heated and exposed to oxygen. The resonance absorption of the 23.875-keV γ-rays of ^{119}Sn in SnO_2 shows considerable line broadening over that calculated from the known lifetime of the 3/2 state ($\tau_{1/2} = 2.75 \times 10^{-8}$ sec, $\Gamma = 2.4 \times 10^{-8}$ ev). It

has been shown that this broadening of the absorption spectrum of SnO_2 is due to an unresolved quadrupole doublet with splitting $\Delta = 0.50 \pm 0.02$ mm/sec.[5,6]

Rf joule heating in the ferromagnetic iron foils causes excessive temperatures leading to the formation of iron oxides, in particular Fe_2O_3. The formation of ferric oxides can change the value of the hyperfine fields at the nuclear sites as well as induce quadrupole effects in the resonance spectra. Therefore, it was necessary to reduce the oxidized foils of iron and tin to their pure metallic forms by heat treating in a purified hydrogen atmosphere.

The chemical reaction for the reduction of Fe_2O_3 and SnO_2 are[7]

$$SnO_2 + 2H_2 = Sn + 2H_2O \qquad (3.2)$$

$$Fe_2O_3 + 3H_2 = 2Fe + 3H_2O \quad . \qquad (3.3)$$

The rates of these reactions are highly temperature dependent and are given by the logarithmic equation[7]

$$\log T + \log M = C \quad , \qquad (3.4)$$

where T is the absolute temperature, M is the time in hours and C is a constant. The time-dependent curve for the reduction of ferric and stannic oxide is shown in Fig. 3.4. From the figure, the shape of the curve indicates that the most advantageous temperatures at which to operate are those over 750°C. Hydrogen gas reduction of the iron foils was usually done around 1000°C; however, tin which has a low melting point (250°C) required lower reduction temperatures for extended periods of time. This was necessary to maintain the integrity of the foils.

As will be discussed in Chapter 5, some of the tin experiments involved using binary metallic alloys of iron/tin and nickel/tin. Since

Figure 3.4

Oxide reduction times for ferric and stannic oxides in a purified hydrogen atmosphere as a function of temperature (after reference 7).

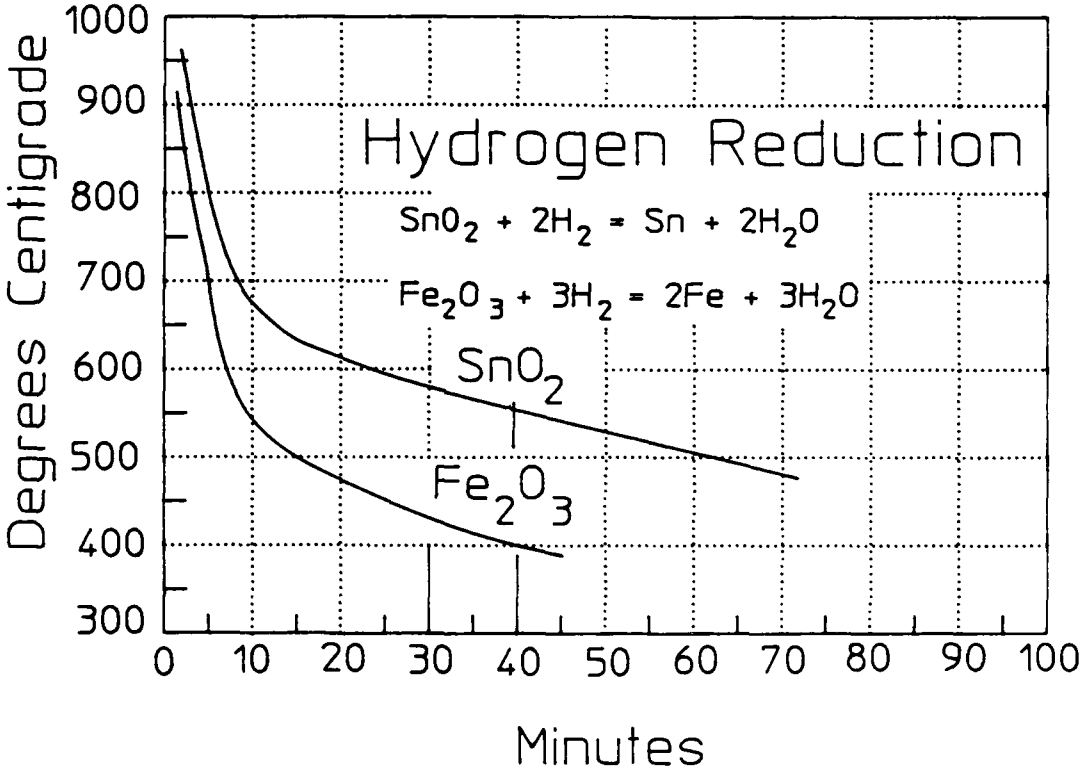
Hydrogen Reduction
$SnO_2 + 2H_2 = Sn + 2H_2O$
$Fe_2O_3 + 3H_2 = 2Fe + 3H_2O$
SnO_2
Fe_2O_3
Degrees Centigrade
1000
900
800
700
600
500
400
300
0
10
20
30
40
50
60
70
80
90
100
Minutes

the reduction of ferric oxide is easier than stannic oxide for a mixture of these oxides the reduction would proceed as follows.[7] First, a reduction of the ferric oxide would occur followed by a period where both oxides were undergoing a reducion. Finally, after a time all of the iron would be reduced with some SnO_2 remaining. The process would then continue until all of the tin oxide was reduced to its metallic form.

The H_2 gas reduction of oxides was accomplished by using a Lindberg 54000 series tube furnace. The maximum operating temperature was 1200°C. The temperature of the oven was monitored by measuring the EMF (millivolt) output of a Platinell II thermocouple which terminated inside the core of the furnace. The oxidized foils were placed in a quartz vessel and inserted into a one inch diameter quartz sleeve that fit into the center bore of the furnace. The flow rate of the hydrogen gas was approximately 4 ft^3/hour. After passing through the furnace the excess hydrogn gas was burned off using a modified bunsen burner.

To circumvent the oxidization of the absorber foils two techniques were used. First, the rf could be pulsed on and off to allow for radiational cooling of the absorber. This radiational cooling of the absorber could be expedited by using a small fan to blow a stream of cool air across the absorber mounted in the induction coil of the LC circuit. A second technique, used primarily in the tin experiments, was to perform the rf experiment inside a sealed plexi-glass box which was filled with an inert gas and held at positive pressures. Performing the tin experiments in this atmospheric isolation chamber in combination with rf pulsing and a cooling fan eliminated most of the oxidation problems.

Ultrasonic Transducer Assembly

Two of the experiments reported in this work involved the use of a quartz pieozelectric transducer to generate ultrasonic sidebands. The absorbers were bonded by a gel or epoxy to the transducer. X-cut quartz crystals were used to generate longitudinal waves, and AT-cut transducers were used to generate transverse waves.[4] The transducers were purchased from Valpey-Fisher and were cut to have their resonance frequency near 25 MHz. The electrodes were vacuum deposited chrome/gold and the transducer was one inch in diameter. A critical concern was to maintain the total thickness of the transducers to a value smaller than the range for the relatively soft γ-rays used in these experiments.

The absorber-transducer assembly was mounted in an aluminum holder to provide mechanical rigidity to the transducer and to allow a means of connecting the output of the rf generator/amplifier to the transducer electrodes. A schematic of the acoutic assembly is shown in Fig. 3.5.

The piezoelectric quartz transducer was driven from the ouput of the rf signal generator and amplifier described earlier. An rf impedance matching network was not necessary since all the experiments were performed at the natural frequency of the quartz transducer. The resonance frequency of the transducer could be "tuned" through a small range of frequencies by changing the dimensions and, hence, the mass of the absorber foils. The added mass would change the load on the transducer and, hence, its resonant frequency would shift slighty.

The mechanical resonance of quartz pieozelectric transducers are very high with typical Q values of about 400 being reported in the literature.[4] The vibrational resonance is Lorentzian with line widths dependent upon the attenuation of the ultrasound in the transducer material.[4]

Figure 3.5

Schematic diagram of the ultrasonic transducer assembly used to mechanically modulate the gamma-ray energies of the 14.4 and 23.875-keV Mössbauer lines of ^{57}Fe and ^{119}Sn respectively.

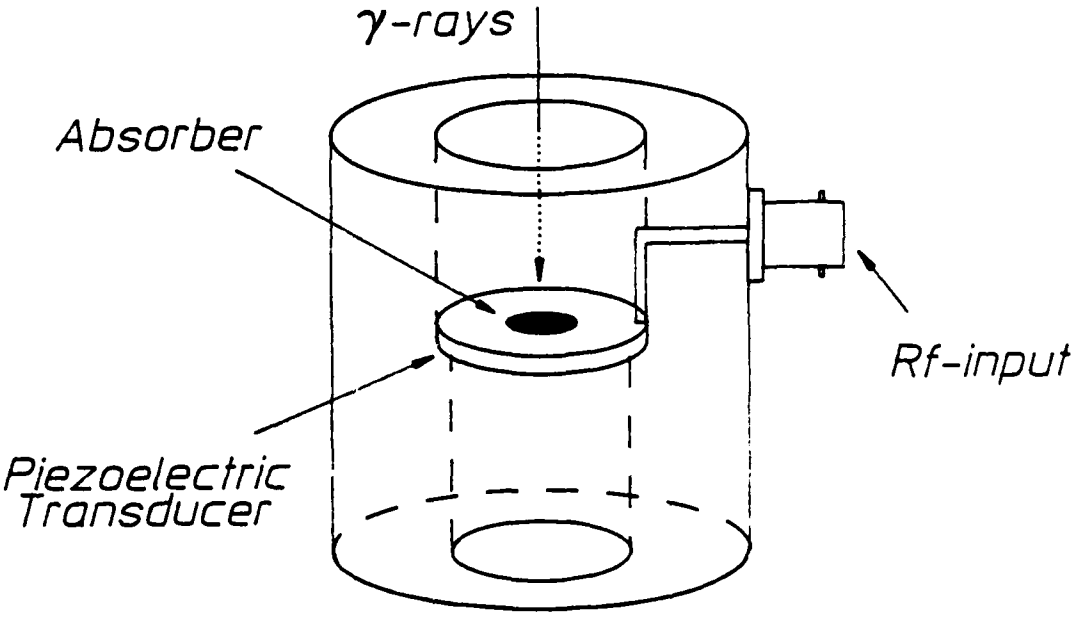
γ-rays
Absorber
Rf-input
Piezoelectric
Transducer

Data Analysis

Several computer programs were available for processing Mössbauer data. The software used was from Coherent Technologies and basically treated the data as vectors representing the counts stored as a function of their channel address. Basic arithmatic operations such as addition or subtraction of data sets and running averages could be easily performed. Figure 3.6a shows an example of an unprocessed spectrum. The signal to noise ratio could be improved by a factor of $(5)^{1/2}$ by performing a running average of the data from five successively resolved channels.[8] An example of a five point running average is shown in Fig. 3.6b.

Since the data is stored as a function of the channel address of the MCS and not as a function of the source velocity (mm/sec) it is necessary to know the calibration constant of the spectrometer (mm/sec/channel). This is calculated from a Mössbauer spectrum with known peak positions by dividing the separation of the peaks in mm/sec by the number of channels spanning the same range. The spectra could also be converted from counts versus mm/sec to frequency units by calculating

$$\nu = \frac{vE_\gamma}{\hbar c} \quad . \tag{3.5}$$

Although the work presented in this dissertation is not concerned with the absolute determination of the Mössbauer parameters for a given sample, there are, none-the-less, certain instrumental errors present due to the Doppler motion of the source which should be noted. They are: Parabolic distortion of the base line due to the inverse square law, Compton scattering, cosine smearing and channel width broadening of the spectra.[10] The distortion of the baseline, due to the inverse square law, is noticable for a moving source when the source/absorber separation is small. Since the

Figure 3.6

Raw data plot of a Mössbauer spectrum of an iron foil (b) the same data set after performing a five point running average which improves the signal to noise ratio by a factor of $(5)^{1/2}$.

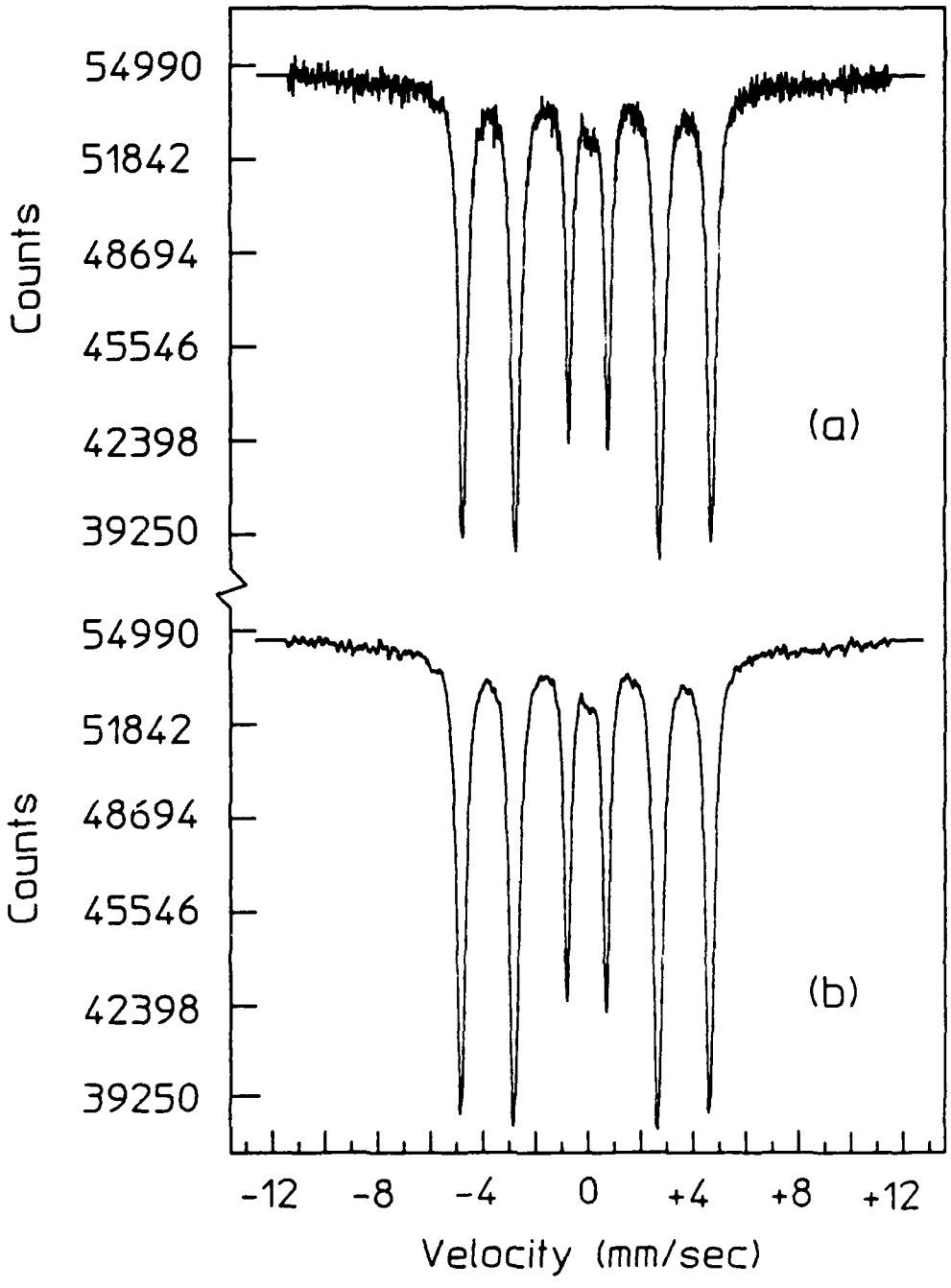
54990
51842
48694
45546
42398
39250
Counts
(a)
54990
51842
48694
45546
42398
39250
Counts
(b)
-12
-8
-4
0
+4
+8
+12
Velocity (mm/sec)

intensity of the γ-rays fall off as $1/r^2$, this distortion may be corrected by increasing the source to absorber separation.

Parabolic distortion of the baseline due to Compton scattering occurs when higher energy radiation is emitted by the source. This can be particularly troublesome when ^{57}Co is the source because of the 137-keV line due to the 5/2 - 1/2 transition.

The two remaing sources of instrumental error are cosine smearing and channel width broadening. Cosine smearing is a natural consequence of the angular dependence of the Doppler effect and will produce a spectrum which is slightly shifted toward higher velocities. This velocity shift is given by $dv = vD^2/16d^2$, where D is the detector diameter and d is the source-detector separation.[10,11] Channel width broadening is due to a change in the velocity of the source while counts are still being accumulated in a channel. The magnitude of the effect is solely dependent upon the calibration constant of the spectrometer (mm/sec/channel).

REFERENCES

1. R. L. Cohen and G. Wertheim, in Methods of Experimental Physics, R. V. Colman ed., Solid State Physics, (Academic Press, New York, 1974), Vol II, p. 307.
2. R. H. Herber and Y. Hazony, in Techniques of Chemistry, A. Weissberger and B. Rossiter eds., (Wiley Interscience, New York, 1972), Vol. IIID, p. 215.
3. T. E. Cranshaw and P. Reivari, Proc. Phys. Soc. (London) 90, 1059 (1967).
4. J. Mishory and D. I. Bolef, in Mössbauer Effect Methodology, I. J. Gruverman ed., (Plenum Press, New York, 1968), Vol. 4, p. 13.
5. R. H. Herber and J. Spijkerman, J. Chem. Phys. 42, 4312 (1965).
6. K. P. Mitrofanov, M. V. Plotnikova, and V. S. Shpinel, Sov. Phys. JETP 21, (3) 524 (1965).
7. C. L. Mantell, Tin: Its Mining, Production, Technology, and its Applications, American Chemical Society Monograph Series, 2nd ed. (Reinhold Publishing Corporation, New York, 1949), Chp. 7.
8. B. D. DePaola, Experimental Studies of the Interaction of the Nucleus with Long Wavelength Radiation, (unpublished Ph.d. Thesis, University of Texas at Dallas, 1984).
9. W. Gilbert Clark, Rev. Sci. Instrum. 35, (3), 316 (1964).
10. Jon J. Spijkerman, in An Introduction to Mössbauer Spectroscopy, Leopold May ed., (Plenum Press, New York, 1971), p. 23.
11. R. Riesenman, J. Steger, and E. Kostiner, Nucl. Instr. Methods 72, 109 (1969).

CHAPTER 4

EXPERIMENTAL RESULTS I

Introduction

In this chapter the results of two experiments are presented. Each yields strong evidence which contradict the accepted hypothesis that magnetostriction is the primary cause of radiofrequency sidebands. The first experiment reexamines the results of Chien and Walker[1] who demonstrated that sidebands could be propagated from a ferromagnetic driver foil into a nonmagnetic sample. The data presented here conclusively demonstrates that the effect of two foils varied from two to four times the effect produced by a single foil, depending upon the static magnetic bias applied; a result inconsistent with the magnetostrive-acoustic model of sideband generation. The second experiment involves a study of radiofrequency modulation of the hyperfine fields of ^{57}Fe in a nonmagnetostrictive iron-nickel alloy. Here it is found that the sideband development corresponds with the permeability of the sample and not with its magnetostriction.

Coherence Experiment

From a current perspective it is the experiment reported by Chien and Walker[1] in 1976 that forms the bulwark of the magnetostrictive-acoustic explanation of Mössbauer sidebands. In that experiment an absorbing foil composed of ferromagnetic and nonmagnetic layers was used to study transport of the causitive agent from the ferromagnetic layer into the nonmagnetic region where the sidebands were produced upon Mössbauer transitions of embedded ^{57}Fe nuclei. Very clear evidence showed that the cause did

arise in the ferromagnetic Ni layers, producing sidebands in the nonmagnetic stainless steel layers. The most ready explanation at that time was a transport of phonons from one layer to the next with a high acoustic Q. Those experiments were repeated in the work reported here, but with extensions which contradict the classic interpretation of Chien and Walker.[1]

Although not unique for all sidebands in a spectrum,[1] the idea of a modulation index m as a measure of the strength of the development of the sidebands offers practical convenience for descriptions. For a magnetostrictive origin,[1]

$$m = x_0/\lambda \quad , \tag{4.1}$$

where x_0 is the amplitude of the periodic displacement of the nuclei and λ = 0.137 A for the 14.4-keV line of ^{57}Fe. In the corresponding magnetodynamic model[2]

$$m = bH \quad , \tag{4.2}$$

where H is the applied magnetic field and b provides proportionality between M_s, the saturation magntization of the medium, and H. For relatively small m, the ratio of the magnitude of the first order sidebands to the intensity in the original parent line is proportional to m^2, which in turn is proportional to P, the applied radiofrequency power.

One of the most compelling results presented by Chien and Walker[1] was a demonstration supposed to show the enhancement of m^2 afforded by tighter acoustic coupling of the layers. They found that electroplating Ni upon a stainless steel foil produced much higher values of m^2 in absorption experiments than could be obtained by gluing a Ni foil to the stainless foil. They attributed the difference to the obviously poorer acoustic

properties of the glue. However, as part of this dissertation it is observed that their stainless steel foil was electroplated on both sides with Ni while the epoxied bond was used to join a single Ni foil to one side of the stainless absorber. While the m defined by Eq. (4.1) for a single foil could not be additive if produced in different magnetostrictive layers, in principle the M_s upon which m depends in Eq. (4.2) could add coherently. Two sources of m arising from distinctly separate sources could give a resulting modulation of $4m^2$ in a magnetodynamic model. Chien and Walker failed to recognize[1] that even in the magnostrictive model two sources of m generated in the two electroplated layers should give a modulation index of $2m^2$ in the absorber foil. Instead, they attributed the increased sideband intensity developed by the two plated sources in comparison to the one glued source only to the advantage they assumed for a plated contact over a glued interface. They reported no comparison of the effects of gluing or plating the *same number of ferromagnetic layers to the absorber foil*. Reported here is a repetition of the Chien and Walker experiment which showed that the effect of two foils varied from two to four times that produced by a single foil joined in the same fashion, depending upon the static magnetic bias applied.

In this experiment the absorber was a 2.5 μm paramagnetic stainless steel (SS) foil with 90.6% enrichment of ^{57}Fe. For the nonabsorbing ferromagnetic drivers, 2.5 μm Ni foils were used, all of which were cut from a single sheet of polycrystalline Ni. The stainless-steel absorber was sandwiched between two Ni foils and held in rigid contact by mounting the foils between glass cover slides of 100 μm thickness. A conventional Mössbauer spectrometer, modified for rf experiments, as shown in Fig. 4.1, utilized a 25 mCi source in a Rh matrix to obtain the ^{57}Fe absorption spectra. The 14.4-keV gamma rays were detected with a Kr gas filled proportional counter biased with 1.8 kV.

Figure 4.1

Schematic drawing of the experimental arrangement used in the coherence experiments. Note the position of the rare earth magnets which are used to apply a magnetic bias to the absorber.

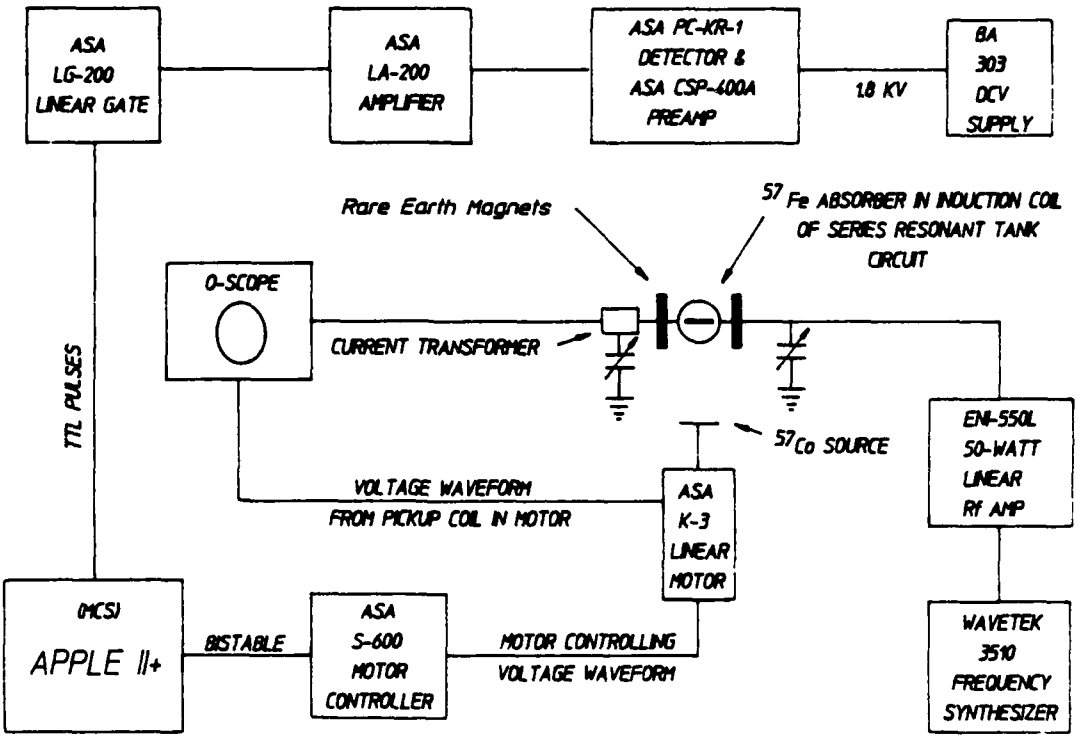
ASA
LG-200
LINEAR GATE
ASA
LA-200
AMPLIFIER
ASA PC-KR-1
DETECTOR &
ASA CSP-400A
PREAMP
1.8 KV
BA
303
DCV
SUPPLY
Rare Earth Magnets
57 Fe ABSORBER IN INDUCTION COIL
OF SERIES RESONANT TANK
CIRCUIT
O-SCOPE
CURRENT TRANSFORMER
TTL PULSES
57 Co SOURCE
ENI-550L
50-WATT
LINEAR
Rf AMP
VOLTAGE WAVEFORM
FROM PICKUP COIL IN MOTOR
ASA
K-3
LINEAR
MOTOR
(MCS)
APPLE II+
BISTABLE
ASA
S-600
MOTOR
CONTROLLER
MOTOR CONTROLLING
VOLTAGE WAVEFORM
WAVETEK
3510
FREQUENCY
SYNTHESIZER

A 25 MHz rf magnetic field was applied by mounting the foils in the cylindrical induction coil of an LC tank circuit. In obtaining data for a direct comparison between the effect of one Ni driver versus two, the product of the applied rf power P and the electrical Q of the circuit containing the rf induction coil was maintained at constant values. Elementary analysis shows that if PQ is constant the rf current in the coil of such a circuit is also constant and, hence, the two absorber arrangements are subjected to applied fields of the same intensity H. The results of the first experiment verified the linearity of the first order sideband amplitudes at 25 MHz for SS with two Ni drivers with PQ products of 75, 150, and 300 W producing the data shown in Fig. 4.2. The spectra are scaled so that the intensity of the central Mössbauer absorption peak of ^{57}Fe in SS is held constant in order to make direct comparisons of the sideband amplitudes.

Having established the linearity of the first order sidebands in the Ni-SS-Ni sandwich, one of the Ni drivers was removed and the experiment was repeated with the same PQ products as before. Figure 4.3 shows a comparison of the sideband amplitude for two Ni drivers versus one; in this configuration two Ni drivers give twice the effect of one driver foil.

In the next experiment a comparison is made between the effect of one source of excitation with that from two sources when both were biased with a static magnetic field. Rare earth magnets were placed about the induction coil such that the static magnetic field was mutually orthogonal to the rf magnetic field and the direction of gamma-ray propagation.

The linearity of the sideband amplitudes at 25 MHz as a function of PQ was again established as seen in Fig. 4.4 in order to insure that the introduction of the static magnetic field did not introduce any nonlinearities to the system. The scale, thus established, was used to measure the decrease in the sideband amplitude when one of the sources of excitation was removed from this biased sandwich. As is clearly shown in Fig. 4.5,

Figure 4.2

Experimental verification of the linearity of the first order sidebands at 25 MHz as a function of the applied rf power. The product of the applied rf power, P, and the quality factor, Q, of the circuit are used to insure reproducibility of the rf field strengths.

Linearity of First Order Sidebands

as a Function of Rf Power

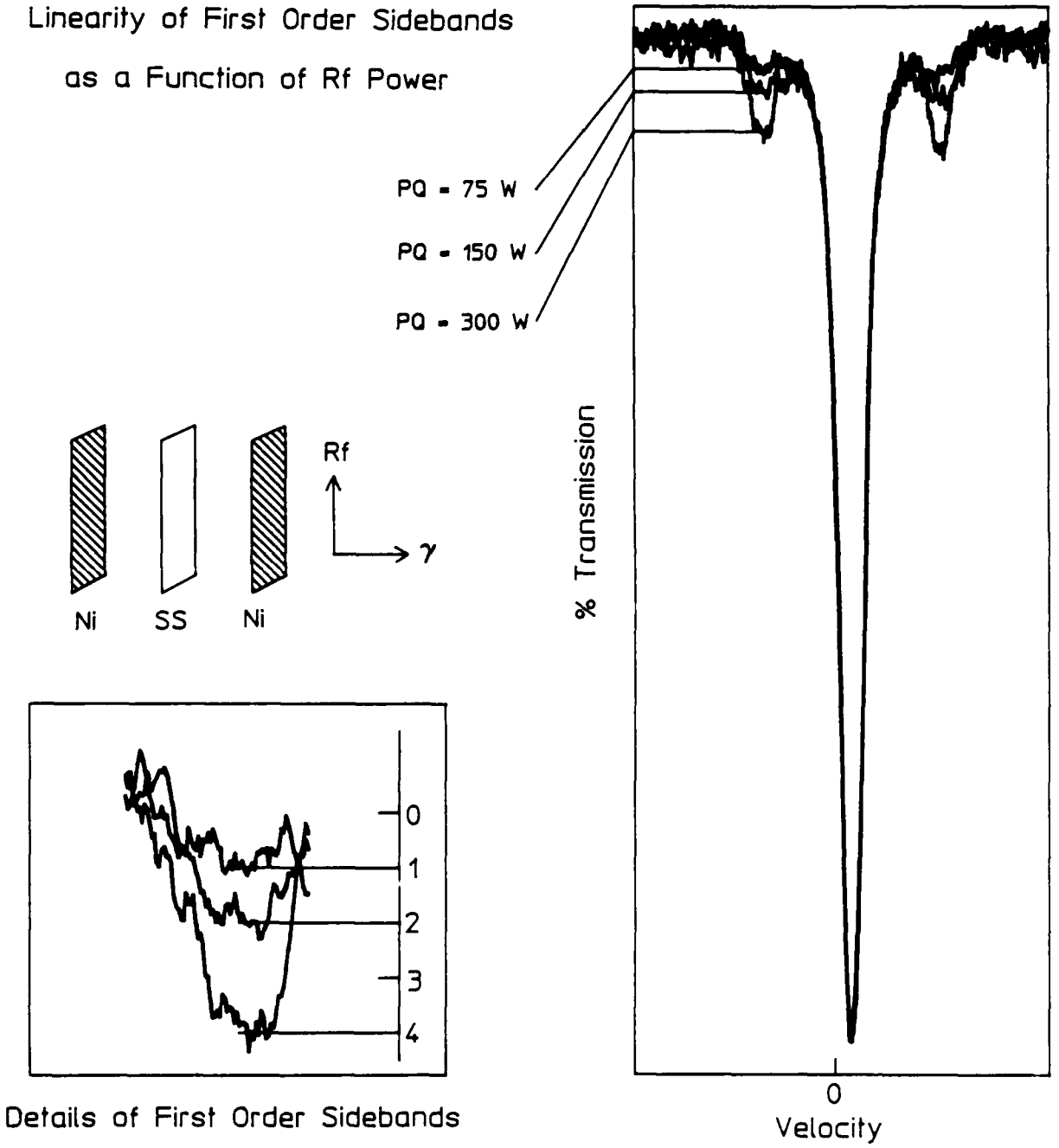

Details of First Order Sidebands

Figure 4.3

Comparison of the first order sideband amplitudes for one Ni driver foil versus two at 25 MHz with a PQ product of 300 W.

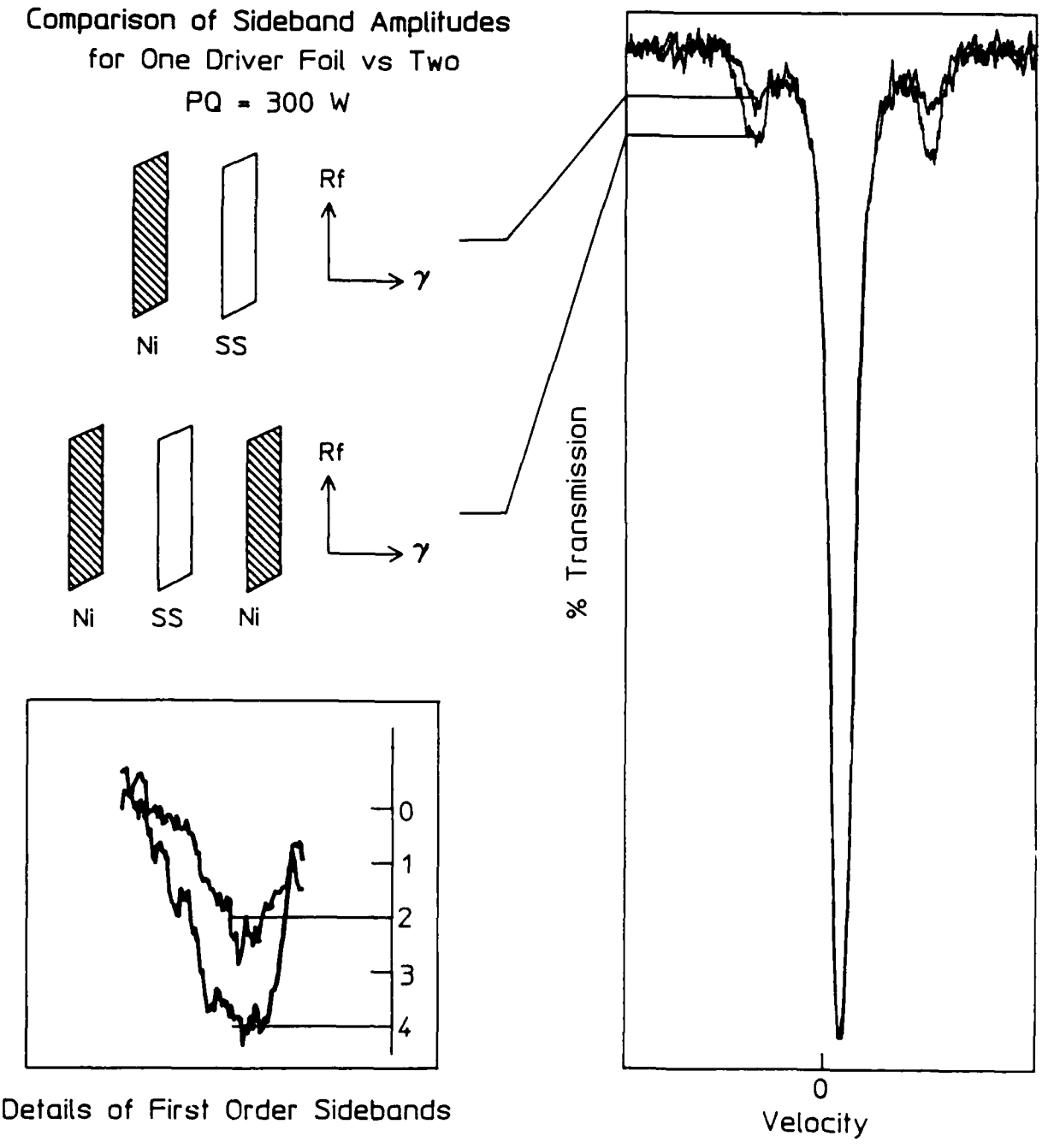

Details of First Order Sidebands

AD-A207 446 THE DEMONSTRATION OF THE FEASIBILITY OF THE TUNING AND STIMULATION OF NUCLEAR RADIATION(U) TEXAS UNIV AT DALLAS RICHARDSON C B COLLINS 31 OCT 88 3/3

UNCLASSIFIED N00014-81-K-0653 F/G 20/8 NL

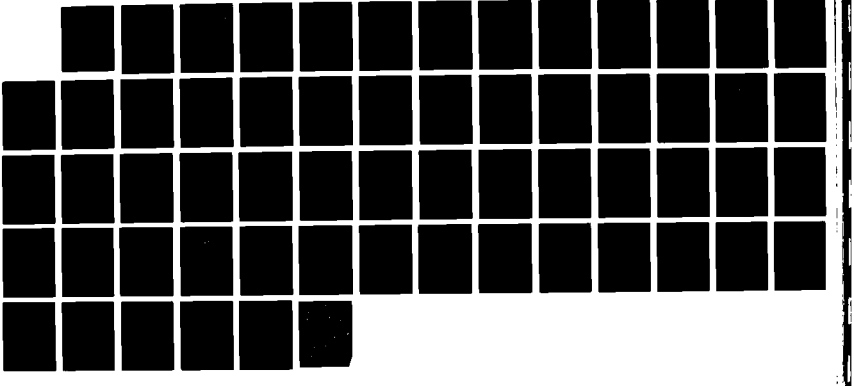

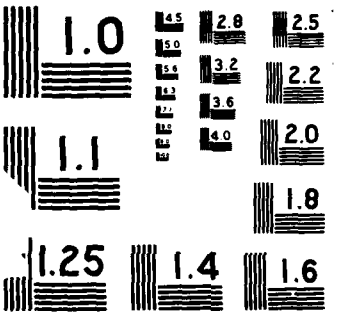
1.0
1.1
1.25
1.4
1.6
1.8
2.0
2.2
2.5
2.8
3.2
3.6
4.0
4.5
5.0
5.6

Figure 4.4

Establishment of linearity of the first order sidebands at 25 MHz with PQ = 75, 150 and 300 W when the foils are biased with a static magnetic field.

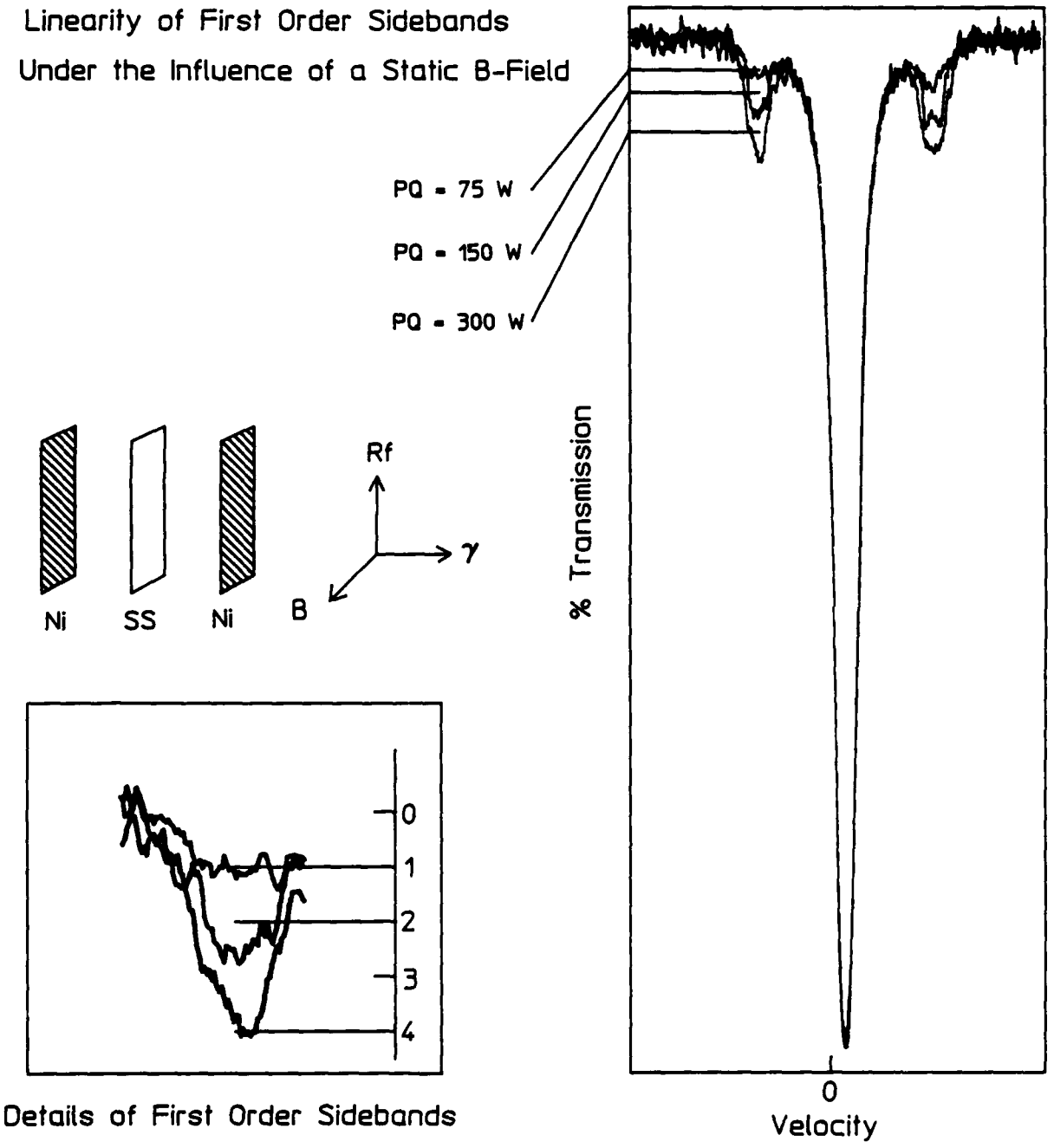

Details of First Order Sidebands

Figure 4.5

Comparison of sideband amplitudes for one driver foil versus two when both are biased by a static B-field with PQ = 300 W. Here two foils give four times the effect of one thus giving a modulation index of $4m^2$.

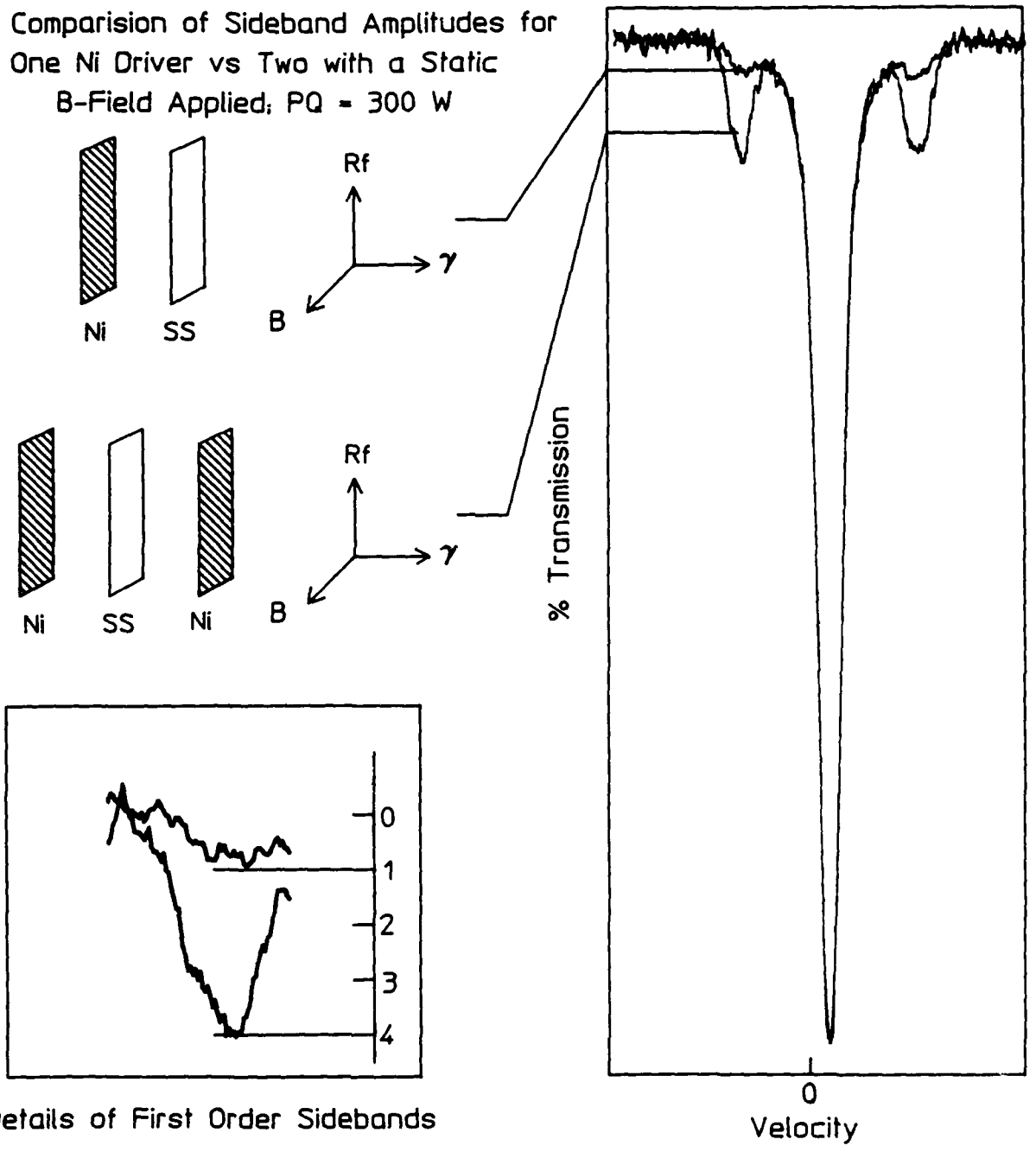
Comparision of Sideband Amplitudes for
One Ni Driver vs Two with a Static
B-Field Applied; PQ = 300 W
Rf
γ
B
Ni
SS
Rf
γ
B
Ni
SS
Ni
% Transmission
0
Velocity
0
1
2
3
4
Details of First Order Sidebands

the sideband amplitudes obtained with two driver foils are four times the amplitudes obtained with one driver foil. Therefore, with the application of a static B-field, two sources of excitation give four times the effect.

The results of this reexamination of the Chien and Walker experiment support only the first conclusion reached in that original work, namely that the causitive agent of rf sidebands can be produced in a ferromagnetic layer and then transported into a nonmagnetic layer. Their other conclusion is completely refuted by this demonstration because the effects they attributed to the type of coupling between layers most probably resulted from the relative numbers of magnetic and nonmagnetic layers.

These new results go beyond the propositions tested by Chien and Walker[1] and display behaviors completely inconsistent with the traditional magnetostrictive-acoustic origin of Mössbauer sidebands. In experiments such as these, acoustic phonons are the bosons associated with vector fields driven by tensor forces, *not vector forces*. Without invoking stimulated emission, there seems to be no way in which tensor sources which are physically separated can produce coherent vector fields in a space between them, even if they are temporally synchronized. As the fields increase, the magnetostrictive foils will become stressed along parallel axes which are displaced by the thickness of the stainless layer between them. There is no mechanism to produce a displacement vector in a particular direction as a consequence of the resulting strains in the Ni foils. Only a small scale buldging or buckling of each Ni foil is to be expected and this is usually described as the scattering of phonons at right angles to the source. Without the stimulated emission of such phonons, there is no way to insure that one foil buckles toward the stainless layer at a particular point while the other buckles away.

The stimulated emission of phonons that would be necessary to produce coherent additions of the displacements arising from the different sources would imply the existence of a threshold of power, above which two modula-

tion indices of m would give an effect of $4m^2$ and below which only $2m^2$. No such threshold was suggested by data similar to that of Fig. 4.5 which was obtained over an adequate range of powers.

Magnetic Phase Modulation in Nonmagnetostrictive Permalloys

In both the ^{181}Ta and ^{67}Zn experiments, which were discussed in Chapter 1, the observed effects were small and required the application of large fields. An enhancement of the amplitude of the rf magnetic field acting on the Mössbauer nuclei would clearly result in a larger effect. However, joule heating and other effects make simply increasing the rf power unattractive. A more elegant technique, which can be used to enhance the magnitude of the field seen by the nucleus, is to embed the nuclei under investigation in a thin ferromagnetic foil[2-4]. In this case the magnetization of the foil is then controlled by the internal magnetic field B_o and a perpendicular radiofrequency field B_{rf}. The applied radiofrequency field at the nuclear site is then enhanced by the ratio of the hyperfine magnetic field to the static field.

Unfortunately, in thin ferromagnetic foils there exists a coupling between the magnetic and elastic energy of the lattice which manifests itself as time-dependent magnetostrictive oscillations of the foil when it is subjected to a radiofrequency field. It is generally believed that this magnetostrictive-acoustic coupling introduces a Doppler motion of the iron nuclei and leads to a mechanical frequency modulation of the recoilless γ-radiation which is great enough to produce sidebands to each of the six allowed magnetic dipole (parent transitions) in the ^{57}Fe Mössbauer spectrum.[5-7] However, in view of the recent observations of magnetically induced transitions in the spectra of ^{181}Ta and ^{67}Zn it seems clear that this phenomena should be observable in ^{57}Fe as well and perhaps play a dominant role in magnetically soft materials, provided that the contribu-

tions to the sideband intensities due to mechanical effects can be eliminated.[8]

In this experiment the first clear evidence of radiofrequency modulation of the hyperfine fields of ^{57}Fe in a nonmagnetostrictive iron-nickel alloy is presented. Iron-nickel alloys, or permalloys as they are called, are of great scientific and technical interest because of their unusual magnetic properties. Permalloys are characterized by their high permeabilities and low magnetostriction. The magnetostriction of a polycrystalline permalloy passes through zero when the composition of the permalloy approaches 81 percent nickel.[9-11] More specifically, Mckeehan[9] established that to a first approximation the net magnetostriction should be a linear function of the concentration of either component (Fe or Ni) with a smooth passage of the magnetostriction through zero at 81 percent nickel. At this critical compositon in well annealed alloys, hystersis losses are at a minimum and the permeability is near maximum. The effect of composition versus magnetostriction is shown in Fig. 4.6.[12] Clearly, an 81 percent nickel permalloy is the ideal candidate in which to look for magnetically induced transitions in the Mössbauer spectrum of ^{57}Fe. With this goal in mind two permalloy foils were specially prepared for us by ONRL, one foil with 81 percent nickel and the other with 82 percent nickel. Each foil has a thickness of 2.5 μm with an ^{57}Fe-enrichment of 92.8 percent of the iron component of the alloy.

A conventional Mössbauer spectrometer using a 2.9 mCi source in a Pd matrix was used to obtain the ^{57}Fe absorption spectra. A Wavetek 3510 signal generator with a frequency range of 1 MHz to 1GHz and a 100-Hz resolution was used along with an ENI 550L 50-W linear amplifier, to generate the rf field at the absorber. Prior to taking the Mössbauer absorption spectra of the permalloys, with and without the presence of an rf field, the permalloy foils were annealed in dry hydrogen at a temperature of 1000°C for six hours.

Figure 4.6

Magnetostriction of the class of magnetically soft iron-nickel alloys, known as permalloys at various fractions of saturation versus the percent nickel in iron (after reference 12). The magnetostriction passes through zero when the composition of the permalloy approaches 81% Ni.

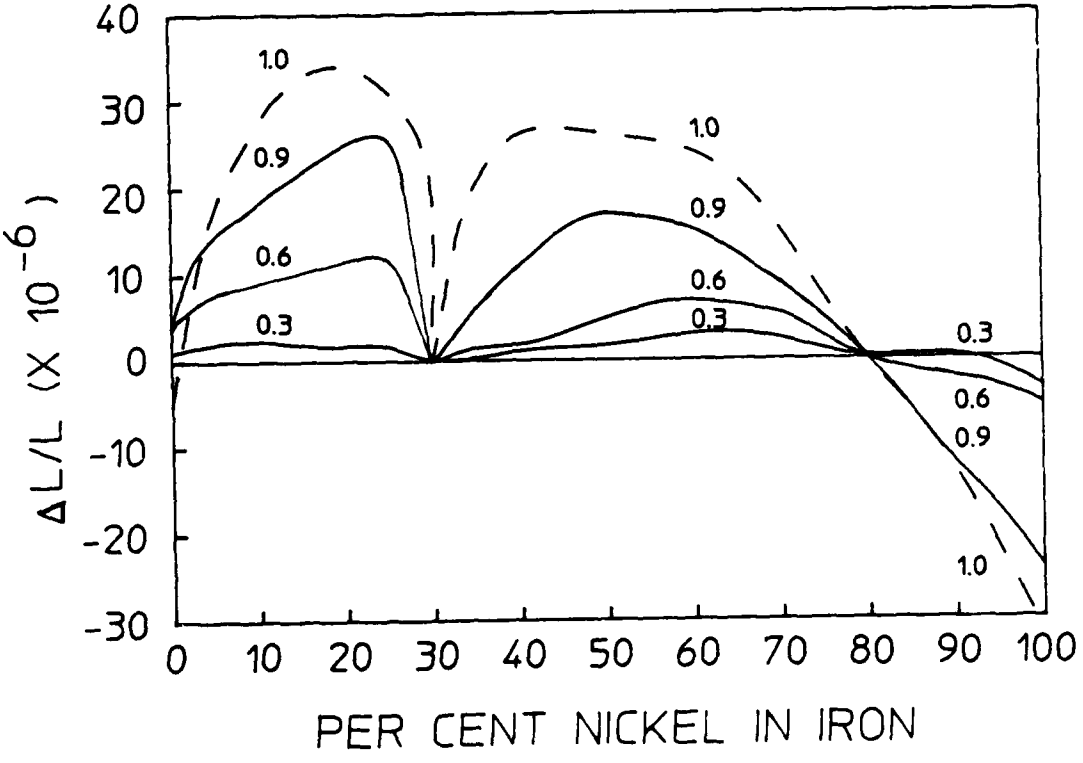
40
30
20
10
0
-10
-20
-30
ΔL/L (X 10⁻⁶)
1.0
0.9
0.6
0.3
1.0
0.9
0.6
0.3
0.3
0.6
0.9
1.0
0 10 20 30 40 50 60 70 80 90 100
PER CENT NICKEL IN IRON

Mössbauer spectra of the 81 and 82 percent permalloy were taken with and without rf, as shown in Fig. 4.7 and 4.8 respectively. The frequency of the applied rf field was 60 MHz and the product of power and Q-factor (PQ) of the resonator in which the foil was mounted was 12.5 watts. This PQ product is proportional to the intensity of the rf field acting on the absorber. Within the context of previous experiments on Mössbauer sidebands this is an extraordinarily low level of input corresponding to only 1.2 Watts of rf power into a Q of 10.42. This is to be contrasted with results reported in the literature[7] to require input powers approaching 1 kW at comparable frequencies.

As is shown by Fig. 4.7b, sideband development is greatest in the foil in which there is little or no magnetostriction. Assay results from ORNL, obtained by mass spectrometry and in-house permeability measurements, confirm that the 81 percent Ni foil has characteristics reported in the literature necessary for the foil to have a minimum or zero in the magnetostriction.

Taking advantage of the unusual magnetic properties of a class of iron-nickel alloys known as permalloys we have, for the first time, demonstrated a direct interaction of the Mössbauer nucleus ^{57}Fe with a periodically oscillating magnetic field. The result of such an interaction is to generate a spectrum in which the six lines (parent transitions) in a normal absorption spectrum of ^{57}Fe are accompanied by additional absorption peaks (rf induced sidebands) when the absorber is subjected to a radiofrequency field.

Figure 4.7

(a) Mössbauer absorption spectrum of the 81% Ni permalloy showing the six parent lines resulting from a magnetic interaction of the dipole moment with the strong internal hyperfine fields present in the foil. (b) Rf spectrum of the same foil subjected to a radiofrequency field oscillating at 60 MHz and a PQ product of 12.5 W. Note the strong sideband development present in the spectrum even though the foil has negligible magnetostriction.

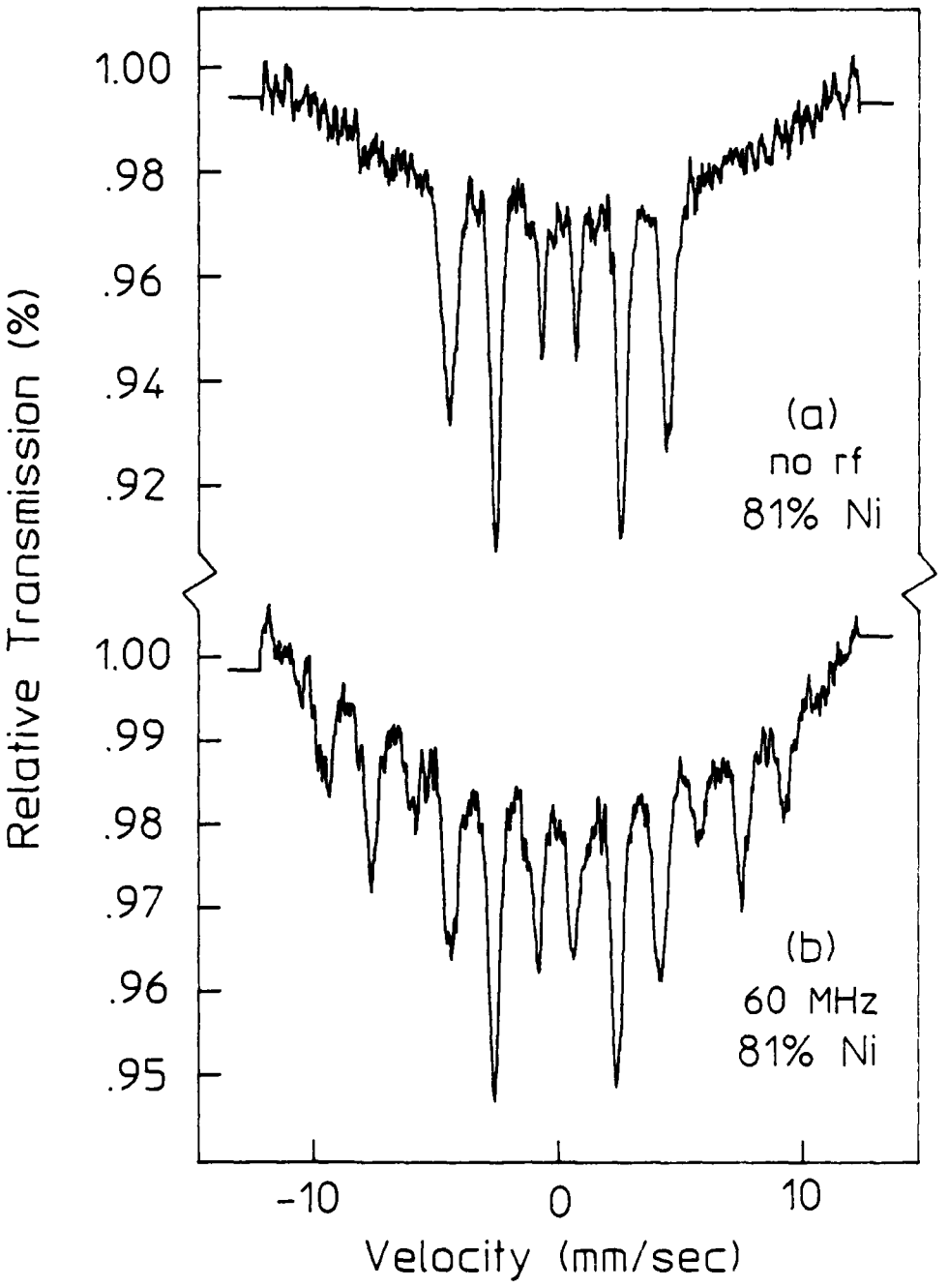
1.00
.98
.96
.94
.92
(a)
no rf
81% Ni
1.00
.99
.98
.97
.96
.95
(b)
60 MHz
81% Ni
Relative Transmission (%)
-10
0
10
Velocity (mm/sec)

Figure 4.8

(a) Mössbauer absorption spectrum of the 82% Ni permalloy foil. (b) Rf spectrum showing weak sideband development under identical rf conditions as that used to obtain the data of Fig. 4.7b. Even though this foil has a non-negligible magnetostriction, the permeability is lower in the 82% Ni permalloy than in the 81% Ni foil; hence, phase modulation effects are also weaker.

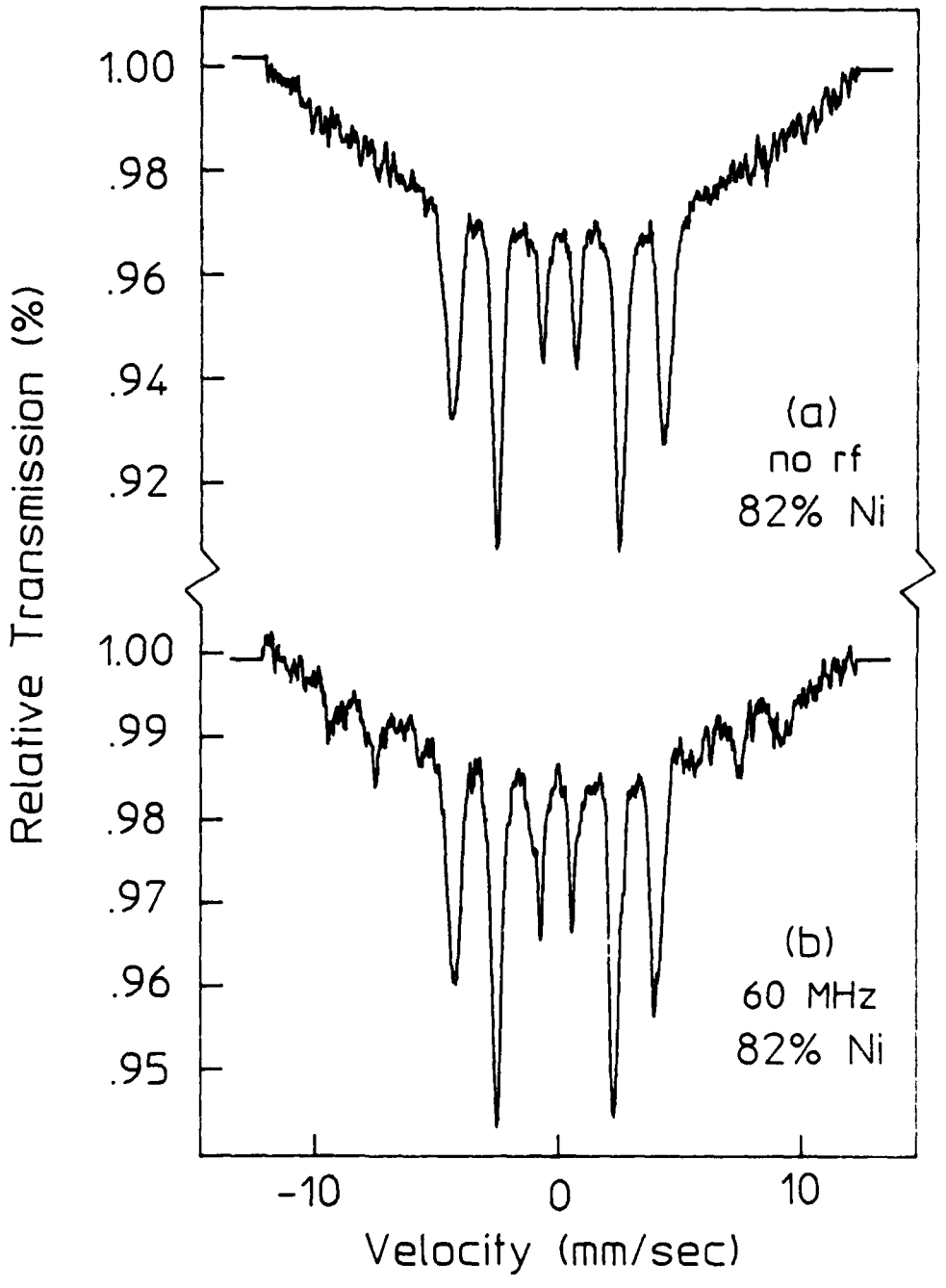
1.00
.98
.96
.94
.92
(a)
no rf
82% Ni
1.00
.99
.98
.97
.96
.95
(b)
60 MHz
82% Ni
Relative Transmission (%)
-10
0
10
Velocity (mm/sec)

REFERENCES

1. C. L Chien and J. C. Walker, Phys. Rev. B 13, 1876 (1976).
2. C. B. Collins and B. D. DePaola, Optics Lett. 10, 25 (1985).
3. B. D. DePaola and C. B. Collins, J. Opt. Soc. Am. B 1, 812 (1984).
4. B. D. DePaola, S. S. Wagal, and C. B. Collins, J. Opt. Soc. Am. B 2, 541 (1985).
5. N. D. Heiman, L. Pfeiffer, and J. C. Walker, Phys. Rev. Lett. 21, 93 (1968).
6. N. D. Heiman and J. C. Walker, Phys. Rev. 184, 281 (1969).
7. L. Pfeiffer, N. D. Heiman, and J. C. Walker, Phys. Rev. B 6, 74 (1972).
8. E. Ikonen, P. Helistö, J. Hietanieni, and T. Katila, Phys. Rev. Lett. 60, 643 (1988).
9. L. W. Mckeehan, Phys. Rev. 28, 158 (1926).
10. M. Kersten, Z. tech. Physik 12, 665 (1931).
11. R. Lichtenberger, Ann. Physik 15, 45 (1932).
12. R. M. Bozorth, Ferromagnetism, (D. Van Nostrand Co. Inc., Princeton New Jersey, 1964), p. 556.

CHAPTER 5

EXPERIMENTAL RESULTS II

Introduction

During the last three decades there has been a tremendous number of publications dealing with ultrasonic and radiofrequency sidebands in Mössbauer spectroscopy. Nearly all of these used ^{57}Fe as the Mössbauer isotope. The only exception to this for ultrasonic sidebands is an experiment performed in 1962 by Burov et. al.,[1] on the ultrasonic splitting of the absorption line of $^{119}SnO_2$. Radiofrequency sidebands have been reported in only two isotopes other than ^{57}Fe;[2,3] they are ^{181}Ta and ^{67}Zn. In this chapter the results of an experimental investigation of ultrasonic and radiofrequency sidebands in ^{119}Sn are presented.

Chien and Walker Experiment with a Diamagnetic Tin Absorber

During the course of preliminary investigations into rf sidebands, one experiment of considerable importance was the demonstration of the inability to produce rf sidebands in the absorption spectrum of ^{119}Sn by using ferromagnetic drivers. By the magnetostrictive hypothesis it should be possible to transfer the sidebands into the tin absorber from ferromagnetic drivers, similar in technique to the Chien and Walker[4] experiment.

In the initial attempts to develop rf sidebands in tin, the absorber consisted of a 5 μm tin foil with 89.90% enrichement of ^{119}Sn sandwiched between two ferromagnetic non-absorbing nickel drivers of either 2.5 or 5 μm thickness. This composite sample was pressed together and rigidly held in contact by mounting the foils between two glass cover slides each of 100 μm thickness. This arrangement replicated the one used to transfer

sidebands to stainless steel. The radiofrequency field was applied by mounting the foils in a flat coil of about eight turns in an L-C circuit. To reduce the rf heating of the sample, the rf power was pulsed with a duty cycle of 1:3 and a pulse duration of 200 msec. Additional cooling of the sample was accomplished by mounting a small cooling fan above the absorber in the L-C tank circuit. Since tin is easily oxidized, the experiments were performed in a nitrogen atmosphere.

A conventional Mössbauer spectrometer using a 2 mCi source in a $CaSnO_3$ matrix was used to obtain the ^{119}Sn absorption spectra. To detect the 23.875-keV gamma-rays of the tin, a high resolution EG&G Ge detector and pre-amplifier which was negatively biased with 1000 V was used. With the use of an EG&G 552 PSA/T-SCA discriminator, it was possible to filter out electronically the 25.8-keV characteristic x-ray line of the tin source.

Experiments with a PQ product of up to 800 W were performed with no clear evidence of sideband development (where P is the applied rf power and Q is the quality factor of the L-C circuit). To make a comparison with a Ni-SS-Ni absorber, we note that pronounced sidebands are propagated into a stainless-steel absorber from the nickel driver foils with PQ products of only few watts.

The failure to transfer rf sidebands into a 5 μm tin foil from a pair of ferromagnetic driver foils is a very significant result. According to the magnetostrictive model, acoustic waves should exist in the ferromagnetic foils when they are subjected to an rf magnetic field. When placed in contact with the tin foil these acoustic vibrations should be detected in the tin Mössbauer spectrum as sidebands. The fact that this is not observed, even with the application of large rf fields, can be explained by assuming: (a) the ultrasonic properties of the Ni-Sn-Ni foils are not conducive to the transport of acoustic vibrations from the nickel to the tin or (b) the magnetostrictive-acoustic model is incorrect. If the conclusions drawn by Chien and Walker are even qualitatively correct this

experiment should work. To assure that this failure is not due to extremely poor acoustic coupling between the driver foils and the tin, a brief discussion of the ultrasonic properties of the foils will now be presented.

Ultrasonic Properties of the Ni-Sn-Ni Absorber

The transfer of ultrasound from one material to another is analogous to the passage of light through materials with different refractive indices. Both phenomena are described by wave equations which are identical in form. For ultrasonic waves, instead of a refractive index to characterize the medium it is the acoustic impedence that is of importance. The acoustic impedence of a material is defined by

$$Z = \rho c \quad , \tag{5.1}$$

where ρ is the density of the material in g/cm^3 and c is the velocity of ultrasound in the material. The acoustic impedence is different for longitudinal (l) and shear (s) waves, so it is necessary to specify the type of wave when discussing impedence values of materials.

Closely following the analogy with light waves, the power transmission coefficient, α_t, can be calculated for the transmission of ultrasound from a material with a high impedence, Z_1, into a material with a lower impedence, Z_2. The power transmission coefficient has been given for ideal materials at normal incidence as[5]

$$\alpha_t = \frac{I_t}{I_i} \frac{4Z_1Z_2}{(Z_1 + Z_2)^2} \quad , \tag{5.2}$$

where I_t/I_i is simply the ratio of the transmitted intensity of the acoustic wave to the incident intensity. For longitudinal acoustic waves

evaluation of Eq. (5.2) yields for a Ni-SS interface (Z_{Ni} = 49.5 g/cm^{3}sec and Z_{SS} = 45.4 g/cm^{3}sec) a value of 99.81% for α_t. The same calculation for a Ni-Sn interface (Z_{Sn} = 24.2 g/cm^{3}sec) yields a value of 88.2% for the power transmission coefficient. For this idealized calculation, we see that even though the Ni-Sn interface is not as efficient for transport of ultrasonic waves, as is the Ni-SS foils, it is none-the-less not so poor as to prevent the formation of sidebands in the tin absorber. Clearly, the transfer of acoustic vibrations into the tin foil is sufficient for sidebands to develop if magnetostrictive-acoustic oscillations of the driver foils are the source of the sidebands in a Ni-SS-Ni absorber. However, even PQ products in excess of 800 W failed to produce the sidebands in tin.

Ultrasonic Sidebands in Tin

For completeness it was decided to repeat the experiment of Burov et al.[1] to determine if tin might have unusual ultrasonic properties making it particularly difficult to develop acoustic sidebands. The experiment was performed using the ultrasonic assembly described in Chapter 3. The absorber was a 1 cm^2 piece of tin with a thickness of 5 μm. The foil, which was annealed in a purified hydrogen atmosphere for six hours at 200°C, was acoustically bonded to an X-cut quartz pieozelectric transducer (PZT). The resonant absorption of ^{119}Sn without rf is shown in Fig. 5.1a. From the figure we see that the resonance is displaced from zero by 2.2 mm/sec. This is the isomer shift due to differing monopole interactions experienced by the tin nuclei in the source ($CaSnO_3$) and the absorber (metallic tin). The Mössbauer resonance is also very broad, with a FWHM of about 18 MHz. Figure 5.1b shows the rf spectra taken at the resonant frequency of the quartz PZT which was 24.0 MHz. Strong first order sidebands developed in the absorption spectra, as shown by the figure, with

Figure 5.1

The Mössbauer absorption spectrum of a 5 μm tin foil enriched with 89.90% ^{119}Sn. (a) Unperturbed spectrum and (b) spectrum of the same foil acoustically bonded to an X-cut piezoelectric transducer oscillating at a frequency of 24.0 MHz. The rf power applied to the transducer was 60 mW. Clear first order sidebands due to mechanical frequency modulation are shown to have developed.

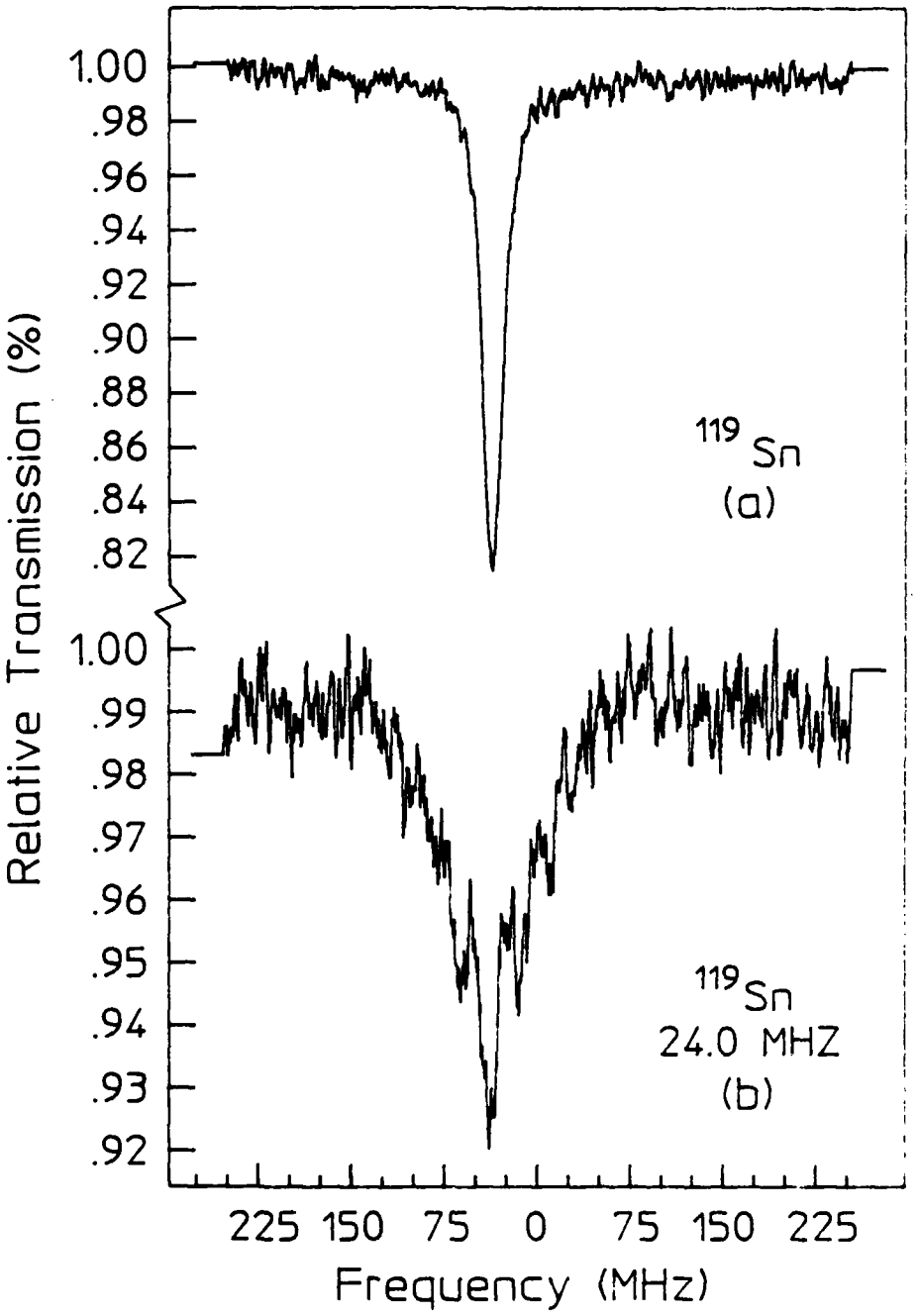
1.00
.98
.96
.94
.92
.90
.88
.86
.84
.82
1.00
.99
.98
.97
.96
.95
.94
.93
.92
Relative Transmission (%)
^{119}Sn
(a)
^{119}Sn
24.0 MHZ
(b)
225 150 75 0 75 150 225
Frequency (MHz)

an applied rf voltage of only 6 mv corresponding to an applied power of only 60 mW. Similar ultrasonic experiments performed using 310 SS and iron foils, as shown in Fig. 5.2, demonstrated that ultrasonic sidebands developed in tin with power levels comparable to that necessary to develop them in stainless steel and iron foils.

The failure to produce rf sidebands in tin with ferromagnetic drivers can easily be explained in the context of magnetic phase modulation theory presented in Chapter 2. Tin is a diamagnetic material with a magnetic susceptibility of $\chi_{Sn} = -31 \times 10^{-6}$ (cgs units). Also, since tin has no uncoupled electrons there is no net spin to allow the propagation of the large amplitude spin waves generated in the ferromagnetic drivers in the the tin foil.

Iron-Tin Layered Alloys

Since ^{57}Fe and ^{119}Sn both have excellant Mössbauer properties, it is not suprising that there exists an abundance of Mössbauer data on Fe-Sn alloys and compounds. In this section we are interested in alloying tin with iron so that the tin nuclei experiences a nonzero internal hyperfine magnetic field which can be coupled to an rf magnetic field to modulate the quantum phases of the nuclear states.

When thin foils of iron and tin are placed in contact and heated, an interphase layer forms at the interface between the foils. The compounds which form in this layer are contingent upon the temperature and duration of the heat treatment. Vertes et al.,[6] demonstrated that at low temperatures (< 300°C) the interface layer will consist primarly of Fe_3Sn_2. At higher temperatures (> 400°C)the interphase layer will consist mainly of $FeSn_2$. Vertes et al.[6] also reports that the thickness of the interphase region will change according to $\Delta x^2 = k\Delta t$, where k is proportional to the diffusion coefficient for tin into iron and t is the time. From their

experimental data they concluded that the thickness of the alloyed layer could be calculated from the Mössbauer absorption spectrum by

$$x = \frac{d}{1 + RS_\beta/S_\alpha} \frac{C_\beta}{C_\alpha} \quad , \tag{5.3}$$

where d is the original thickness of the tin layer, S_β and S_α are the corresponding areas under the Mössbauer resonance for both the alloyed and unalloyed tin. The values C_β and C_α are the concentrations of the unused tin and the alloyed tin and R is the ratio of the recoilless fractions.

The construction of the iron-tin layered alloys is as follows. A 6 μm foil of natural iron was held in rigid contact with a 5 μm foil of ^{119}Sn and placed in an oven and baked at 425°C for six hours in a purified hydrogen atmosphere to reduce any oxides present in the foils. Under these conditions a layered alloy was formed with the composition Fe + $FeSn_2$ + Fe_3Sn + Sn. Figure 5.3a shows the resulting absorption spectra of this composite absorber. The compond $FeSn_2$ is antiferromagnetic with a Neel temperature, T_N of 393 K.[7] The absorption spectrum consist of a paramagnetic component and hyperfine structure of magnetic origin in the form of an unresolved doublet which is characteristic of $FeSn_2$ with $T < T_N$. With increasing temperature, the separation of the lines would decrease until $T > T_N$; at which point they would coalesce into a single line.[8] The observed spectrum corresponds to an incomplete resolution of the hyperfine pattern. The isomer shift of the center of gravity of the doublet is + 2.2 ± 0.1 mm/sec. In the literature it is reported that the cross-section for the absorption of the 23.875-keV γ-rays of $FeSn_2$ is approximately the same as that for SnO_2.[8]

A study of the magnetic structure of $FeSn_2$ by neutron diffraction has been reported by G. Le Caër et al.,[9] who found that at room temperature the magnetic structure is collinear and characterized by ferromagnetic (100)

Figure 5.2

Ultrasonic sidebands generated in (a) a 2.5 μm foil of 310-SS and (b) a 2.5 μm iron foil. Both absorbers were enriched with 90.89% ^{57}Fe. The sidebands were generated using an X-cut quartz piezoelectric transducer oscillating at 24 MHz. The value of the applied rf to the piezoelectric quartz transducer was 60 mW.

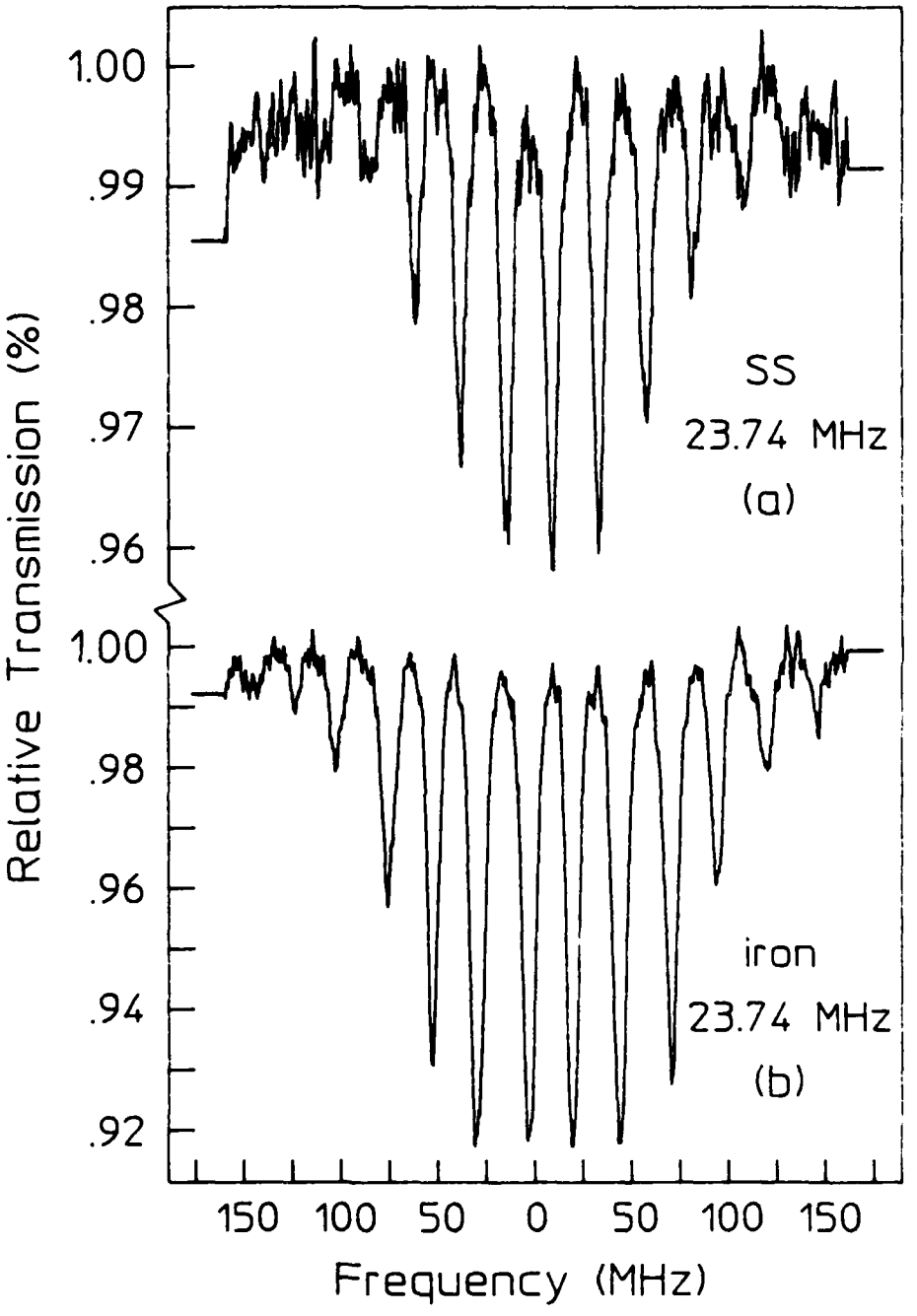
1.00
.99
.98
.97
.96
1.00
.98
.96
.94
.92
Relative Transmission (%)
SS
23.74 MHz
(a)
iron
23.74 MHz
(b)
150 100 50 0 50 100 150
Frequency (MHz)

Figure 5.3

The Mössbauer absorption spectrum of an $FeSn_2$ interphase region of a layered absorber constructed by pressing thin foils of iron and tin together and heat treating in a purified hydrogen atmosphere. The doublet structure is due to a magnetic dipole interaction. (a) Spectrum obtained without rf. (b) Rf spectrum at a frequency of 77.5 MHz with a PQ of 620 W.

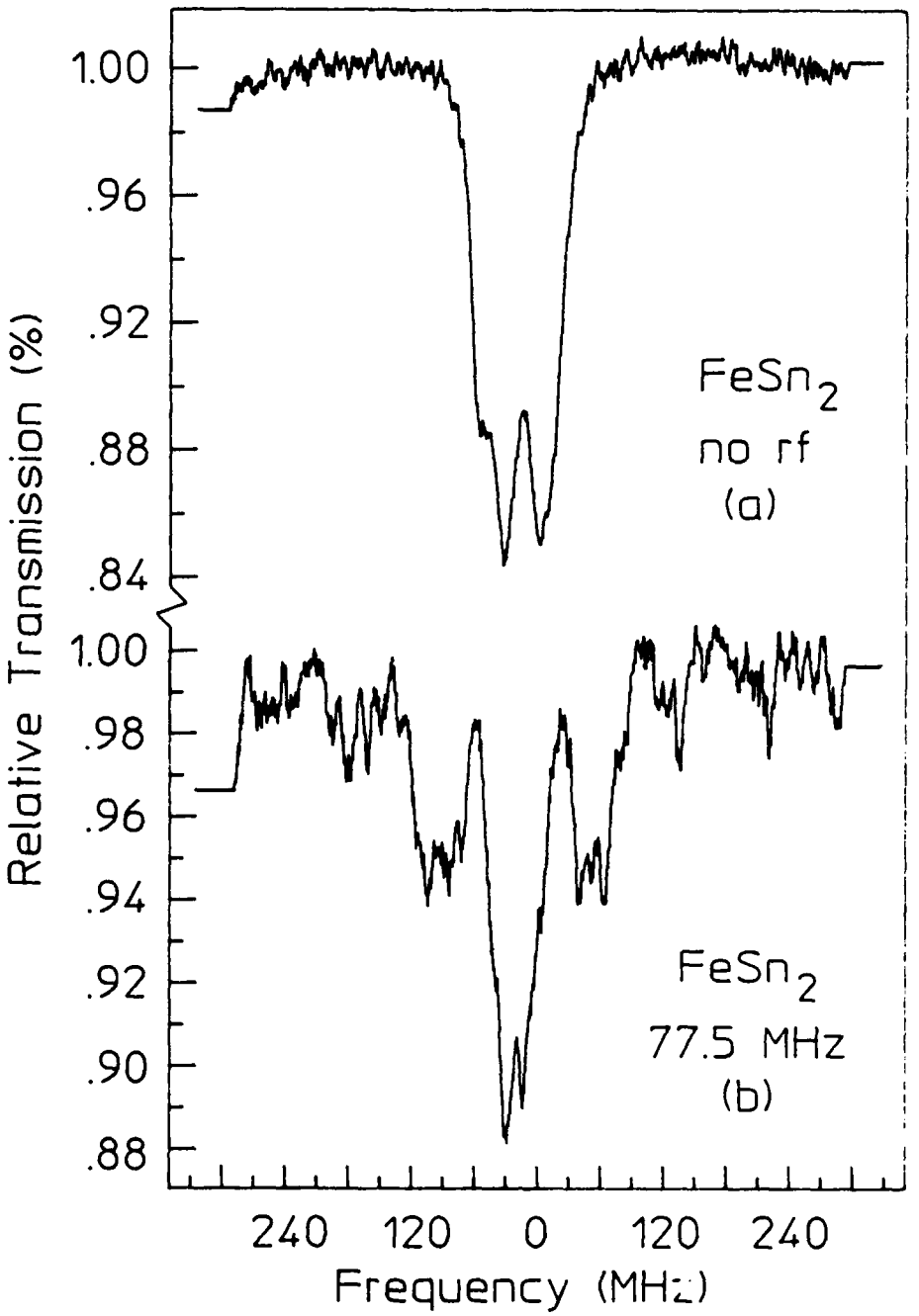
1.00
.96
.92
.88
.84
1.00
.98
.96
.94
.92
.90
.88
Relative Transmission (%)
FeSn2
no rf
(a)
FeSn2
77.5 MHz
(b)
240
120
0
120
240
Frequency (MHz)

planes coupled to [100] directions. The hyperfine magnetic field felt by the tin nuclei can be calculated from the splitting of the absorption line by using Eq. (2.9). From the spectrum in Fig. 5.3a this calculation yields a magnetic field of approximately 25 kOe at the tin nuclear sites.

The rf spectrum of this layered iron-tin absorber is shown in Fig. 5.3b. The absorber was mounted in a flat coil of a L-C circuit and an rf magnetic field was applied. With a PQ product of 620 W and a frequency of 75.5 MHz, sidebands up to third order were observed in the ^{119}Sn absorption specrum.

Nickel-Tin Layered Alloys

Many Mössbauer studies have been carried out on the intermetallic compounds of FeSn and $FeSn_2$, but limited studies have been carried out on the intermetallic compounds of nickel and tin. The work of Leideiser et. al.,[10] represents the first such attempt to study the Mössbauer properties of nickel-tin systems.

Tin and nickel alloy readily, forming compounds such a Ni-Sn, Ni_3Sn_2 and Ni_3Sn_4. Which compound actually forms again depends upon the temperature and duration of the heat treatment. Nickel-tin alloys have a ^{119}Sn absorption spectrum similar to that of $FeSn_2$ (Fig. 5.4a) both of which are due to magnetic dipole interactions. The NiSn alloys have much narrower line separation than that for the $FeSn_2$ spectra (30 MHz vs. 70 MHz); therefore, lower rf frequencies could be applied without sacrificing the clarity of the spectrum (i.e. no overlapping resonances), resulting in sideband development at much lower powers (sideband generation requires lower rf power at lower frequencies) The magnetic field at the tin nuclear sites in the NiSn absorbers indicate that they experience an internal hyperfine field of about 8 kOe. The rf Mössbauer spectrum of the NiSn layer of the composite absorber is shown in Fig. 5.4b. The rf

Figure 5.4

Mössbauer spectrum of the NiSn interphase region of a composite absorber constructed by pressing thin foils of nickel and tin together and heat treating in a purified hydrogen atmosphere. The doublet is characteristic of the compound NiSn as reported by Leidheiser et. al.,[10] and is the result of a magnetic dipole interaction. The separation of the two peaks is 30 MHz. (a) Spectrum obtained without rf. (b) Rf spectrum at 77.5 MHz showing strong sideband development with a PQ product of 620 W.

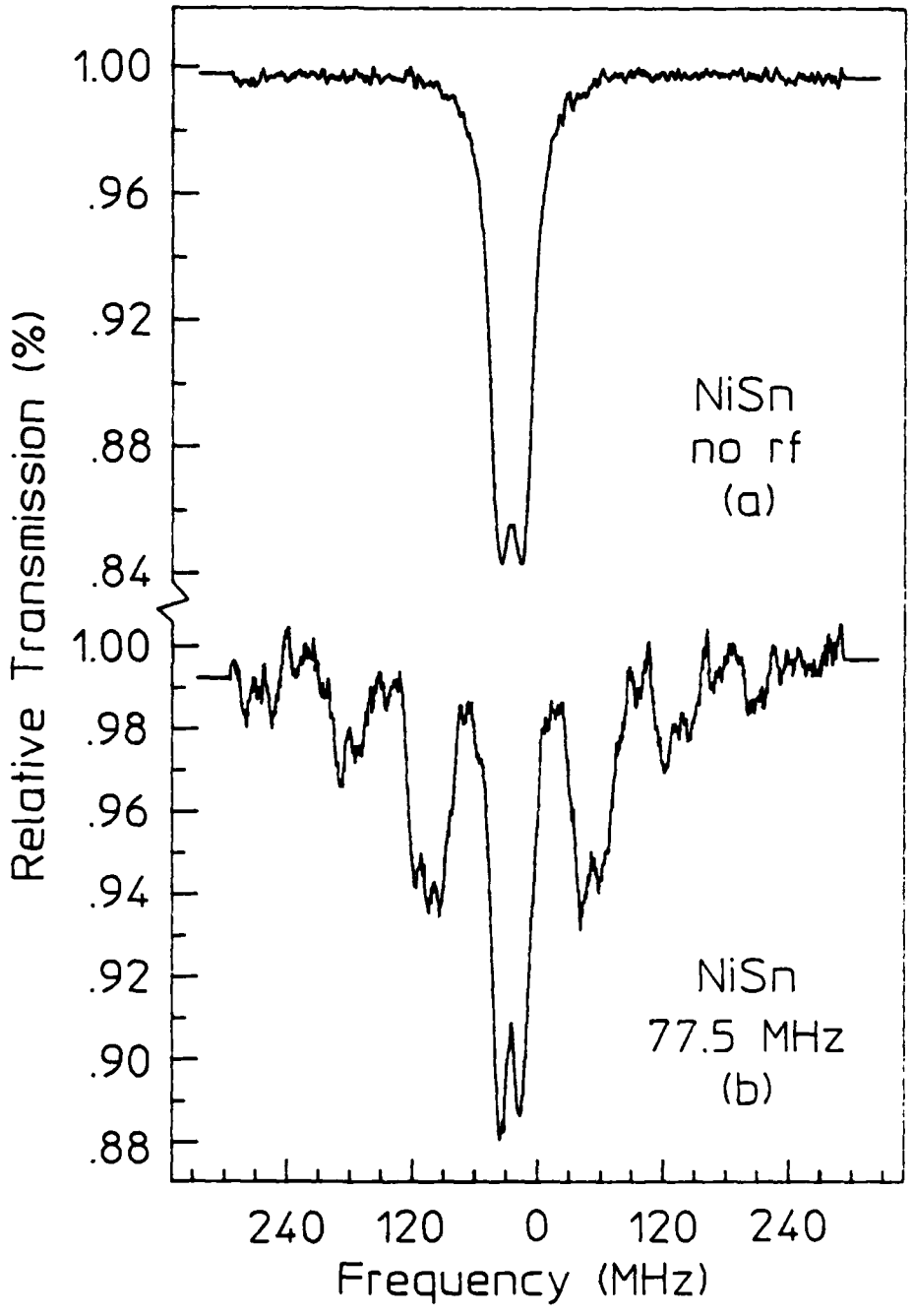
1.00
.96
.92
.88
.84
1.00
.98
.96
.94
.92
.90
.88
Relative Transmission (%)
NiSn
no rf
(a)
NiSn
77.5 MHz
(b)
240
120
0
120
240
Frequency (MHz)

spectrum was collected at a frequency of 77.5 MHz with a PQ product of 620 W.

The magnetostrictive hypothesis would explain the above experiments if it were assumed that the acoustic coupling between the tin and driving foils were greatly increased by the alloying, thereby producing acoustic waves in the sample. However, the dramatic failure of a Chien and Walker experiment with a tin absorber sandwiched between ferromagnetic Ni foils rules out this possibility. Since hyperfine structure is present in the spectra of the alloys, the sideband development must result from the modulation of the interaction energy of the applied radiofrequency field with the nuclear magnetic moments, thereby resulting in phase modulation of the nuclear states.

REFERENCES

1. V. A. Burov, V. A. Krasil'nikov, and O. Yu Sukharevskaya, Sov. Phys. JETP 43, 837 (1962).
2. E. Ikonen, P. Helisto, J. Hietanieni, and T. Katila, Phys. Rev. Lett. 60, 643 (1988).
3. P. J. West and E. Matthias, Z. Phys. A 288, 369 (1978).
4. C. L. Chien and J. C. Walker, Phys. Rev. B 13, 1876 (1976).
5. Lawrence E. Kinsler and Austin R. Frey, Fundamentals of Acoustics, 2nd ed., (John Wiley & Sons, Inc., New York, 1962), Chp. 6, p. 128.
6. A. Vertes, S. Nagy and M. Z. Awas, Nuclear Instrum. and Methods 199, 367, (1982).
7. V. A. Varnedk, L. I. Strugova, and E. G. Avvakumov, Sov. Phys. Solid State 16, 1186 (1974).
8. V. I. Nikolaev, Yu.I. Slacherbina, and A. I. Karchevskii, Sov. Phys. JETP 44, 775 (1963).
9. G. Le Caër, B. Malaman, G. Venturini, D. Fruchart and B. Roques, J. Phys. F: Met. Phys. 15, 1813 (1985).
10. H. Leidheiser, I. Czako-Nagy, M. L. Varsanyi, and A. Vertes, J. Electrochem. Soc. 126, 204 (1979).

CHAPTER 6

EXPERIMENTAL RESULTS III

Introduction

The excitation of coherent transients in Mössbauer spectra has been previously limited to a low range of frequencies by the high powers required to modulate the nuclear phases.[1] Reported in this chapter is an eleven orders-of-magnitude increase in the efficiency through which such phenomena can be produced. Magnetic modulation of the quantum phases of ^{57}Fe nuclei has been produced by magnetostatic spin waves excited at large amplitudes in a paramagnetic stainless steel foil. Transport of the waves allowed the observation of coherent effects in a region where spurious acoustic vibrations were absent. Sidebands were found on the 14.4-keV line of ^{57}Fe with less than a 1% contribution from the phonons.

The propagation of magnetoelastic waves is a complex problem which has been intensively studied since 1958.[2] For many magnetic media the dispersion equation for such waves displays several branches[3,4] which can be individually identified with spin waves, magnetostatic waves or elastic waves, as shown in Figure 6.1. Mixed waves coupling magnons and phonons occur principally when branches intersect, so that the frequencies and wavelengths for both are nearly equal.[2] Away from those values of parameters magnetic and acoustic waves can be separated. In principle this offers a means to propagate only the former to a sample in which it is desired to magnetically modulate the phases of the states of the nuclei to be observed there without the concomitant introduction of acoustic noise.

The most convenient of the Mössbauer transitions for modulation experiments is the 14.4-keV transition of ^{57}Fe diluted in a thin metal foil. The propagation of magnetic waves in conductive foils presents a

Figure 6.1

Dispersion curve showing a plot of the wavevector k of spin waves as a function of energy (after reference 4). Away from the cross-over region the waves are essentially purely magnetic or purely elastic.

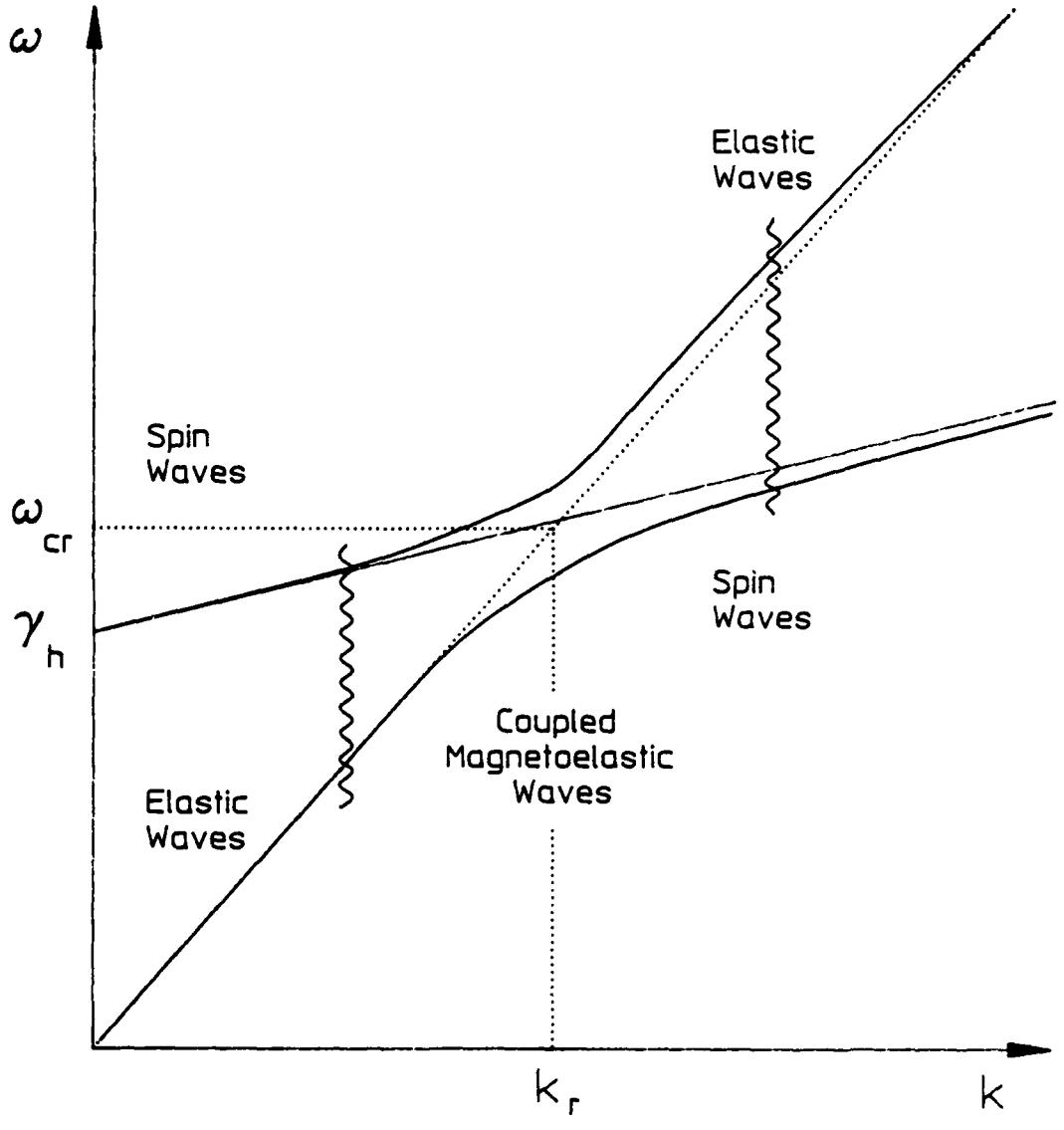
ω
Elastic
Waves
Spin
Waves
ω cr
γ h
Spin
Waves
Coupled
Magnetoelastic
Waves
Elastic
Waves
k r
k

special problem because of eddy current losses and Kittel has given an approximation[2] which would limit the mean free path for a magnon to a few wavelengths for the frequencies of tens of MHz which would be interesting for use with ^{57}Fe. For this reason the preferred choices for the propagation of magnetization in such thin metallic foils are the magnetostatic waves characterized by long wavelengths and high group velocities[3-5] that are quite removed from intersections with acoustic branches. Wavelengths can readily reach the scale of millimeters and it has been demonstrated that dispersion properties are little affected by raising the temperature of the foil above the Curie point[6] so that the material becomes paramagnetic.

The stainless steel used in these experiments was a nonmagnetic alloy, 310 which was expected[7] to have a susceptibility of about 4000 ($\times 10^{-6}$). When enriched in ^{57}Fe, it displays a single absorption line at 14.4-keV. Relatively recently, it has been shown[8] how to communicate the large values of magnetization characteristic of ferromagnetic materials into thin foils of paramagnetic media, such as stainless at room temperature, by sandwiching it between ferromagnetic layers. Such an arrangement was used in the experiments reported here to launch a wave of oscillating magnetization into a stainless tape, enriched in ^{57}Fe so that nuclear phase modulation might be observed at a distance from the source of the disturbance that was greater than the range for the transport of acoustic phonons.

This experiment employed a conventional Mössbauer spectrometer with a 2mCi ^{57}Co source in a Pd matrix to obtain the ^{57}Fe resonance spectra in a transmission geometry. To detect the 14.4-keV gamma rays we used a high resolution EG&G high purity Ge detector. A Wavetek Model 3000 signal generator and a 50 db ENI-325LA linear radiofrequency (rf) amplifier provided the oscillating magnetic field.

To calibrate the contributions from ultrasonic and phase modulation effects two independent techniques of sideband generation were used. As a

basis for comparison, ultrasonic sidebands were excited on the unsplit absorption line of ^{57}Fe nuclei in a stainless steel foil by sinusodial vibrations injected with a 25 MHz piezoelectric transducer. As shown in Fig. 6.2a, an 8 mm × 10 mm section of a larger ^{57}Fe-enriched stainless steel foil of 2.5 μm thickness was acoustically bonded to the transducer. The remaining length of the 10 mm × 20 mm stainless foil was gently curved, forming a 90 degree angle with the plane of the transducer. Mechanical support was provided for the transverse section of foil by mounting it between glass cover slides which were then fastened to the transducer cell.

In the usual longitudinal geometry for a transmission experiment, a convenient level of input power of 0.06 W produced the reference level of sideband development seen in Fig. 6.3 in which the 4th order contained 34% of the intensity remaining in the parent transition. In the transverse geometry, the effect of phonons transported in the foil about 1 cm around a bend of 90 degrees could not be detected even with a tenfold increase in power above the reference level. Such an absence of phonons seems consistent with the difficulties expected in propagating transverse vibrations through a medium thin in comparison to a wavelength of sound. This experiment was performed with both X- and AT-cut quartz crystals for transducers as shown in Figs. 6.2a and 6.2b. Sidebands were not observed in the transverse geometry in either case, and the AT-cut transducer required a larger input power of 2.9 W in the longitudinal geometry in order to obtain the same reference level of sideband development.

In the second experimental arrangement, the piezoelectric transducer was replaced with a pair of 2.5 μm foils of ferromagnetic Ni (8 mm × 10 mm) which were periodically magnetized as shown in Fig. 6.2c. The foils (Ni-SS-Ni) were held in rigid contact by sandwiching them between glass cover slides. The protruding section of the stainless foil was again bent at an angle of 90 degrees and enclosed between glass cover slides in the

Figure 6.2

Schematic representation of the mounting arrangements used in the excitation of sidebands on the Mössbauer absorption line of ^{57}Fe in a 2.5 μm thick stainless steel (SS) foil shown as shaded. The optical path from gamma source to detector is shown by the dotted arrow for the orthogonal directions marked as longitudinal and transverse. Excitation is injected into the horizontal face of the SS-foil and the vertical face is mechanically stabilized by the 100 μm thick glass cover slides sandwiching the absorber foils.

(a) Vibrational excitation injected by the X-cut quartz crystal transducer connected to a radiofrequency oscillator.

(b) Vibrational excitation injected by the AT-cut quartz crystal transducer connected to a radiofrequency oscillator.

(c) Spin waves injected by the periodic oscillation of the Ni foils pressed onto the absorber foil by additional cover slides not shown and excited by the magnetic field in an inductor containing the Ni foils. The vertical section protrudes from the coil between windings.

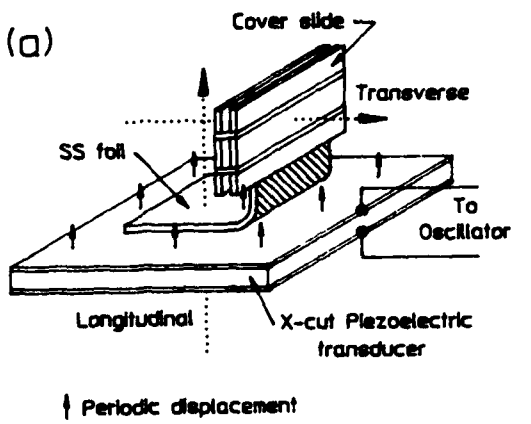
(a)
Cover slide
Transverse
SS foil
To
Oscillator
Longitudinal
X-cut Piezoelectric
transducer
Periodic displacement

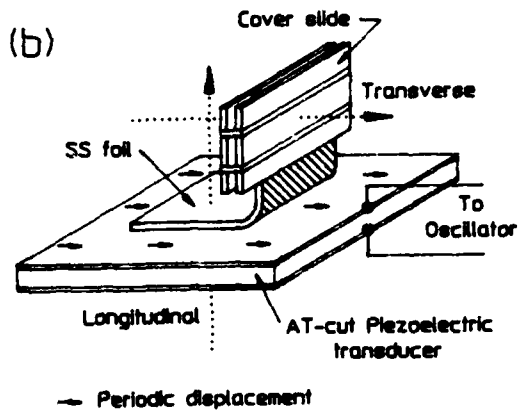
(b)
Cover slide
Transverse
SS foil
To
Oscillator
Longitudinal
AT-cut Piezoelectric
transducer
Periodic displacement

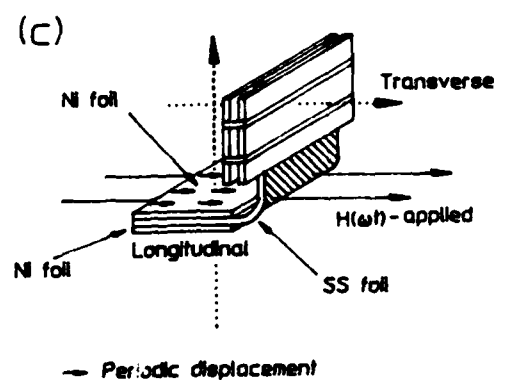
(c)
Ni foil
Transverse
H(ωt) - applied
Longitudinal
Ni foil
SS foil
Periodic displacement

Figure 6.3

Absorption spectra of ^{57}Fe in stainless showing sidebands developed by phonons present in the sample foil.

(a) Reference spectrum observed in the longitudinal geometry at a level of excitation of 0.06 W in the piezoelectric crystal.

(b) Sidebands observed in the transverse geometry of Fig. 6.2a for an excitation level of 0.7 W. Only the unsplit parent line is seen.

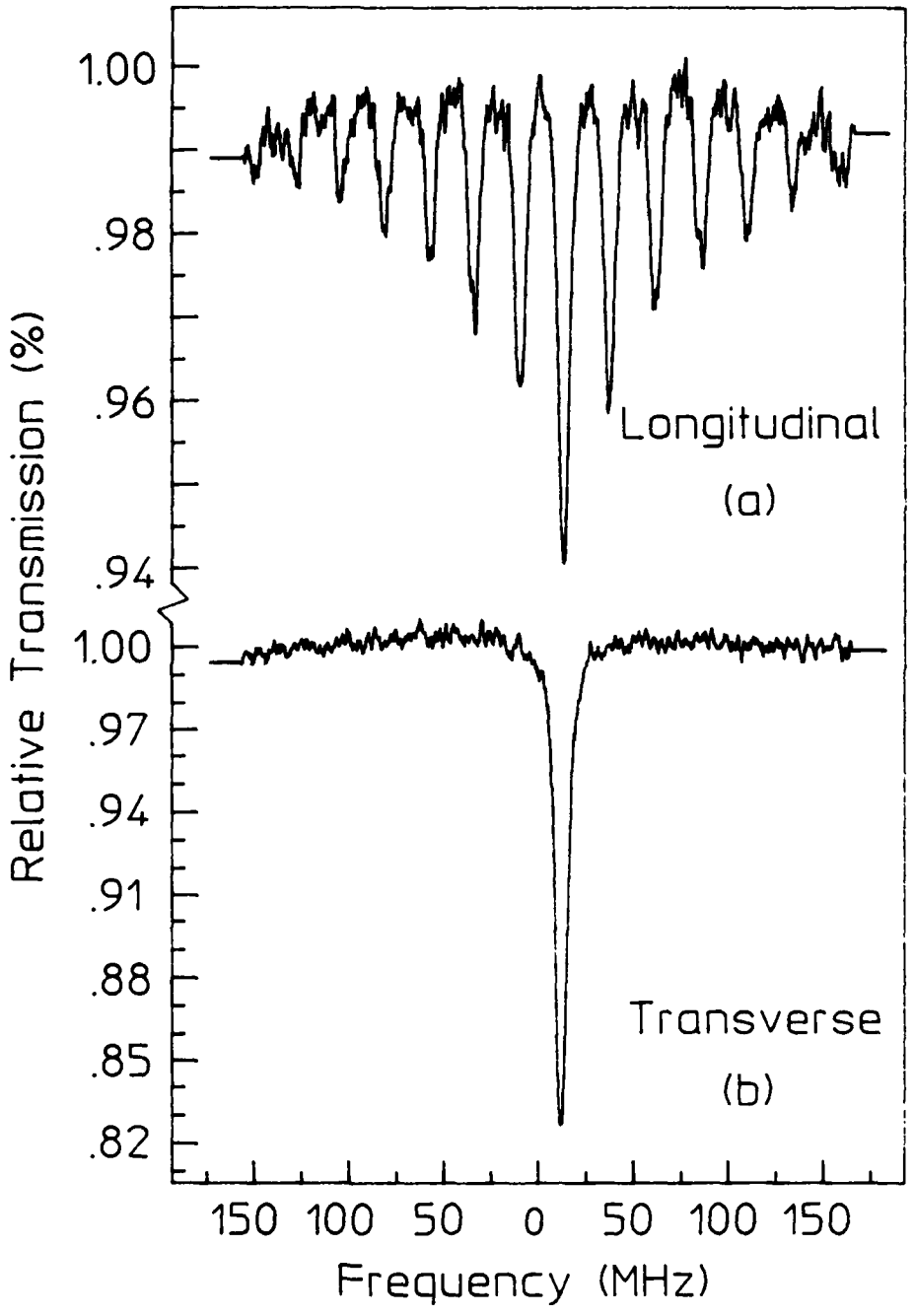
1.00
.98
.96
.94
1.00
.97
.94
.91
.88
.85
.82
Relative Transmission (%)
Longitudinal
(a)
Transverse
(b)
150 100 50 0 50 100 150
Frequency (MHz)

same way as before. Mechanical rigidity was provided to the absorber assembly by a plastic frame.

An rf magnetic field of 0.07 mT was applied to the absorber via a flattened induction coil of a tuned L-C circuit. In the longitudinal geometry for observation the rf power level was adjusted to give about the same reference level of sideband development as had been generated with the piezoelectric transducer, thus facilitating a direct comparison of the propagation of ultrasonic sidebands with those induced by phase modulations generated by magnetostatic waves.

The spectra obtained in the longitudinal and transverse geometries of Fig. 6.2c are shown in Fig. 6.4. In the transverse geometry at this same level of input power, first order sidebands containing about 22 percent of the intensity of the parent line developed. This represents a level 10 times the threshold for detection and hence 100 times any component contributed by acoustic phonons as determined from the data of Fig. 6.3 obtained with the experimental arrangement of Fig. 6.2a. It seems that these experiments have shown that an oscillating alignment of spins can be propagated through such a stainless foil better than mechanical vibrations can be transported under the same condition.

Excited on one end by the oscillating magnetization of a strip of ferromagnetic Ni, the absorber foil showed the strong development of sidebands at the other end where mechanical vibrations were shown to contribute less than 1% of the signal. In these experiments the driving amplitude, H_o in the Ni, was only 0.07 mT while the frequency was 23.74 MHz. Without the excitation of spin waves the effect should have been smaller by at least the ratios of the scaling parameters,[1] $(B_o/\omega)^2$, a factor of 10^{11} for this case. Even with some attenuation of the spin waves during transport, the great enhancement in the effects of coherent modulation which they produced in this arrangement makes possible the examination of

Figure 6.4

Absorption spectra of ^{57}Fe in stainless showing sidebands resulting from the modulation of nuclear phases by spin waves present in the sample foil.
(a) Reference level of excitation observed in the longitudinal geometry of Fig. 6.1b at a field amplitude of 0.07 mT.
(b) Sidebands observed in the transverse geometry for the same driving field of 0.07 mT.

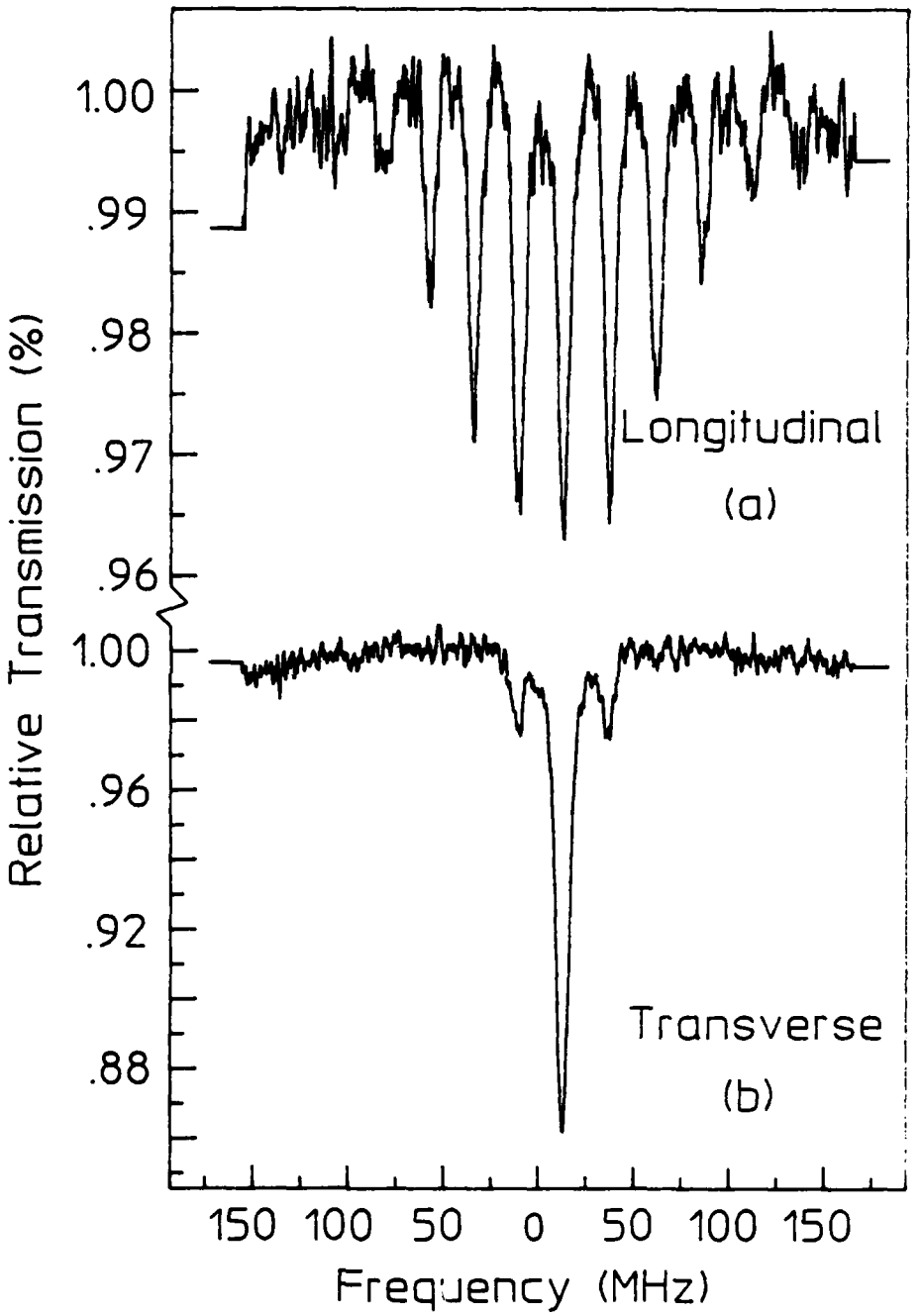
1.00
.99
.98
.97
.96
1.00
.96
.92
.88
Relative Transmission (%)
Longitudinal
(a)
Transverse
(b)
150 100 50 0 50 100 150
Frequency (MHz)

many predicted coherent phenomena over practical ranges of tuning at accessible levels of input powers.

Bridging Experiments

In the previous section it was shown that radiofrequency sidebands induced in a paramagnetic stainless foil from a pair of ferromagnetic drivers could be transported away form the source foil along a length of stainless tape. It was demonstrated that the acoustic vibrations in the foils contributed less than 1% of the signal of the transported sidebands. Without the excitation of spin waves the effect should have been smaller by at least the ratios of the scaling parameters, $(B_0/\omega)^2$, a factor of 10^{11} for this case. If indeed spin waves are the transport mechanism for these magnetically induced sidebands then it should be possible to transport this effect through any paramagnetic material. In this section the results of a series of experiments designed to qualitatively verify that spin waves are the transport mechanism of magnetic sidebands in paramagnetic materials and also provides the remarkable amplification of the phase modulation of nuclear states observed in the last section.

Spin waves (or magnons) are low-lying excitations that occur in ordered magnetic materials. In ferromagnetic or anitferromagnetic materials the long-range magnetic ordering decreases as the temperature increases until eventually there is a phase transition to a disordered (paramagnetic) state. This critical temperature is known as the Curie temperature T_C in ferromagnets and as the Neel temperature T_N in antiferromagnetic materials.

The concept of spin waves, as the lowest lying magnetic states above the ground state, was introduced by Bloch in 1930. He hypothesized the spin waves as deviating slightly from their ground state, and that these disturbances would then propagate with a wavelike behavior through the material.

Several techniques are used to study spin waves. Light scattering from magnons and inelastic neutron scattering are the most useful techniques for studying the dispersion of magnons. Electron energy loss spectroscopy is another scattering technique used to study excitation on crystal surfaces. Magnetic resonance spectroscopy can also be used.

The absorber arrangement for the sideband transport experiments reported in this section is shown in Figure 6.5. A 2.5 μm, ferromagnetic nickel foil with a surface area of 1 cm^2 was used as the source of large amplitude magnetic oscillations which were injected into a variety of foils with varying magnetic susceptiblilites. The bridging foils were chosen on the basis of whether or not they have a positive or negative magnetic susceptibility which would indicate whether the material is paramagnetic ($\chi > 0$) or diamagnetic ($\chi < 0$). If spin waves are the transport medium, then large amplitude spin waves generated in the nickel foil should propagate across a paramagnetic bridge which connects the nickel and stainless foils. In diamagnetic materials where there are no unpaired electrons, the medium for spin wave transport is nonexistent and the waves of oscillation magnetization quickly die out once they enter the material. The resulting phase modulation of the nuclear states is then detected in the 310 SS paramagnetic absorber enriched with 90.82% ^{57}Fe of the iron component of this alloyed foil.

The results of these experiments for a variety of bridging materials is summarized in Table 6.1. All of the data for the bridging experiments was collected with an rf frequency of 24.0 MHz and a PQ product of 150 W. The second column of the table gives the magnetic susceptibility of the bridging material. A cursory examination of table reveals the mechanism responsible for the transport of nuclear phase modulation effects can propagate only through paramagnetic bridging foils, a result consistent with the spin wave hypothesis.

Figure 6.5

Absorber configuration of the rf bridging experiments. The foils were mounted between glass cover slides for mechanical rigidity. The rf field was applied to the foils by mounting the assembly in the induction coil of a tuned LC-circuit.

Absorber Arrangement for

Sideband Transport Experiments

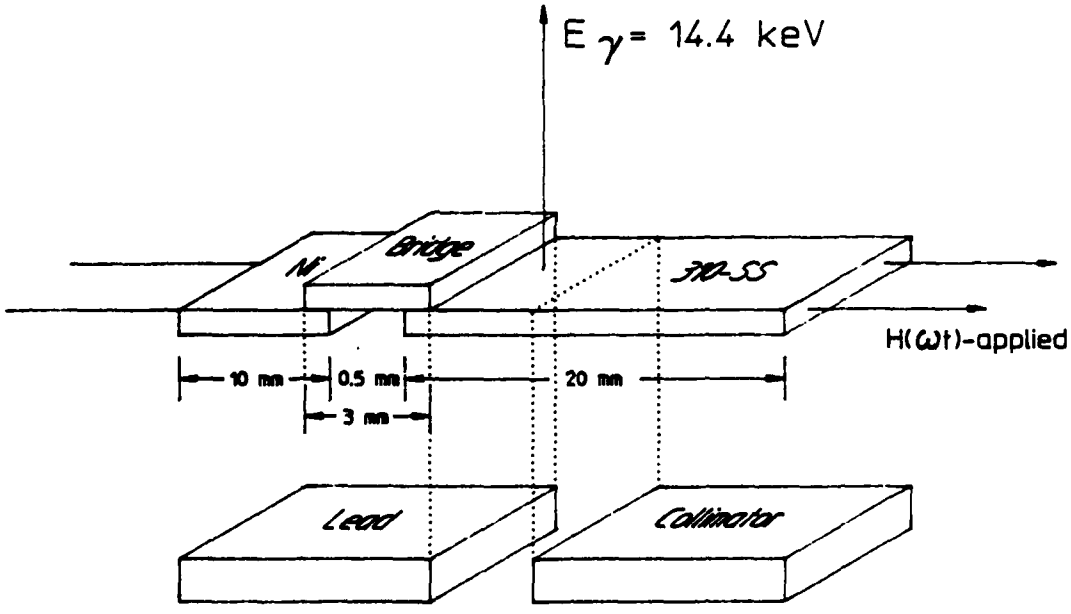

Table 6.1

Summary of experimental results for the rf bridging experiments. As can be seen the mechanism responsible for transporting the magnetically induced sidebands from the nickel source to the stainless steel absorber can be propagated only by paramagnetic materials. The transport of this effect is also independent of the acoustic coupling between the foils. The results of the bridging experiments are consistent with the spin wave hypothesis discussed in the text.

Bridging Material (25 μm)	Susceptibility χ (10^{-6} cgs)	Acoustic Impedence $Z = \rho c$ (10^5 g/cm^{2}sec)	Effect Transported
Aluminum	+ 16.5	17.33	yes
Copper	- 5.46	44.74	no
Silver	- 19.5	37.96	no
310-SS	+ 4000	45.4	yes
Tin	- 37.0	24.24	no
Titanium	+ 153.0	27.32	yes

As a basis of comparision the acoustic impedences of the bridging foils are also given in Table 6.1. The acoustic impedance, as was discussed in Chapter 5, is simply a measure of how well acoustic vibrations can be propagated through a material. As can be seen from the table there is no correlation between the acoustic coupling of the foils and the transport of the effect, whereas the correlation between the transport of the effect and the magnetic properties of the bridging foil is excellent. For example, consider the case for Al which has a magnetic susceptibliity of + 16.5 ($\times 10^{-6}$ cgs) and shows a strong transport of sidebands as seen in Figure 6.6a, yet it has very poor acoustic properties compared to the nickel source and the stainless absorber. In contrast, Cu which has very good acoustic matching with the Ni and SS foils does not transport the effect as seen in Figure 6.6b. From the results of these bridging experiments it is possible to conclude that the sidebands transported across a paramagnetic bridging foil is the result of nuclear phase modulation and not mechanical frequency modulation. The results of this experiment furthur supports the spin wave transport hypothesis presented in the previous section.

Figure 6.6

Representative data sets showing (a) the transport of sidebands across a paramagnetic Al bridge and (b) no transport of the effect across a diamagnetic Cu bridge foil. The bridging foils were both 25 μm thick. The frequency of the rf was 24.0 MHz with a PQ product of 150 W for the applied rf.

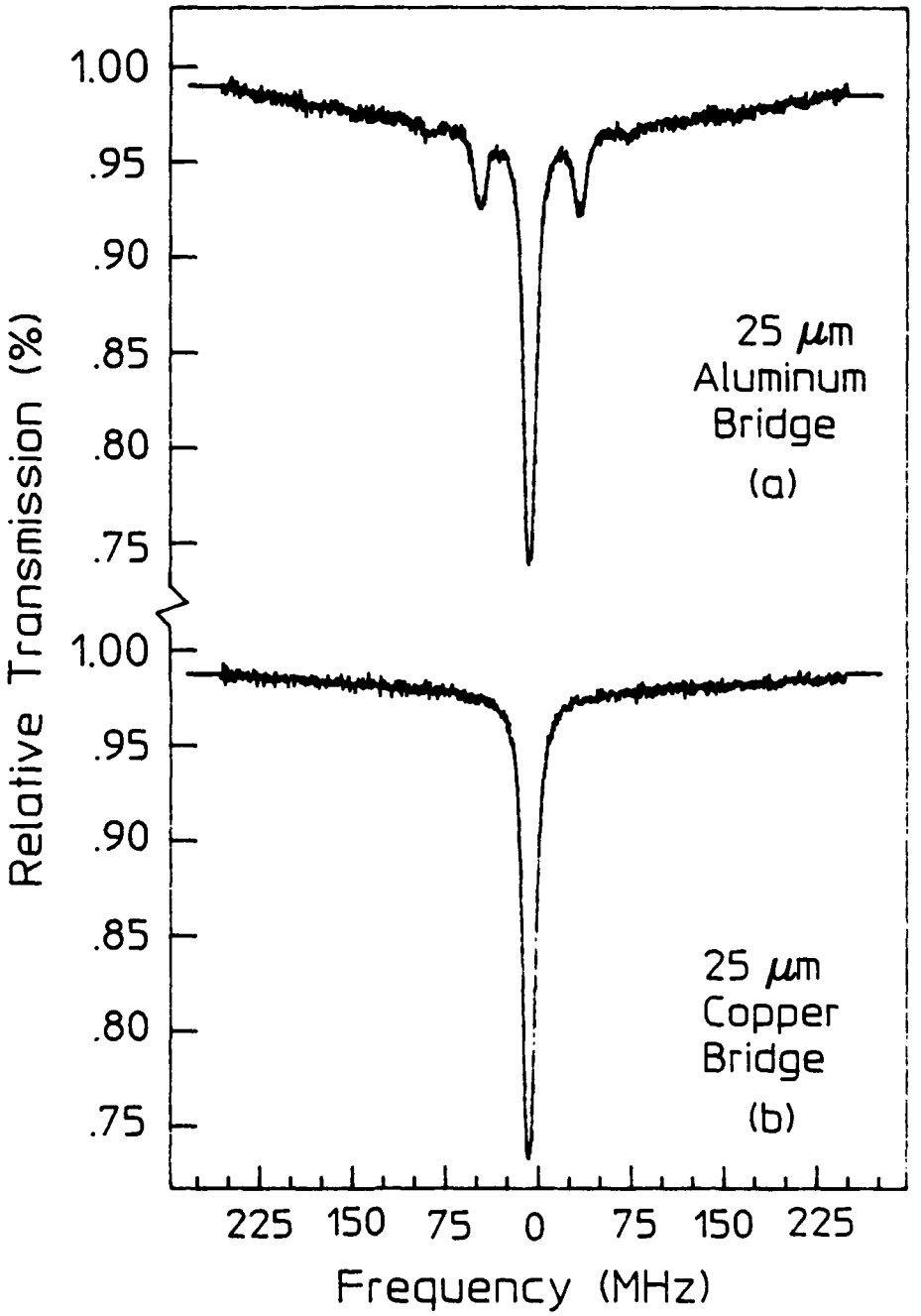
1.00
.95
.90
.85
.80
.75
25 μm
Aluminum
Bridge
(a)
1.00
.95
.90
.85
.80
.75
25 μm
Copper
Bridge
(b)
Relative Transmission (%)
225 150 75 0 75 150 225
Frequency (MHz)

REFERENCES

1. E. Ikonen, P. Helisto, J. Hietaniemi and T. Katila, Phys. Rev. Lett. 60, 643 (1988).
2. C. Kittel, Phys. Rev. 110, 836 (1958).
3. P. C. Fletcher and C. Kittel, Phys. Rev. 120, 2004 (1960).
4. E. Schlömann, J. Appl. Phys. 31, 1647 (1960).
5. R. W. Damon and J. R. Eshback, J. Appl. Phys. Supp. 31, 1045 (1960).
6. H. A. Mook, J. W. Lynn, and R. M. Nicklow, Phys. Rev. Lett. 30, 556 (1973).
7. T. Lyman, Metals Handbook, 8th ed. (Am. Soc. for Metals, Ohio, 1961), Vol. I, p. 793.
8. P. Grünberg, J. Appl. Phys. 51, 4338 (1980).

CHAPTER 7

SUMMARY AND CONCLUSIONS

The interaction of the nucleus with long wavelength (rf) radiation has been studied using the Mössbauer effect for more than two decades. As first proposed by Mitin,[1] this interaction could result from a multiphoton interaction where a quantum of rf is simultaneously absorbed along with a quanta of gamma-ray energy under Mössbauer conditions. These multiphoton effects should be observed as sidebands accompanying the usual Mössbauer transitions. While probably observed for 20 years[2] the effects, however, were initially confused with mechanical frequency modulation first reported by Ruby and Bolef[3]. Later researchers,[4-5] studying the influence of rf magnetic fields on the Mössbauer transitions in iron foils enriched with ^{57}Fe, incorrectly assumed that the rf sidebands thus observed were the result of a periodic displacement of the Mössbauer nuclei driven by the magnetostrictive oscillations of the foils. This conceptual error was later compounded by the work of Chien and Walker[7] who developed a scheme where sidebands could be transfered into nonmagnetic absorbers from ferromagnetic driver foils. They incorrectly assumed that under the influence of rf magnetic fields acoustic waves were set up in the ferromagnetic foils and then transferred in to the absorber foil. The acoustic vibrations were then believed to be detected as sidebands on the Mössbauer transitions. This dissertation reports the reexamination of rf sidebands in various absorber arrangements and concludes that the magnetostiction model of rf sideband development is incorrect.

In chapter 4 the results of two experiments were presented which demonstrate that the magnetostrictive model of rf sidebands does not explain the new experimental evidence reported in this work. The first experiment reexamined and extended the Chien and Walker experiment which

from current perspective was considered to be the bulwark of the magnetostrictive-acoustic hypothesis. The results of this experiment supported only the first conclusion reached in that original work, namely that the causitive agent of rf sidebands can be produced in a ferromagnetic layer and then transported into a nonmagnetic layer. Their other conclusion was completely refuted by data presented in Chapter 4 because the effects they attributed to the type of coupling between layers was seen to result from the relative number of magnetic and nonmagnetic layers. In this dissertation it was found that the effect of two ferromagnetic source foils varied from two to four times the effect produced by a single foil, depending upon the static magnetic bias applied, a result not explained by the magnetostrictive-acoustic hypothesis.

The second experiment reported in Chapter 4 demonstrated that the magnetostrictive properties of the absorber foils does not correlate with the observed sideband development. In this experiment two iron-nickel alloys professionally prepared for us by ORNL served as the absorber foils. These alloys or permalloys as they are called, possessed unusual magnetic properties in that at a composition near 81% Ni the magnetostriction of the foil passed through zero in at least two crystalographic directions. By comparing the sideband development in two foils with compositions near this critical point it was demonstrated that sideband development anticorrelated with magnetostriction and correlated with the higher permeability of the nonmagnetostrictive foil.

In Chapter 5 the results of an experimental investigation into the rf sideband development in the absorption spectra of ^{119}Sn were reported. Here it was found that sidebands could not be propagated into a diamagnetic tin foil from a pair of ferromagnetic drivers, even with the application of rf powers nearly three orders of magnitude greater than that necessary to induce sidebands in a paramagnetic 310 stainless steel foil. Even considering the slightly poorer acoustic coupling between the nickel and tin, as

compared to a nickel-stainless interface, the magnetostrictive-acoustic model cannot explain this failure.

In the remaining two experiments reported in Chapter 5, tin was alloyed with iron and nickel forming the magnetic compounds $FeSn_2$ and NiSn. Here it was found that sidebands easily developed with application of reasonable rf powers. The results were explained using nuclear phase modulation theory presented in Chapter 2. By coupling the naturally occuring hyperfine magnetic fields at the nuclear sites with the rf fields, large scale phase modulation effects were observed in these binary metallic compounds.

The experimental results of Chapter 6 represents the most convincing argument against the magnetostrictive-acoustic model. In the first experiment discussed, a direct comparision between ultrasonic and magnetic sidebands was made. As a basis for comparision, sidebands were excited upon the unsplit absorption line of ^{57}Fe nuclei embedded in a paramagnetic 310 stainless steel foil by the sinusoidal vibrations injected with X and AT-cut transducers. In the usual longitudinal geometry for transmission experiments, a convenient level of input power produced a reference level of sideband development that resulted in sideband development up to 4th order which contained 34% of the intensity remaining in the parent line. In the transverse geometry, the effect of phonons transported in the foil about 1 cm around a bend of 90 degrees could not be detected even with a tenfold increase in rf power above the reference level.

Replacing the piezoelectric source of ultrasonic phonons with a pair of 2.5 μm foils of ferromagnetic nickel subjected to an rf magnetic field, gave the opportunity to launch what is believed are large amplitude spin waves into the magnon fluid of the paramagnetic foil. The longitudinal geometry was used to set the same reference level of sideband development at the source. In the transverse geometry at this same level of input power, the first order sidebands were found to have 20% of the intensity of

the parent transition, a level 10 times the threshold for detection and, hence, 100 times any component contributed by acoustic phonons. It is believed that these sidebands are the result of nuclear magnetic phase modulation of the quantum phases of ^{57}Fe nuclei which were produced by spin waves of large amplitude transported from the ferromagnetic source. This represents an eleven orders-of-magnitude increase in the efficiency through which phase modulation effect can be produced.

The second experiment reported in Chapter 6 further strengthens the argument in favor of spin waves as the transport mechanism of the magnetically induced sidebands. Here it was shown that these sidebands could be propagated from a ferromagnetic source across a paramagnetic "bridge" and then detected in a stainless tape enriched with ^{57}Fe. It was found that sidebands could only be propagated through materials which have a nonzero spin, that is to say sidebands cannot be propagated across a bridge of diamagnetic material.

In summary, the results presented in this dissertation resolve a controversy which has existed in the literature for over 20 years. It was shown that nuclear magnetic phase modulation is indeed observed and that the effect can be transported a considerable distance through a foil by first coupling the rf field to the individual magnons in a material and then coupling to the nucleus, to modulate the quantum phases of the nuclear states.

REFERENCES

1. A. V. Mitin, Sov. Phys. JETP 25, 1062 (1967).
2. G. L. Perlow, Phys. Rev. 172, 319 (1968).
3. S. L. Ruby and D. I. Bolef, Phys. Rev. Lett. 5, 5 (1960).
4. N. D. Heiman, L. Pfeiffer, and J. C. Walker, Phys. Rev. Lett. 21, 93 (1968).
5. L. Pfeiffer, N. D. Heiman, and J. C. Walker, Phys. Rev. B 6, 74 (1972).
6. N. Heiman, R. K. Hester, and S. P. Weeks, Phys. Rev. B 8, 8 (1973).
7. C. L. Chien and J. C. Walker, Phys. Rev. B 13, 1876 (1976).

END

6-89

DTIC